Petrology and Partial Melting of Garnet-bearing Mafic Granulites from the Gondwana Orogeny

January 2015

Yohsuke SAITOH

Contents

Contents	i
Abstract	ii
List of figures	v
List of tables	vii
Chapter 1 Introduction	1
Chapter 2 Geological setting	10
Chapter 3 Petrography	19
Chapter 4 Mineral Chemistry	35
Chapter 5 Mineralogy and compositions of CMI	45
Chapter 6 Metamorphic *P-T* conditions	48
Chapter 7 Phase equilibrium modeling	58
Chapter 8 Discussion	68
Chapter 9 Conclusion	79
Acknowledgement	81
References	82

ABSTRACT

Partial melting of meta-basic rocks (e.g., mafic granulite, amphibolite), which has been regarded as the major constituent of the lower to middle crust, probably plays a critical role of formation of felsic to andesitic magma and crustal differentiation. It is also generally accepted that partial melting has considerable influence on mineralogy and stability field of minerals during high-grade metamorphism. Numerous studies on partial melting processes of meta-basic rocks have been done for the last several decades mostly on the basis of high *P-T* experiments. However, detailed approach on the process based on outcrop- to hand specimen-scale, or even mm- to micro-scale petrological investigations is limited. Recently micro-scale (<100 μm) crystallized melt inclusions (CMIs) as a direct evidence of partial melting were investigated from several high-grade terranes, yet they are mostly found in felsic to pelitic granulites. This study therefore reports new petrological data of such CMIs in mafic granulite and associated pelitic to felsic granulites using detailed petrological approach and phase equilibrium modeling of minerals, and quantitatively discuss the effect of partial melting on *P-T* evolution of high-grade metamorphic terrane.

The examined mafic granulites were corrected from the Neoproterozoic to Cambrian Lützow-Holm Complex (LHC), East Antarctica, which corresponds to the collisional orogeny formed during the amalgamation of Gondwana Supercontinent. CMIs were found from 10 mafic granulite samples which show variation of mineral assemblages such as garnet + clinopyroxene + quartz + ilmenite and garnet + quartz + plagioclase + clinopyroxene + hornblende + biotite ± rutile. These rocks preserve several decompression textures such as Grt + Cpx/Hbl + Qtz → Opx + Pl ± H_2O and Grt + Qtz

→ Opx + Pl probably formed by clockwise *P-T* evolution. The CMIs are 50 to 200 μm in size, preserved only in porphyroblastic garnet, and mainly consist of quartz, biotite, K-feldspar, and plagioclase. Two samples of mafic granulite with abundant CMIs; Type A (sample TS11010802) from Skallevikshalsen in the highest-grade region of the LHC, and Type B (sample TS11020610I) from Ongul in slightly lower-grade area were selected for detailed pseudosection analysis. Type A is characterized by the peak assemblage of garnet + clinopyroxene + quartz + ilmenite, while the peak mineralogy of Type B is garnet + clinopyroxene + ilmenite + orthopyroxene + biotite + hornblende. The inferred melt composition based on modal abundance and composition of minerals in CMIs suggest generation of potassium-rich and andesitic to dacitic melts probably by dehydration melting of hornblende and biotite which often occur as inclusions in garnet. The maximum degree of melt extraction has been estimated based on pseudosection analysis as about 6.5 % (Type A) and 4.5 % (Type B). As the degree of partial melting increases, the stability field of quartz expands toward lower pressure, clinopyroxene becomes unstable, and liquid becomes more stable. The phase equilibria modeling also suggests that the melt extraction probably took place during the prograde stage.

This study subsequently adopted integrated bulk compositions calculated using melt composition and the degree of melt extraction, and inferred *P-T* conditions of melt extraction stage at 820-830 °C and 9-10 kbar (Type A) and about 750 °C and 15.5 kbar (Type B). The estimated solidus temperatures of the samples are 750 °C and 780 °C, respectively, at 10 kbar, which are consistent with previous estimations of high P-T experiments. The estimated peak *P-T* condition (>920 °C) and *P-T* path (clockwise) of Type A are well consistent with the results of previous studies of Skallevikshalsen, while the peak pressure condition of Type B (15.5 kbar) is slightly higher (1-1.5 kbar)

than that obtained from pelitic granulite in Ongul but nearly consistent. This study successfully traced the evidence of prograde partial melting and melt extraction in mafic granulites from the LHC, and determined prograde and peak *P*-*T* conditions based on pseudosection approach using integrated bulk compositions, which confirmed that the influence of partial melting should be taken into consideration for evaluation of high-grade metamorphism.

Key words: partial melting, mafic granulite, crystallized melt inclusions (CMIs), phase equilibrium modeling, Lützow-Holm Complex (LHC)

List of Figures **page**

Fig. 1. Geological map of the Lützow Holm Complex. 94
Fig. 2. Exposures map in the Lützow Holm Complex. 95
Fig. 3. Geological map of the Skallevikshalsen. 96
Fig. 4. Geological map of the Skallen. 97
Fig. 5. Geological map of the Austhovde. 98
Fig. 6. Geological map of the Ongul. 99
Fig. 7. Field occurrence of the examined samples from Skallevikshalsen. 101
Fig. 8. Field occurrence of the examined samples from Austhovde. 102
Fig. 9. Field occurrence of the examined samples from Ongul. 102
Fig. 10. Thin sections photographs of the examined samples. 103
Fig. 11. Compositional diagrams of garnet. 107
Fig. 12. Compositional diagrams of pyroxene. 109
Fig. 13. Compositional diagrams of feldspar. 111
Fig. 14. Compositional diagrams of amphibole. 117
Fig. 15. Back Scattered Electron (BSE) images of CMIs within mafic to ultramafic granulites. 122
Fig. 16. Back Scattered Electron (BSE) images of CMIs within pelitic to felsic granulites. 123
Fig. 17. Estimated *P-T* conditions obtained from Skallevikshalsen and Skallen. 124
Fig. 18. Estimated *P-T* conditions obtained from Austhovde. 125
Fig. 19. Estimated *P-T* conditions obtained from Ongul. 126
Fig. 20. *P-T* diagram showing calculated pseudosections of mineral assemblages in mafic granulite from Skallevikshalsen. 127
Fig. 21. *P-T* diagram showing calculated pseudosections of mineral assemblages in mafic granulite from Austhovde. 128
Fig. 22. *P-T* diagram showing calculated pseudosections of mineral assemblages in garnet amphibolite from Ongul. 129
Fig. 23. *P*-X diagram showing calculated pseudosections of mineral assemblages in mafic granulite from Skallevikshalsen. 130
Fig. 24. *P*-X diagram showing calculated pseudosections of mineral assemblages in garnet amphibolite from Ongul. 131
Fig. 25. *P-T* diagram showing calculated pseudosections for integrated-bulk composition of mafic granulite from Skallevikshalsen. 132
Fig. 26. *P-T* diagram showing calculated pseudosections of mineral assemblages in mafic granulite from Skallevikshalsen. 132

Fig. 27. *P-T* diagram showing calculated pseudosections for integrated-bulk composition of garnet amphibolite from Ongul. 133
Fig. 28. *P-T* diagram showing calculated pseudosections of mineral assemblages in garnet amphibolite from Ongul. 133
Fig. 29. *P-T* diagram showing stability field of plagioclase in examined samples and previous experimental study. 134
Fig. 30. Simplified *P-T* paths of the mafic granulite and garnet amphibolite. 135
Fig. 31. Detailed *P-T* diagram in Fig. 26 with mineral modal isopleth. 136
Fig. 32. Comparison of *P-T* path of the mafic granulites from Skallevikshalsen and Previous studies. 137

List of Tables **page**

Table 1. Mineral abbreviations. 138
Table 2. Approximate abundance of minerals of examined samples. 139
Table 3. Measured grain sizes of minerals of examined samples. 149
Table 4. Representative electron microprobe analysis of garnet. 159
Table 5. Representative electron microprobe analysis of pyroxene. 162
Table 6. Representative electron microprobe analysis of plagioclase. 164
Table 7. Representative electron microprobe analysis of amphibole. 166
Table 8. Composition of the CMI. 167
Table 9. Summary of the *P-T* calculations. 170
Table 10. Whole rock chemistry of the mafic granulites. 171

Chapter 1. Introduction

1.1. Mafic granulite

Mafic granulite is regarded as one of the important components of granulite terrains and lower crust (e.g., Rudnick and Fountain, 1995). It is generally characterized by abundant ferromagnesian minerals (e.g., hornblende, pyroxene, biotite, garnet etc.) and basaltic to andesitic composition. Particularly, garnet-bearing mafic granulites preserve important geological and petrological information of orogenic processes because garnet often includes prograde minerals, fluid inclusion, and melt inclusions, and shows compositional zoning as a result of changing *P-T* conditions. Such prograde mineralogy and compositional zoning provides early history of the metamorphic evolution (e.g., Spear, 1993), and fluid inclusions provide key information of fluid-rock interaction (e.g., Walther and Wood, 1986). Previous petrological studies demonstrated that garnet-bearing mafic granulites generally formed under higher-pressure condition than garnet-free granulites (e.g., Green and Ringwood, 1967; López and Castro, 2001). This study thus focuses on petrology of the garnet-bearing mafic granulite (also refer as high-pressure mafic granulite). Such high-pressure (HP) metamorphic rocks provide important insights into exhumation history of the rocks to the Earth's surface from deep crustal levels or mantle depths (O'Brien and Rötzler, 2003).

1.2. High-pressure mafic granulite

Green and Ringwood (1967) performed experimental studies of basaltic rocks with

various compositions under high *P-T* conditions. Their results of quartz tholeiite (quartz-saturated basalt), suggest that garnet + clinopyroxene + quartz ± plagioclase assemblage is stable at high *P* conditions while orthopyroxene-bearing assemblage is stable under lower pressure. The phase relation proposed by Green and Ringwood (1967) is therefore essential to investigate the metamorphic process of mafic granulites. O'Brien and Rötzler (2003) summarized *P-T* conditions and mineral assemblages of the high-pressure granulites, and divided the granulites into two groups based on *P-T* ranges; 700-850 °C and 10-14 kbar, and 900 °C and above 15 kbar. In the case of mafic rocks, garnet + clinopyroxene + plagioclase ± hornblende ± quartz is a key indicator of high-pressure metamorphism, while garnet + K-feldspar + kyanite is a diagnostic assemblages of high-pressure metamorphism in pelitic to felsic granulites (O'Brien and Rötzler, 2003). Pressure-temperature-time (*P-T-t*) paths of such rocks could preserve significant information for understanding of thermal and tectonic processes particularly for the deeply eroded orogen as well as the protoliths (MORB, island arc and oceanic Island). This chapter introduces previous studies of the high-pressure-mafic granulite (HPMG) and partial melting process of the granulite. Pressure-temperature evolutions of the HPMG have been investigated by many authors. For example, Sajeev et al. (2010) reported HPMG from the Imjingan belt in South Korea. The granulites in the belt occur as blocks with leucosome within amphibolite which is in turn surrounded by metasediments (paragneiss). Peak assemblage of the granulite is garnet + clinopyroxene + quartz + rutile followed by formation of retrograde symplectite of hornblende + titanite + plagioclase. They obtained peak *P-T* condition of 20 kbar and 900 °C by phase equilibrium modeling, and they argued collisional tectonic setting involving the Imjingan belt. Liu et al. (2013) reported HPMG from the North China Craton. The

granulite occurs as blocks within tonalite-trondhjemite-granodiorite (TTG) gneiss or thin layers within TTG gneiss. Peak assemblage of the granulite is garnet + clinopyroxene + plagioclase (albite rich) + quartz which is replaced by symplectite of orthopyroxene + plagioclase + hornblende. The peak *P-T* condition of the granulite is 14.5-16.5 kbar and 850-880 °C along a clockwise *P-T* path. They further performed trace element study of the garnet in the granulite, suggesting that garnet in the sample crystalized under high-grade conditions related to subduction and collision tectonic settings. Zhang et al. (2010) reported HPMG with the peak mineral assemblage of garnet + clinopyroxene + rutile + quartz, from the Amdo basement, central Tibet. The granulite occurs as small blocks within low-grade metasedimentary rocks. Two types of symplectites composed of orthopyroxene + plagioclase ± spinel and hornblende + plagioclase were identified around garnet. *P-T* estimation suggests that peak metamorphic condition was about 860-920°C and 1.46-1.56 GPa, which was retrogressed during post-peak stage at 820-890°C and 0.88-1.15 Gpa, and to amphibolite-facies stage at 550-670°C and 0.52-0.65 GPa. These three stages define a clockwise *P-T* path with near-isothermal decompression and cooling following the peak-high-pressure metamorphism. This suggests that the Amdo granulites underwent an initial subduction to a deep crustal level of ~50 km and then were rapidly exhumed to a shallow crustal level (~20 km). The formation of Amdo granulites is considered to have resulted from arc-continent collision between the Amdo basement and the Qiangtang terrane during the middle Jurassic, which is a crucial step to the tectonic evolution of the Tibetan Plateau, while most radiometric ages for the gneisses from the Amdo basement fall in a narrow range of 490 Ma to 530 Ma. Zhang et al. (2005) reported HPMG in the Bashiwake area of the south Altyn Tagh (SAT)

subduction-collision complex which encloses mafic granulites and garnet peridotite-hosted sapphirine-bearing metabasites. Quartz-bearing mafic granulite contains the peak pressure assemblage of garnet + clinopyroxene + ternary feldspar (now mesoperthite) + quartz + rutile. Petrographic data suggests the peak assemblage of garnet + clinopyroxene + kyanite + rutile. Application of thermobarometry indicates that all the rock types in the studied area experienced peak *P-T* conditions of 18.5–27.3 kbar and 870-1050 °C. A medium- to high-pressure granulite-facies overprint (780–820 °C, 9.5-12 kbar) is defined by the formation of secondary clinopyroxene ± orthopyroxene + plagioclase at the expense of garnet and early clinopyroxene in the mafic granulites. Occurrence of the mafic granulite and *P-T* conditions of available lithologies (mafic granulite and felsic granulite) suggest they experienced similar metamorphism. In summary, peak *T* condition of HPMG and associated pelitic to felsic granulite is *T* >750 °C from different localities in the world, which is below solidus of the rocks. In the case of mafic granulites, experimental studies of amphibolite under fluid absent conditions suggest that solidus is below 750 °C (López and Castro, 2001) while pelitic rocks could generated melt below 750 °C (Vielzeuf and Holloway, 1988). Therefore, partial melting is probably a common process under granulite facies. This study thus particularly focuses on the partial melting process of various granulites (mafic, pelitic, and felsic granulites).

1.3. Partial melting of pelitic to felsic granulite

Partial melting process of pelitic granulites have been reported from many localities. They are characterized by the concentration of felsic mineral (leucosome), abundant

incompatible elements in the leucosome (e.g., Ba, P, and Sr), and occurrences of glassy-melt inclusions, and crystalized melt inclusions (CMIs). For example, garnet-sillimanite gneiss (pelitic gneiss) from the Lützow-Holm Complex shows migmatitic textures composed of leucocratic and melanocratic portions in hand specimen scale (Yoshimura et al., 2004). Based on the texture, mineral chemistry, and *P-T* estimations, they argued that the progress of partial melting. High-Ba content of potassium feldspar within the leucosome also support it corresponds to crystallized melt, because Ba behaves as incompatible element during partial melting (Rollinson, 1993). Indares et al. (2008) performed petrological studies of kyanite-bearing anatectic gneiss (pelitic granulite), and also discussed feldspar-rich domains (leucosome) in the rock are interpreted as products of melt crystallization. The rocks yielded peak *P-T* condition of 14.5-15.5 kbar and 840-890 °C, which is typical of high-pressure granulite according to the classification of O'Brien and Rötzler (2003). Compositions of such anatectic melt and *P-T* conditions of partial melting have been investigated by several authors. For instance, Vielzeuf and Holloway (1988) performed high-temperature experimental studies in the system of pelitic rocks under fluid-absent conditions at 7-12 kbar and 750-1250 °C. The results show that S-type-granitic melt was generated within a narrow temperature range of 850-875 °C resulting from the reaction Bt + Als + Qtz + Pl→Liq + Grt ± Kfs suggesting the progress of dehydration melting. Mineral textures and trace element chemistry of such migmatitic rocks have been well studied, because they are easily identified and investigated if compared to crystalized melt inclusions and glassy inclusions due to their small size (micrometer scale). Recently, micro-scale textures which are possibly direct evidence of the progress of partial melting have also been investigated. Several authors reported the occurrence of micro- to millimeter-scale

crystallized melt inclusions (CMIs) and quenched glassy inclusions trapped in porphyroblastic minerals in granulites (e.g., Tsunogae and Santosh, 2006; Cesare et al., 2009; Hiroi et al., 2014). Such inclusions are thought to be a key not only to infer post-peak exhumation process but also to discuss the evolution of granulite terrains. Some authors concluded that the formation of CMIs requires rapid cooling and uplifting from the lower crust (e.g., Hiroi et al., 2014), whereas Cesare et al. (2009) argued that such glassy inclusions are products of slow cooling. The petrogenesis of such micro-scale inclusions are therefore now in debate. Cesare et al. (2009) reported glassy inclusions and crystalized-melt inclusions (also called "nanogranite") included in porphyroblastic garnet within graphite-bearing granulites (khondalite) and pelitic granulites from the Kerala Khondalite belt (KKB), South India. They argued that such glassy inclusions and nanogranite are products of slow cooling. Bartori et al. (2013) performed remelting experiment of the nanogranite reported by Cesare et al. (2009) using piston cylinder. The results show that product of the experiment is comparable with original melt composition with a few amounts of volatile loss. Compositions of the nanogranite are ultrapotassic and rhyolitic with $K_2O > Na_2O$, and are characterized by the considerable amounts of volatile (up to 10 wt. %). Hiroi et al. (2014) reported "felsic inclusions" within garnet from pelitic and psammitic granulites from the Highland Complex, Sri Lanka, and concluded that quenched textures of felsic inclusions require rapid cooling. They hypothesized that the granulites ascended episodically along discrete high-strain zones and cooled as fast as some felsic magmas. CMIs have so far been mostly reported from felsic and pelitic granulites probably because such quarzto-feldspathic rocks commonly experienced partial melting during prograde stage. In contrast, they are generally rare in mafic granulites, although minor dehydration

melting of mafic granulites has been also reported (e.g., Garrido et al., 2006). Experimental studies of partial melting in several lithologies suggest pelitic rocks forms more abundant liquid phase than amphibolites (mafic rocks) at given temperatures (e.g., Vielzeuf and Holloway, 1988; Skjerlie and Johnston, 1993; Lopes and Castro, 2001). This study thus attempt to investigate textures of the CMIs in mafic to ultramafic granulites to discuss the partial melting process.

It is generally accepted that melt loss and partial melting had a considerable influence on mineralogy and stability field of the mineral (e.g., White et al., 2007). Such influence has been constrained in the case of pelitic granulites. For instance, Indares et al. (2008) performed phase equilibrium modeling to pelitic granulites which might have experienced partial melting during prograde stage. The results show that stability field of the peak mineralogy is expanded toward lower temperature if they adopted melt-integrated composition for the modeling. They also reported shift in the muscovite-out line toward lower temperature. It is unclear that in phase equilibrium modeling for mafic granulite, whether the partial melting and melt extraction effects mineralogy and stability fields of the minerals because previous studies did not take into consideration the melt composition. Thus, it is necessary to evaluate the influence of the partial melting on phase diagrams. This study thus focuses on mafic to ultramafic granulites from the Neoproterozoic to Cambrian Lützow-Holm Complex (LHC), because the mafic to ultramafic granulites from the region contain abundant CMIs. Various lithologies are observed in the LHC, which enables us to compare partial melting processes not only in mafic granulites but also in pelitic to felsic granulites.

1.4. Partial melting of the mafic granulites

Partial melting process of mafic granulites has been investigated based on experimental studies. For example, López and Castro (2001) performed experimental study of dehydration melting in the system of amphibolite under dry condition. Solidus of the examined system is around 800 °C and mode of the produced liquid depends on given temperature. At P >10 kbar, garnet is present in the system, suggesting that the formation of garnet-bearing restite in the system. The composition of liquid (granodioritic to granitic) suggests presence of considerable amount of volatile (e.g., H_2O and brine) in the liquid (up to 15 wt. %). Garrido et al. (2006) discussed origin of the garnet-granulite in the Jijal complex, which is considered to be a lower crustal part of the Kohistan paleo arc, North Pakistan. REE modeling indicates that they are consistent with dehydration melting of hornblende gabbronorite. Experimental study, field observation, and petrological date suggest that dehydration melting of basaltic rock (amphibolite) plays a considerable role to form garnet-bearing mafic granulite and felsic melt in lower crust, which is a key process to create andesitic crust (Garrido et al., 2006). Thus, it is important to investigate partial melting process of basaltic rock (amphibolite and mafic granulite) to discuss crustal evolution.

1.5. Purpose of this study

1. To investigate textures, mineralogy and petrogenesis of the CMIs, and determine pressure-temperature conditions of partial melting of mafic and pelitic to felsic granulites from the LHC.
2. To investigate the influence of the partial melting to phase diagram, mineralogy,

and *P-T* conditions of mafic granulites.

Chapter 2. Geological setting

2.1. Geology of the Lützow-Holm Complex (LHC)

The LHC is one of Cambrian high-grade terrains bounded by the Proterozoic Rayner Complex to the east and the Yamato-Belgia Complex to the west in East Antarctica (e.g., Hiroi et al., 1991; Shiraishi et al., 2003). Shiraishi et al. (1987) inferred that the Yamato-Belgia complex and LHC formed paired-metamorphic belts and the two complexes were situated in subduction zone based on *P-T* evolutions and geochronlogic data. The dominant lithology in the LHC comprises well-layered pelitic to psammitic and intermediate gneisses with minor amounts of mafic to ultramafic and calcareous rocks. Mafic to ultramafic rocks occur as a thin layer or lenticular block in orthogneiss or pelitic rock (Hiroi et al., 1991). Younger granitoid intrusions also occur widely.

Structural studies have been performed by several workers. Yoshida (1978) identified four stages of deformation events (D1, D2, D3, and D4) in the LHC. D1 and D2 events occurred during granulite-facies metamorphism, while D3 and D4 events are contemporaneous with amphibolite-facies metamorphism. Kawakami and Ikeda (2004a, 2004b) discussed three stage deformation events within the LHC, and concluded that these events are contemporaneous with high-grade metamorphism. Ikeda and Kawakami (2004) argued that major deformation events occur under low-pressure and high-temperature conditions (granulite to ultrahigh temperature) and never involve prograde-high-pressure conditions based on the field analysis at Skallevikshalsen. Nogi et al. (2013) performed geophysical study along the LHC. They conclude that the Lützow-Holm Complex can be sub divided into four blocks based on the inferred

strike-slip faults. These strike-slip faults may have been generated during a younger stage of Pan-African orogeny, after the formation of NW-SE-striking geological structures. Cape Hinode situated at low-grade part of the LHC is regarded as an exotic block which may have originated from the Rayner Complex and been displaced by right lateral strike-slip motions.

Several authors discussed tectonic scenario of the LHC based on geochronlogic and geochemical data. Available geochronological data including U-Pb zircon and EPMA monazite ages indicate that the rocks along the LHC underwent an episode of high-grade metamorphism at *ca*. 520-550 Ma (Shiraishi et al., 1994, 2003, 2008). Hiroi et al. (1991) discussed the tectonic significance of mafic to ultramafic rocks from southeast part of the LHC, and concluded that these rocks were originated from ophiolitic complex. Recently, Suda et al. (2008) reported petrological and geochemical investigations of mafic to ultramafic rocks in several localities in the LHC, and suggested that they were involved by multiple subduction and high-grade metamorphism as a result of the final collision of East and West Gondwana during the Pan-African orogeny. Satish et al. (2008) performed oxygen and strontium isotopic study of the high-grade marbles from Skallen region and, suggested that these rocks deposited around 730-830 Ma and the deposition age are consistent with carbonate deposition in the Mozambique Ocean that separated East and West Gondwana. Tsunogae et al. (2014) reported SHRIMP U-Pb ages of zircon in charnockitic orthogneiss from Vesklesnausen, and protolith ages of 2507.9 ±7.4 Ma corresponding to magmatic emplacement, while they regarded the timing of high-grade metamorphism as 581-549 Ma.

Recent petrological investigations of high-grade metamorphic rocks around

Lützow-Holm Bay identified high- to ultrahigh-temperature metamorphism along a clockwise metamorphic evolutions and westward increase of metamorphic grade (e.g., Hiroi et al., 1991; Yoshimura et al., 2008). Metamorphic grade varies from upper amphibolite along a Prince Olav Coast to granulite around the Lützow-Holm Bay with a presence of the thermal axis, i.e. the region of the highest metamorphic grade. It is inferred that the metamorphic grade decrease westward from the thermal axis, although few available petrological data including *P-T* paths have been published so far. Yoshimura et al. (2008) first reported sapphirine + quartz assemblage which is regarded as a diagnostic indicator of UHT metamorphism, within porphyroblastic garnet in pelitic granulite from Rundvågshetta located on the thermal axis. They also reported orthopyroxene + sillimanite + quartz assemblage which indicated relatively high-pressure and UHT metamorphism. They concluded a clockwise *P-T* path characterized by isothermal decompression and subsequent UHT condition (T > 1000 °C). Metastable kyanite within garnet and plagioclase are also reported by several authors from several localities in the LHC (e.g., Hiroi et al., 1983; Kawakami and Motoyoshi 2004), which is typical of medium-pressure-type metamorphism. Hiroi et al. (1991) reported clockwise *P-T* paths of mafic to ultramafic rocks from the southeast part of the LHC and suggested that metamorphism of the LHC is not identical to the medium-pressure type (Barrovian type) and the LHC might have been involved prograde high-pressure metamorphism. Hiroi et al. (2008) reported kyanite bearing meta-tonalites and associated pelitic and calc-silicate from Cape Hinode located in the northeastern part of LHC. They argued the meta-tonalite originated from resite of basaltic magma melting under conditions at 15-20 kbar. They regarded these rocks as allochthonous blocks in the LHC at the waning stage of its regional metamorphism,

related to the final amalgamation of East and West Gondwana supercontinents. Kawasaki et al. (2011) reported osumilite and spinel + quartz bearing pelitic granulite from Rundvågshetta, which supported that the locality attains UHT conditions. They obtained high-pressure and UHT condition (P > 15 kbar , T > 1000°C) along a clockwise *P-T* path. Tsunogae et al. (2014) argued that UHT condition from Rundvågshetta is a local event based on phase equilibrium modeling of charnockite from Rundvågshetta. They suggested that peak condition of charnockite does not exceed 900 °C. They implied peak condition reported by Yoshimura et al. (2008) might have resulted from local heating. Kawasaki et al. (2013) reported armalcolite-psuedomorph-bearing pelitic granulite from Skallevikshalsen. They applied Fe^{3+}-in-sillimanite geothermometer and titanium-in-garnet geothermobarometer to the granulite, and estimated peak *P-T* conditions of > 1050 °C at 7-11kbar. Iwamura et al. (2013) reported Mg-Al-rich mafic granulite from Akarui Point situated at low-grade part of the LHC. They concluded that peak condition of the granulite is 900-920 °C and 7-8 kbar, which are extremely higher than the results of previous studies, along a clockwise *P-T* path. They suggested Akarui Point might be an exotic block juxtaposed within the amphibolite-granulite transition zone.

2.2. Geology of the study areas

Samples of granulites and associated rocks discussed in this study were collected from Skallevikshalsen/Skallen (Figs. 3 and 4), Austhovde (Fig. 5), and Ongul (Fig. 6). The examined samples were collected by 39th and 52th Japanese Antarctica Research Expedition (JARE 39 and 52). The four exposures are situated on the granulite-facies

zone of the LHC (Figs. 1 and 2). Below this study summarizes general geology of the areas.

2.2.1. Skallevikshalsen/Skallen

This area exposes 7 km in length and 1.7km in width. Brief geology of the area is summarized in Yoshida et al. (1976) and Osanai et al. (2004). The dominant lithologies of this area are paragneisses, metabasites, marbles, skarn, allied rocks, quartzite, garnet gneissose granite, charnockite, and minor intrusives (Yoshida et al., 1976; Osanai et al., 2004) (Figs. 3 and 4). The foliation trends show NE and NW dipping towards southeast or northwest. Yoshida et al. (1976) reported overturned recumbent anticline in this area. Kawakami and Ikeda (2004a) reported the evidence of ductile deformation (mineral lineation and micro scale folds) observed within retrograde stage characterized by the alignment of sillimanite in leucocratic garnet-sillimanite gneiss. They also pointed out that no deformation occurred during prograde stage. Available data of metamorphic *P-T* evolution of the region were proposed by several authors. Banno et al. (1964) identified orthopyroxene in mafic to intermediate rock, and suggested the region experienced granulite-facies metamorphism. Metastable kyanite preserved within porphyroblastic minerals (e.g., garnet and plagioclase), suggests that the progress of regional metamorphism from kyanite stability field to sillimanite stability field (Hiroi et al., 1991; Osanai et al., 2004). Kawakami et al. (2004) reported Spl + Qtz assemblage within garnet-sillimanite gneiss, which is a possible indicator of UHT metamorphism if Zn content of spinel is low. They also reported the metastable kyanite and staurolite within garnet suggesting that this region experienced a clockwise *P-T* path. Yoshimura

et al. (2004) estimated *P-T* conditions of garnet-biotite gneiss and mafic gneiss from Skallevikshalsen area, and obtained *P-T* conditions of 770-940 °C and 6.5-12 kbar for garnet biotite gneiss and 780-960 °C and 6-11 kbar for mafic gneiss. In Skallen region, metamorphic *P-T* conditions have been discussed in Yoshida and Akiwa (1983) (823 °C 4.1-6.5 kbar), Suzuki (1983) (825± 25 °C and 6.3±1.3 kbar). Santosh and Yoshida (1992) performed petrologic and fluid inclusion study of charnockite from Skallen, and estimated *P-T* conditions as 600-750 °C and 6-8 kbar. They also reported high-density-CO_2-rich fluid inclusions (up to 1.05 g*cm^-3) within garnet. They argued that CO_2 originated from sub-continental mantle based on carbon-isotope study. Geochronological data from Skallen region suggest that presence of narrow ranges of metamorphic event. Nicolaysen et al. (1961) reported Rb-Sr biotite age of 530-500 Ma. U-Th-Pb chemical ages (CHIME) of monazite in garnet-biotite-quarzto-feldspathic gneiss yielded 539 ±14 Ma and 543 ±14 Ma (Hokada unpublished data). These data are roughly consistent with the Pan-African metamorphic event (550-520 Ma) in the Lützow-Holm Complex (Osanai et al., 2004). Satish-Kumar et al. (2008) reported petrological and geochemical data of marble collected from Skallen. Depositional age of protolith was estimated as 730-830 Ma based on carbon isotopic data, which may corresponds to the timing of closure of Mozambique Ocean that separated East and West Gondwana. This study focused on mafic granulites (samples TS10122506, TS10122601K, TS10122604B, TS11010802, TS11010704B, and TS11010803A) which occur as lenticular blocks within brownish gneissose granodiorites, marble and calc-silicate rocks (Figs.3 and 7). These granulites mainly consist of coarse-grained garnet and clinopyroxene or hornblende (Figs. 7-a, 7-b, and 7-c). They show sharp contact with surrounding gneisses and no migmatite texture can be seen in outcrop and

hand-specimen scale. This study also describes petrological characters of felsic granulites (samples TS10122502D and TS97122003-2), garnet-biotite gneiss (B97122708B) and pelitic granulite (sample TS10122502B2). Localities of garnet-sillimanite gneiss reported by Kawakami et al. (2004), and those of mafic gneiss and garnet-biotite gneiss reported by Yoshimura et al. (2004) are also plotted in Fig. 3.

2.2.2. Austhovde

Austhovde is located about 15 km northeast of the thermal axis. This region consists of three outcrops, Austhovde-kita Rocks, Austhovde-naka Rocks, and Austhovde Minami Rocks (Shiraishi and Yoshida, 1987). This area shows E-W trending foliations and southward dipping in the north (Austhovde-kita Rocks), and N-S trending foliation and westwards dipping in the south (Austhovde-minami Rocks) where the mineral lineation plunges gently toward south. Thus, Shiraishi and Yoshida (1987) inferred that the presence of megascopic folding in this area. Samples discussed in this study were collected from the Austhovde-minami Rocks which is composed of alteration of pyroxene-hornblende gneiss, siliceous garnet-gneiss, quartzite garnet-biotite gneiss, biotite gneiss, and skarn (Fig. 5). Lesser amounts of mafic to ultramafic rocks occur as thin concordant layer among the gneiss and lenticular blocks (Fig. 5), and it shows sharp contact with surrounding garnet-biotite gneiss (Fig. 8-a). Metamorphic *P-T* conditions of this region have not been investigated in detail although occurrences of orthopyroxene in several lithologies suggest that this region experienced granulite-facies metamorphism (Shiraishi and Yoshida, 1987). Shiraishi et al. (2008) reported SHRIMP age of zircon separated from garnet-biotite gneiss in Austhovde.

They obtained 533 ± 9 Ma of metamorphic age which is consistent with the geochronological investigations from other exposures of the LHC (e.g., Shiraishi et al., 2008; Tsunogae et al., 2014).

Mafic granulite is mainly composed of garnet, clinopyroxene, hornblende, plagioclase, and quartz. It is unclear that the sample experienced partial melting in outcrop or hand-specimen scale because the sample shows no migmatitic texture. This study also discusses petrology of felsic granulite (sample TS11011407D, Fig. 8-b) that occurs as thin layers in garnet gneiss, kyanite-bearing meta-quartzite (sample TS11011702G, Fig. 8-c) and kyanite-bearing garnet-biotite gneiss. (sample TS1101154C, Fig. 8-d).

2.2.3. Ongul

Ongul is located about 75 km NNE of the thermal axis in the LHC (Fig. 2). The exposure is composed of more than ten small islands. The largest island is West Ongul Island with approximate diameter of 3.5 km (Yanai et al., 1974a, 1974b). Samples discussed in this study were collected from West Ongul Island and East Ongul Island. East Ongul Island is structurally characterized by an isoclinal fold plunging to the south. The mantle of the fold consists of charnockitic pyroxene gneiss. Ishikawa et al. (1994) described structural data of the region in detail. Regional foliations are generally N-S to NNW-SSE with dipping 60-25 °E in the Ongul Island. Four stages of folding events were identified in the area, suggesting all kinds of lithologies of the Islands behaved as ductile materials at the earlier stage. They also reported large-scale faults in West Ongul Island. The faults show dextral-ENW-WSW trending. Kawakami and Ikeda (2004b)

concluded that major folding events took place under amphibolite-facies condition based on structural analysis, and they suggest these deformations are chronologically close to the peak stage of the region. The folding events can be correlated with other exposures in the LHC (Kawakami and Ikeda, 2004a, 2004b; Ikeda and Kawakami, 2004). The dominant lithologies of the Ongul Island are garnet-gneiss, hornblende gneiss, pyroxene gneiss, garnet-biotite gneiss, and garnet-bearing granitic gneiss with minor amount of metabasites, calc-silicate rock, and marble (Yanai et al., 1974a; Ishikawa et al., 1994) (Fig. 6). The pyroxene gneiss alternates with hornblende gneiss in the western part of the island. Lenses or thin beds of metabasites occur in certain horizons. Widespread occurrences of orthopyroxene within metabasite and intermediate granulite suggest that this region experienced granulite-facies metamorphism (Yanai et al., 1974; Ishikawa et al., 1994). Geochronological studies were performed by several authors. Shibata et al. (1985) reported Rb-Sr-mineral ishochoron age and K-Ar ages of biotite and hornblende of 502-469 Ma, which were regarded as cooling age (Ishikawa et al., 1994). SHRIMP zircon ages of garnet-biotite gneiss suggest that the timing of high-grade metamorphism is 532±8 Ma (Shiraishi et al., 2003, 2008).

Mafic granulites discussed in this study were collected from hinge of isoclinal fold of metabasite (samples TS11020610G and TS11020610I, Figs. 6 and 9-a). They are characterized by medium- to coarse-grained garnet and hornblende. Pelitic granulite (sample TS11020604B) corresponds to leucocratic layer of migmatitic garnet-biotite gneiss. The rock texture suggests the progress of partial melting in the sample (Fig. 9-b). This study also discusses petrology of intermediate granulite (sample TS11020606A) collected from the northern part of West Ongul Island (Fig. 9-c).

Chapter 3. Petrography

This charter discusses with general petrography of the examined samples. Mineral assemblages and modal occurrence of minerals in each sample are described in Tables 2 and 3.

3.1. Garnet-bearing mafic granulite

3.1.1. Garnet-clinopyroxene granulite

This rock is massive and shows no obvious evidence of migmatization in hand-spacemen scale. The mineralogy of a representative sample TS11010802 is garnet (50-60%), clinopyroxene (20-30%), plagioclase (3-5%), orthopyroxene (3-5%), calcic amphibole (3-5%), and ilmenite (3-5%) with accessory ilmenite, zircon, and quartz (Fig. 10-a). Garnet is medium- to coarse-grained (0.8-6 mm) and porphyroblastic. It often contains fine-grained (<0.5 mm) inclusions of quartz, calcic amphibole, biotite, and ilmenite. Matrix subidioblastic clinopyroxene is medium- to coarse grained (0.4-3 mm). These textures suggest that the equilibrium assemblage of this sample during the peak stage is probably garnet + clinopyroxene. The grain boundaries between garnet and clinopyroxene or calcic amphibole are filled by fine- to medium-grained (0.1-0.4 mm) symplectic intergrowth of orthopyroxene and plagioclase (Fig 10-a). The textures indicate the progress of the following reactions.

$$\text{Grt} + \text{Ca-Amp} + \text{Qtz} \rightarrow \text{Opx} + \text{Pl} + H_2O \quad (1)$$

$$\text{Grt} + \text{Cpx} + \text{Qtz} \rightarrow \text{Opx} + \text{Pl} \quad (2)$$

The occurrence of quartz in the garnet, while it is absent in matrix of the sample, suggests that quartz was completely consumed by the progress of reactions (1) and (2), suggesting that garnet + clinopyroxene + quartz was the probable peak assemblage. Reaction (1) suggests dehydration of calcic-amphibole during prograde to peak stage. The progress of reaction (2) implies isothermal decompression during peak to retrograde stage. Therefore, the peak assemblage of this rock will be garnet + clinopyroxene + quartz + ilmenite. As discussed in a later section, this study adopted the assemblage for *P-T* calculations. The garnet often contains inclusion of hornblende, biotite, ilmenite, quartz, and CMI. The CMI consists of fine-grained quartz, orthopyroxene, biotite, K-feldspar, plagioclase, and ilmenite which size varies from 1 to 50 μm (Fig. 15-c). The size of CMI grains is up to 100 μm, and they show negative crystal shapes of the host garnet (Fig. 15-c). Such fine-grained nature of each crystal and the shape of the CMI might require quench processes of liquid during cooling stage of the inclusions (e.g., Hiroi et al., 2014).

Sample TS10122506 is amphibole- and quartz-rich variety of the lithology. The sample is characterized by medium- to coarse-grained garnet (0.8-3.0 mm) and clinopyroxene (0.4-1.6 mm). The mineralogy of the sample is garnet (30-35%), clinopyroxene (20-25%), quartz (5-10%), calcic amphibole (10-15%), orthopyroxene (5-10%), and plagioclase (5-10%) with accessory ilmenite, zircon, and apatite (Figs. 10-b and 10-c). The medium- to coarse-grained garnet is subidioblastic. The mineral contains inclusions of fine- to medium-grained quartz (0.1-0.3 mm), clinopyroxene (0.2-0.3 mm), plagioclase, ilmenite (0.05-0.2 mm), and CMI (~0.1 mm). The CMI consist of fine-grained quartz, biotite, K-feldspar, plagioclase, and ilmenite which size varies from 1 to 50 μm. The size of CMI grains is up to 100 μm, and they show negative

crystal shapes of the host garnet (Fig. 15-a). As the garnet is in contact with clinopyroxene and quartz, this study regards that the equilibrium assemblage of this sample during the peak stage is probably garnet + clinopyroxene + quartz. Clinopyroxene is a dominant mineral in the matrix. It is fine- to coarse-grained (0.4-1.6 mm) and subidioblastic in shape. The grain boundaries between garnet and clinopyroxene or calcic amphibole are filled by fine- to medium-grained (0.1-0.4 mm) symplectic intergrowth of orthopyroxene and plagioclase (Fig. 10-b). The textures indicate the progress of reactions (1) and (2).

Sample TS11010704B is characterized by medium- to coarse-grained garnet (0.8-3 mm) and clinopyroxene (0.4-1.6 mm). Its mineralogy is garnet (45-50%), clinopyroxene (35-45%), and ilmenite (3-5%) with accessory quartz, calcic amphibole, orthopyroxene, and plagioclase (Fig. 10-d). The medium- to coarse-grained garnet is subidioblastic, and contains inclusions of fine- to medium-grained quartz (0.1-0.3 mm) and clinopyroxene (0.2-0.3 mm). As the garnet is in contact with clinopyroxene and quartz, this study regards that the equilibrium assemblage of this sample during the peak stage is probably garnet + clinopyroxene + quartz. Clinopyroxene is a dominant mineral in the matrix. It is fine- to coarse-grained (0.4-1.6 mm) and subidioblastic in shape. No obvious reaction texture is present in the sample except for the occurrence of retrograde greenish amphibole partly replacing clinopyroxene. Rare orthopyroxene occurs in matrix. The garnet often contains inclusion of hornblende, biotite, ilmenite, quartz, and CMIs. The CMIs consist of fine-grained quartz, biotite, K-feldspar, plagioclase, muscovite, and ilmenite which size varies from 1 to 50 μm (Fig. 15-b). The mineralogy of the CMIs suggests that S-type granitic melt was generated during high-grade metamorphism. The size of CMI grains is up to 200 μm, and they show negative crystal shapes of the host

garnet. The presence of CMIs within garnet and mineral mode of the sample implies that this sample is restitic in composition.

Sample TS11010803A is characterized by medium- to coarse-grained garnet (0.8-3.0 mm) and clinopyroxene (0.4-1.6 mm). Its mineralogy is garnet (45-50%) and clinopyroxene (35-45%) with accessory quartz, calcic amphibole, orthopyroxene, and ilmenite (Fig.10-e). The medium- to coarse-grained garnet is subidioblastic. The mineral often contains inclusions of fine- to medium-grained quartz (0.1-0.3 mm) and clinopyroxene (0.2-0.3 mm). As the garnet is in contact with clinopyroxene and quartz, this study regards that the equilibrium assemblage of this sample during the peak stage is probably garnet + clinopyroxene + quartz. Clinopyroxene is a dominant mineral in the matrix. It is fine- to coarse-grained (0.4-1.6 mm) and subidioblastic in shape. No obvious reaction texture is present in the sample except for the occurrence of retrograde greenish amphibole partly replacing clinopyroxene. Rare orthopyroxene occurs in matrix.

3.1.2. Garnet-bearing-two-pyroxene granulite

This rock corresponds to pyroxene- and garnet-rich part of a lenticular blocks of mafic granulite (Fig. 9-a). It consists of medium-grained garnet (~0.5 mm) and medium- to coarse-grained pyroxenes (~0.4 mm). The mineralogy of a representative sample (TS11011405A-2) is garnet (20-30%), clinopyroxene (15-20%), orthopyroxene (10-15%), quartz (10-20%), and plagioclase (10-15%) with accessory calcic amphibole, apatite, and ilmenite (Fig. 10-f). The medium- to coarse-grained garnet (0.3-3.0 mm) is subidioblastic and contains fine-grained quartz (0.05-0.3 mm), plagioclase, CMI, and

ilmenite. The CMI consists of biotite, quartz, plagioclase, and K-feldspar (Fig 15-e). Each grain comprising the CMIs is 1 μm to 10 μm. Fine- to medium-grained orthopyroxene (0.2-1.0 mm), plagioclase (0.3-1.0 mm), and clinopyroxene (0.4-1.0 mm) also occur in matrix. Quartz in the matrix is medium- to coarse grained (0.4-3.0 mm). All the minerals are subidioblastic to xenoblastic. No obvious reaction texture is present in the sample. This study thus regards the peak assemblage of the rock as garnet + clinopyroxene + orthopyroxene + quartz. Calcic amphibole occurs as inclusions in the garnet, while orthopyroxene is not included in the garnet. This study thus regards prograde mineralogy as garnet + calcic amphibole + quartz + melt + plagioclase + clinopyroxene.

3.1.3. Garnet-bearing-orthopyroxene granulite

This rock is characterized by very coarse-grained and deformed garnet in thin section scale. A representative sample (TS10122604B) consists of garnet (35-45%), orthopyroxene (15-25%), plagioclase (5-15%), and quartz (5-15%) with accessory clinopyroxene, calcic amphibole, biotite, and ilmenite (Fig. 10-g). Garnet is very coarse-grained (up to 3 cm) and subidioblastic. It contains numerous inclusions of quartz (0.1-0.4 mm), plagioclase (0.1-0.4 mm), and ilmenite. Quartz is the most abundant inclusions within the garnet in this sample. The mineral in the matrix (0.3-3.0 mm) is coarser than plagioclase in the matrix (0.3-1.2 mm). No obvious reaction texture is observed in the sample except for the occurrence of retrograde greenish calcic amphibole partly replacing orthopyroxene.

The mineralogy of a representative sample B97122302F2 is garnet (5-7%),

orthopyroxene (15-20%), plagioclase (15-25%), biotite (15-20%), and hornblende (10-15%) with accessory quartz, rutile, and ilmenite (Fig. 10-h). The coarse-grained garnet is subidioblastic, and contains inclusions of fine- to medium-grained quartz (0.1-0.3 mm), plagioclase (0.2-0.5 mm), biotite (0.1-0.5 mm), ilmenite (0.2-0.3 mm) rutile (~0.1 mm), and CMI (0.1-0.3 mm). The CMI consists of fine-grained quartz, biotite, K-feldspar, plagioclase, and ilmenite which size varies from 1 to 20 μm (Fig. 15-d). The size of CMI grains is up to 100 μm, and they show negative crystal shapes of the host garnet. The garnet is surrounded by fine- to medium-grained (0.1-0.4 mm) symplectic intergrowth of orthopyroxene and plagioclase (Fig. 10-h). The textures indicate the progress of the following reactions.

$$\mathrm{Grt + Qtz \rightarrow Opx + Pl} \qquad (3)$$

This reaction indicated progress of post-peak decompression event. It is notable that CMI and rutile are observed in the same garnet grain, suggesting that partial melting took place in the stability conditions of rutile. This study thus regards the peak assemblage as garnet + rutile + ilmenite + melt + plagioclase + quartz. Medium- to coarse-grained orthopyroxene (0.2-1.2 mm), plagioclase (0.1-1.1 mm), and hornblende (0.3-1.0 mm) are dominant minerals in the matrix, and they are subidioblastic to xenoblastic in shape (Fig. 10-i). This study adopted this assemblage for *P-T* calculations as discussed in later sections.

Another type of garnet-orthopyroxene granulite (e.g., sample TS11020206H) contains garnet (15-25%), orthopyroxene (5-15%), biotite (5-15%), plagioclase (10-15%), quartz (10-15%), and Fe-Ti oxides (5-15%) with accessory zircon, apatite, and spinel (Fig. 10-j). This sample is characterized by fine- to medium-grained (0.6-2 mm) garnet and orthopyroxene (0.2-0.8 mm). Quartz is present as elongated grains up

to 3 mm along the rock foliation or as fine-grained (0.05 - 0.2 mm) inclusions in garnet. Fine- to medium-grained (0.2-1.3 mm) biotite is also aligned along the foliation. Plagioclase is medium- to coarse-grained (0.2-1.5 mm), and subidioblastic to xenoblastic, and present only in the matrix (Fig. 10-e). No obvious reaction texture is present in the sample. Rare greenish spinel occurs with Fe-Ti oxides. This study thus regards garnet + orthopyroxene + quartz + plagioclase as the peak assemblage of this sample. We adopted this assemblage for *P-T* calculations as discussed in later sections.

3.1.4. Garnet amphibolite

This rock corresponds to a hornblende- and garnet-rich part of the lenticular blocks of mafic granulite. It consists of fine- to coarse-grained garnet (0.3-3.0 mm) and fine- to medium-grained calcic amphibole (0.05-1.0 mm). The mineralogy of a representative sample (TS11011601M) is garnet (10-15%), calcic-amphibole (15-20%) clinopyroxene (10-15%), orthopyroxene (10-15%), and plagioclase (10-15%) with accessory quartz, apatite, and ilmenite. The medium- to coarse-grained garnet (0.3-3.0 mm) is subidioblastic and contains fine-grained quartz (0.05-0.3 mm), plagioclase and ilmenite. Fine- to coarse-grained calcic amphibole (0.2-2.0 mm) is predominant in the matrix. Fine- to medium-grained orthopyroxene (0.2-1.0 mm), plagioclase (0.3-1.0 mm), and clinopyroxene (0.4-1.0 mm) also occur in the matrix. All the minerals are subidioblastic to xenoblastic. Along the grain boundaries of the garnet and calcic amphibole, symplectic orthopyroxene and plagioclase occur as fine-grained minerals (0.02-0.3 mm), suggesting the progress of reaction (1) (Fig. 10-k). As the quartz is present only in the garnet, this study regards the prograde assemblage as garnet + clinopyroxene + quartz +

calcic amphibole.

Sample TS11020610G-2 corresponds to a garnet- and calcic amphibole-rich part of lenticular blocks of mafic granulite. It mainly consists of fine- to coarse-grained garnet (~0.4 cm) and fine- to medium-grained calcic amphibole (~1 mm). The mineralogy of the sample is garnet (50-60%), plagioclase (5-10%), hornblende (25-30%), and orthopyroxene (5-10%) with accessory biotite (Fig. 10-l). Fine- to coarse-grained garnet (0.1-50 mm) is subidioblastic and contains fine-grained plagioclase (0.2-0.5 mm), ilmenite (<0.1 mm), and CMI. CMI consists of biotite, quartz, plagioclase, and K-feldspar. Hydrous minerals such as biotite and calcic amphibole are present in garnet, which suggests that dehydration melting might have taken place in this sample during prograde to peak stage. Fine- to medium-grained orthopyroxene (0.5-0.3mm), plagioclase (0.1-0.3 mm) occur as symplectite suggesting the progress of the reaction (1). Greenish calcic amphiboles are observed both in the matrix and in the garnet, which suggest the mineral was stable under prograde to peak conditions. This study thus regards prograde to peak assemblage as garnet + plagioclase + liquid + ilmenite + calcic amphibole. Retrograde mineralogy of the sample is probably plagioclase + ilmenite + calcic amphibole + orthopyroxene.

Sample TS11020610I corresponds to a plagioclase-rich part of lenticular blocks of mafic granulite (Fig. 9-a). It consists of fine- to coarse-grained garnet (0.2-5.0 mm) and fine- to medium-grained pyroxenes (~1 mm). Its mineralogy of a representative sample is garnet (10-15%), plagioclase (30-40%), hornblende (15-20%), orthopyroxene (10-15%), and clinopyroxene (3-5%) with accessory quartz, biotite, rutile, and ilmenite (Figs. 10-m and 10-n). The medium- to coarse-grained garnet (0.2-5.0 mm) is subidioblastic, and contains fine-grained quartz (0.05-0.1 mm), plagioclase (0.2-0.5

mm), CMI (0.05-0.1 mm), ilmenite (<0.1 mm), and rutile (<0.1 mm). The CMI consists of biotite, quartz, plagioclase, K-feldspar (Fig. 15-f), rutile, and ilmenite. Some CMIs show clearly negative crystal shape implying interaction between the melt and the host garnet is minimum or ignorable. Hydrous minerals such as biotite and calcic amphibole present in garnet (Fig. 10-m) suggest that dehydration melting might have taken place in this sample. Fine- to medium-grained orthopyroxene (0.3-0.5 mm) and plagioclase (0.1-0.3 mm) occur as symplectite suggesting the progress of reaction (1). Orthopyroxene and plagioclase are also present in fine- to coarse-grained matrix (0.3-2.5 mm). Brownish calcic amphibole is observed both in matrix and within garnet, which suggests that the mineral is stable under prograde to peak conditions. Quartz is present only in garnet and CMI (Figs. 10-m and 15-f). This study thus regards mineralogy of prograde to peak stage as garnet + quartz + plagioclase + liquid + rutile + ilmenite + calcic amphibole.

3.2. Pelitic and felsic granulite

3.2.1. Pelitic granulite

This rock type (e.g., sample TS10122502B2) is composed of garnet, (15-20%), K-feldspar (20-25%), quartz (10-15%), biotite (5-10%), plagioclase (<1%), and muscovite (10-15%) with accessory rutile and ilmenite. Fine- to coarse -grained garnet (0.1-5 mm) is subidioblastic, and contains abundant inclusions of quartz (0.05-0.75 mm), biotite (0.1-0.4 mm), rutile (0.02-0.1 mm), and CMI (0.1-0.3 mm). The CMI consists of quartz, biotite, plagioclase, K-feldspar, and rutile (Fig. 16-a), suggesting that partial

melting occur under the stability field of rutile or rutile crystallized directly from melt. Fine- to coarse-grained matrix is occupied by quartz (0.05-3.5 mm), K-feldspar (0.1-2.5 mm), biotite (0.1-2.0 mm), and cordierite (0.25-2.0 mm). No obvious reaction texture is present in the sample except for the cordierite which is now replaced by aggregate of fine grained white mica (<0.02 mm). This study thus regards prograde to peak stage as garnet + rutile + quartz + plagioclase + melt ± biotite.

Sample B97122003-2 is composed of garnet (15-25%), quartz (10-15 %), sillimanite (5-10%), plagioclase (25-35%), and K-feldspar (5-10%) with accessory rutile and ilmenite. Fine- to coarse- grained garnet (1.4-4.0 mm) is subidioblastic, and contains abundant inclusions of quartz (0.1-2.5mm), rutile (0.02-0.1 mm), K-feldspar (0.15-0.3 mm), and CMI. CMI occurs as aggregate of fine-grained quartz, biotite, and rutile. Their irregular shapes of the CMI (Fig. 16-c) indicate that they probably reacted with the host garnet. Fine- to coarse-grained matrix is occupied by quartz (0.05-3.5mm) and K-feldspar (0.1-2.5 mm). Sillimanite only occurs along the rim of the garnet. CMI, which are coexisting with rutile, ilmenite, and quartz, is observed in the core of the garnet. We thus regard peak mineral assemblage as garnet + melt + quartz + rutile + ilmenite + plagioclase ± sillimanite.

Sample TS11011401B is a massive rock without any obvious foliation in hand specimen scale. It is characterized by well-defined occurrence of melanosome and leucosome parts. It is composed dominantly of garnet (10-15%), quartz (25-35%) plagioclase (3-5%), biotite (10-15%), K-feldspar (10-15%), and sillimanite (10-15%) with accessory ilmenite, rutile, and CMIs. Medium- to coarse-grained garnet (0.3-2.5 mm) is concentrated in melanosome which is mainly composed of garnet, biotite (0.3-2.5 mm), sillimanite (0.3-5.0 mm), and quartz (0.3-2.5 mm). Leucosome mainly

consists of K-feldspar and quartz. Matrix of the leucosome is composed of coarse-grained (0.5-5.0 mm) quartz, medium-grained plagioclase (0.1-1.0 mm), and fine- to coarse-grained biotite (0.1-4.0 mm).

Sample TS11011702B is a massive rock without any obvious foliation in hand specimen. It is composed dominantly of garnet (15-25%), biotite (10-15%), spinel (10-15%), K-feldspar (10-15%), plagioclase (3-5%), and quartz (3-5 %), with accessory ilmenite. Medium- to coarse-grained garnet (0.5-4.0 mm) is subidioblastic. Garnet often contains fine- to medium-grained K-feldspar (0.3-0.7 mm), biotite (~0.2 mm), and spinel (0.05-0.1 mm). Matrix is composed of fine- to coarse-grained spinel (0.1-2.5 mm), sillimanite (0.3-1.7 mm), and K-feldspar (0.1-2.5 mm). The minerals in the matrix are all xenoblastic to subidioblastic.

Sample TS11020604B is a well-foliated rock in hand specimen scale. The foliation is defined by alignment of sillimanite. This sample is composed dominantly of garnet (10-15%), biotite (7-10%), plagioclase (10-15%), K-feldspar (10-15%), sillimanite (7-10%), and rutile (2-3%) with accessory spinel, kyanite, and zircon. Medium- to coarse-grained garnet (0.2-2.5 mm) often contains quartz (0.05-0.1 mm), plagioclase (0.02-0.1 mm), K-feldspar (0.05-0.1 mm), rutile (0.02-0.2), kyanite (0.3-0.5 mm), and spinel (<0.1 mm). Matrix consists of plagioclase (0.05-5.0 mm), quartz (0.1-5.0 mm), K-feldspar (0.1-3.5mm), rutile (0.05-0.5 mm), sillimanite (0.07-2.5 mm), and biotite (0.1-1 mm) (Fig. 10-r). All the grains in the sample are subidioblastic to xenoblastic. Kyanite is only present in garnet (Fig. 10-s), suggesting that prograde *P*-*T* path passed through the kyanite stability field. This study thus regards a prograde assemblages as garnet + plagioclase + K-feldspar + kyanite +rutile, which is a typical mineralogy of high-pressure pelitic granulite (e.g., O'Brien and Rötzler, 2003). As discussed in later

sections, this sample is adopted for *P-T* calculations.

3.2.2. Felsic granulite

Sample TS10122502D is a massive rock without any obvious foliation in hand specimen scale. This sample consists of orthopyroxene-rich mafic part and orthopyroxene-free felsic part (Figs. 10-o and 10-q). This sample is composed dominantly of garnet (15-25%), quartz (15-20%), plagioclase (15-20%), K-feldspar (15-20%), orthopyroxene (5-10%), and rutile (2-3%), with accessory ilmenite, zircon, and monazite. Medium- to coarse-grained garnet (0.5-4.0 mm) is observed in the matrix of coarse-grained (~3 mm) quartz, medium-grained plagioclase (0.2-1.0 mm) (Fig. 10-o), and fine- to medium-grained orthopyroxene (0.1-0.5 mm). The garnet contains inclusions of fine- to medium-grained quartz (0.1-0.3mm), plagioclase (0.2-0.5 mm), biotite (0.1-0.5 mm), ilmenite (0.2-0.3mm), rutile (~0.1 mm), kyanite (0.3 mm, only one grain), and CMI. CMI consists of biotite, quartz, K-feldspar, ilmenite, and rutile. Each grain within CMI ranges from 3 μm to 10 μm (Fig. 16-b). No obvious reaction texture is present in the sample except for the occurrence of retrograde biotite partly replacing orthopyroxene. This study therefore regards the prograde assemblage of this rock as garnet + rutile + ilmenite + kyanite + plagioclase + quartz + melt and peak assemblage of this rock as garnet + orthopyroxene + quartz + plagioclase + ilmenite. The minerals are all subidioblastic to xenoblastic in shape. As discussed in later sections, this sample is adopted for *P-T* calculations.

Garnet charnockite (sample TS11011407D) is a massive rock without any obvious foliation in hand specimen. It is composed dominantly of quartz (35-45%), biotite

(10-20%), plagioclase (10-15%), orthopyroxene (10-15%), and garnet (5-10%), with accessory zircon and magnetite. Fine- to coarse-grained garnet (0.2-1.3 mm) and orthopyroxene (0.2-1.4 mm) are observed in the matrix of coarse-grained (~3 mm) quartz and medium-grained plagioclase (0.2-1.0 mm) (Fig. 10-t). No obvious reaction texture is present in the sample except for the occurrence of retrograde biotite partly replacing orthopyroxene. This study therefore regards the peak assemblage of this rock as garnet + orthopyroxene + quartz + plagioclase. The minerals in the sample are all subidioblastic to xenoblastic in shape (Fig. 10-t). As discussed in later sections, this sample is adopted for *P*-*T* calculations.

Sample TS11011702G is composed of quartz (85-90%), garnet (2-5%), and sillimanite (1-2%) with accessory plagioclase, kyanite, and K-feldspar. Fine- to coarse -grained quartz (0.5.-5.0 mm) is subidioblastic. Sillimanite is observed as subidioblastic and fine- to coarse-grained (0.4-1.0 mm) crystal within quartz. Kyanite, plagioclase, and K-feldspar are in contact with garnet (Fig. 10-u), suggesting that kyanite + garnet +quartz + plagioclase + K-feldspar is a peak assemblage of this sample.

3.2.3. Garnet-biotite gneiss

Sample B97122708B shows rock foliation defined by aligned of biotite. It is composed of garnet (20-25%), biotite (15-20%), K-feldspar (15-20%), plagioclase (15-20%), quartz (10-15 %), ilmenite (<2 %), and rutile (<2 %) with accessory apatite and monazite (Fig. 10-v). Medium- to coarse-grained garnet (0.3-3.5mm) is porphyroblastic and subidioblastic. It contains quartz (0.05-0.2 mm), plagioclase (0.2-0.7 mm), K-feldspar (0.07-0.4 mm), rutile (0.05-0.1 mm), and minor ilmenite.

Inclusions within the garnet tend to occur in the core of the garnet, suggesting these inclusions were trapped during prograde stage. Matrix is composed of quartz (0.1-1.3 mm), biotite (0.07-1.3 mm), plagioclase (0.3-1.3 mm), and K-feldspar (0.3- 1.5 mm) with minor amount of ilmenite. All the minerals occurring in the matrix are subidioblastic to xenoblastic.

Sample TS11011504C is characterized by abundant garnet. It is composed dominantly of garnet (40-45%), biotite (25-30%), plagioclase (5-10%), and K-feldspar (1-2 %) with accessory ilmenite, rutile, spinel, and kyanite. Medium- to coarse-grained garnet (1-7 mm) is observed in the matrix of coarse-grained (0.5-5.0 mm) quartz, medium-grained plagioclase (0.1-1.0 mm), and fine- to coarse-grained biotite (0.1-4.0 mm). The garnet contains inclusions of fine- to medium-grained quartz (0.1-0.3mm), plagioclase (0.2-0.5 mm), biotite (0.1-0.5 mm), ilmenite (0.2-0.3 mm), rutile (~0.1 mm), kyanite (0.1-0.5 mm), spinel (0.05-0.1 mm), and CMI (Figs. 10-w and 10-x). The CMI consist of quartz, biotite, plagioclase, K-feldspar, rutile, and ilmenite. Most of the CMI show irregular shape, which suggests that CMI reacted with host garnet (Fig. 16-e). Because the CMI, plagioclase, quartz, ilmenite, rutile, and K-feldspar are included in the same garnet grain, this study regards the prograde to peak assemblage as garnet + rutile + ilmenite + plagioclase + quartz + K-feldspar + melt. As discussed in later sections, this sample is adopted for *P-T* calculations.

3.3. Ultramafic granulite

Sample TS10122601C is a massive rock without any obvious foliation in hand specimen. It is composed dominantly of clinopyroxene (30-35%), orthopyroxene

(20-25%), hornblende (10-15%), and biotite (10-15%). Clinopyroxene (0.5-2.5 mm) is fine- to coarse-grained and subidioblastic. Orthopyroxene is subidioblastic and medium- to coarse-grained (0.5-4.0 mm). Fine- to coarse-grained hornblende (0.3-2.5 mm) and biotite (0.1-3.5 mm) occupy grain boundaries of clinopyroxene and orthopyroxene. No obvious reaction texture is present in the sample.

Sample TS11011504E is a massive rock without any obvious foliation in hand specimen. It is composed dominantly of clinopyroxene (70-80%), orthopyroxene (5-10%), and hornblende (5-10%) with accessory plagioclase and biotite. Clinopyroxene (0.2-2.4 mm) is fine- to coarse-grained and subidioblastic. Orthopyroxene and hornblende are fine- to medium-grained (0.3-1.0 mm) and subidioblastic.

3.4. Other lithologies

3.4.1. Calc-silicate granulite

Sample TS10122401K1 is a massive rock without any obvious foliation in hand specimen. It is composed dominantly of scapolite (50-60%), hornblende (10-15%), and biotite (10-15%) with accessory zircon and clinopyroxene. Fine- to coarse-grained and subidioblastic scapolite (0.5-3.0 mm) is observed in a matrix. Hornblende and biotite are fine- to medium-grained (0.1-3.0 mm) and subidioblastic. Clinopyroxene is subidioblastic and fine- to coarse-grained (0.3-2.5 mm). The minerals are all subidioblastic to xenoblastic in shape and they show no reaction texture, suggesting peak assemblage of this sample is scapolite + clinopyroxene + titanite + hornblende.

Sample TS11011602A shows foliation defined by orientation of clinopyroxene and titanite. It is composed dominantly of scapolite (70-80%), clinopyroxene (5-10%), and titanite (3-5%) with accessory zircon. Fine- to coarse-grained and subidioblastic scapolite (0.1-4.0 mm) is observed in the matrix. Clinopyroxene is subidioblastic and fine- to coarse-grained (0.3-2.5 mm). Fine- to coarse grained titanite (0.5-5.0 mm) is included in scapolite and clinopyroxene. The minerals in the sample are all subidioblastic to xenoblastic in shape, and show no reaction texture, which suggests peak assembly of this sample is scapolite + clinopyroxene + titanite.

3.4.2. Garnet-bearing intermediate granulite

Sample (TS11020606A) is a massive sample without foliation. It is composed dominantly of garnet (45-50%), orthopyroxene (5-10%), plagioclase (5-10%), and quartz (10-15%) with accessory biotite, rutile, and zircon. Garnet is subidioblastic and occurs as aggregate of fine- to coarse-grained crystals (0.1-1.7 mm) (Fig. 10-y). The mineral often contains quartz (0.05-0.1 mm), rutile (0.05-0.1 mm), plagioclase (<0.1 mm), and CMI. The matrix of the rock consists of plagioclase (0.05-5 mm), quartz (0.1-5 mm), rutile (0.05-0.5 mm), ilmenite (0.07-2.5 mm), and biotite (0.1-1 mm). As orthopyroxene is not observed in garnet, this study regards prograde mineralogy as garnet + rutile + plagioclase + ilmenite + liquid + quartz, while the peak assemblage is inferred as garnet + orthopyroxene + plagioclase + quartz + rutile + ilmenite. These assemblages are adopted for *P*-*T* calculations.

4. Mineral Chemistry

Chemical analyses of all minerals were carried out using a WDS electron microprobe analyzer (JEOL JXA8530F) at the University of Tsukuba. The analyses were performed under conditions of 15 keV accelerating voltage and 10 nA beam current, and the data were regressed using oxide-ZAF correction method. Below, this study describes a mineral chemistry of the examined samples. Representative compositions of minerals in the analyzed samples are given in Tables 4-7. Fe_2O_3 content of ilmenite is calculated by the method proposed by Droop (1987).

4.1. Garnet

4.1.1. Garnet in mafic granulite

Garnet in garnet-clinopyroxene granulite in Skallevikshalsen is essentially a solid solution of pyrope, almandine, and grossular with X_{Mg} = Mg/(Fe+Mg) = 0.14-0.32 and low content of spessartine (Table 4 and Fig. 11). The mineral shows a general rimward increase of almandine content. For example, garnet in sample TS11010802 shows slightly pyrope-enriched core (Alm_{55-56} Prp_{25-26} Grs_{18}) than rim (Alm_{57-59} Prp_{21-23} Grs_{18}). The mineral in garnet-bearing orthopyroxene granulite (sample TS1012122604B) shows compositional zoning from slightly pyrope- and grossular-enriched core (Alm_{65} Prp_{16} Grs_{25-26}) to rim (Alm_{64-65} Prp_{14} Grs_{19-20}). In contrast, garnet in sample TS11010704B (garnet-clinopyroxene granulite) shows no compositional variation within single grain (Alm_{66} Prp_{9} Grs_{23}). Garnet in mafic granulite (sample TS11011405A-2) from Austhovde

shows X_{Mg} ratio (=0.16-0.19) consistent with that from Skallevikshalsen. It shows slightly pyrope-enriched core (Alm_{63-64} Prp_{14} Grs_{20}) than rim (Alm_{65} Prp_{12-13} Grs_{20}). The mineral in sample TS11011601M also shows slightly pyrope-enriched core (Alm_{54-57} Prp_{25-26} Grs_{17-18}) than rim (Alm_{58} Prp_{23} Grs_{17-18}). Similar relationships are observed for garnet in the mafic granulite from Ongul. Garnet in garnet amphibolite from Ongul (sample TS11020610I) shows compositional zoning from slightly pyrope-enriched core (Alm_{54} Prp_{28-29} Grs_{16}) than rim (Alm_{56} Prp_{26} Grs_{15}). The mineral in another garnet amphibolite from Ongul (sample TS11020610G-2) also shows slightly pyrope-enriched core (Alm_{46} Prp_{35-36} Grs_{16}) than rim (Alm_{51-52} Prp_{26-30} Grs_{16}). The mineral in garnet-orthopyroxene granulite from Innhovde (sample TS11020206H) shows little compositional variation (Alm_{63} Prp_{25} Grs_{10-11}).

4.1.2. Garnet in pelitic and felsic granulites

Garnet in pelitic granulite from Skallevikshalsen essentially is a solid solution of pyrope, almandine, and grossular with X_{Mg} = Mg/(Fe+Mg) = 0.32-0.45 and low content of spessartine (1-2 mol. %) (Fig. 11-c). The mineral shows a general rimward increase of almandine content. For example, garnet in sample TS10122502B2 shows slightly pyrope-enriched core (Alm_{53-54} Prp_{42-43} Grs_{3}) than rim (Alm_{63-64} Prp_{33} Grs_{2}), while the mineral in sample TS10122502D shows heterogeneous composition depending on its occurrence. The mineral in orthopyroxene-bearing domain shows slightly grossular-enriched core (Alm_{56-57} Prp_{24-25} Grs_{16-17}) than rim (Alm_{61} Prp_{29} Grs_{7-8}), while the mineral in orthopyroxene-free domain is nearly homogeneous in composition (Alm_{56-58} Prp_{35-36} Grs_{6-7}). In sample TS97122003-2, the mineral shows slightly

pyrope-enriched core (Alm_{59-60} Prp_{33-34} Grs_{7}) than rim (Alm_{64-65} Prp_{28-29} Grs_{6}). Garnet in garnet-biotite gneiss and garnet-sillimanite-spinel gneiss from Austhovde is a solid solution of pyrope, almandine, and grossular with X_{Mg} =0.27-0.40 and low content of spessartine (1-3 mol. %) (Fig. 11-c). The mineral shows a general rimward increase of almandine content. For example, garnet in sample TS11011504C shows slightly pyrope- and grossular-enriched core (Alm_{54-55} Prp_{36-37} Grs_{7-8}) than rim (Alm_{67-68} Prp_{25-26} Grs_{5}), while the mineral in garnet sillimanite gneiss (sample TS11011702B) shows homogenous in composition (Alm_{64-67} Prp_{25-26} Grs_{5-7}). The mineral in pelitic granulite from Ongul (sample TS11020604B) is homogeneous in composition (Alm_{57} Prp_{38-39} Grs_{3}). Garnet in intermediate granulite (sample TS11020606A) from Ongul shows no compositional zoning (Alm_{54-55} Prp_{34-35} Grs_{8-10}). Garnet in felsic granulite from Austhovde (sample TS11011407D) is slightly enriched in X_{Mg}=0.28-0.29, if compared to the mineral in the mafic granulite (sample TS11011405A-2), and is nearly homogeneous in composition (Alm_{63} Prp_{25} Grs_{10-11}). Garnet in felsic granulite from Austhovde (sample TS11011702G) is nearly homogeneous in composition (Alm_{66-67} Prp_{30} Grs_{2}).

4.2. Clinopyroxene

Clinopyroxene in garnet clinopyroxene granulite from Skallevikshalsen is compositionally augite with X_{Mg} = 0.65-0.67 (Table 5 and Fig. 12-a). Slight compositional variation in Acmite ($Ca_{0.5}\square_{0.5}AlSiO_6$; Ac), and Ca-Tschermak ($Ca_{0.5}Al_2SiO_6$; Ca-Ts) components can be seen depending on samples (Table 5). Clinopyroxene in sample TS11010802 shows Ac and Ca-Ts components of 0-5 mol. %

and 7-9 mol. %, respectively, whereas the mineral in sample TS11010803A show lower Ac (1-2 mol. %) and Ca-Ts (3-5 mol.%) contents. The mineral in sample TS11010704B is also Fe-rich (X_{Mg} = 0.40-0.41) with moderate components of Ac (2-4 mol. %). The mineral in garnet-two-pyroxene granulite shows slightly Ca-Ts-rich core (X_{Mg} = 0.53-0.54, Ca-Ts=5.9-6.1 mol. %) than rim (X_{Mg} = 0.53, Ca-Ts=3.9-4.4 mol. %). The mineral in mafic granulites from Austhovde is also compositionally augite with X_{Mg} =0.50-0.60 (Table 5) with little compositional variation in terms of Ca-Ts components from core to rim. For example, the mineral in mafic granulite (sample TS11011405A-2) shows slightly Ca-Ts-enriched core (5-6 mol. %) than that of rim (3-4 mol. %) (Table 5). The mineral in mafic granulites from Ongul (e.g., sample TS11020610I) is also compositionally augite with X_{Mg} =0.61 and moderate Ca-Tschermak composition (3-4 mol. %).

4.3. Orthopyroxene

4.3.1. Orthopyroxene in mafic granulite

Orthopyroxene in garnet-clinopyroxene granulite from Skallevikshalsen shows compositionally variation depending on samples in terms of Fe-Mg ratio (X_{Mg} = 0.40-0.55) (Table 5). The mineral in sample TS11010802 shows Mg-rich (X_{Mg} = 0.54-055) and Al-poor (X_{Al} = Al/2 =0.04) compositions with no compositional variations whereas the mineral in sample TS11010803A shows Fe-rich (X_{Mg} = 0.40) and Al-poor (X_{Al} = 0.04) compositions. There is no significant compositional variation between the core (X_{Mg} = 0.42, X_{Al} =0.02) and rim (X_{Mg} = 0.42, X_{Al} =0.02) of the sample

TS10122604B (garnet-two-pyroxene granulite). The mineral in mafic granulite from Austhovde shows a rimward increase of Mg content. For example, the mineral in sample TS11011405A-2 shows slightly Fe-enriched core (X_{Mg} = 0.56, X_{Al} =0.02) than rim (X_{Mg} = 0.58-0.59, X_{Al} =0.02). Orthopyroxene in garnet-orthopyroxene granulite from Innhovde shows compositional zoning from Mg-rich rim (X_{Mg} = 0.58-0.59, X_{Al} =0.05-0.06) to Fe-rich core (X_{Mg} = 0.56, X_{Al} =0.06-0.07) (Table 5).

4.3.2. Orthopyroxene in felsic and intermediate granulites

Orthopyroxene in felsic granulite (e.g., sample TS11011407D) from Austhovde shows slightly Al-rich core (X_{Mg} = 0.53, X_{Al} =0.06) than rim (X_{Mg} = 0.53, X_{Al} =0.05) (Table 5). The mineral in the felsic granulite (TS10122502D) shows nearly homogeneous compositions (X_{Mg} = 0.58, X_{Al} =0.05-0.06) (Fig. 12-b). The mineral in intermediate granulite from Ongul (sample TS11020606A) is magnesium rich and nearly homogeneous in composition (X_{Mg} = 0.62-63, X_{Al} =0.06) (Table 5).

4.4. Plagioclase

4.4.1. Plagioclase in mafic granulite

Plagioclase in garnet clinopyroxene granulite from Skallevikshalsen shows significant compositional variations depending on its occurrence (Fig. 13). For example, symplectic fine-grained plagioclase in sample TS11010802 formed by reaction (2) shows the highest anorthite content of An_{89-92} with minor orthoclase content (less than 2

mol. %). The mineral coexisting with calcic amphibole in coarse-grained matrix has higher albite contents (An_{71-72}). The mineral in the grain boundary of garnet and clinopyroxene in sample TS11010803A (garnet-clinopyroxene granulite) shows the moderate-albite content (An_{52-53}) (Table 6). Plagioclase in garnet-two-pyroxene granulite (sample TS10122604B) also shows higher albite content (An_{59-63}) (Table 6).

Plagioclase in mafic granulites (e.g., samples TS11011405A-2 and TS11011405C) of Austhovde is also anorthite rich (An_{52-71}). Plagioclase in equilibrium with garnet (sample TS11011405A-2) shows no compositional variation (An_{60-61}). The mineral in the matrix of mafic granulite (sampleTS11011405C) shows slightly albite-rich compositions (An_{52-53}), if compared to that occurring as fine-grained symplectite, which is significantly, anorthite rich (An_{71}) (Table 6). The mineral in garnet-orthopyroxene granulite from Innhovde is also albite rich (An_{48}) and homogeneous in composition.

Plagioclase in sample B97122302F2 shows significant compositional variation depending on its occurrence. The mineral in garnet shows higher-albite content (An_{55-56}), whereas the mineral occurring as symplectite is anorthite rich (An_{80-81}). In contrast, plagioclase in garnet amphibolite from Ongul, symplectic fine-grained plagioclase in sample TS11020610I formed by reaction (2) shows the highest anorthite content of An_{71-72}. The mineral coexisting with calcic amphibole in coarse-grained matrix and inclusion in garnet in the same sample has higher albite contents (An_{42-47}). The mineral in garnet amphibolite (sample TS11020610G-2) shows the highest anorthite contents (An_{82-85}).

4.4.2. Plagioclase in pelitic and felsic granulites

Plagioclase in felsic to pelitic granulite from Skallevikshalsen shows significant compositional variations depending on sample and its occurrence (Fig. 13). For example, the mineral in garnet in sample TS97122003-2 (pelitic granulite) shows the higher anorthite content of An_{50-51} with minor orthoclase content (less than 2 mol. %). The mineral in coarse-grained matrix have higher albite content of the sample (An_{43-45}). The mineral in the felsic granulite (sample TS10122502D) also shows significant compositional variations depending on its occurrence. The mineral in orthopyroxene-rich matrix have higher anorthite content (An_{53-55}) than that (An_{41-43}) in orthopyroxene-free matrix. The mineral in garnet shows slightly higher anorthite contents (An_{54-55}) than that in matrix. Plagioclase in pelitic granulite (sample TS10122502B2) has no compositional variation (An_{41-42}). The mineral in garnet-biotite gneiss from Austhovde (sample TS11011504C) shows compositional variations depending on its occurrence. Plagioclase in garnet has higher albite content (An_{37-39}) than that in matrix (An_{41-43}). There is no compositional variation of the mineral in garnet-sillimanite-spinel gneiss (An_{42-43}) (sample TS11011702B) and the mineral in kyanite-bearing felsic granulite (An_{14-15}) (sample TS11011702G). The mineral in pelitic granulite from Ongul (TS11020604B) is albite rich (An_{33}) whereas the mineral in intermediate granulite (sample TS11020606A) is anorthite rich (An_{73-74}).

4.5. Amphibole

Amphibole in the examined samples is essentially classified as ferropargasite or pargasite after the classification of Leake et al. (1997) (Figs.14-1and 14-2). The mineral in garnet-clinopyroxene granulite from Skallevikshalsen has a compositional variation

depending on samples and its occurrences. Brownish intergranular amphibole in matrix in sample TS11010802 is compositionally pargasite (X_{Mg} = 0.60, Si =6.2-6.3, $Na+K^A$ = 0.89-0.90), while fine-grained retrograde phase around clinopyroxene in sample TS11010803A is ferropargasite (X_{Mg} = 0.40-0.41, Si = 6.2-6.3, $Na+K^A$ =0.82-0.90). Ferropargasite (X_{Mg} = 0.42-0.43, Si = 6.3, $Na+K^A$ =0.75-0.86) also occurs as retrograde phase replacing orthopyroxene in garnet-two-pyroxene granulite (sample TS10122604B). Amphibole in mafic granulite from Austhovde is ferropargasite (X_{Mg} = 0.43-0.44, Si = 6.1-6.2, $Na+K^A$ =0.88-0.91) (sample TS11011405A-2). Pargasite also occurs in coarse-grained matrix (X_{Mg} =0.61-0.62, Si = 6.1-6.2, $Na+K^A$ =0.94-0.97) and inclusion in garnet (X_{Mg} =0.53-0.54, Si =6.1-6.2, $Na+K^A$ =0.95-1.00) in garnet amphibolite (sample TS11020610I). Pargasite in sample TS11020610G-2 shows compositional variation depending on its occurrence. Pargasite in garnet is slightly Mg-rich (X_{Mg} =069-0.70, Si =6.1-6.2, $Na+K^A$ =0.87-091) than coarse-grained matrix phases (X_{Mg} =0.63-0.64, Si =6.1-6.2, $Na+K^A$ =0.88-0.90)

4.4. Biotite

4.4.1. Biotite in mafic granulites

Biotite in the examined samples occurs as a prograde inclusion phase in garnet or retrograde phase surrounding most porphyroblastic minerals. For example the mineral in garnet clinopyroxene granulite (TS11010802) shows strong compositional variation on its occurrence. The mineral in garnet is Mg and Ti rich (X_{Mg} = 0.73-0.74, TiO_2=5.5-5.6 wt. %), while the matrix retrograde phase is slightly Ti- poor

(TiO_2=3.5-3.6 wt. %). The mineral occurring in matrix of garnet amphibolite (sample TS11020610I) is Mg rich (X_{Mg} = 0.59-060, TiO_2=4.4-4.7 wt. %), while the mineral in CMI shows wide compositional variation of Ti (X_{Mg} = 0.54-0.55, TiO_2=1.2-4.3 wt. %). The mineral coexisting with rutile and ilmenite shows higher Ti content (TiO_2=3.9-4.3 wt. %) than that in the Ti-phase-free CMI (TiO_2=1.2-2.0 wt. %). The mineral in garnet is enriched in Mg and Ti (X_{Mg} = 0.73-0.74, TiO_2=5.5-5.6 wt. %).

4.4.2. Biotite in pelitic and felsic granulites

The mineral in pelitic granulite (sample TS1012250B2) from Skallevikshalsen shows significant compositional variations depending on its occurrence. For instance, biotite in matrix is enriched in Ti component (TiO_2=5.1-5.2 wt. %) than that in CMIs (TiO_2=~0.9 wt. %). Similar relationships are observed in the mineral in felsic granulite (Sample TS10122502D). The mineral in garnet has higher titanium component (TiO_2=~6.7 wt. %) than that in CMI (TiO_2=0.07-0.08 wt. %). The mineral in felsic granulite (sample TS11011407D) is titanium and magnesium rich (X_{Mg} = 0.54-0.55, TiO_2=4.8-4.9 wt. %). The mineral in garnet-biotite gneiss (TS11011504C) from Austhovde is titanium and magnesium rich (X_{Mg} =0.65-0.75, TiO_2=4.1-4.9 wt. %). Biotite in garnet is Mg rich (X_{Mg} =0.74-0.75, TiO_2=4.1-4.2 wt. %) than that in the matrix (X_{Mg} =0.64-0.65, TiO_2=4.6-4.9 wt. %).

4.5. Fe-Ti oxides

Most ilmenites in the examined samples are close to their ideal formula as $FeTiO_3$ with minor content of Mg (MgO=~2.4 wt. %), although some of the minerals contain considerable amounts of hematite components (X_{hem}=50*Fe^{3+} pfu~ 10 mol. %). For example, ilmenite in garnet-clinopyroxene granulite (sample TS11010802) shows the highest Fe^{3+} content (Fe_2O_3=0.15 pfu., X_{hem}~ 7.5 mol. %). Ilmenite in garnet-biotite gneiss (sample TS11011504C) is also hematite rich (Fe_2O_3=0.15 pfu., X_{hem}~ 7 mol. %). Almost all rutiles in the various lithologies are close to their identical formula as TiO_2, although the mineral contains few amounts of iron and zirconium. For instance, the mineral in garnet-biotite gneiss (sample TS11011504C) contains considerable amounts of Fe (FeO=~1.4 wt. %) and zirconium (ZrO_2=2300-4500 ppm). The mineral in CMI is clearly zirconium poor in composition (ZrO_2=600-1100 ppm).

4.7. Other minerals

The compositions of sillimanite and kyanite in the samples are close to the ideal chemistry (Al_2SiO_5), although they also contain small amounts of Fe_2O_3 (up to 1.12 wt. %) and Cr_2O_3 (up to 0.03 wt. %). K-feldspar in the examined samples is essentially orthoclase with minor content of albite (Fig. 13). For example, the mineral coexisting with plagioclase in garnet-biotite gneiss (sample TS11011504C) is $Or_{84\text{-}86}$ $Ab_{12\text{-}14}$. K-feldspar in pelitic granulite (sample TS11020604B) is also orthoclase rich as $Or_{83\text{-}84}$ $Ab_{16\text{-}17}$. Spinel in the examined samples shows compositional variations of hercynite and Zn contents. For instance, spinel in pelitic granulite (sample TS11020604B) is Mg and Zn rich (X_{Mg} = 0.60, ZnO=12.0-12.3 wt. %), while that in garnet-biotite gneiss (sample TS11011504C) is Fe rich and Zn poor in composition (X_{Mg} = 0.46-47, ZnO=2.1-2.2 wt. %).

Chapter 5. Mineralogy and composition of CMI

5.1. Mineralogy of CMI

5.1.1. Mineralogy of CMI in mafic to ultramafic granulites

This study identified CMI in mafic granulites from several localities in the LHC. All the CMIs are observed only in garnet. Some CMIs show clear negative crystal in shape, whereas others display irregular shape probably due to the progress of interaction between CMI and host garnet (Figs. 15 and 16). The mineralogy of the CMI is characterized by the presence of quartz, biotite, plagioclase, and K-feldspar. CMI in the sample TS11010802 contains orthopyroxene while others not. As discussed in a later section, composition of orthopyroxene-bearing CMI is intermediate (andesitic composition). Muscovite is observed only for the CMI in sample TS11011704B (Fig. 15-b). Such occurrence of muscovite suggests the formation of alumina-oversaturated melt by partial melting of mafic granulite. This study attempted to calculate original composition of the CMI to investigate partial melting processes as discussed in later sections.

5.1.2. Mineralogy of CMIs in pelitic and felsic granulites

CMIs are also identified in pelitic and felsic granulites in the examined samples from Skallevikshalsen and Austhovde. Quartz and biotite occur within each CMI. Muscovite is also present in some CMIs (Figs. 16-a and 16-b), implying the formation

of alumina-saturated melt during partial melting. Some CMIs lack plagioclase (Figs.15-b and 15-c), which suggest heterogeneous distribution of the minerals within the CMIs in three dimension scales. Chlorite occurs in sample TS11011504C, suggesting the progress of post-crystallization alternation.

5.2. Compositions of CMI

This study attempted to recalculate the original composition of the CMI based on mineral modal abundance (estimated by BSE images), mineral chemistry, and mineral density. Table 8 shows mode occurrence of the CMI together with the calculated results. First, mineral mode was multiplied by mineral density to estimate volume ratio of each minerals within CMI. Then, volume ratio of each mineral was multiplied by oxide composition of the minerals in CMI. The integrated each oxide compositions correspond to the original melt chemistry. For the calculation, this study selected CMI with sharp and negative-crystal shape, because this study attempted to avoid influence of melt-host interaction. Integrated composition of CMI in sample TS10122506 is dacitic in composition (SiO_2=62.1 %). It is enriched in potassium than sodium (Table 8), because of the high-modal abundance of biotite. Such potassium-rich composition suggests that decomposition of K-rich mineral (e.g., biotite) related to the formation of the CMI. Integrated composition of CMI in sample TS11010802 is depleted in Si if compared to the CMI in sample TS10122506. It is andesitic in composition (Table 8). CMI within garnet amphibolite (Table 8) shows the highest Si content (SiO_2=67.8 %) with higher potassium content (K_2O=3.10 %) than sodium (Na_2O=1.91 %). Volume ratios of biotite within each CMI show similar range (0.326-0.348, Table 8). In contrast,

volume ratio of quartz shows wide range (0.21-0.41, Table 8). All the three CMIs show similar total wt. % (around 97 %) which indicates that considerable amount of volatile (e.g., H_2O, fluorine, and chlorine) is included in the CMI.

Chapter 6. Metamorphic *P-T* conditions

This chapter discusses the results of *P-T* calculations based on conventional geothermobarometers which are applicable for mafic granulites and associated rocks from the studied areas. Here, different geothermobarometers calibrated on the basis of experimental, empirical and thermodynamic parameters using different composition-activity models for the various minerals are used. However the calculated *P-T* ranges could be minimum as the effect of Fe-Mg re-equilibrium between the minerals during further cooling cannot be neglected (e.g., Pattison et al., 2003).

6.1. Grt-Cpx-Pl-Qtz geothermobarometers

The Grt-Cpx geothermometer was applied to porphyroblastic garnet and clinopyroxene in mafic granulites. For the calculations, compositional data of core of the minerals were adopted in order to obtain the condition of peak metamorphism, because compositional date of rim might be modified by mineral reactions (e.g., reactions 1 and 2) at retrograde stage. Application of the method of Ellis and Green (1979), which is based on experimental calibration of Fe-Mg fractionation between garnet and clinopyroxene at 750 °C to 1350°C and 24-30 kbar, and widely applied for granulite terranes, gave a temperature range of 840-850 °C (sample TS11010802) at 8 kbar, a reference pressure based on the peak pressure condition estimated by phase equilibrium modeling as discussed in the next section. This study also adopted the method of Ganguly et al. (1996), which is based on revised solution model of garnet. The method is more realistic than the method of Ellis and Green (1979), because the

method of Ganguly et al. (1996) took into consideration the influence of CaO in the calibration. This study thus adopted the method of Ganguly et al. (1996). The temperature range for sample TS11010704B (760-850 °C) is nearly consistent with that for sample TS11010802 (840-850 °C). The mineral pair in Grt-two-pyroxene granulite from Austhovde (e.g., sample TS11011405A-2) gave a similar range of 770-810°C. This study also applied this method to the mineral pairs in garnet amphibolite (sample TS11020610I), and yielded a temperature range of 820-830 °C at 8 kbar.

Metamorphic pressure of Austhovde was calculated using Grt-Cpx-Pl-Qtz assemblage in sample TS11011405A-2 based on experimental calibration of Perkins and Newton (1981). The estimated results are 4.5-5.5 kbar at 800°C. These results are considerably low, if compared to the petrographic observation (the occurrence of Grt + Cpx + Pl + Qtz + Opx assemblage) which indicates high-pressure condition (*P* around 12 kbar). This study thus adopted the method of Moecher et al. (1988), which is based on improved Grt-Cpx-Pl-Qtz geobarometer using new thermodynamic and experimental data, and obtained a pressure range of 7-8 kbar. The results are also considerably low if taking into consideration the occurrence of Grt-Cpx-Opx-Pl-Qtz assemblage, which suggests high-pressure condition, as discussed later. Thus these results imply that the assemblages using the calculation are possibly reequibirated during retrograde stage. If it is the case, the results indicated the minimum *P-T* range. The estimated *P-T* box obtained useing the methods of Ganguly et al. (1996) and Moecher et al. (1988) for the assemblages is shown in *P-T* diagrams (Figs. 17, 18, and 19).

6.2. Grt-Opx geothermobarometers

The Grt-Opx geothermometer was applied to porphyroblastic garnet and matrix orthopyroxene in mafic granulite, pelitic granulite, felsic granulite, and intermediate granulite. The estimated temperature range for garnet-orthopyroxene pairs is 830-890 °C at 8kbar for mafic granulite (sample TS10122604B) using the method of Lee and Ganguly (1998), which is based on experimental calibration of Fe-Mg fractionation between the minerals in the FMAS system and widely applied for granulite terrenes. The method of Ganguly et al. (1996), which revised the method of Lee and Ganguly (1998), gives a lower temperature range of 760-810 °C. This study adopted the methods of Ganguly et al. (1996). The condition was calculated at 8 kbar, a reference pressure based on the peak pressure condition estimated by Grt-Opx-Pl-Qtz geobarometer of Moecher et al. (1988) as discussed later. The estimated temperature range of pelitic granulite (sample TS10122502D) is 820-840 °C at 8 kbar. A similar temperature range of 830-880°C is obtained from the assemblages in felsic granulite from Austhovde (sample TS11011407D). This study also applied the method for the mineral pairs in intermediate granulite (sample TS11020606A), and obtained the ranges of 820-830 °C at 8 kbar.

Metamorphic pressure was obtained by Grt-Opx-Pl-Qtz geobarometer of Moecher et al. (1988). The estimated pressure condition for garnet-orthopyroxene pairs is 8 kbar for mafic granulite at 800°C (sample TS10122604B). The mineral assemblage in felsic granulite (sample TS11011407D) from Austhovde gave a condition of 8 kbar at 800°C, which is nearly consistent with the value from sample TS10122604B. A similar but slightly higher pressure range of 8.5-8.9 kbar was obtained from the assemblages in intermediate granulite from Ongul (sample TS11020606A). *P-T* boxes obtained from the methods of Ganguly et al. (1996) and Moecher et al. (1988) are plotted in *P-T*

diagrams (Figs. 17, 18, and 19).

6.3. Isopleths of Ti-Al contents in Ca-amphibole

Ti- and Al-isopleths of Ernst and Liu (1998), which is based on the experiment of calcic amphiboles in MORB-like protolith, are adopted for semi-quantitative estimation of *P-T* conditions for calcic amphiboles in mafic granulites from Skallevikshalsen, Austhovde, and Ongul. The examined samples contain rutile or ilmenite as excess Ti-bearing phases, and plagioclase or garnet as excess Al-bearing phases. The calculated results are 6-8 kbar and 820-860°C (sample TS11010802) and 9 kbar and 830-860°C (sample TS11011405C). In contrast, higher-temperature range of 900-950 °C and 6-8 kbar is obtained from garnet-amphibolite (sample TS11020610I). The estimated *P-T* conditions using the method of Ernst and Liu (1998) are plotted in *P-T* diagrams (Figs .17, 18, and 19).

6.4. Garnet-hornblende-plagioclase-quartz geothermobarometry

Garnet-hornblende-plagioclase-quartz geothermobarometry is applied to hornblende included in garnet to estimate prograde *P-T* conditions. This study adopted garnet-hornblende geothermometry proposed by Graham and Powell (1987). Metamorphic pressure is calculated by the method of Kohn and Spear (1990). This study obtained 700-720 °C and 7-7.2 kbar from the mineral assemblage in the garnet-two-pyroxene granulite from Austhovde (Sample TS11011405A-2). As hornblende used for estimation occurs as inclusions in garnet, the result might

correspond to a prograde *P-T* condition. The mineral assemblage from garnet amphibolite in Ongul (sample TS11020610I) yields *P-T* ranges of 700-720 °C and 8.1-9.1 kbar, which could also imply a prograde *P-T* condition, because this study adopted the compositions of hornblende and plagioclase occurring in garnet. This study also estimated metamorphic temperature of garnet amphibolite (sample TS11020610G-2) occurring in the same locality of sample TS11020610I. The estimated temperature is 690-780 °C, which is consistent with the result obtained from sample TS11020610I. As this sample (TS11020610G-2) lacks quartz inclusion the garnet, metamorphic pressure could not be calculated.

6.5. Garnet-rutile-ilmenite-plagioclase geobarometery

The garnet-rutile-ilmenite-plagioclase-quartz geobarometery (GRIPS) was applied to porphyroblastic garnet, and its inclusion of rutile, ilmenite, and plagioclase, which are considered to preserve prograde to peak conditions in several lithologies. This study estimated pressures based on the experimental study of Bohlen and Liotta (1986), and adopted activity models of Newton et al. (1980) for plagioclase and Ganguly and Saxena (1984) for garnet. Ilmenite is regarded as an ideal solution. A pressure range of a pelitic granulite from Skallevikshalsen (sample TS10122502D) is 15.2-15.4 kbar at 800 °C with range of Kd= $a_{Ilm}^{6} * a_{An}^{3} * a_{Gr}^{-1} * a_{Alm}^{-2}$ =0.90-0.93, whereas pressure range of a mafic granulite from Skallen (sample B97122302F2) is 15.8-16.0 kbar at 800 °C (Kd=0.24-0.27). A similar pressure range of 15.5-15.6 kbar at 800 °C (Kd=0.40-0.44) is obtained from the garnet-biotite gneiss from Skallen (sample B97122708B). This study also obtained a similar pressure range of 15.6 -15.8 kbar at 800 °C (Kd=0.32-0.40) from

garnet-biotite gneiss (sample TS11011504C) in Austhovde. In contrast, the estimated pressure range for the mineral assemblage within the matrix in intermediate granulite (sample TS11020606A) is 8-8.5 kbar at 800 °C (Kd=6.30-6.78). This study also adopted composition of plagioclase in the garnet within the sample, and obtained a pressure range of 12.2-12.7 kbar at 800 °C (Kd=3.79-4.01). Since the composition of plagioclase in matrix is used for pressure estimation, the calculated pressure (8-8.5 kbar) is regarded as the peak pressure, which is well consistent with the result calculated by garnet-orthopyroxene-plagioclase-quartz geothermobarometry (Table 9), while the higher-pressure range of 12.2-12.7 kbar is regarded as prograde to peak condition, because the composition of plagioclase within garnet is used the calculation. As discussed in a later section, GRIPS assemblages are coexisting with CMI (liquid phase), pressure ranges obtained by GRIPS are considered to be the prograde pressure. The estimated pressure conditions using the GRIPS geobarometer are plotted in *P-T* diagrams (Figs. 17, 18, and 19). In summary, GRIPS assemblages in garnet gives high-pressure conditions (P = 15-16 kbar), although sample TS11020606A yields medium- to high-pressure record (*P* = 8-8.5 kbar and 12-12.7 kbar). These results suggest that granulite terrain of the LHC experienced medium- to high-pressure metamorphism.

6.6. Garnet-aluminosilicate-plagioclase-quartz geobarometery

The garnet-aluminosilicate-plagioclase-quartz geobarometery (GASP) was applied to porphyroblastic garnet, aluminosilicate (kyanite or sillimanite), plagioclase, and quartz, which are considered to preserve prograde to peak conditions in several

lithologies. Activity models of Newton et al. (1980) for plagioclase and Gangly and Saxena (1984) for garnet are adopted for calculations. Pressures were estimated based on the equation presented by Spear (1993). The estimated pressure range for the mineral assemblage in the matrix in a felsic granulite from Austhovde (sample TS11011702G) is 11.5-11.6 kbar at 800°C with $Kd=a_{Pl}*a_{Grs}^{-1}$ =59-68. As the mineral assemblage occurs in matrix (Fig. 10-u), this study considered that the estimated pressure as the peak condition. In contrast, a pressure range of 14.7-15.3 kbar at 800°C (Kd=6.2-6.4) is obtained from the mineral assemblage in a pelitic granulite from Ongul (TS11020604B). As the compositions of plagioclase in the garnet are used for pressure estimation, the obtained pressures are regarded as prograde to peak conditions. The estimated pressure conditions using the GASP geobarometer are plotted in *P-T* diagrams (Figs. 18 and 19).

6.7. Zirconium-in-rutile geothermometry

The zirconium in rutile geothermometer is applied to rutile in garnet in various lithologies in order to obtain the condition of prograde to peak metamorphism. Based on the experimental study of Zack et al. (2004), this study selected rutile grains coexisting with quartz and zircon. Tomkins et al. (2007) performed an experimental study to natural rutile-bearing lithologies to evaluate pressure dependence of zirconium content in rutile. They concluded considerable pressure dependence of the geothermometer in the system of SiO_2-TiO_2-ZrO_2 in the presence of silicate melt, which is similar the phase relation of our samples that rutile and CMI coexist. This study thus adopted the equation proposed by Tomkins et al. (2007). Temperature calculation is performed under 12 kbar. Compositions of rutile are analyzed at least 5 points for each grains. Temperature range

of 850-910 °C is obtained from pelitic granulite (sample TS10122502D) from Skallevikshalsen. Rutile adopted for temperature estimation occurs as inclusion in garnet, which are coexisting with plagioclase, ilmenite, quartz, and CMI. As rutile also coexisting with melt, the obtained temperature range might suggest prograde to peak condition. A similar temperature range of 870-930 °C is obtained from a pelitic granulite (TS10122502B2) collected from the same outcrop as sample TS10122502D (Fig. 7-d). Rutile in the samples occurs in garnet, which contains plagioclase, quartz, and CMI, suggesting that estimated temperature range probably corresponds to prograde to peak stage. This study also adopted this method to rutile coexisting with quartz, ilmenite, and CMI within garnet in pelitic granulite (sample TS97122003-2) from Skallen. The estimated temperature range is 860-950 °C. Because rutile adopted for temperature estimation occurs with CMI, calculated temperature might imply prograde to peak condition. A temperature range of 890-930 °C is obtained for rutile inclusion in garnet in a mafic granulite (sample B97122302F2) from Skallen. Plagioclase, ilmenite, quartz, zircon, and CMI are also included in the garnet, which implies that calculated temperature might correspond to a prograde to peak condition. A similar temperature range of 860-960 °C is obtained from a garnet-biotite gneiss (TS11011504C) from Austhovde. Rutile in the sample is a part of GRIPS assemblages and coexisting with CMI within garnet, which suggest that estimated temperature probably corresponds to the condition of prograde to peak stage.

6.8. Summary of the *P-T* estimations from geothermobarometry

Estimated *P-T* conditions are summarized in Table 9. Most of the calculated-*P-T*

conditions correspond to amphibolite- to granulite-facies field. They are possibly of prograde to peak conditions. Peak *P-T* conditions of granulites in Skallevikshalsen and Skallen yields *P-T* ranges of 800-950 °C and 6-11 kbar. The peak conditions of Austhovde are 790-860 °C and 7-9 kbar, which is consistent with the estimation obtained from the lithologies in Skallevikshalsen and Skallen. Peak *P-T* estimations of the granulites from Ongul show *P-T* ranges of 810-840 °C and 8.5-8.9 kbar. An interpretation of the results of GRIPS calculation is complicated. GRIPS mineralogy is preserved in garnet, which are coexisting with CMI (e.g., samples TS10122502D, B97122302F2, B97122708B, and TS11011504C). This study adopted zirconium in rutile geothermometer to rutile grains which are parts of GRIPS mineralogy. Temperature ranges of the result are 850-930 °C. If this study assumes that CMI is stable at prograde to peak stages, GRIPS and CMIs are probably stable at the temperature ranges of 850-930 °C. Peak 1 condition is thus defined by the combination of GRIPS geobarometery and zirconium in rutile geothermometer (850-930 °C and 16.2-17.5 kbar). Similar Peak 1 conditions of 860-960 °C and 16.5-17.5 kbar were also obtained from Austhovde region. *P-T* ranges obtained by garnet-two-pyroxene geothermobarometry to the mineral pairs in the matrix are regarded as Peak 2 stage (820-900 °C and 6-11 kbar) of the Skallevikshalsen and Skallen. Peak 2 stage (780-870 °C and 7-9 kbar) is also defined from the Austhovde region. This study therefore defined two possible stages of the peak metamorphism from the examined samples. The *P-T* conditions of prograde stage are also discussed below. In Austhovde region, *P-T* range of 700-720 °C and 7-7.2 kbar by garnet-hornblende-quartz geobarometery, which is regarded as a prograde stage, due to occurrence of the hornblende within garnet. In Ongul region, *P-T* ranges of 700-710 °C and 8.9-9.1 kbar

are assumed as prograde *P-T* conditions. As the examined samples from the Skallevikshalsen and Skallen lack suitable mineral assemblages for prograde *P-T* estimation, this study could not determine *P-T* condition of prograde stage of the areas by conventional geothermobarometry. As discussed in Chapter 7, this study adopted mineral equilibrium modeling for the mafic granulites from Skallevikshalsen, Austhovde, and Ongul to discuss prograde *P-T* evolution.

Chapter. 7 Phase equilibrium modeling

7.1. *P-T* pseudosection of mafic granulites

This study applied mineral equilibrium modeling technique to estimate metamorphic *P-T* conditions of the stability of mineral assemblages in three mafic granulites (samples TS11010802, TS11011405A-2, and TS11020610I). For the phase equilibrium calculations, this study adopted THERMOCALC 3.33 software (Powell and Holland, 1988, updated October 2009) based on an internally consistent dataset of Holland and Powell (1998; dataset tcds55s, file created November 2003). The computations using this software are based on the stable mineral assemblage and phase compositions for a given bulk composition at specified *P-T* conditions, and the results are used to construct rock-specific equilibrium assemblage diagrams (also called pseudosections). Calculations were performed in the system Na_2O-CaO-K_2O-FeO-MgO-Al_2O_3-SiO_2-H_2O-TiO_2-Fe_2O_3 (NCKFMASHTO) (White et al., 2003, 2007). Because the examined samples contain considerable amounts of Fe-Ti oxide and un-negligible quantity of Fe_2O_3 in whole rock chemistry, this study adopted NCKFMASHTO or NCFMASHTO system for calculations. The phases considered in the modeling and the corresponding *a-x* models used are garnet, biotite, and melt (White et al., 2007), plagioclase (Holland and Powell, 2003), clinopyroxene (Green et al., 2007), amphibole (Diener et al., 2007), orthopyroxene, spinel, and magnetite (White et al., 2002), and ilmenite-hematite (White et al., 2000). Quartz, rutile and H_2O are treated as pure end-member phases. For the analysis, a slab of relatively homogeneous part of the examined granulite used for thin-section preparation was used

for chemical analysis. Bulk rock compositions for the rocks were determined by X-ray fluorescence spectroscopy at Activation Laboratories, Canada. The chemical composition (in wt. %) of the samples are listed in Table 10. Mn is neglected in the modeling because the MnO content of these samples are low (<0.37 wt. %). The examined samples contain considerable amounts of P_2O_5, which is up to 0.7 wt. % as the examined samples contain minor apatite. As we neglect P_2O_5 from the system, the CaO content equivalent to apatite should be extracted from the calculation. The corrected CaO content is adopted for the pseudosection calculation.

Sample TS11010802 contains garnet, clinopyroxene, quartz, plagioclase, orthopyroxene, biotite, calcic amphibole, ilmenite, and inferred melt. Garnet and clinopyroxene occurs as idioblastic to subidioblastic minerals. Quartz is only present in garnet, and absent in the matrix, which suggests that quartz is consumed by the progress of reactions 1 and 2. Orthopyroxene and plagioclase are not observed within the garnet, and occur as retrograde phases around garnet (fine-grained symplectite). Hornblende and biotite are observed both in the garnet and in the matrix. The minerals in the garnet are regarded as the relict of prograde stage, while the minerals in the matrix replace clinopyroxene and garnet or occur as symplectite, suggesting that they are products during retrograde stage. This study thus regards the mineral assemblage of garnet + clinopyroxene + quartz + ilmenite + inferred melt as the probable peak assemblage. Fig. 20 shows a *P-T* pseudosection for the sample with the compositional factors for calculation listed in the figure. Water content of the rock in mole ($M(H_2O)$) was fixed to be 1.0 mol.%. The stability field of the peak mineral assemblage of the rock plotted in the NCKFMASHTO pseudosection suggests a narrow *P-T* range of T > 920 °C and P >10 kbar (purple-colored area in Fig. 20) for the assemblage. The lower-temperature

stability limit of the assemblage is defined by the disappearance of biotite. The upper pressure stability limit of the assemblage is defined by the absence of rutile in the sample. Retrograde hornblende formed by reaction 1 is observed in the sample. The stability field of the retrograde hornblende is defined by the appearance of quartz and magnetite, because quartz is not present in the matrix, magnetite is not observed in the sample, and hornblende coexists with plagioclase and orthopyroxene. As the retrograde hornblende does not coexist with liquid phase, upper temperature stability limit of the assemblage is defined by the presence of liquid (pale-purple-colored area in Fig. 20). This study could not define the stability field of a prograde assemblage of garnet + hornblende + quartz + ilmenite + clinopyroxene + biotite (plagioclase and rutile free), because there is no stability field without plagioclase and rutile (Fig. 20). Stability field of the prograde mineralogy and *P*-*T* condition is discussed in Chapter 8.

Sample TS11011405A-2 contains clinopyroxene, hornblende, plagioclase, quartz, and ilmenite in garnet. Magnetite and orthopyroxene are not observed in garnet. As biotite is accessory and the sample contains very low potassium in whole rock chemistry, this study adopted NCFMASHTO system for the modeling. This study regards prograde assemblage as garnet + clinopyroxene + hornblende + plagioclase + quartz + ilmenite. The stability field of the prograde assemblage is shown in Fig. 21 with pale-purple colored area. Upper pressure limit of the field is defined by the appearance line of rutile which is not observed in the sample. Lower-pressure limit of the area is defined by appearance of the magnetite. Matrix of the rock is characterized by medium- to coarse-grained garnet, clinopyroxene, orthopyroxene, plagioclase, and quartz. Ilmenite and magnetite also present in the matrix. Coarse-grained hornblende is not observed in the matrix. The mineral assemblage indicates that mineralogy of the peak stage is garnet

+ clinopyroxene + orthopyroxene + quartz + plagioclase + ilmenite + magnetite. This assemblage is shown in Fig. 21 with purple-colored area. The upper pressure limit of the field is defined by the disappearance line of orthopyroxene. Lower pressure limit of the area is defined by the disappearance of ilmenite which is likely to be a product of peak stage in the matrix. Lower temperature limit of the field is defined by the appearance of hornblende. Hornblende is not present as a relict of peak stage. The *P*-*T* range of the stability field is therefore defined as $T > 790$ °C and $P > 7$kbar (Fig. 21). This study also attempted to draw compositional isopleth (refer as z(g)) to further constrain *P*-*T* condition of the peak stage. Grossular content of the garnet rim is defined in the diagram (dashed lines in Fig. 21). The field defined by the isopleths might correspond to the constrained stability field of the peak mineralogy, because this study adopted the composition of the garnet (composition of rim) which is likely to be a product of the peak stage. The peak *P*-*T* range of the field is 870-990 °C and 9.3-10.6 kbar, which is consistent with the inferred peak conditions of the granulite terrain in the LHC (e.g., Yoshimura et al., 2004). The style of the *P*-*T* path of the sample is likely to be clockwise, because of the absence of magnetite and orthopyroxene in the garnet. Detailed discussion of *P*-*T* evolution is described in Chapter 8.

This study also attempts to draw phase diagram for sample TS11020610I to discuss the *P*-*T* evolution of garnet amphibolite from Ongul. Garnet contains quartz, plagioclase, hornblende, biotite, ilmenite, and rutile. Quartz is only present in garnet, suggesting that the mineral might have been consumed during retrograde stage. Hornblende also occurs in garnet, which indicates that prograde assemblage includes hornblende + quartz. In the phase diagram (Fig. 22), stability field of the prograde mineralogy of garnet + clinopyroxene + quartz + hornblende + rutile + biotite is colored in purple. Prograde

P-T condition shows a wide range. Quartz is absent in a matrix, whereas magnetite and orthopyroxene, and coarse-grained hornblende and plagioclase are observed in a matrix. This study thus regards peak assemblage of the sample as garnet + clinopyroxene + magnetite + orthopyroxene + plagioclase + hornblende + biotite. Probable peak stability field is shown in Fig. 22 with pale-purple colored area. Upper pressure limit of the area is defined by the disappearance line of rutile and lower pressure limit is defined by the disappearance line of garnet. Upper temperature limit of the field is defined by the appearance line of liquid which is not observed in the matrix of sample. As magnetite is absent and quartz present only in the garnet, this sample is likely to have experienced clockwise *P-T* evolution.

7.2. *P*-X pseudosections and the estimation of degree of partial melting

7.2.1. *P*-X pseudosection of the garnet-clinopyroxene rock

This study also constructed *P*-X pseudosection to estimate the degree of partial melting during prograde stage. As discussed in Chapter 5, this study selected two samples which are likely to have undergone partial melting (samples TS11010802 and TS11020610I). Sample TS11010802 was collected from Skallevikshalsen in the highest-grade region of the LHC, and sample TS11020610I was collected from Ongul in slightly lower-grade area. Sample TS11010802 is regarded as a restitic rock in composition, because it is characterized by low Si contents (SiO_2= 39.6 wt. %), Fe-enriched whole rock chemistry (FeO= 21.3 wt. %), high modal abundance of mafic mineral (up to 90%), and occurrence of well-preserved CMI within garnet. A procedure

to estimate compositions of CMI are described in Chapter 5. This study attempted to mix the compositions of the bulk rock and CMI at various ratios to infer degree of partial melting at high-grade metamorphism. This study first drew *P*-X pseudosections (Pressure - X: mixing rate of CMI and bulk chemistry) at 700 °C to evaluate the stability field of the prograde mineralogy in the examined samples. Mixing ratio of Bulk: CMI = 85: 15 and Bulk: CMI = 100:0 in wt. % is fixed as end members of the X axis (Fig. 23). It should be noted that the presence of clinopyroxene-out line is located around 'Melt 6.5%' (bold-red line in Fig. 23). The stability field of quartz shifted toward lower pressure side as rate of melt increases (bold-black line in Fig. 23). At melt > 6.5%, diopside is not stable in the phase diagram, which is not consistent with the presence of diopside in the examined sample. This study thus assumes that maximum melt addition of the sample is melt = 6.5% (Bulk: Melt = 93.5:6.5%) which is corresponding to the amount of extracted melt from the system about 6.5-7%. If this study assumes the integrated melt composition, 6.5-7% amount of melt has been lost during partial melting (Fig. 23). Fig. 23 also defines the appearance of liquid (bold-orange line in Fig. 23) which suggests that increasing amount of melt induced the shift of solidus in the examined system toward lower temperature.

7.2.2. *P*-X pseudosection of garnet amphibolite

This study also constructed *P*-X pseudosection for the garnet amphibolite (sample TS11020610I) which contains abundant CMIs. Whole rock chemistry shows SiO_2 content of this sample is 44.9 wt. %, and plagioclase rich in modal ratio, if comparted to sample TS11010802. Bulk rock chemistry indicated that melt loss is likely to be low

compared to sample TS11010802. The result of modeling is shown in Fig. 24. This sample contains hornblende and quartz in porphyroblastic garnet, and coarse-grained clinopyroxene in the matrix, which implies that garnet + hornblende + quartz + clinopyroxene is a prograde assemblage, and the stability field of this assemblage is critical to determine the degree of melt loss. The stability field of the hornblende + quartz + clinopyroxene assemblage is defined by the disappearance lines of quartz (bold-black line in Fig. 24) and clinopyroxene (bold-red line in Fig. 24) and is colored in purple. In this sample, disappearance line of clinopyroxene might define maximum rate of melt addition, because clinopyroxene occurs both in matrix and in garnet. This study also calculated modal isopleth of clinopyroxene (<3%). The phase diagram shows modal isopleth of clinopyroxene=3% (labeled as Cpx=3%), which is almost consistent with maximum rate of melt addition = 4.5%. (dashed line in Fig. 24) in the system. This study thus assumes that the amount of extracted melt is about 4.5-5%. The phase diagram also characterized the appearance of liquid, which suggests amount of melt increasing caused decreasing of solidus temperature. This study thus succeeded to create the melt-bulk pseudosection to discuss the degree of the partial melting and stability field of the prograde mineralogy before melting.

7.3. *P-T* pseudosection for integrated bulk composition

Based on estimation of the degree of the melt loss by *P*-X pseudosections, this study adopted integrated bulk compositions for calculation of *P-T* pseudosection (Figs. 25 and 27). Fig. 25 shows the *P-T* pseudosection for the bulk chemistry with bulk: melt=93.5:6.5% in Fig. 23 (sample TS11010802). Petrographic data indicated that

plagioclase is not observed in garnet, and rutile is not found in the sample, which suggest plagioclase is not stable at prograde to peak stage, and does not coexist with rutile. Thus, the prograde assemblage of the sample is regarded as garnet + clinopyroxene + quartz + ilmenite + hornblende + biotite, which is colored in purple in the phase diagram (Fig. 25). As melt coexists with garnet + clinopyroxene + quartz + ilmenite + hornblende + biotite, the stability field of melt-bearing assemblage might be liquid + garnet + clinopyroxene + quartz + ilmenite + hornblende + biotite, which is colored in pale purple in the figure. The line of liquid present defines the initiation of partial melting of the examined sample. According to the diagram, partial melting started at 770-780 °C and 9-9.3 kbar (Fig. 25). This study also calculated modal isopleth of liquid = 6.5% which is considered to have been extracted from the system as determined by *P*-X pseudosection. If this study assumes that amount of extracted melt is identical to the amount of melt generated in the system, melt loss might have occurred at *P*-*T* range of 820-830 °C and 9.3-10.3 kbar (Fig. 25). After melt extraction, this study adopted the pseudosection which does not consider the influence of melt (Fig. 26), because the peak mineralogy is characterized by anhydrous phases, suggesting restitic composition. Peak assemblage of garnet + clinopyroxene + quartz + ilmenite is colored in purple in Fig. 26. The stability field of the peak stage is defined by the disappearance of biotite and plagioclase, and appearance of rutile. Stability field of the peak assemblage is $T > 910$ °C and $P > 10.5$ kbar. Retrograde stage is also defined in the diagram, which is colored in pale purple. The retrograde mineralogy is characterized by the absence of quartz and magnetite. Pale-purple-colored area in Fig. 26 is thus corresponds to the *P*-*T* field of the retrograde assemblage of garnet + clinopyroxene + orthopyroxene + ilmenite + hornblende + biotite. This study combined *P*-*T* conditions

obtained from the sample (after partial melting and before melt extraction), and inferred clockwise *P-T* evolution (Fig. 26). Dashed line of the *P-T* path represents the *P-T* evolution before partial melting.

P-T pseudosection of sample TS1020610I for the bulk chemistry of melt=4.5% in the Fig. 24 (Fig. 27) shows quite different topology if compared to the *P-T* diagram of Fig. 28 which does not consider the melt composition. The inferred prograde mineralogy of garnet + clinopyroxene + hornblende + biotite + quartz + rutile + plagioclase (below solidus), is colored in purple area. As the area is too broad to discuss the precise prograde *P-T* condition, this study drew compositional isopleth of plagioclase (Xan=0.52-0.53) in the diagram. Plagioclase in the garnet is used for the isopleth calculations. At higher temperature than solidus, as quartz might be stable, a possible mineralogy with melt is quartz + liquid + garnet + clinopyroxene + hornblende + biotite + rutile + plagioclase. The stability field of the mineralogy is colored in pale purple, which is also a broad area (Fig. 27). This study thus calculated modal isopleth of liquid=4.5% which is determined by *P*-X pseudosection in Fig. 27. Compositional isopleth of liquid (X_{Fe} =Fe/ (Fe + Mg) $_{mole}$ of liquid =0.61) is also calculated and shown in the figure. Composition of the liquid is determined based on the melt composition described in Table 8. If this study assume that amount of produced melt in the examined sample is identical to the amount of extracted melt, a cross point of the compositional isopleths and mode isopleth of the liquid possibly corresponds to the *P-T* condition of melt extraction. The *P-T* condition of melt extraction is therefore estimated as 750 °C and 15.2 kbar. This study further discusses the *P-T* evolution after melt extraction by phase diagram in Fig. 28 which does not consider the effect of melt loss (also correspond to the bulk chemistry after melt extraction). The peak mineralogy includes

magnetite and orthopyroxene which are observed in the matrix. This study assumes that peak mineralogy is garnet + orthopyroxene + clinopyroxene + magnetite + hornblende + plagioclase + biotite. The stability field of the peak assemblage is colored in pale purple (Fig. 28). To constrain peak *P-T* condition, this study adopted hornblende-plagioclase geothermometer (Holland and Blundy, 1994) for the mineral pairs in the matrix. The result of the temperature estimation is shown in the diagram (refer as T(HB)). The results suggest that style of *P-T* path of the sample is clockwise (Fig. 28). Dashed-line part of the *P-T* path represents a possible *P-T* evolution before partial melting.

Chapter 8. Discussion

8.1. Mineralogy and *P-T* conditions of mafic granulite

This chapter discusses petrographic data, inferred *P-T* conditions, and *P-T* paths of the mafic granulite collected from the LHC. Peak assemblages of the examined samples are categorized into the following assemblages (a) Grt + Cpx + Qtz + Ilm (samples TS11010704B, TS11010803A and TS11010802), (b) Grt + Cpx + Opx + Qtz + Pl + Ilm ± Mag (samples TS10122604B and TS11011405A-2), (c) Grt + Cpx + Pl + Opx + Hbl + Ilm (samples TS10122506, TS11011601M, and TS11020610G-2), (d) Opx + Pl + Ilm + Hbl (sample B97122302F2) and (e) Grt + Opx + Cpx + Pl + Hbl + Bt + Ilm+ Mag (sample TS11020610I). Most of the peak assemblages include garnet and orthopyroxene, which suggests that the examined samples experienced granulite-facies metamorphism. This is consistent with previous studies that report widespread occurrences of orthopyroxene within mafic granulites (e.g., Osanai et al., 2004; Shiraishi and Yoshida, 1987). Furthermore some peak assemblages (c and d) include hydrous phases (hornblende and biotite), while others do not, implying difference of peak *P-T* conditions among them. Mafic granulites examined in this study (e.g., samples TS11010802 and TS11020610I) are also characterized by several reaction textures: (1) Grt +Hbl + Qtz →Opx + Pl + H_2O, (2) Grt + Cpx + Qtz → Opx + Pl, and (3) Grt + Qtz → Opx + Pl. Similar textures have been reported from granulite terrains worldwide (e.g., Osanai et al., 2004, 2006; Zhang et al., 2010; Saitoh et al., 2011; Koizumi et al., 2014). Previous reports inferred decompressional and clockwise *P-T* evolutions from the reaction textures. According to the experimental study of Green and Ringwood (1967), the following reaction takes place about 10 kbar at 900 °C.

Grs-Alm-Prp Grt + Qtz→Opx + An (4)

The reaction corresponds to reaction (3) of this study. Their experimental data demonstrated that reactions (2) and (4) take place in quartz tholeiite system by a decrease in pressure or an increase in temperature, leading to the consumption of garnet, clinopyroxene, and quartz, and formation of orthopyroxene + plagioclase assemblage at the lower-pressure (or higher-temperature) side of "disappearance of plagioclase" (Pl-out) curve of Green and Ringwood (1967) in Fig. 29 at P > 14 kbar at 900 °C or P > 12 kbar at 800 °C. As fine-grained orthopyroxene and plagioclase were regarded as products in the examined samples (e.g., samples TS10122506 and TS11010802), this study assumes that the samples were involved by decompressed along a clockwise P-T path (e.g., Fig. 20).

Green and Ringwood (1967) also discussed mineral assemblages of basaltic rocks based on experimental study, and they suggested plagioclase-free assemblage (garnet + clinopyroxene + quartz ± rutile) is formed under higher-pressure condition than plagioclase-bearing assemblage (garnet + two-pyroxene + plagioclase ± rutile ± ilmenite) (Pl-out line in Fig. 29). Fig. 29 shows plagioclase-out line (disappearance of plagioclase in the phase diagram) of the examined samples and the results of high P-T experiments of Green and Ringwood (1967). The results of this study demonstrated that the stability field of plagioclase strongly depends on samples, and should be evaluated by phase equilibrium modeling, implying that occurrence of plagioclase is not always a good indicator for quantitative evaluation of metamorphic pressure. For instance at 750 °C, plagioclase in sample TS11010802 becomes unstable at 9 kbar (Fig. 29), whereas the mineral in sample TS11011405A-2 is stable up to 16 kbar at 750 °C. Based on phase equilibrium modeling, plagioclase-free assemblages (garnet + clinopyroxene +

quartz + ilmenite + hornblende + biotite) in sample TS11010802 from Skallevikshalsen, the assemblages is stable under relatively lower pressure of P = 8.5-9 kbar at 750 °C (Fig. 25). In contrast, this study shows that peak P condition of sample TS11020610I from Ongul is relatively high, P = 15.5 kbar, T = 750 °C (Fig. 26), of which peak assemblages is garnet + clinopyroxene + plagioclase + hornblende + biotite + rutile. Furthermore, occurrence of quartz seems to be an important factor to discuss metamorphic evolution. Quartz in some samples (samples TS11010802, TS11011601M, and TS11020610I) is present only in garnet but not in matrix, suggesting that the mineral might have been consumed by the progress of reactions (1), (2) and (3). Saitoh et al. (2011) reported high-pressure mafic granulite from Palghat-Cauvery-suture zone, Southern India, and described a similar reaction texture (reaction 2) and argued complete consumption of quartz by reaction (2) during decompression stage. This study thus assumes that the absence of quartz is a good indicator of decompression event as well as fine-grained symplectitic orthopyroxene and plagioclase. Furthermore, phase equilibrium modeling demonstrated that stability field of quartz in the examined samples varies depending on samples. For example, Fig. 21 (results of phase equilibrium modeling of sample TS11011405A-2 from Austhovde) shows that quartz is stable at all fields in the diagram, while quartz in sample TS11020610I from Ongul is only stable at P > 10 kbar (bold-black line in Fig. 22). This study thus infers that occurrence and stability field of quartz is critical to determine P-T evolution, and it is useful to adopt phase equilibrium modeling to determine the stability field of quartz.

This study also discusses that occurrence of CMI within eleven mafic to ultramafic granulites from four exposures in the LHC (Skallevikshalsen, Skallen, Austhovde, and Ongul). CMI is dominant in core to mantle part of garnet, which suggests that CMI

might have been formed during prograde stage, garnet might have been crystalized under the presence of liquid, and garnet and CMI were regarded as in equilibrium. Widespread occurrence of CMI within pelitic to felsic granulites implies formation of CMI is not unique process in the granulites from the LHC. All CMIs are hosted in porphyroblastic garnet which always contains hydrous mineral (biotite and/or hornblende), suggesting that breakdown of these minerals are related to the formation of the CMI. Several authors argued that formation of anatectic melt during high-grade metamorphism is induced by the breakdown of hydrous mineral (e.g., Wolf and Wyllie, 1994; White et al., 2007). Similar CMIs are reported from other high-grade terrains (e.g., Sri Lankan pelitic granulite by Hiroi et al. (2014) and South Indian pelitic and felsic granulite by Cesare et al. (2009)). The occurrence of the CMI preserved in our sample is very similar in size and shape to these reports. Cesare et al. (2009) reported CMI consisting of quartz, K-feldspar, biotite, and plagioclase. Hiroi et al. (2014) reported CMI which is comprised of quartz, K-feldspar, biotite, plagioclase, aluminosilicate, and orthopyroxene. However, mineralogy of CMI reported by previous study is more aluminous (e.g., occurrence of alminosilicate and muscovite) than CMI in mafic to ultramafic granulites presented in this study, suggesting that host rock of CMI controlled mineral assemblages and mineral chemistry of the CMI.

Previous studies did not report CMI within metabasic rocks (mafic to ultramafic granulites) in detail because rare occurrence and very small size of the inclusions might have caused overlooking. It should be noted that CMI might be a direct evidence of the trace of partial melting of the host mafic to ultramafic granulites, although the examined samples show no evidence of migmatization.

8.2. *P-T* conditions and process of partial melting

This study divided partial melting processes into three stages: (1) before melt generation (below solidus), (2) during melt generation and melt extraction and (3) after melt extraction. *P-T* conditions of the three stages are discussed below.

8.2.1. Partial melting process before melt generation.

Fig. 30 shows the summary of *P-T* estimations and *P-T* paths of the examined two samples (TS11010802 from Skallevikshalsen and TS11020610I from Ongul). Solidus curves of the samples are similar each other. For example at P =10 kbar, difference of the two solidus curves is only 20-30 °C (Fig. 30). Wolf and Wyllie (1994) performed high *P-T* experiments in the system of amphibolite under 10 kbar at given temperatures, and suggested that melt generation initiated at 750 °C. Their experimental data is consistent with the results of this study, because solidus temperatures of the samples at 10 kbar are 750-760 °C (Fig. 30). Results of this study also suggest that difference of bulk chemistry (Fig. 30) does not play a critical role to determine solidus of mafic rocks.

8.2.2. Partial melting process during melt generation

This study also discusses partial melting process such as mineral reaction and *P-T* conditions of melt extraction during melt generation. Fig. 25 demonstrates that *P-T* condition of melt extraction is about 820-830 °C and 9-10 kbar. According to the

experiment of dehydration process of amphibolite by Wolf and Wyllie (1994), following dehydration reaction takes places with increasing temperature (a); Hbl + Pl → Liquid + Cpx + Ca-Al-Hbl + Grt + Opx. López and Castro (2001) also argued dehydration reaction based on high-*T* experiment and concluded that formation of liquid phase takes place through reaction (b); Hbl +Pl → Liquid ± Ep ± Grt ± Cpx ± Opx + Liquid. hornblende + plagioclase are therefore key assemblage to confirm the presence of liquid phase in the two experiments. In contrast, this study demonstrated that progress of melt extraction took place within plagioclase-free field in the phase diagram (Fig. 25). These results therefore suggest that partial melting process under plagioclase-free condition is also possible. Fig. 31 is a detailed phase diagram of a part of Fig. 25 with modal isopleths of garnet, clinopyroxene, liquid, biotite, and hornblende. As shown in the figure, modal abundance of garnet, clinopyroxene, and liquid increase as temperature rises, whereas, modal abundance of hornblende and biotite decrease with increasing temperature. This implies that decomposition of hornblende and biotite produced liquid phase, garnet, and clinopyroxene, suggesting the progress of the following reaction (c); Hbl + Bt ± Qtz → Grt + Cpx + Liq. The results are different from the melting reactions discussed in the previous studies possibly because they did not take into account the effect of potassium-bearing phases (e.g., biotite and potassium feldspar). It is therefore inferred that potassium-bearing phases should be taken into consideration during evaluation of partial melting process, because liquid phase contains considerable amount of potassium (Table 8).

Fig. 30 shows that melt extraction of sample TS11020610I from Ongul took place at *P*-*T* condition of 750 °C and 15.2 kbar, which is higher in *P* and lower in *T* than the melt extraction stage in sample TS11010802 from Skallevikshalsen (Fig. 30). In the

case of this sample, plagioclase was stable during melt generation stage (Fig. 27). Occurrence of plagioclase suggests the progress of reactions (a), (b) and (c). Peak pressure which corresponds to the stage of melt extraction is estimated by compositional isopleth of liquid in pseudosection, which confirms phase equilibrium modeling is a useful tool for evaluating partial melting process.

8.2.3. Mineralogy and *P-T* evolution after melt extraction

Mineralogy and peak *P-T* conditions after melt extraction of these rocks are obviously different between the two samples. Garnet-clinopyroxene rock (sample TS11010802) from Skallevikshalsen might be a restitic rock with CMI in garnet. Peak *P-T* condition is $T > 910$ °C and $P > 10$ kbar based on pseudosection analysis (Fig. 26). Mineralogy of the peak stage of the rock is characterized by a dry assemblage (garnet + clinopyroxene + quartz + ilmenite), which suggest that H_2O derived by decomposition of hydrous phases within garnet was concentrated into melt, and then it might have been completely removed from the system by melt extraction. Previous studies of high *P-T* experiment on modeling of amphibolites (López and Castro, 2001) and CMIs (Bartoli et al., 2013) as well as the results of this study demonstrated that considerable amount of volatile is included in liquid phases (up to 10 wt. %). Thus, after melt extraction, restitic phases should have become anhydrous. In contrast, mineral assemblage of peak stage of garnet amphibolite (sample TS11020610I) from Ongul is garnet + orthopyroxene + plagioclase + hornblende + biotite + magnetite (Fig. 28). The peak *P-T* condition of the garnet amphibolite is low (800-820 °C and 7-8 kbar) if compared to that of sample TS11010802 (garnet-clinopyroxene rock) from Skallevikshalsen. Similar peak *P-T*

condition (800-830 °C and 8-8.5 kbar) is obtained for intermediate granulite from Ongul where sample TS11020610I was collected, which suggests peak *T* condition of Ongul region is about 810-830 °C. Based on phase equilibrium modeling and estimation of peak *P-T* condition, the shape of *P-T* path after melt extraction of the sample is almost parallel to hornblende-out line (Fig. 28). This suggests that the Hbl-out line might have buffered pressure and temperature, and prevented decomposition of hornblende. Thus, sample TS11020610I preserve hornblende and biotite in the matrix as products of peak stage.

8.3. *P-T* paths of the examined areas

This study adopted *P-T* pseudosection and *P*-X pseudosection to evaluate partial melting processes. The results show partial melting of the examined samples significantly affected mineralogy, stability field of minerals, and *P-T* conditions of the rocks. In the case of sample TS11010802 from Skallevikshalsen, the bulk composition without addition of melt composition could not account for the stability field of the prograde mineralogy assemblage (Fig. 20). In contrast, pseudosection for integrated bulk composition could calculate the prograde *P-T* condition, *P-T* condition of initiation of partial melting, and *P-T* condition of melt extraction (Fig. 30). *P-T* path and peak *P-T* condition obtained from the phase equilibrium modeling of the sample is well consistent with the *P-T* estimation by conventional geothermobarometry and previous *P-T* estimations from the area (Kawakami et al., 2004; Yoshimura et al., 2004) (Figs. 17 and 32). Although, higher-pressure conditions (4-5 kbar) were obtained from another samples (TS10122502D, B97122302F2 and B97122708B) collected from the same

exposures as sample TS11010802 (Figs. 3 and 4), this study could not obtain such a high-pressure condition from sample TS11010802 because bulk chemistry might have buffered high *P* condition, and this sample does not record high *P* condition. Previous studies did not reported evidence of high *P* metamorphism from the region (e.g., garnet + kyanite + K-feldspar, jadeite-rich clinopyroxene, and magnesian staurloite), although this study and previous reports confirmed the occurrence of kyanite within porphyroblastic mineral (e.g., garnet and plagioclase), suggesting that the region experienced medium *P* type (P~12 kbar) metamorphism (Barovian type metamorphism). On the other hand, some previous petrological investigations around Lützow-Holm Bay suggested that the trace of high *P* metamorphism (e.g., Yoshida., 1978; Hiroi et al., 1991; Kawasaki et al., 2011) as discussed below. Yoshida. (1978) reported high *P* condition (P ~13.5 kbar) from charnockitic gneiss collected from Lützow-Holm Bay region, based on combination of several geothermobarometry and experimental data.
Hiroi et al. (1991) also suggested that metamorphism of the LHC is not identical to the medium-pressure type (Barrovian type) and the LHC might have been involved prograde high-pressure metamorphism. Kawasaki et al. (2011) reported high-pressure condition of $P > 15$ kbar around 1000 °C from Rundvågshetta situated on the thermal axis determined based on high *P*-*T* experimental study (Kawasaki and Motoyoshi, 2006), and occurrence of kyanite within garnet. This study thus regards such high *P* condition (P~ 15kbar) as appropriate, and characterized regional metamorphism around Lützow-Holm Bay region. Furthermore, Yoshida et al. (1976) argued there are no obvious structural boundary (major thrust and/or fault zone) in the exposure, implying that all the lithologies in the area undergone similar metamorphic evolution.

In the case of sample TS11020610I from Ongul, if the melt composition is not

considered, decompressional *P-T* evolution has been inferred (Fig. 22). If this study adopted integrated-bulk chemistry for phase equilibrium modeling, this study could determine the prograde *P-T* condition and the *P-T* condition of melt extraction (Fig. 28). Thus it is meaningful to take into consideration the effect of partial melting to discuss metamorphic evolution, even if the amount of melt extraction is small. Fig. 19 also shows the results of *P-T* estimation by conventional geothermobarometry (e.g., garnet-orthopyroxene geothermobarometer and garnet-aluminosilicate-plagioclase-quartz geobarometer) for samples from Ongul (same exposure as the garnet amphibolite for phase equilibrium modeling). A prograde *P-T* estimation by isopleth of plagioclase in the phase diagram (Fig. 27) is well consistent with the result of garnet-hornblende-plagioclase-quartz geobarometery applying to the mineral assemblage presenting as inclusions in garnet (Figs. 18 and 27). Peak-pressure condition determined by compositional isopleth and modal isopleth of liquid is slightly higher (about 1 -1.5 kbar) but nearly consistent (Figs. 19 and 27). This study thus assume the region experienced high *P* metamorphism (P~14-15 kbar) along a clockwise *P-T* path.

P-T trajectory of Austhovde is also constrained by conventional geothermobarometry and pseudosection analysis. The results are shown in Figs. 18 and 21, suggesting that the region might have experienced clockwise *P-T* path. Peak *P-T* condition of felsic granulite (830-860 °C and 8-8.5 kbar, sample TS11011407D) is consistent with the result of phase equilibrium modeling (Fig. 18). Prograde pressure condition obtained by garnet-aluminosilicate-plagioclase-quartz geobarometery to the felsic granulite (sample TS11011702G) is also consistent with the *P-T* trajectory obtained from mafic granulite (Fig. 18). These results suggest that the mafic granulite

and felsic granulite might have experienced similar metamorphic evolution. GRIPS geobarometery indicates higher-pressure condition than the estimated *P-T* path (Fig. 18). The high *P* condition is only obtained from one sample (sample TS11011504C), but it does not contain the diagnostic mineralogy of high *P* metamorphism (e.g., garnet + kyanite + K-feldspar and magnesia staurolite) like Skallevikshalsen, although the sample contains kyanite within garnet. The occurrence of kyanite is similar to the samples from Skallevikshalsen (e.g., sample TS10122502D). As style of the *P-T* paths, *P-T* conditions (Fig. 17), and occurrence of aluminosilicate of the Austhovde region (Fig. 10-u) are consistent with those of Skallevikshalsen (Figs. 10-l and 18), this study considers that Austhovde and Skallevikshalsen regions experienced similar *P-T* evolution, although relationships between medium *P* type metamorphism determined by pseudosection and geothermobarometry and high *P* condition obtained by GRIPS geobarometery is still unclear. Further petrological study related to *P-T* conditions and *P-T* paths is required. Some authors suggested that the LHC was involved high *P* metamorphism (P >13.5 kbar, e.g., Yoshida., 1978; Kawasaki et al., 2011), while several authors inferred that peak *P* conditions are below 12 kbar (e.g., Kawakami et al., 2004; Tsunogae et al., 2014). Kawasaki et al. (2011) proposed a series of *P-T* path (from P > 15 kbar to UHT condition), which imply that high *P* metamorphism is prior to the medium *P* and high *T* metamorphism along a clockwise *P-T* evolution. This study further confirmed that the evidence of high *P* metamorphism from three exposures (Skallevikshalsen, Austhovde, and Ongul). The results of this study further imply that the LHC underwent regional high *P* and high *T* metamorphism.

9. Conclusion

(1) CMIs were found from 10 mafic granulite samples which show variation of mineral assemblages such as garnet + clinopyroxene + quartz + ilmenite and garnet + quartz + plagioclase + clinopyroxene + hornblende + biotite ± rutile. These rocks preserve several decompression textures such as Grt + Cpx/Hbl + Qtz → Opx + Pl ± H_2O and Grt + Qtz → Opx + Pl probably formed by clockwise *P-T* evolution. The CMIs are 50 to 200 μm in size, preserved only in porphyroblastic garnet, and mainly consist of quartz, biotite, K-feldspar, and plagioclase.

(2) Two samples of mafic granulite with abundant CMIs; Type A (sample TS11010802) from Skallevikshalsen in the highest-grade region of the LHC, and Type B (sample TS11020610I) from Ongul in slightly lower-grade area were selected for detailed pseudosection analysis. The inferred melt composition based on modal abundance and composition of minerals in CMIs suggest generation of potassium-rich and andesitic to dacitic melts probably by dehydration melting of hornblende and biotite which often occur as inclusions in garnet. The maximum degree of melt extraction has been estimated based on pseudosection analysis as about 6.5 % (Type A) and 4.5 % (Type B). As the degree of partial melting increases, the stability field of quartz expands toward lower pressure, clinopyroxene becomes unstable, and liquid becomes more stable. The phase equilibria modeling also suggests that the melt extraction probably took place during the prograde stage.

(3) This study subsequently adopted integrated bulk compositions calculated using melt composition and the degree of melt extraction, and inferred *P-T* conditions of melt extraction stage at 820-830 °C and 9-10 kbar (Type A) and about 750 °C and

15.5 kbar (Type B). The estimated solidus temperatures of the samples are 750 °C and 780 °C, respectively, at 10 kbar, which are consistent with previous estimations of high *P-T* experiments. The estimated peak *P-T* condition (>920 °C) and *P-T* path (clockwise) of Type A are well consistent with the results of previous studies of Skallevikshalsen, while the peak pressure condition of Type B (15.5 kbar) is slightly higher (1-1.5 kbar) than that obtained from pelitic granulite in Ongul but nearly consistent. This study successfully traced the evidence of prograde partial melting and melt extraction in mafic granulites from the LHC, and determined prograde and peak *P-T* conditions based on pseudosection approach using integrated bulk compositions, which confirmed that the influence of partial melting should be taken into consideration for evaluation of high-grade metamorphism.

Acknowledgement

I would like to express my gratitude to my supervisor, Dr. T. Tsunogae at the Faculty of Life and Environmental Science, University of Tsukuba for all his support and sample collection in Antarctica. This work would not be accomplished without his continuous guidance and critical reading of the manuscript. Prof. M. Santosh at Kochi University and T.R.K Chetty at National Geophysical Research Institute are specially thanked for their supported and guidance during my field works in India.

I also wish to acknowledge to Prof. Yoji Arakawa, Masanori Kurosawa and Ken-ichiro Hayashi for their helpful discussion and encouragement.

I am deeply indebted to Dr. N. Nishida and Dr. N. Chino at the Chemical Analysis Division of the Research Facility Center for Science and Technology, University of Tsukuba for their kind assistance and guidance in the microprobe analysis.

I also thank to H. Shimizu, Oyun-Erdene, T. Endo, T. Koizumi, M. Iinuma, S. Iwamura, A. Kobayashi, A. Hiraga, and Y. Takamura of metamorphic petrology laboratory for their support and help. I want to thank to my family for their constant encouragement and support. Without their help, I could not study at the University of the Tsukuba for 3 years. Thanks are extended to graduate students at the University of Tsukuba, especially T. Shimono, D. Endo, and Y. Miyake for their helpful support and suggestion.

This study was supported by a Grant-in-Aid for JSPA Fellows to Saitoh (No.24･237).

References

Banno, S., Tatusmi, T., Kuno, H., Katura, T., 1964. Mineralogy of granulite facies rocks in the area around Lützow-Holm Bay, Antarctica. JARE Sci. Rep., Ser. C, 1,12p.

Bartoli, O., Cesare, B., Poli, S., Acosta-Vigil, A., Esposito, R., Turina, A., Bodnar, R. J., Angel, R.J., Hunter, J., 2013. Nanogranite inclusions in migmatitic garnet: behavior during piston-cylinder remelting experiments. GEOFLUIDS 13, 405-420.

Bohlen, S, R., Liotta, J, J., 1987. A Barometer for Garnet Amphibolite and Garnet Granulites. Journal of Petrology 27, 1025-1034.

Cesare, B., Ferreol, S., Salvioli, M, E., Pedron, D., Cacallo, A., 2009. "Nanogranite" and glassy inclusions: The anatectic melt in migmatites and granulites. Geology 37, 627-630.

Diener, J.F.A., Powell, R., White, R., Holland, T.J.B., 2007. A new thermodynamic model for clino- and orthoamphiboles in the system Na_2O–CaO–FeO–MgO–Al_2O_3–SiO_2–H_2O–O. Journal of Metamorphic Geology 25, 631–656.

Droop, G.T.R., 1987. A general equation for estimating Fe^{3+} concentration in ferromagnesian silicates and oxides from microprobe analyses, using stoichiometric criteria. Mineralogical Magazine 51, 431-435.

Ellis, D.J., Green, D.H., 1979. An experimental study of the effect of Ca upon garnet-clinopyroxene Fe-Mg exchange equilibria. Contributions to Mineralogy and Petrology 71, 13-22.

Ernst, W.G., Liu, J., 1998. Experimental phase-equilibrium study of Al- and Ti-contents of calcic amphibole in MORB - A semiquantitative thermobarometer. American

Mineralogist 83, 952-969.

Ganguly, J., Saxena, S, K., 1984. Mixing properties of aluminosilicate garnets: constraints from natural and experimental data, and applications to geothermo-barometry. American Mineralogist 69, 88-97.

Ganguly, J., Cheng, W., Tirone, M., 1996. Thermodynamics of aluminosilicate garnet solid solution: new experimental data, an optimized model, and thermometric applications. Contribution to Mineralogy and Petrology 126, 137-151.

Garrido, C.J., Boudiner, J.L., Burg, J.P., Zeilinger, G., Hussain, S.S., Daywood, H., Chaudhry, M.N., Gervilla, F., 2006. Petrogenesis of Mafic Garnet Granulite in the Lower Crust of the Kohistan Paleo-arc Complex (Northern Pakistan): Implications for Intra-crustal Differentiation of Island Arcs and Generation of Continental Crust. Journal of Petrology 47, 1873-1914.

Graham, C, M., Powell, R., 1984. A garnet–hornblende geothermometer: calibration, testing, and application to the Pelona Schist, Southern California. Journal of Metamorphic Geology 2, 13-31.

Green, D.H., Ringwood, A.E., 1967. An experimental investigation of the gabbro to eclogite transformation and its petrological applications. Geochimica et Cosmochimica Acta 31, 767-833.

Green, E., Holland, T., Powell, R., 2007. An order-disorder model for omphacitic pyroxenes in the system jadeite-diopside-hedenbergite-acmite, with applications to eclogitic rocks. American Mineralogist 92, 1181-1189.

Hiroi, Y., Shiraishi, K., Yanai, K., Kizaki, K., 1983. Aluminum silicates in the Prince Olav and Soya Coasts, East Antarctica. Memoirs of National Institute of Polar Research, Special issue 28, 115-131.

Hiroi, Y., Shiraishi, K., Motoyoshi, Y., 1991. Late Proterozoic paired metamorphism complexes in East Antarctica , with special reference to the tectonic significance of ultramafic rocks. Geological Evolution of Antarctica, Cambridge University Press 1991.

Hiroi, Y., Motoyoshi, Y., Ishikawa, N., Hokada, T., Shiraishi K., 2008. Origin of xenocrystic garnet and kyanite in clinopyroxene–hornblende-bearing adakitic meta-tonalites from Cape Hinode, Prince Olav Coast, East Antarctica. Geological Society of London Special Publication 308, 333-350.

Hiroi, Y., Yanagi, A., Kato, M., Kobayashi, T., Prame, B., Hokada, T., Satish, K, M., Ishikawa, M., Adachi, T., Osanai, Y., Motoyoshi, Y., Shiraishi, K., 2014. Supercooled melt inclusions in lower-crustal granulites as a consequence of rapid exhumation by channel flow. Gondwana Research 25, 226-234.

Holland, T.J.B., Powell, R., 1990. An enlarged and updated internally consistent thermodynamic dataset with uncertainties and correlations: the system K_2O–Na_2O–CaO–MgO–MnO–FeO–Fe_2O_3–Al_2O_3–TiO_2–SiO_2–C–H_2–O_2. Journal of Metamorphic Geology 8, 89-124.

Holland, T., Blundy, J., 1994. Non-ideal interactions in calcic amphiboles and their bearing on amphibole-plagioclase thermometry. Contributions to Mineralogy and Petrology 116, 433-447.

Holland, T., Powell, R., 2003. Activity–composition relations for phases in petrological calculations: an asymmetric multicomponent formulation. Contributions to Mineralogy and Petrology 145, 492-501.

Ikeda, T., Kawakami, T., 2004. Structural analysis of the Lutzow-Holm Complex in Akarui Point, East Antarctica, and overview of the complex. Polar Geoscience 17,

22-34.

Indares, A., White, R., Powell, R., 2008. Phase equilibria modelling of kyanite-bearing anatectic paragneisses from the central Grenville Province. Journal of Metamorphic Geology 26, 815-836.

Ishikawa, M., Shiraishi, K., Motoyoshi, Y., Tsuchiya, N., Shimura, T., Yanai, K., 1994. Geological map of the Ongul Island Lützow-Holm Bay, Antarctica. Antarctica Geological Map series, Sheet 36 (with explanatory text 21p). Tokyo, National Institute of Polar Research.

Iwamura, S., Tsunogae, T., Kato, M., Koizumi, T., Dunkley, D., 2013. Petrology and phase equilibrium modeling of spinel-sapphirine-bearing mafic granulite from Akarui Point, Lützow-Holm Complex, East Antarctica: Implications for the P-T path. Journal of Mineralogical and Petrological Sciences 108, 345-350.

Kawakami, T., Ikeda, T., 2004a. Timing of ductile deformation and peak metamorphism in Skallevikshalsen, Lutzow-Holm Complex, East Antarctica. Polar Geoscience 17, 1-11.

Kawakami, T., Ikeda, T., 2004b. Structural evolution of the Ongul Islands, Lutzow-Holm Complex, East Antarctica. Polar Geoscience 17, 12-21.

Kawakami, T., Motoyoshi, Y., 2004. Timing of attainment of the spinel + quartz coexistence in garnet-sillimanite leucogneiss from Skallevikshalsen, Lützow-Holm Complex, East Antarctica. Journal of Mineralogical and Petrological Sciences 99, 311-319.

Kawasaki, T., Motoyoshi, Y., 2006. Experimental constraints on the decompressional *P-T* path of Rundvågshetta Granulites, Lützow–Holm complex, East Antarctica. Fütterer, D.K., Damaske, D., Kleinschmidt, G., Miller, H., Tessensohn, F., (Eds.), Antarctica:

Contributions to Global Earth Sciences, Berlin, Springer (2006), 23–36.

Kawasaki, T., Nakano, N., Osanai, Y., 2011. Osumilite and a spinel + quartz association in garnet–sillimanite gneiss from Rundvågshetta, Lützow-Holm Complex, East Antarctica. Gondwana Research 19, 430-445.

Kawasaki, T., Adachi, T., Nakano, N., Osanai, Y., 2013. Possible armalcolite pseudomorph-bearing garnet–sillimanite gneiss from Skallevikshalsen, Lützow-Holm Complex, East Antarctica: Implications for ultrahigh-temperature metamorphism. Geological Society, London, Special Publications 383, 135-167.

Kohn, M, J., Spear, F, S., Two new geobarometers for garnet amphibolites, with applications to southeastern Vermont. American Mineralogist 75, 89-96.

Koizumi, T., Tsunogae, T., Santosh, M., Tsutsumi, Y., Chetty, T.R.K., Saitoh, Y., 2014. Petrology and zircon U–Pb geochronology of metagabbros from a mafic–ultramafic suite at Aniyapuram: Neoarchean to Early Paleoproterozoic convergent margin magmatism and Middle Neoproterozoic high-grade metamorphism in southern India. Journal of Asian Earth Sciences 95, 51-64.

Leake, B.E., Woolley, A.R., Arps, C.E.S., Birch, W.D., Gilbert, M.C., Grice, J.D., Hawthorne, F.C., Kato, A., Kisch, H.J., Krivovichev, V.G., Linthout, K., Laird, J., Mandarino, J.A., Maresch, W.V., Nickel, E.H., Rock, N.M.S., Schumacher, J.C., Smith, D.C., Stephenson, N.C.N., Ungaretti, L., Whittaker, E.J.W., Youzhi, G., 1997. Nomenclature of amphiboles: Report of the Subcommittee on Amphiboles of the International Mineralogical Association, Commission on New Minerals and Mineral Names. American Mineralogist 82, 1019-1037.

Lee, H.Y., Ganguly, J., 1988. Equilibrium Compositions of Coexisting Garnet and Orthopyroxene: Experimental Determinations in the System FeO-MgO-Al_2O3-SiO_2,

and Applications. Journal of Petrology 29, 93-113.

Liu, P., Liu, F., Liu, C., Wang, F., Liu, J., Yang, H., Cai, J., Shi, J, C., 2013. Petrogenesis, P–T–t path, and tectonic significance of high-pressure mafic granulites from the Jiaobei terrane, North China Craton. Precambrian Research 233, 237-258.

López, S., Castro, A., 2001. Determination of the fluid-absent solidus and supersolidus phase relationships of MORB-derived amphibolites in the range 4-14 kbar. American Mineralogist 86, 1396-1403.

Moecher, D.P., Essene, E.J., Anovitz, L.M., 1988. Calculation and application of clinopyroxene-garnet-plagioclase-quartz geobarometers. Contributions to Mineralogy and Petrology 100, 92-106.

Newton, R.C., Charlu, T.V., Kleppa, O.J., 1980. Thermochemistry of the high structural state plagioclases. Geochimica et Cosmochimica Acta 44, 933-941.

Nicolaysen, L.O., Burger. A.J., Tatsumi, T., Ahrens, L.H., 1961. Age measurements on pegmatites and a basic charnockite lens occurring near Lützow-Holm Bay, Antarctica. Geochimica et Cosmochimica Acta 22, 94-98.

Nogi, Y., Jokat, W., Kitada, K., Steinhage, D., 2013. Geological structures inferred from airborne geophysical surveys around Lützow-Holm Bay, East Antarctica. Precambrian Research 234, 279-287.

O'Brien, P, J., Rötzler, J., 2003. High-pressure granulites: formation, recovery of peak conditions and implications for tectonics. Journal of Metamorphic Geology 21, 3-20.

Osanai, Y., Toyoshima, T., Owada, M., Tsunogae, T., Hokada, T., Crowe, T., Ikeda, T., Kawano, U., Kawasaki, T., Ishikawa, M., Motoyoshi, Y., Shiraishi, K., 2004. Geological map of Skallen, Antarctica (Revised version). Antarctica Geology Map

Series, Sheet 39 (with explanatory text 23). Tokyo, National Institute of Polar Research.

Osanai, Y., Sajeev, K., Owada, M., Kehelpannala, K.V.W., Prame, W.K.B., Nakano, N., Jayatileke, S., 2006. Metamorphic evolution of high-pressure and ultrahigh-temperature granulites from the Highland Complex, Sri Lanka. Journal of Asian Earth Sciences 28, 20-37.

Pattision, D.R.M., Chacko, T., Farquhar, J., McFarlance, C.R.M., 2003. Temperatures of Granulite-facies Metamorphism: Constraints from Experimental Phase Equilibria and Thermobarometry Corrected for Retrograde Exchange. Journal of Petrology 44, 867-900.

Perkins, D., Newton, R.C., 1981. Charnockite geobarometers based on coexistence garnet-pyroxene-plagioclase-quartz. Nature 292, 144-146.

Rollinson, R, H., 1993. Using Geochemical Data: Evaluation, Presentation, Interpretation. Longman, 352p.

Rudnick, R, L., Fountain, D, M., 1995. Nature and composition of the continental crust: A lower crustal perspective. Reviews of Geophysics. 33, 267-309.

Saitoh, Y., Tsunogae, T., Santosh, M., Chetty, T.R.K., Horie, K., 2011. Neoarchean high-pressure metamorphism from the northern margin of the Palghat–Cauvery Suture Zone, southern India: Petrology and zircon SHRIMP geochronology. Journal of Asian Earth Sciences. 42, 268-285.

Sajeev, K., Jeong. J., Kwon, S., Kee, W-S., Kim. S.W., Komiya , T., Itaya, T., Jung, H-S., Park, Y., 2010. High P-T granulite relicts from the Imjingang belt, South Korea: tectonic significance. Gondwana Research 17, 75-86.

Santosh, M., Yoshida, M., 1992. A petrologic and fluid inclusion study of charnockites

from the Lützow-Holm Bay region, East Antarctica: Evidence for fluid-rich metamorphism in the lower crust. Lithos 29, 107-126.

Satish-Kumar, M., Miyamoto, T., Hermann, J., Kagami, H., Osanai, Y., Motoyoshi, Y., 2008. Pre-metamorphic carbon, oxygen and strontium isotope signature of high-grade marbles from the Lützow-Holm Complex, East Antarctica: apparent age constraints of carbonate deposition. Geological Society of London Special Publication 308, 145-164.

Shibata, K., Yanai, K., Shiraishi, K., 1985. Rb-Sr mineral isochron ages of metamorphic rocks around Syowa Station and from Yamato Mountains, East Antarctica. Mem. Natl Inst. Polar Res., Spec. Issue 37, 164-171.

Shiraishi, K. Yoshida, M., 1987. Geological map of the Botnneset, Antarctica. Antarctica Geology Map series, Sheet 25 (with explanatory text 9p). Tokyo, National Institute of Polar Research.

Shiraishi, K., Hiroi, Y., Motoyoshi, Y., Yanai, K., 1987. Plate tectonic development of late proterozoic paired metamorphic complexes in eastern Queen Maud Land, East Antarctica. Gondwana Six: Structure, Tectonics, and Geophysics 40, 309-318.

Shiraishi, K., Ellis, D.J., Hiroi, Y., C. M. Fanning, Motoyoshi, Y., Y, Nakai., 1994. Cambrian Orogenic Belt in East Antarctica and Sri Lanka: Implications for Gondwana Assembly. The Journal of Geology 102, 47-65.

Shiraishi, K., Hokada, T., Fanning, C.M., Misawa, K., 2003. Timing of thermal events in eastern Dronning Maud Land, East Antarctica. Polar Geoscienice 16, 76-99.

Shiraishi, K., Dunkley, D.J., Hokada, T., Fanning, C.M., Kagami, T., Hamamoto, T., 2008. Geochronological constraints on the late Proterozoic to Cambrian crustal evolution of Eastern Dronning Maud Land, East Antarctica: a synthesis of SHRIMP

U-Pb age and Nd model age data. Geological Society, London, Special Publications 308, 21-67

Skjerlie, K, P, Johnston, A, D., 1993. Fluid-Absent Melting Behavior of an F-Rich Tonalitic Gneiss at Mid-Crustal Pressures: Implications for the Generation of Anorogenic Granites. Journal of Petrology 34, 785-815.

Spear., F, S., 1993. Metamorphic Phase Equilibria and Pressure-Temperature-Time Paths. Mineralogical Society of America, 799p.

Suda, Y., Kawano, Y., Yaxley, G., Korenaga, H., Hiroi, Y., 2008. Magmatic evolution and tectonic setting of metabasites from Lützow-Holm Complex, East Antarctica. Geodynamic Evolution of East Antarctica: A Key to the East-West Gondwana Connection. Geological Society of London Special Publication 308, 211-233.

Suzuki, M., 1983. Preliminary note on the metamorphic conditions around Lützow -Holm Bay, East Antarctica. Mem. Natl Inst. Polar Res., Spec. Issue 28, 132-143.

Tomkins, H.S., Powell, R., Ellis, D.J., 2007. The pressure dependence of the zirconium-in-rutile thermometer. Journal of Metamorphic Geology 25, 703-713.

Tsunogae, T., Santosh, M., 2006. Spinel–sapphirine–quartz bearing composite inclusion within garnet from an ultrahigh-temperature pelitic granulite: Implications for metamorphic history and P–T path. Lithos 92, 524-536.

Tsunogae, T., Dunkley, D.J., Horie, K., Endo, T., Miyamoto, T., Kato, M., 2014. Petrology and SHRIMP zircon geochronology of granulites from Vesleknausen, Lützow-Holm Complex, East Antarctica: Neoarchean magmatism and Neoproterozoic high-grade metamorphism. Geoscience Frontiers 5, 167-182.

Vielzeuf, D., Holloway, J, R., 1988. Experimental determination of the fluid-absent melting relations in the pelitic system Consequences for crustal differentiation.

Contributions to Mineralogy and Petrology 98, 257-576.

Walther, J.V., Wood, B.J., (Eds.) 1986. Fluid-Rock Interactions during Metamorphism. Springer, 218p.

White, R.W., Powell, R., Holland, T.J.B., Worley, B.A., 2000. The effect of TiO_2 and Fe_2O_3 on metapelitic assemblages at greenschist and amphibolite facies conditions: mineral equilibria calculations in the system K_2O–FeO–MgO–Al_2O_3–SiO_2–H_2O–TiO_2–Fe_2O_3. Journal of Metamorphic Geology 18, 497-511.

White, R.W., Powell, R., Clarke, G.L., 2002. The interpretation of reaction textures in Fe-rich metapelitic granulites of the Musgrave Block, central Australia: constraints from mineral equilibria calculations in the system K_2O–FeO–MgO–Al_2O_3–SiO_2–H_2O–TiO_2–Fe_2O_3 . Journal of Metamorphic Geology 20, 41-55.

White, R.W., Powell, R., Holland, T.J.B., 2007. Progress relating to calculation of partial melting equilibria for metapelites. Journal of Metamorphic Geology 25, 511-527.

Wolf, M, B., Wyllie. P, J., 1994. Dehydration-melting of amphibolite at 10 kbar: the effects of temperature and time. Contributions to Mineralogy and Petrology 115, 369-383.

Yanai, K., Kizaki, K., Tatsumi, T., Kikuchi, T., 1974a. Geological map of East Ongul Island, Antarctica. Antarctica Geology Map Series, Sheet 1 (with explanatory text 13p). Tokyo, National Institute of Polar Research.

Yanai, K., Tatsumi, T., Kikuchi, T., 1974b. Geological map of West Ongul Island, Antarctica. Antarctica Geology Map Series, Sheet 2 (with explanatory text 5p).

Tokyo, National Institute of Polar Research.

Yoshida, M., Yoshida, Y., Ando, H., Ishikawa, T., Tatsumi, T., 1976. Geological map of the Skallen, Antarctica. Antarctica Geology Map series, Sheet 9 (with explanatory text 16p). Tokyo, National Institute of Polar Research.

Yoshida, M., 1978. Tectonics and petrology of charnockites around Lützow-Holmbukta, East Antarctica. Journal of Geosciences, Osaka City University 21, 65-152.

Yoshida, M., Akiwa, N., 1983. Petrography of a discordant metabasite from Skallen, Lützow-Holmbukuka, East Antacctica. Mem. Natl Inst. Polar Res., Special. Issue, 28, 144-165.

Yoshimura, Y., Motoyoshi, Y., Miyamoto, T., Grew, S. E., Carson, J. Christopher., Dunkley, J. Daniel., 2004. High-grade metamorphic rocks from Skallevikshalsen in the Lützow-Holm Complex, East Antarctica: metamorphic conditions and possibility of partial melting. Polar Geoscience 17, 57-87.

Yoshimura, Y., Motoyoshi, Y., Miyamoto, T., 2008. Sapphirine + quartz association in garnet: implication for ultrahigh-temperature metamorphism in Rundvågshetta, Lützow-Holm Complex, East Antarctica. Geodynamic Evolution of East Antarctica: A Key to the East-West Gondwana Connection. Geological Society of London Special Publication 308, 377-390.

Zack, T., Moraes, R., Kronz, A., 2004. Temperature dependence of Zr in rutile: empirical calibration of a rutile thermometer. Contributions to Mineralogy and Petrology 148, 471-478.

Zhang, J, X., Mattinson, F, C., Meng, F, C., Wan, Y, S., 2005. An Early Palaeozoic HP/HT granulite–garnet peridotite association in the south Altyn Tagh, NW China: P–T history and U-Pb geochronology. Journal of Metamorphic Geology 23, 491-510

Zhang, X, R., Shi, R, D., Huang, Q, S., Liu, D, L., Cidan, S, L., Yang, J, S., Ding, L., 2010. Finding of high-pressure mafic granulites in the Amdo terrane, central Tibet Chinese Science Bulletin 55, 3694-3702

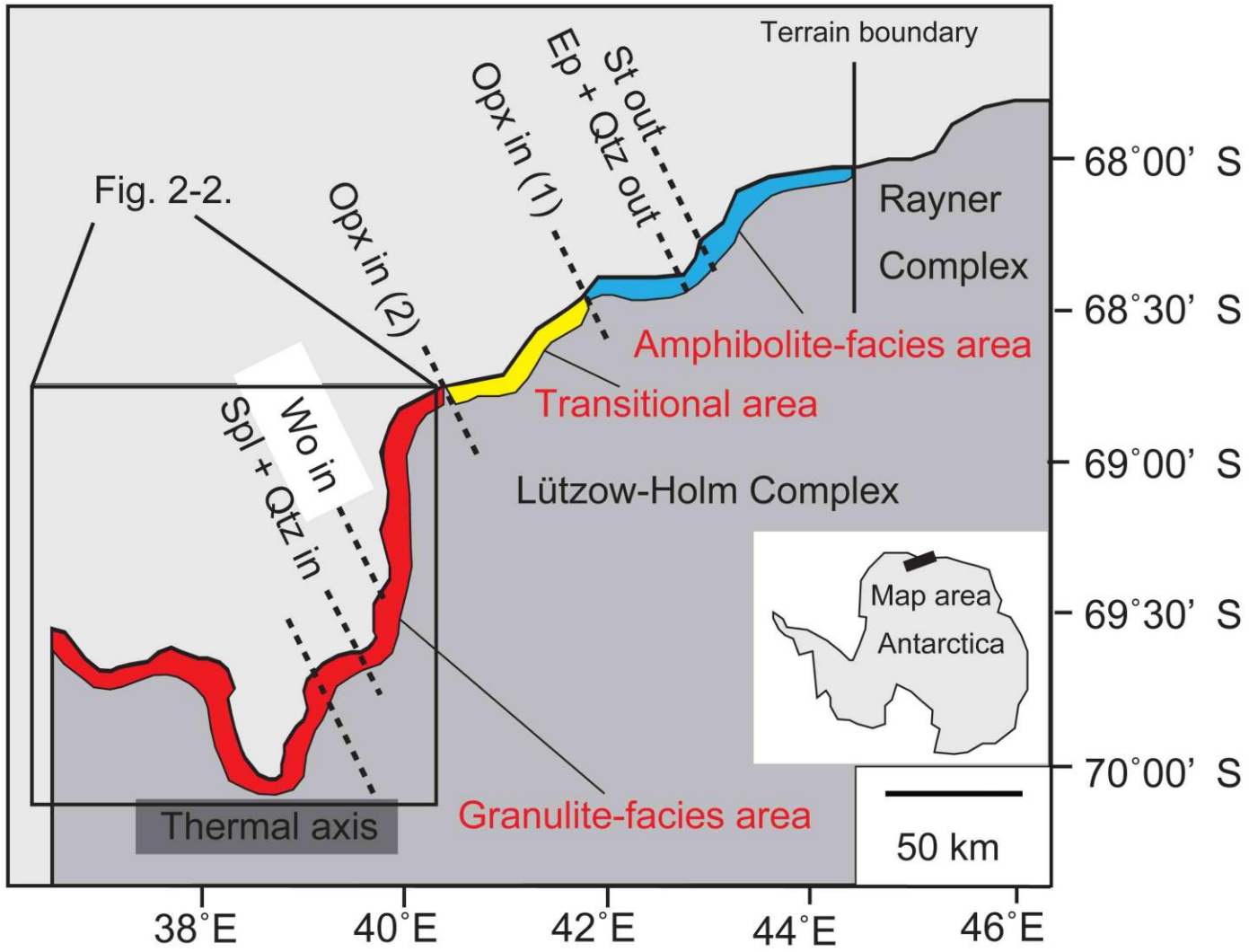

Fig. 1. Simplified map of the LHC showing terrain boundary, their metamorphic facies and localities of isograds modified after Hiroi et al. (1991).

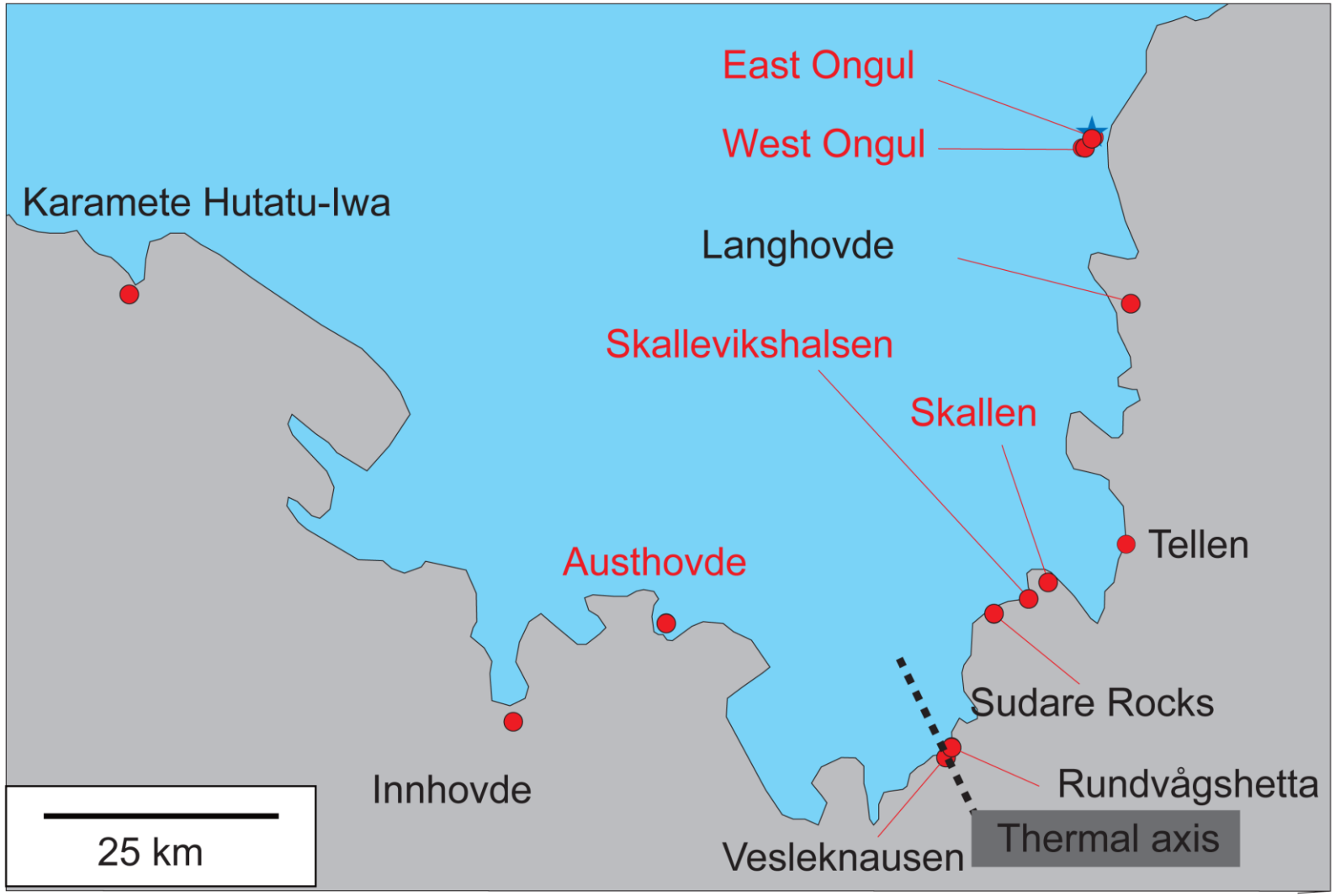

Fig. 2. Location map of exposures in granulite-facies area. Exposures in red imply localities of examined samples.

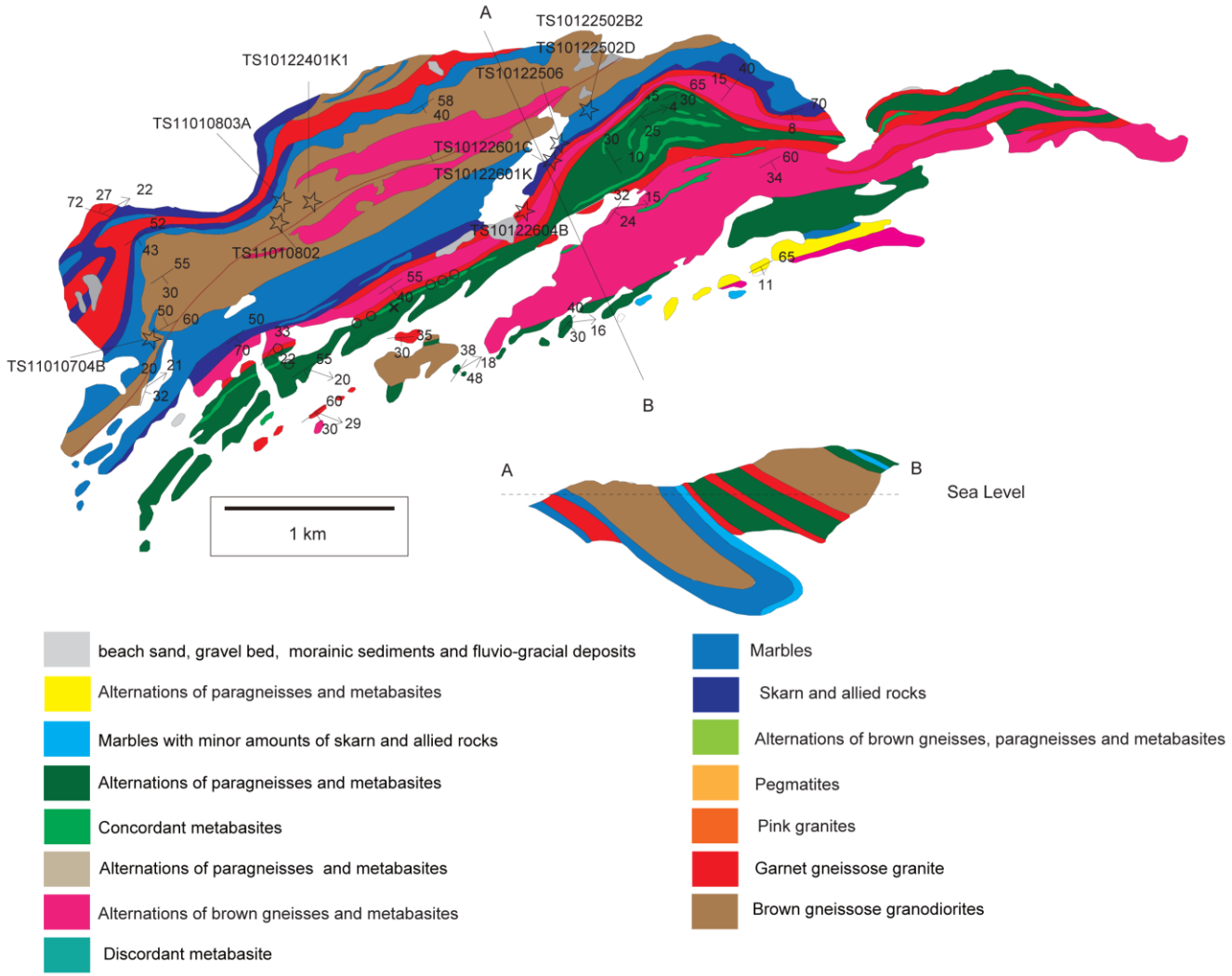

Fig. 3. Geological map of the Skallevikshalsen region after Yoshida et al. (1976). Stars denote sample localities discussed in the text.
Circle points show localities of the examined samples discussed in Yoshimura et al. (2004). "×" point indicates the locality of Spl + Qtz bearing rock reported by Kawakami et al. (2004).

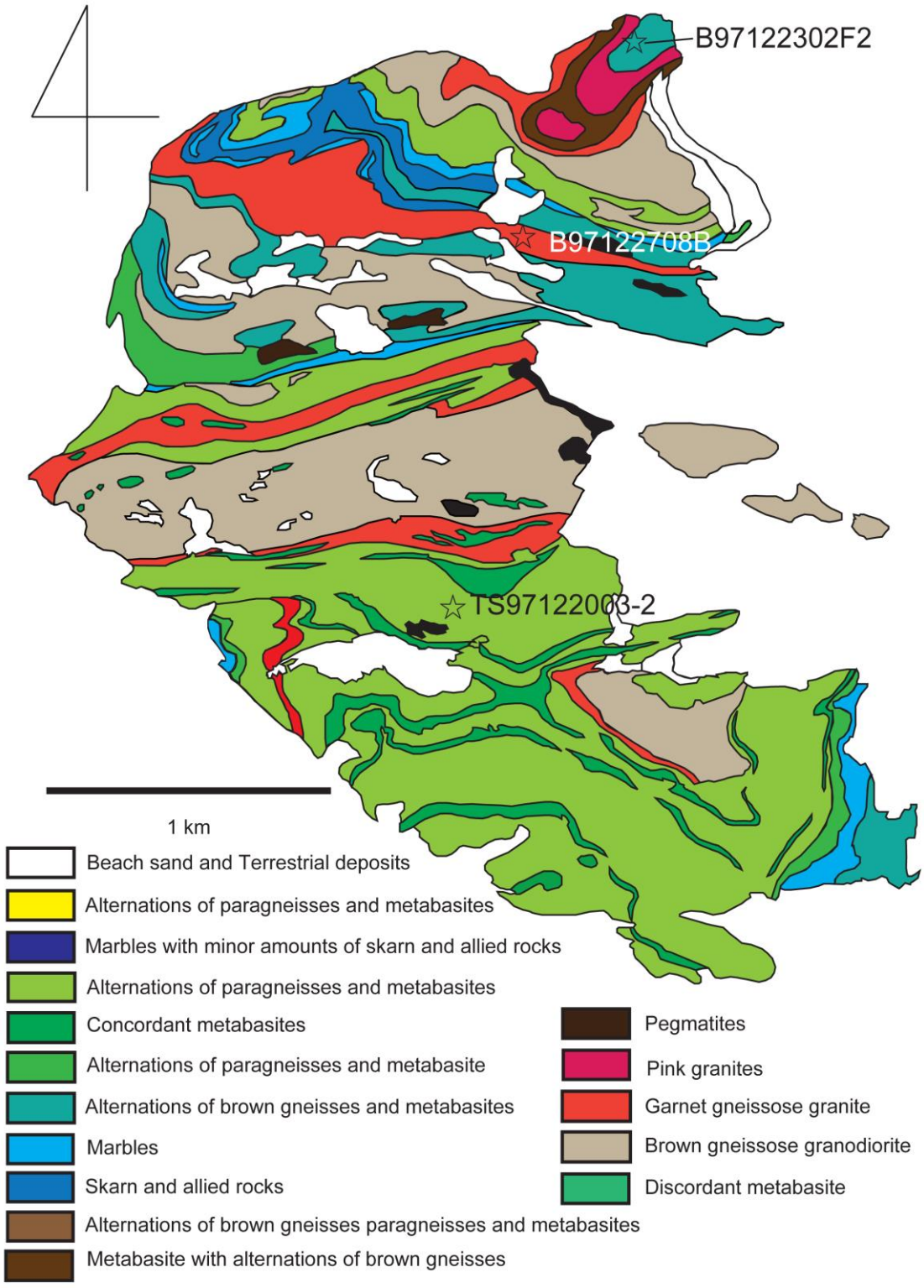

Fig. 4. Geological map of the Skallen region after Yoshida et al. (1976). Stars denote sample localities discussed in the text.

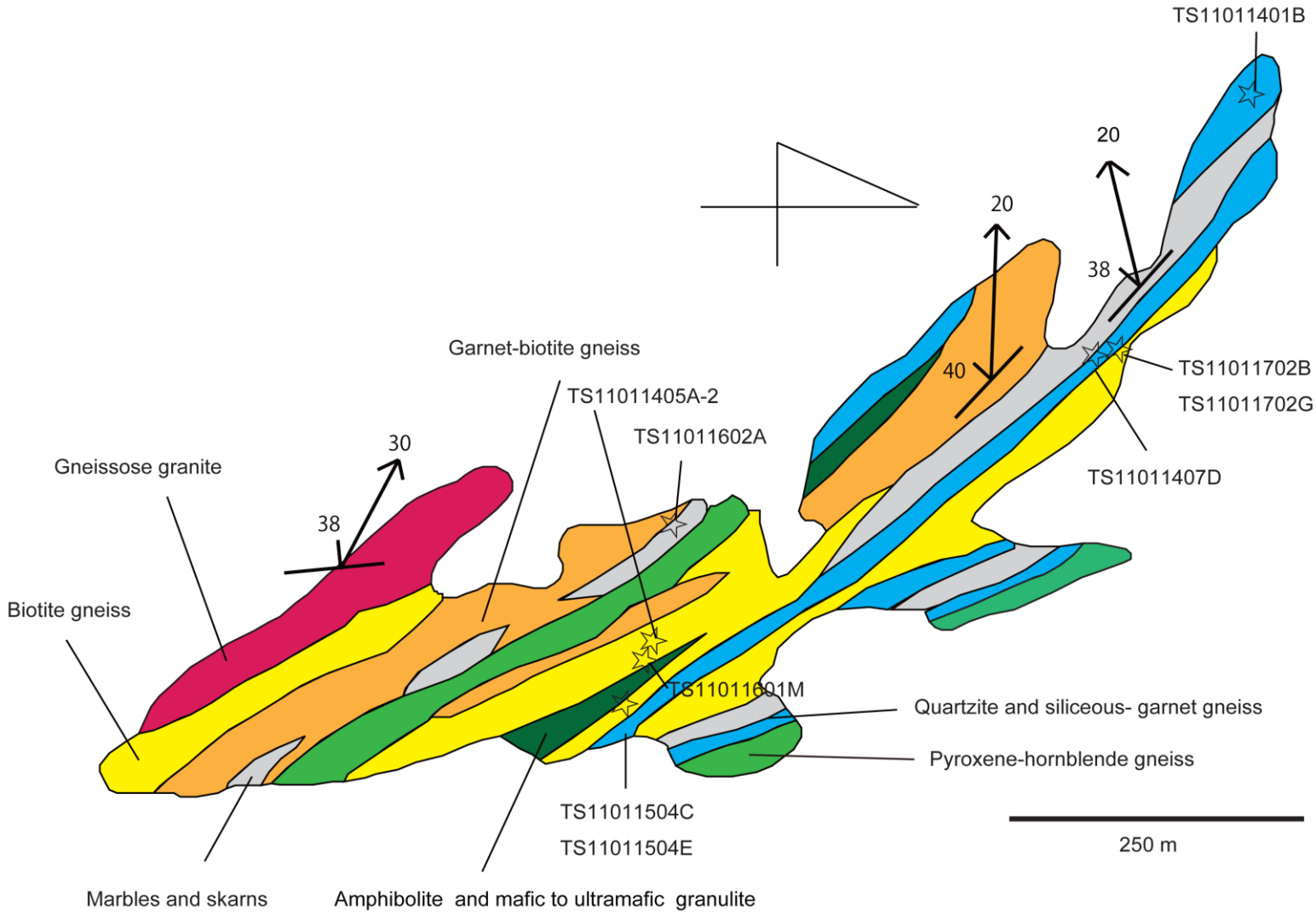

Fig. 5. Geological map of the Austhovde region after Shiraishi and Yoshida (1987). Stars denote sample localities discussed in the text.

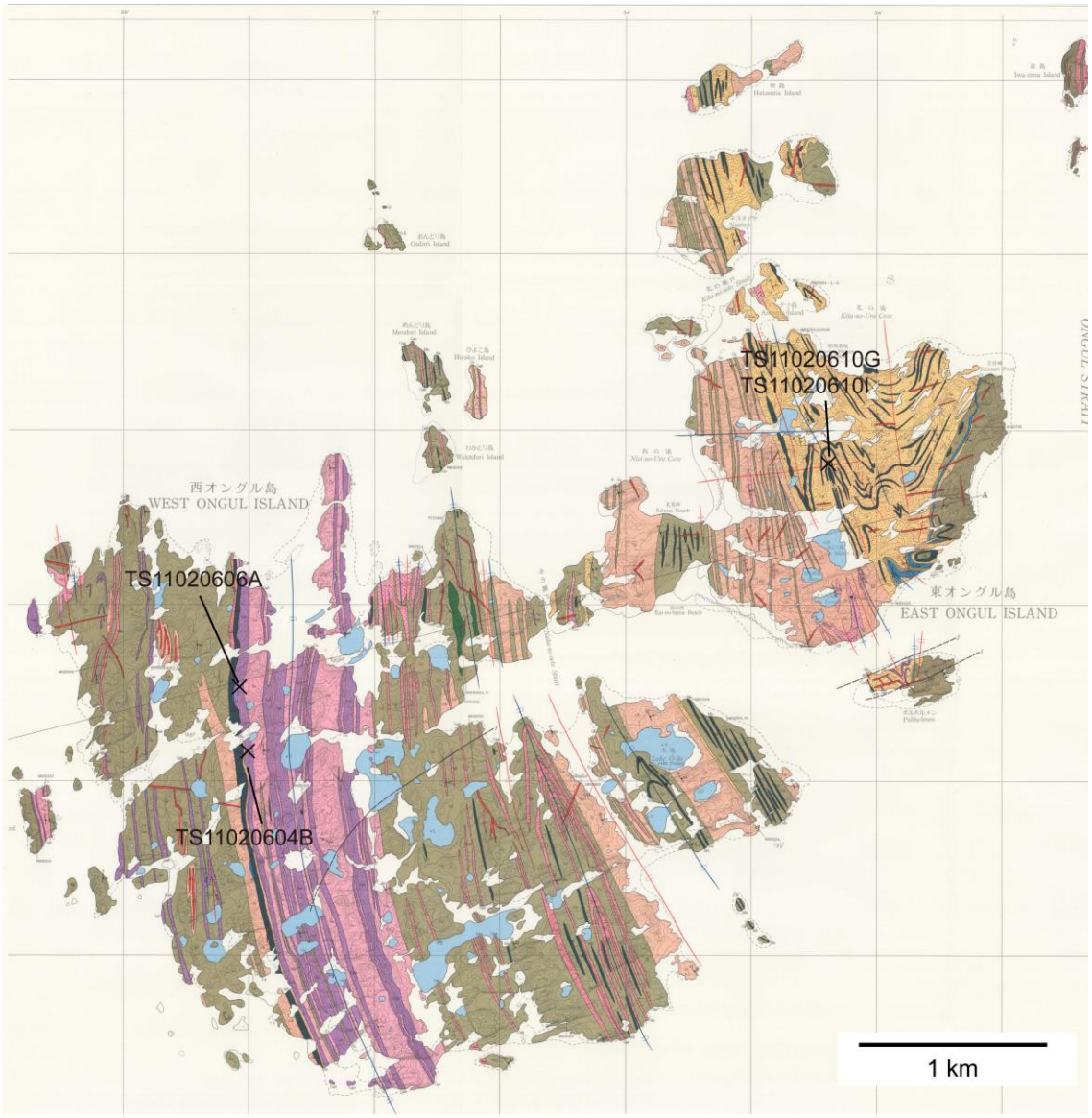

Fig. 6. Geological map of the Ongul region after Ishikawa et al. (1996). “×” show localities of samples discussed in the text.

Fig. 6. Continued.

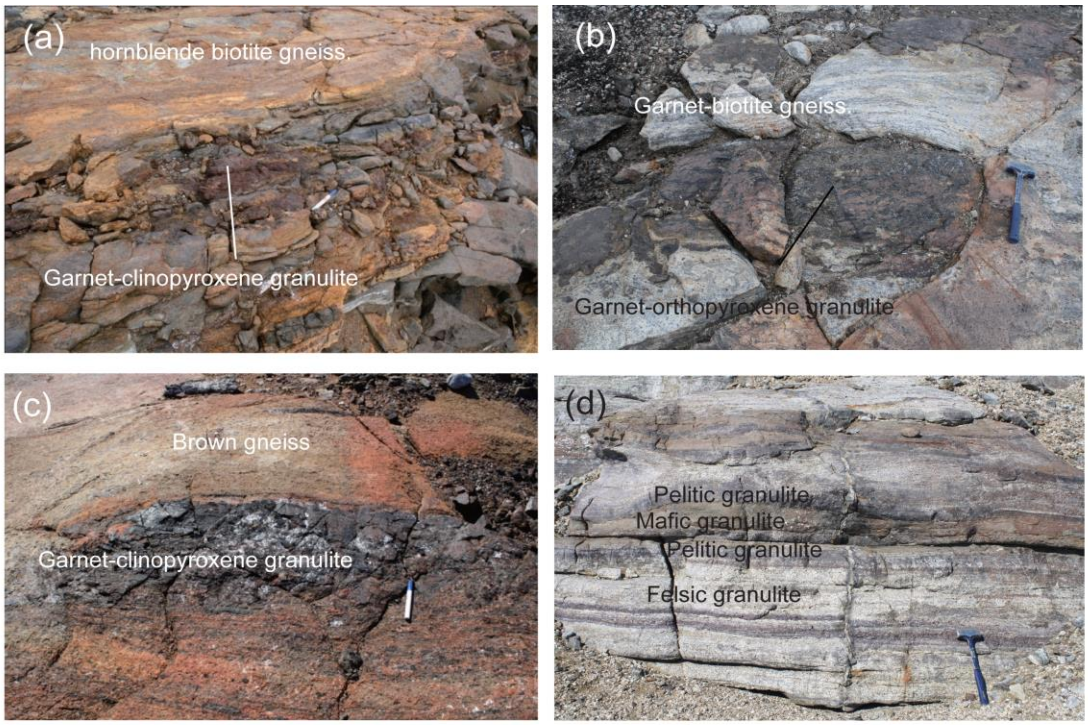

Fig. 7. Field occurrence of garnet-clinopyroxene granulite, garnet-orthopyroxene granulite, and felsic granulite in Skallevikshalsen. (a) Garnet-clinopyroxene granulite occuring as a lenticular block in hornblende-biotite gneiss. (b) Garnet-orthopyroxene granulite enclosed in garnet-biotite gneiss. (c) Garnet-clinopyroxene granulite enclosed in brown gneiss. (d) Felsic granulite, pelitic granulite, and mafic granulite showing alternative layering.

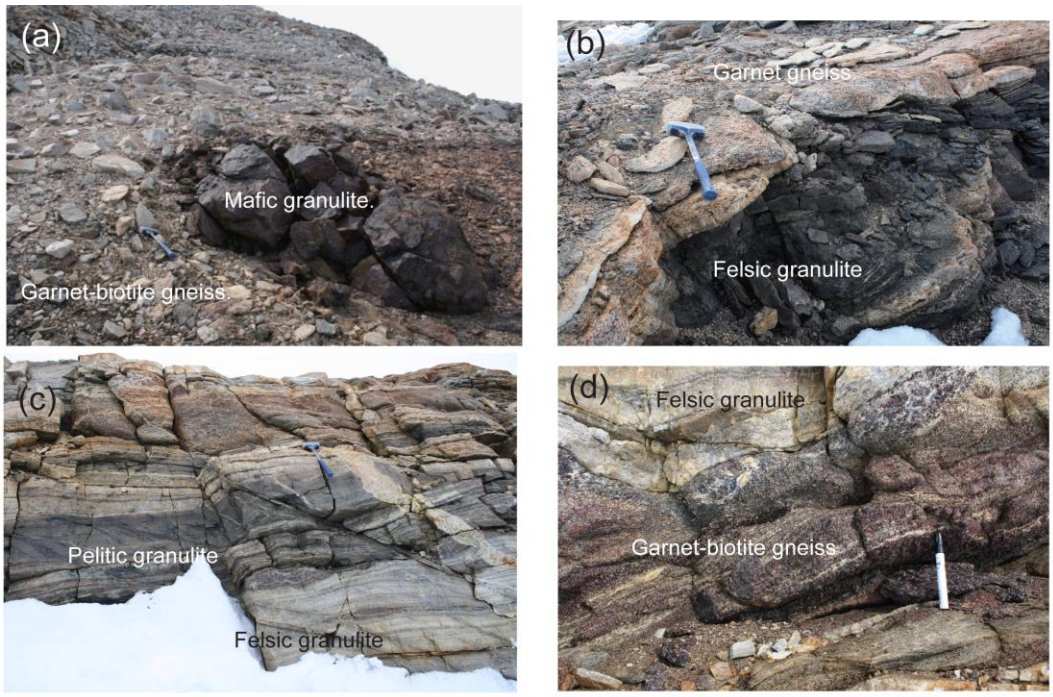

Fig. 8. Field occurrence of mafic granulite, felsic granulite, and garnet-biotite gneiss in Austhovde. (a) Mafic granulite occuring as a lenticular block in garnet-biotite gneiss. (b) Felsic granulite enclosed in garnet gneiss. (c) Felsic granulite showing alternative layering with pelitic granulite. (d) Garnet-biotite gneiss and felsic granulite occuring as alternative layers.

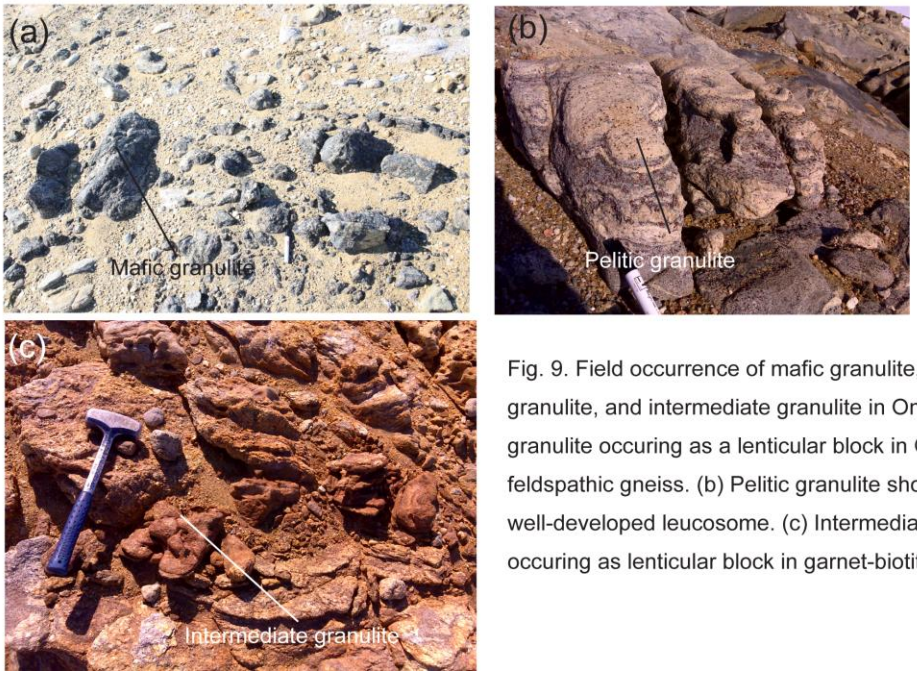

Fig. 9. Field occurrence of mafic granulite, pelitic granulite, and intermediate granulite in Ongul. (a) Mafic granulite occuring as a lenticular block in Quarzto-feldspathic gneiss. (b) Pelitic granulite showing well-developed leucosome. (c) Intermediate granulite occuring as lenticular block in garnet-biotite gneiss.

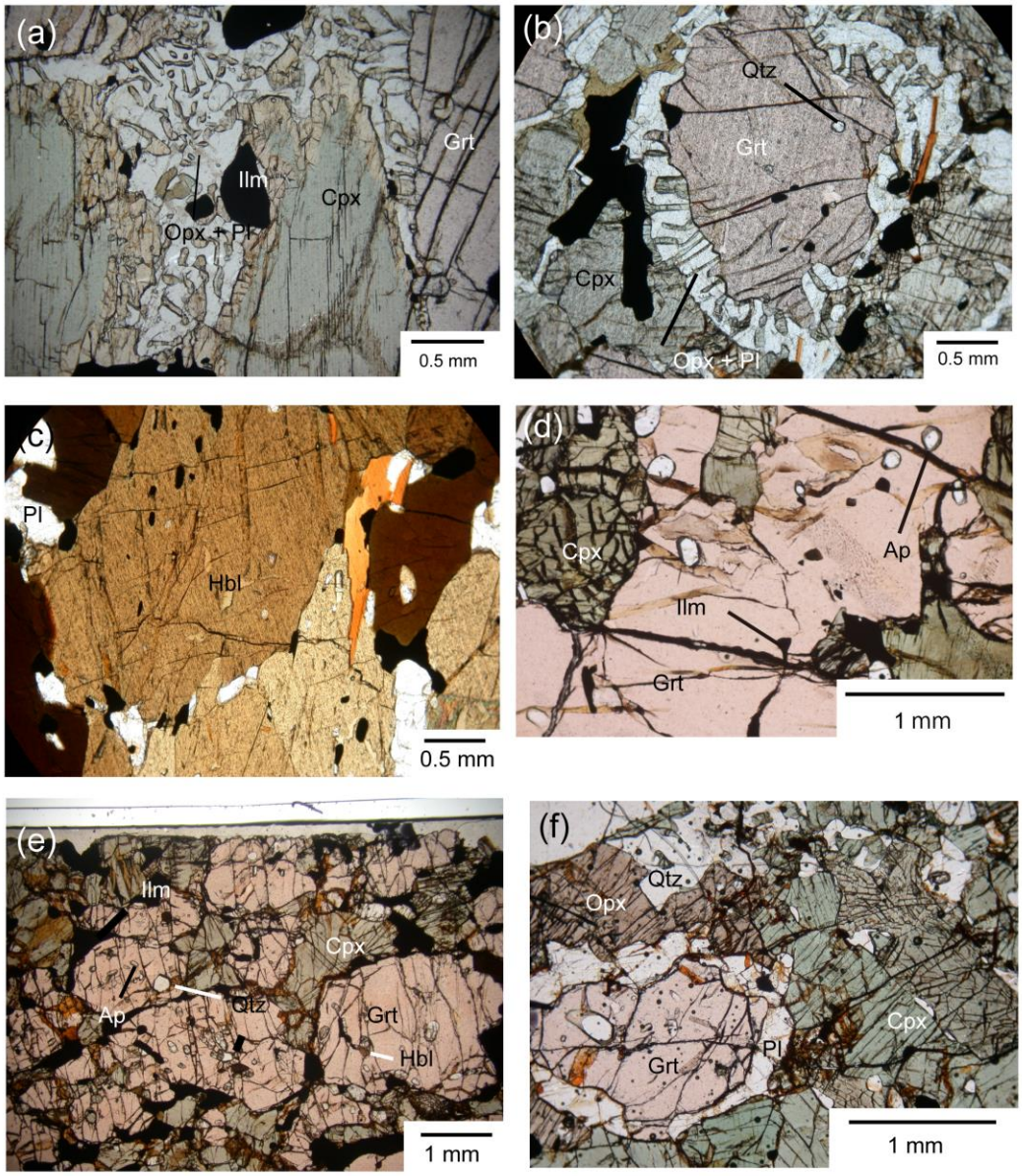

Fig. 10. Various textures of granulites of examined samples. (a) Coarse-grained garnet and clinopyroxene partly replaced by fine-grained orthopyroxene + plagioclase intergrowth (sample TS11010802). (b) Coarse-grained garnet and clinopyroxene partly replaced by fine-grained orthopyroxene + plagioclase intergrowth (sample TS10122506). (c) Hornblende-rich part of sample TS10122506. (d) Garnet-clinopyroxene rock with garnet, clinopyroxene, and ilmenite (sample TS11010704B). (e) Garnet-clinopyroxene rock (sample TS11010803A). It is characterized by abundant garnet, clinopyroxene, and ilmenite without any reaction textures. (f) Garnet-two-pyroxene granulite from Austhovde. It is characterized by occurrence of garnet + two pyroxenes + plagioclase + quartz with no reaction texture (TS11011405A-2).

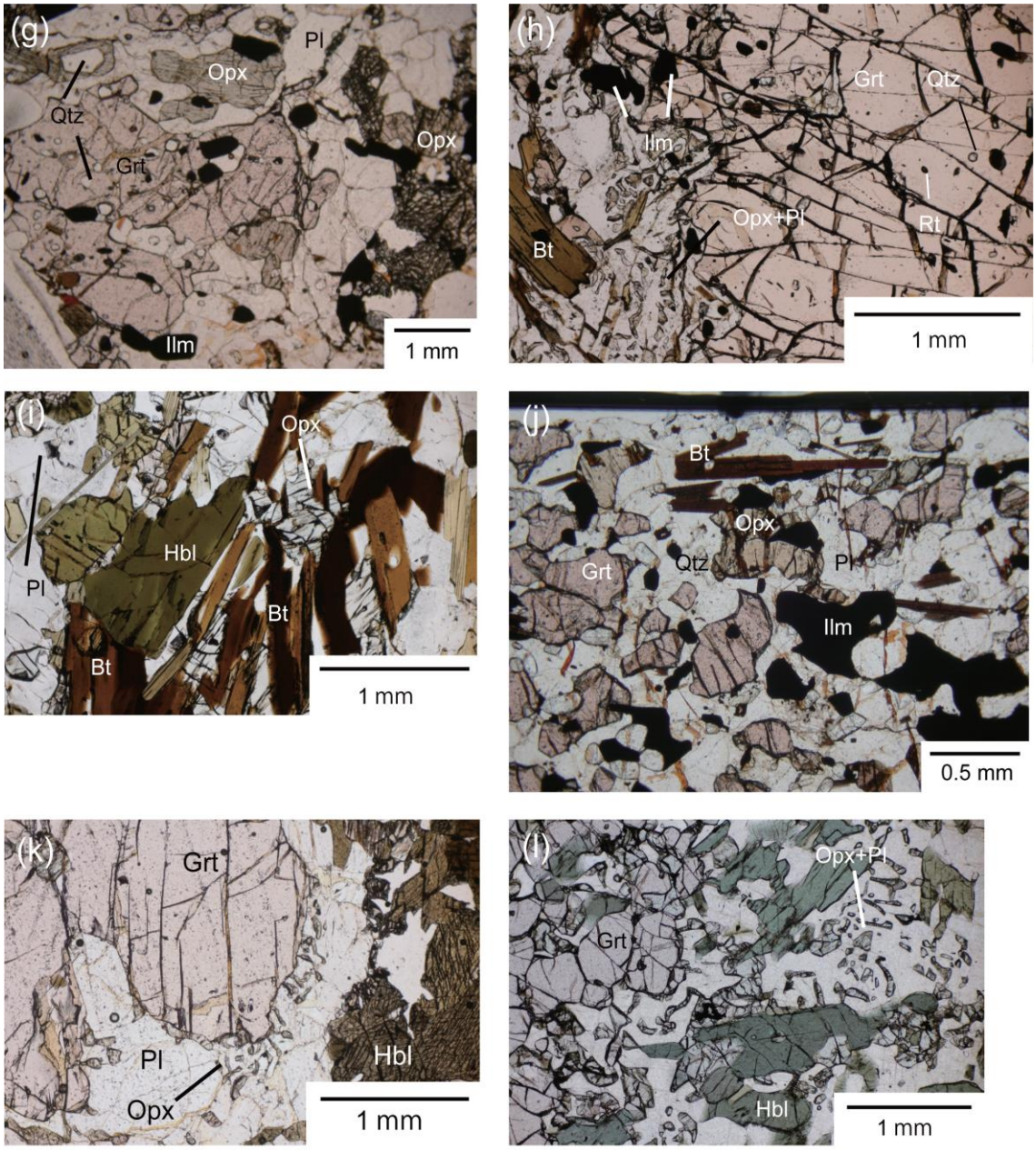

Fig. 10. Continued. (g) Garnet-orthopyroxene granulite characterized by coarse-grained garnet and orthopyroxene (sample TS10122604B). (h) Garnet-orthopyroxene granulite characterized by coarse-grained garnet and occurrence of rutile (sample TS97122302F2). (i) Hornblende and biotite occuring in matrix (sample TS97122302F2). (j) Garnet-orthopyroxene granulite (sample TS11020206H). (k) Garnet amphibolite showing intergrowth of orthopyroxene + plagioclase between grain boundaries of garnet and hornblende (sample TS11011601M). (l) Garnet amphibolite characterized by well-developed intergrowth of orthopyroxene and plagioclase (sample TS11020610G-2).

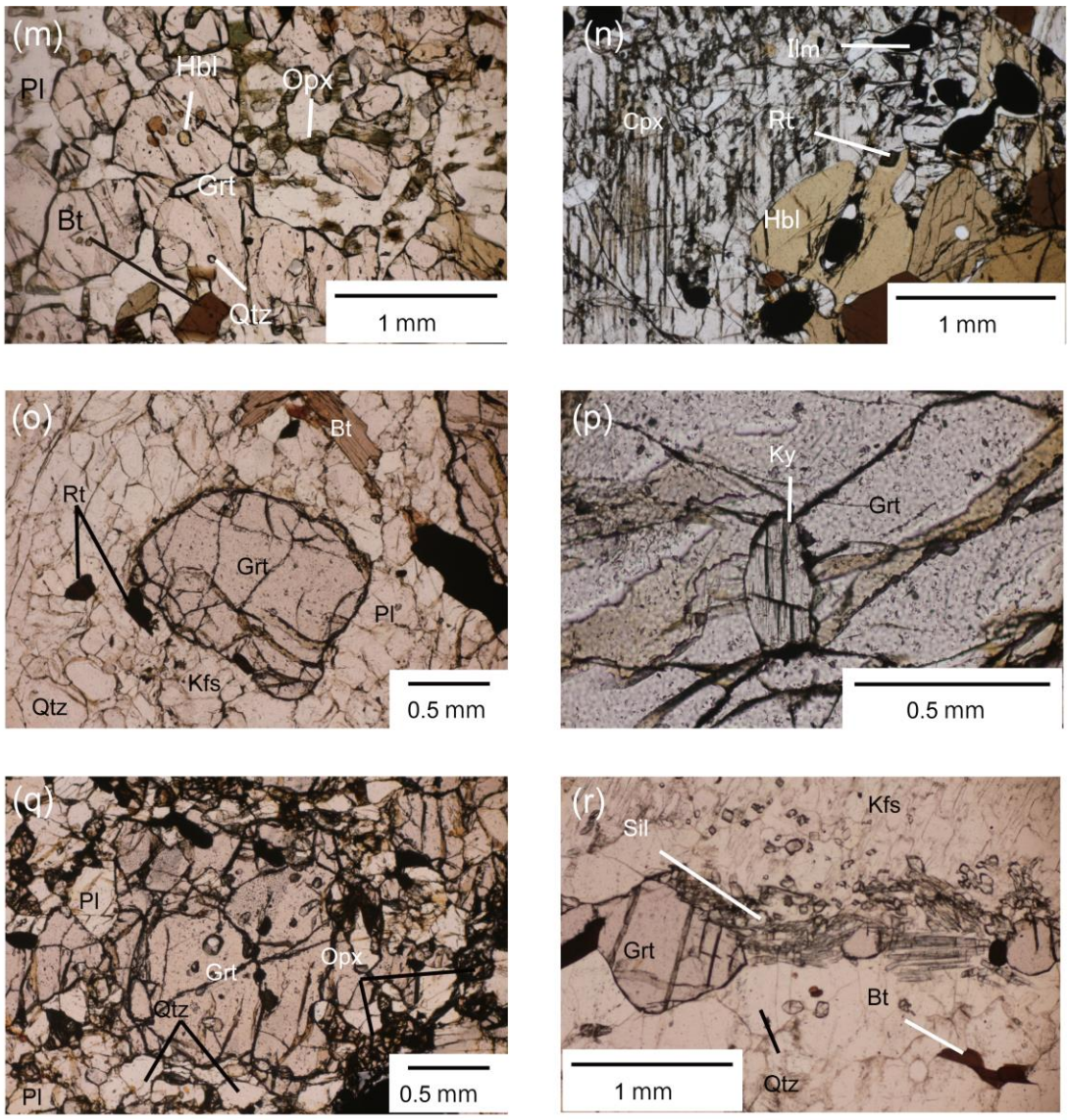

Fig. 10. Continued. (m) Garnet amphibolite characterized by coarse-grained garnet, clinopyroxene, and hornblende. Garnet contains hornblende and quartz. (sample TS11020610I). (n) Coexistence of clinopyroxene, hornblende, and rutile (sample TS11020610I). (o) Felsic granulite from Skallevikshalsen (sample TS10122502D). (p) Garnet in orthopyroxene-free domain containing kyanite (sample TS10122502D). (q) Orthopyroxene-bearing domain of the sample (sample TS110122502D). (r) Pelitic granulite containing garnet, sillimanite, K-feldspar, quartz, and biotite in a matrix (sample TS11020604B).
(s) Garnet containing kyanite, plagioclase, K-feldspar, and rutile (TS11020604B).

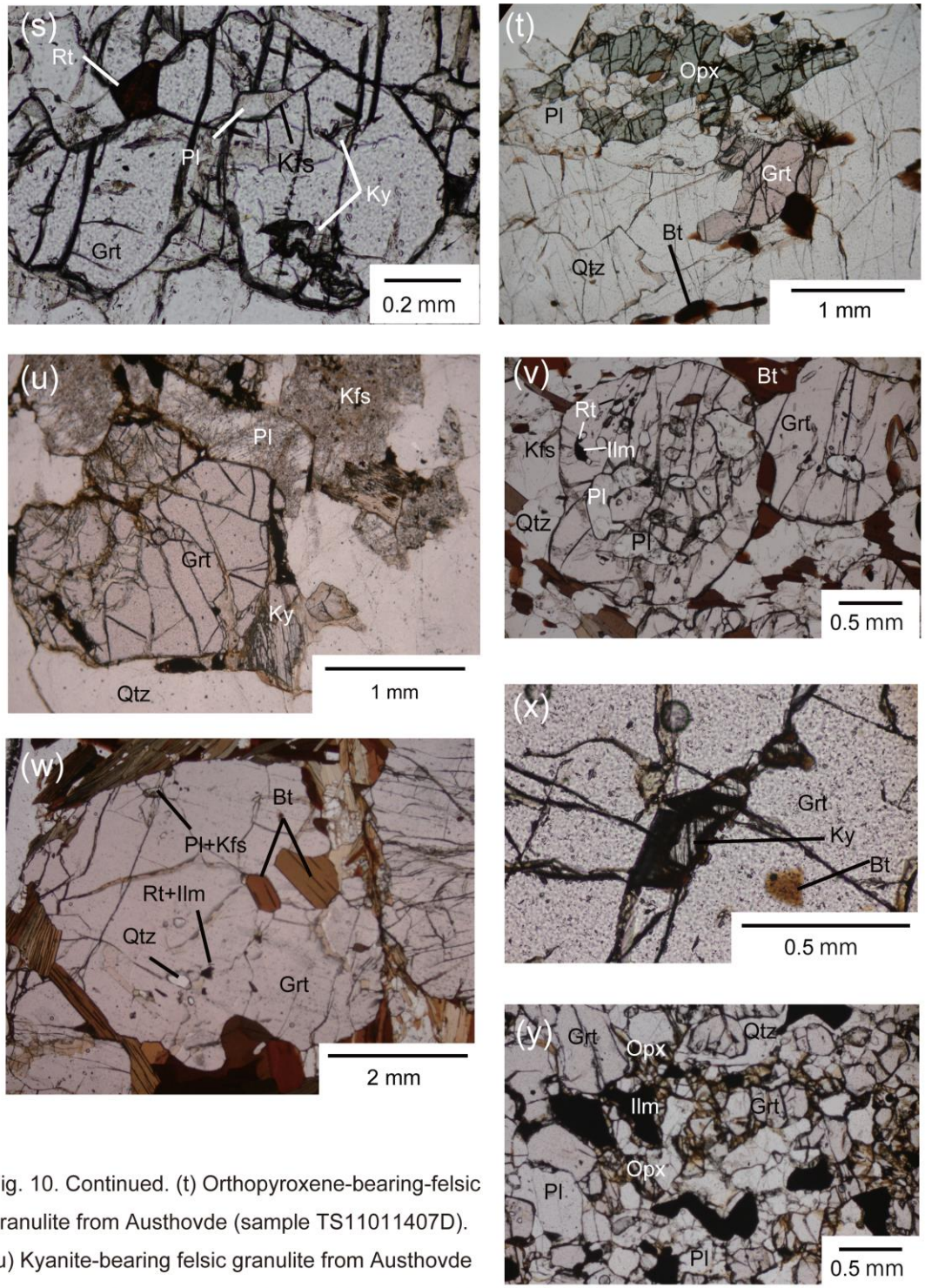

Fig. 10. Continued. (t) Orthopyroxene-bearing-felsic granulite from Austhovde (sample TS11011407D). (u) Kyanite-bearing felsic granulite from Austhovde (sample TS11011702G). (v) Garnet-biotite gneiss from Skallen (sample B97122708B). Garnet contains quartz, plagioclase, biotite, rutile, and ilmenite. (w) Garnet-biotite gneiss characterized by coarse-grained garnet. (sample TS11011504C). (x) Occurence of kyanite within garnet (sample TS11011504C). (y) Orthopyroxene-bearing intermediate granulite (sample TS11020606A).

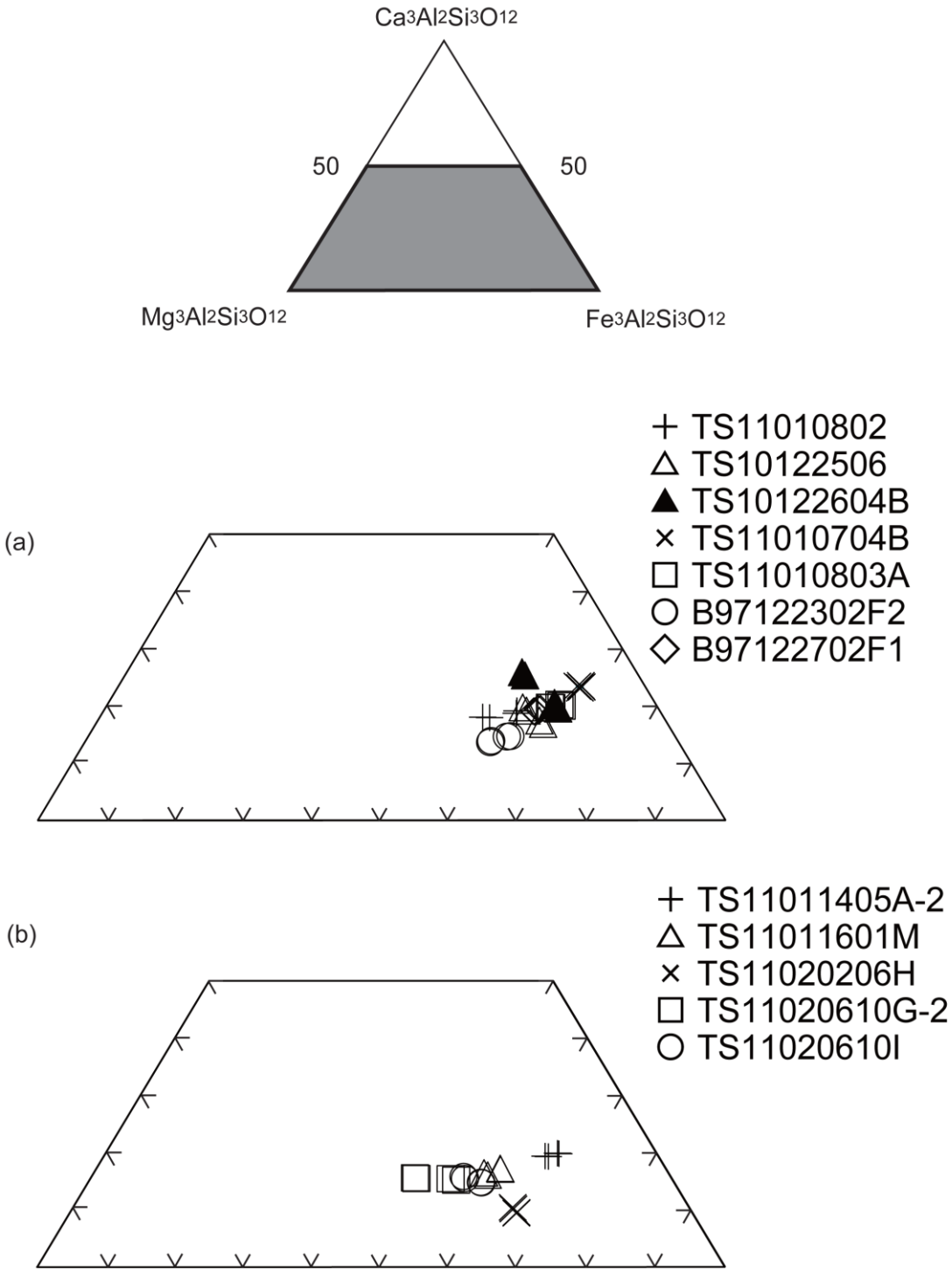

Fig. 11. Compositional diagram of garnet in the examined samples.

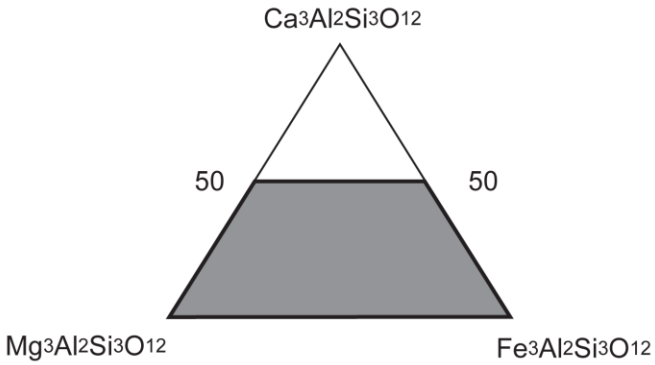

(c)

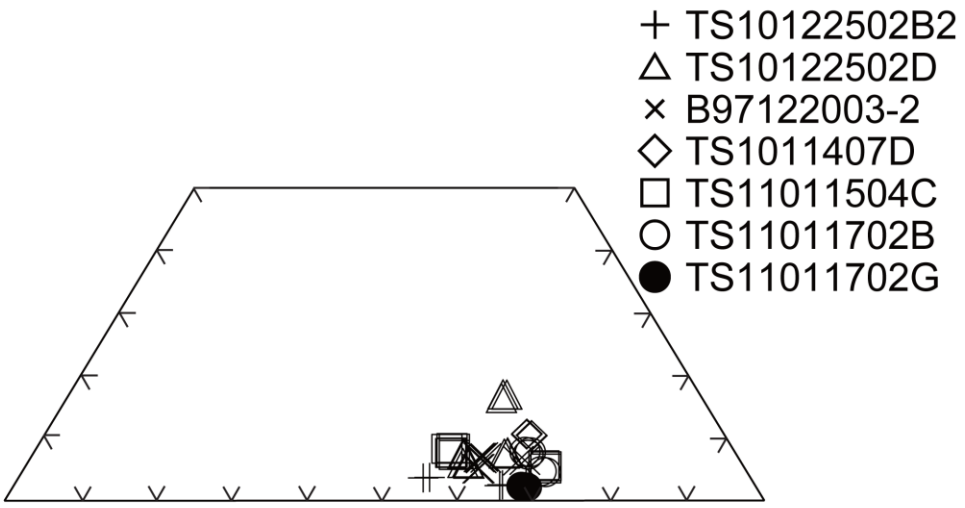

(d)

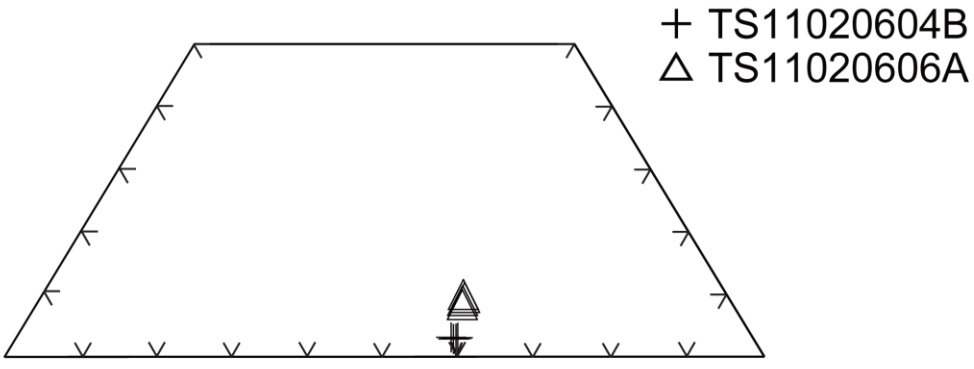

Fig. 11. Continued.

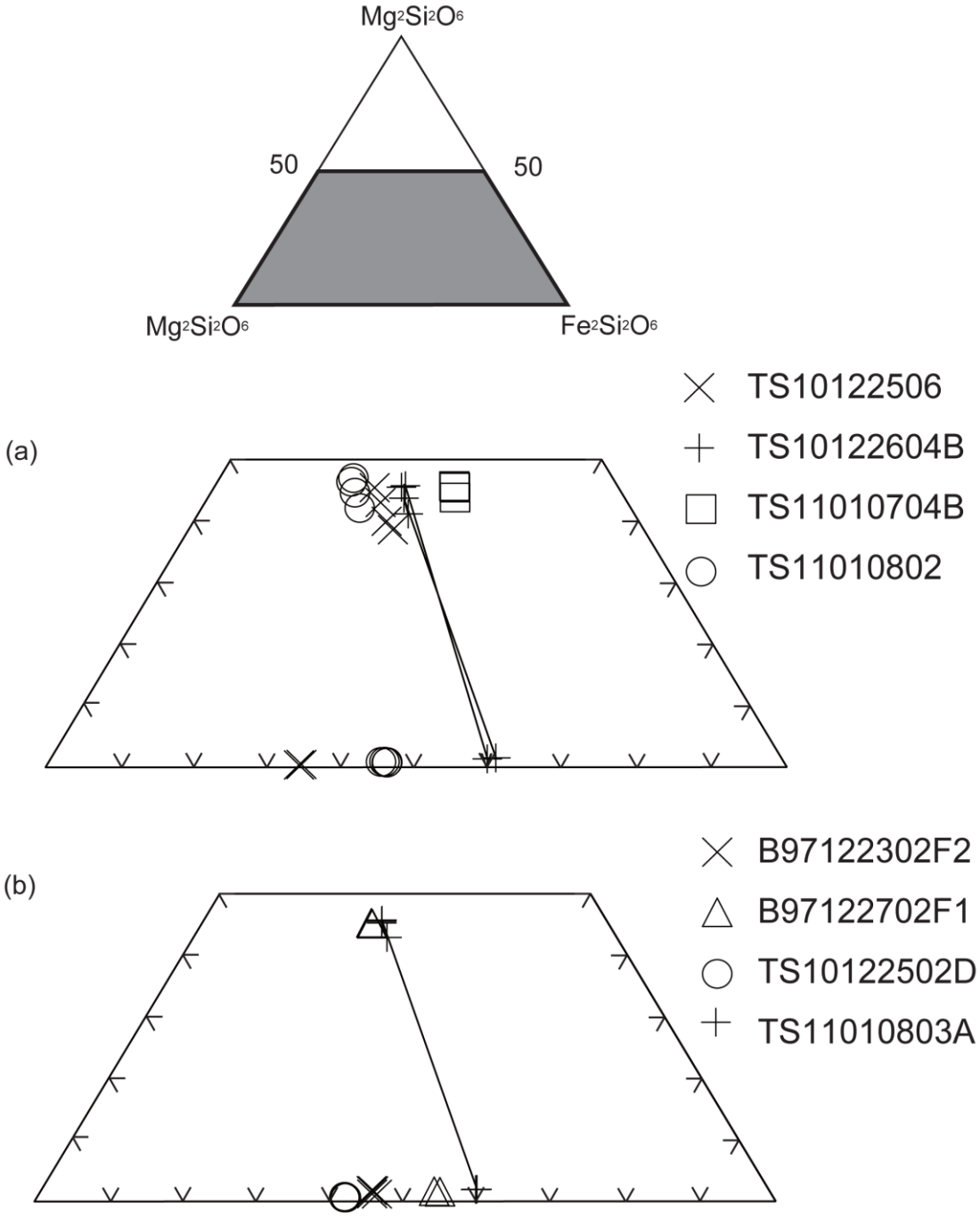

Fig. 12. Compositional diagram of pyroxene in the examined samples.

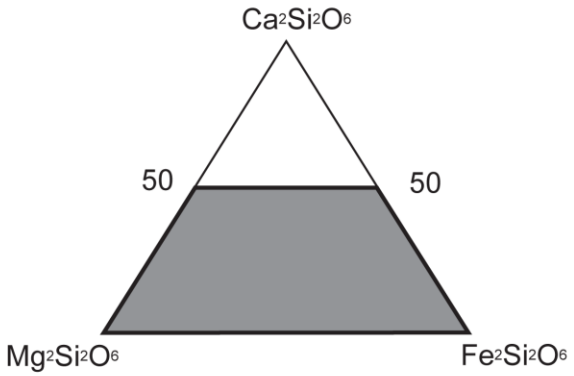

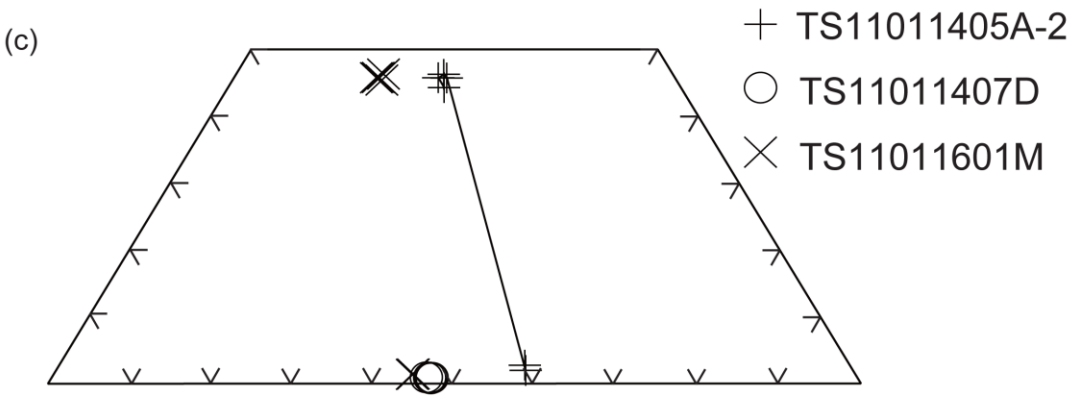

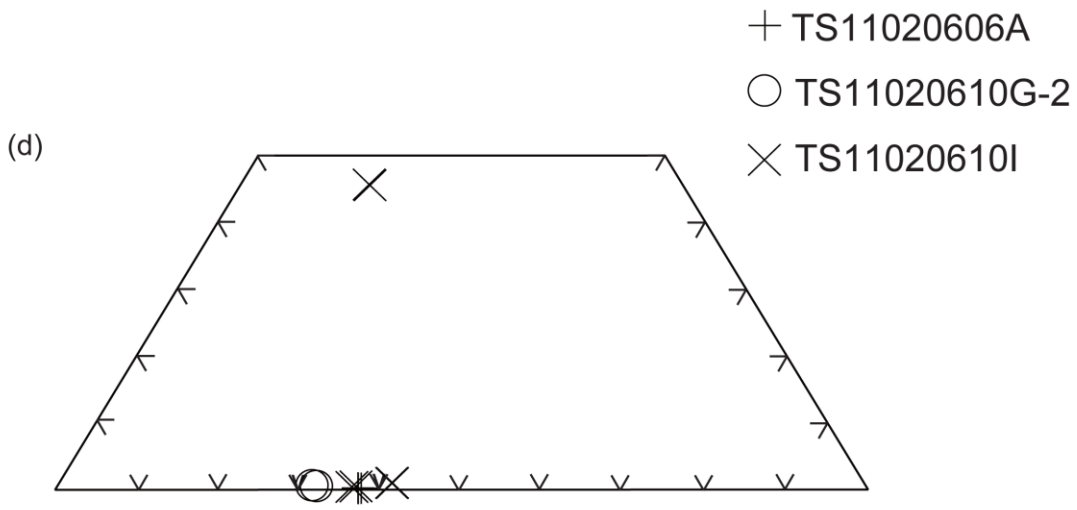

Fig. 12. Continued.

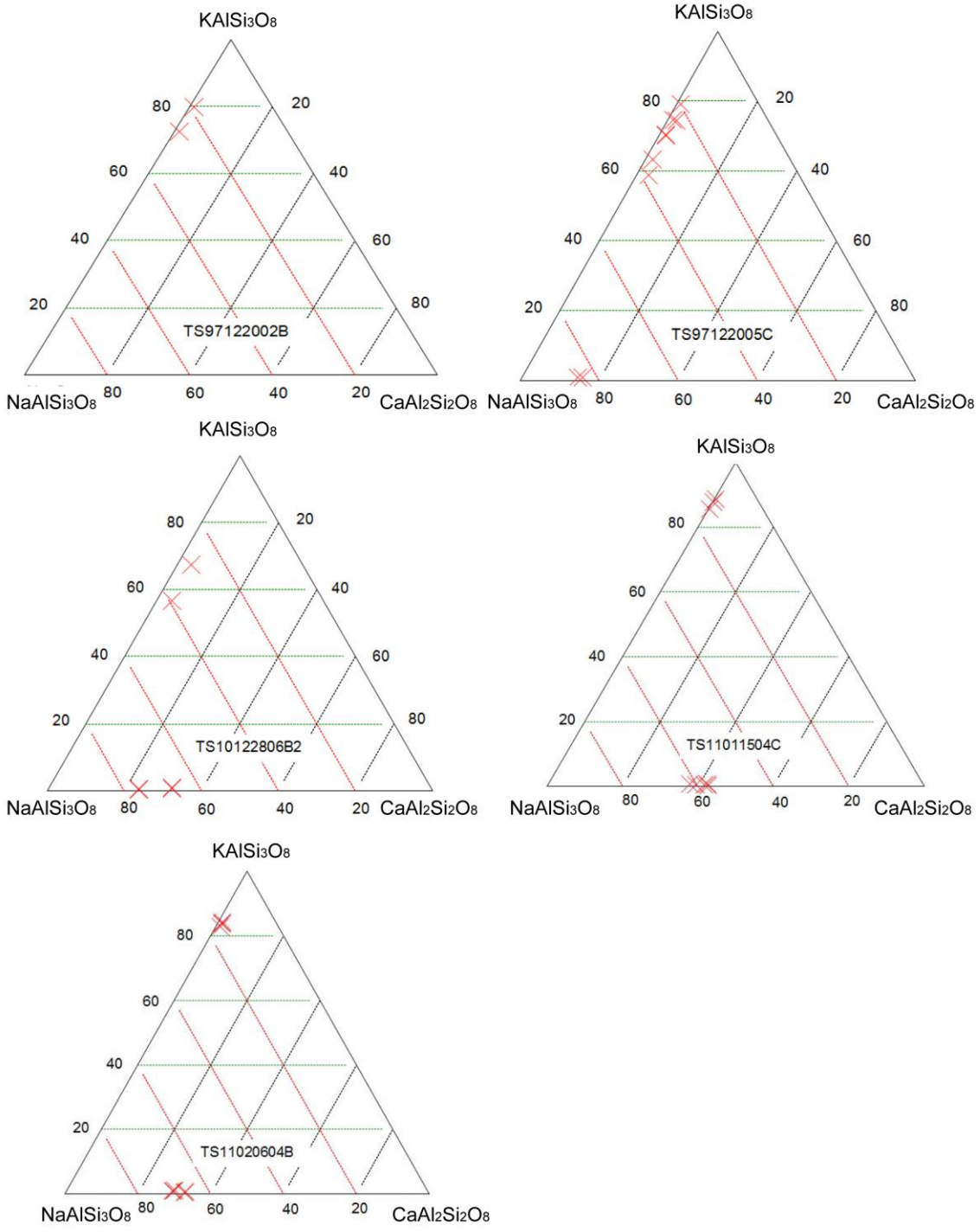

Fig. 13. Compositional diagram of feldspar in the examined samples.

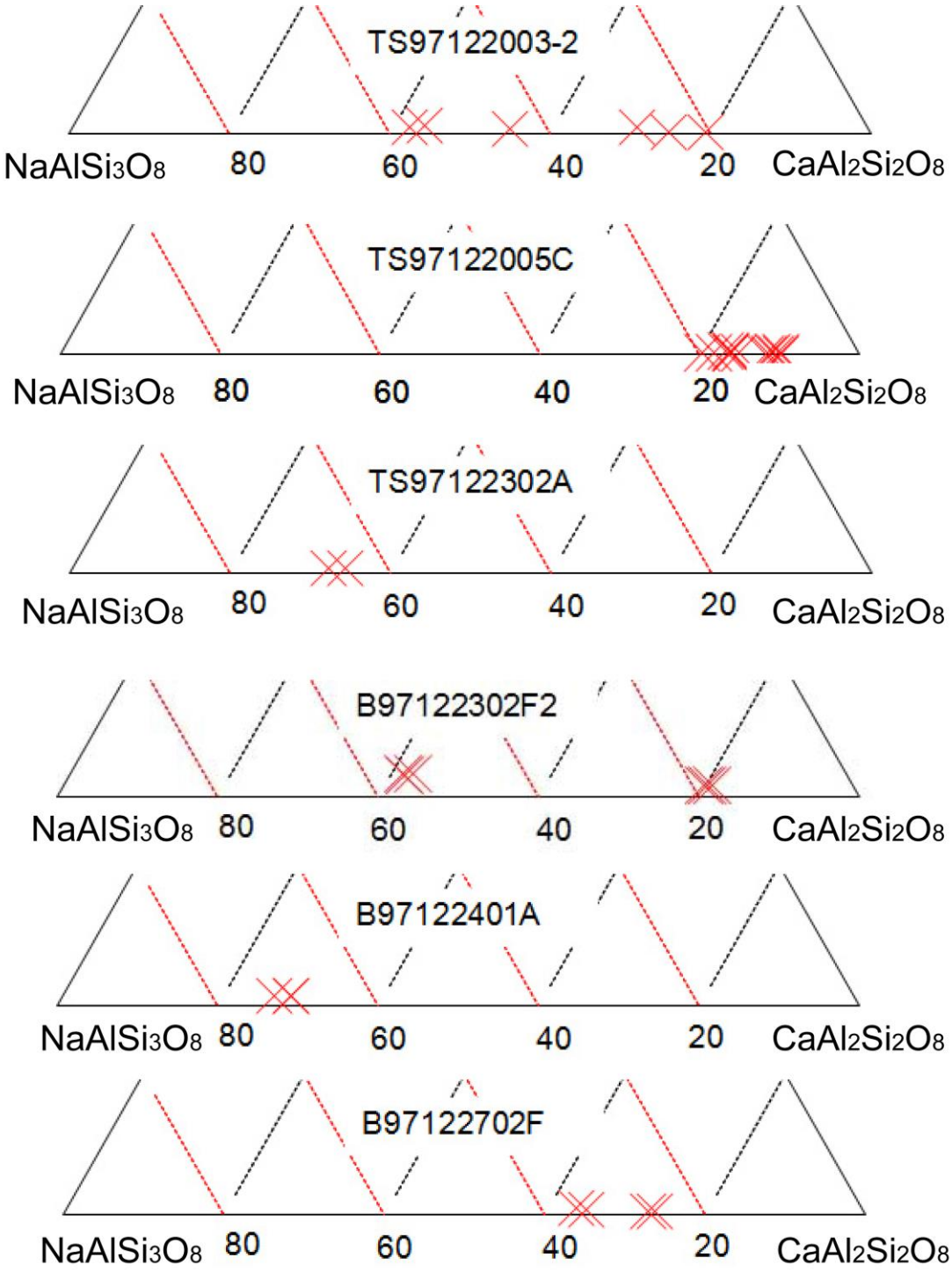

Fig. 13. Continued.

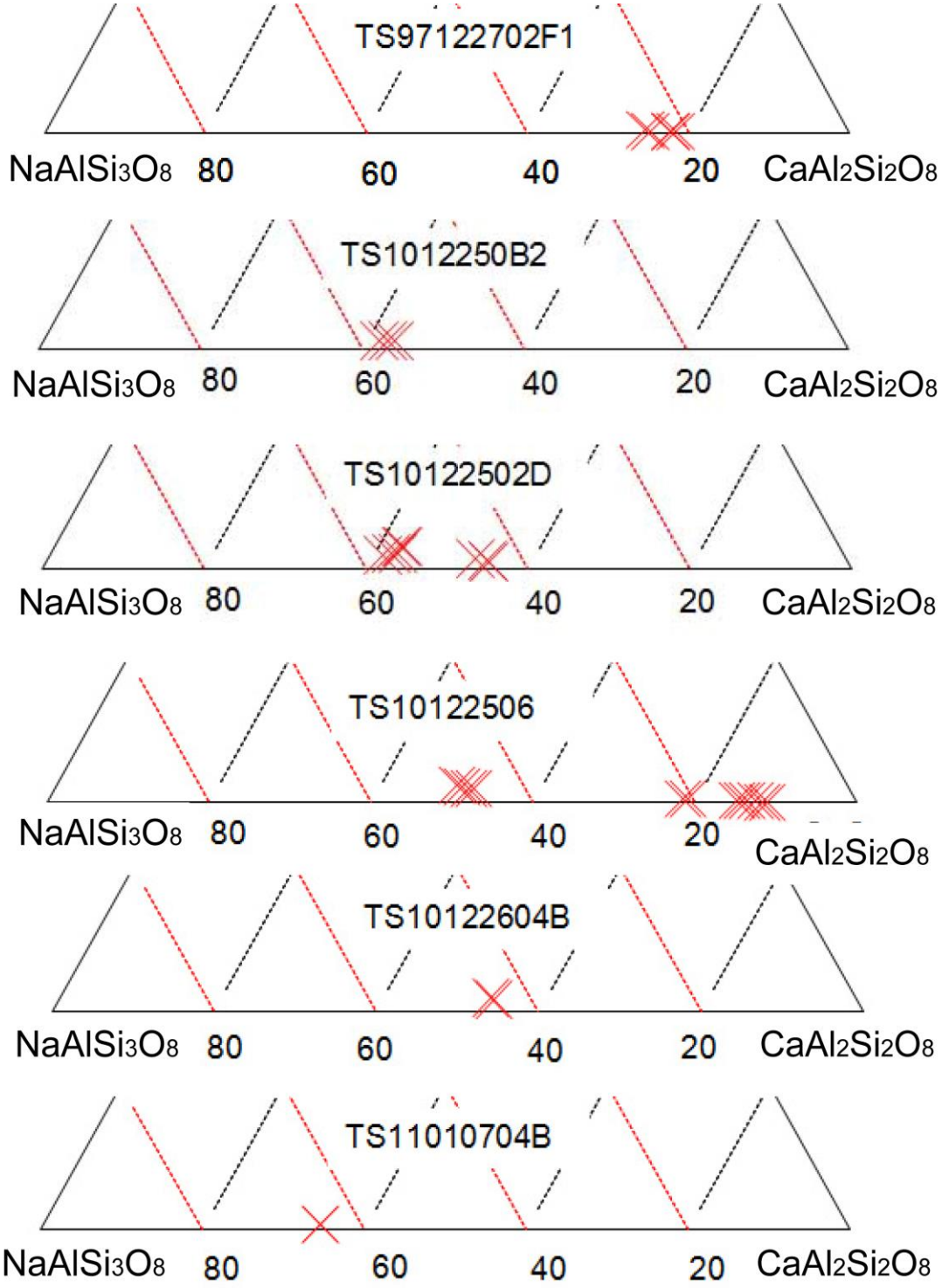

Fig. 13. Continued.

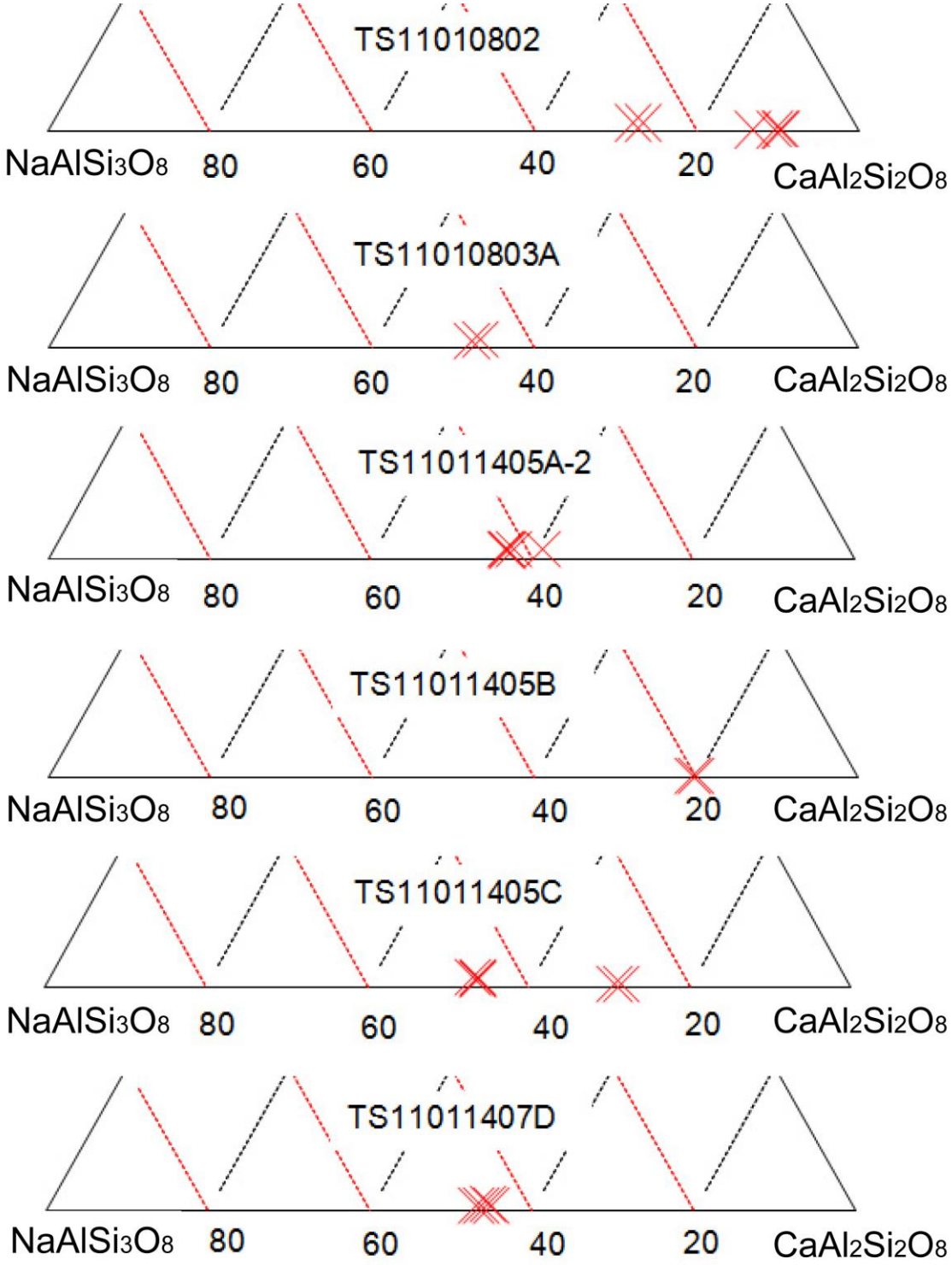

Fig. 13. Continued.

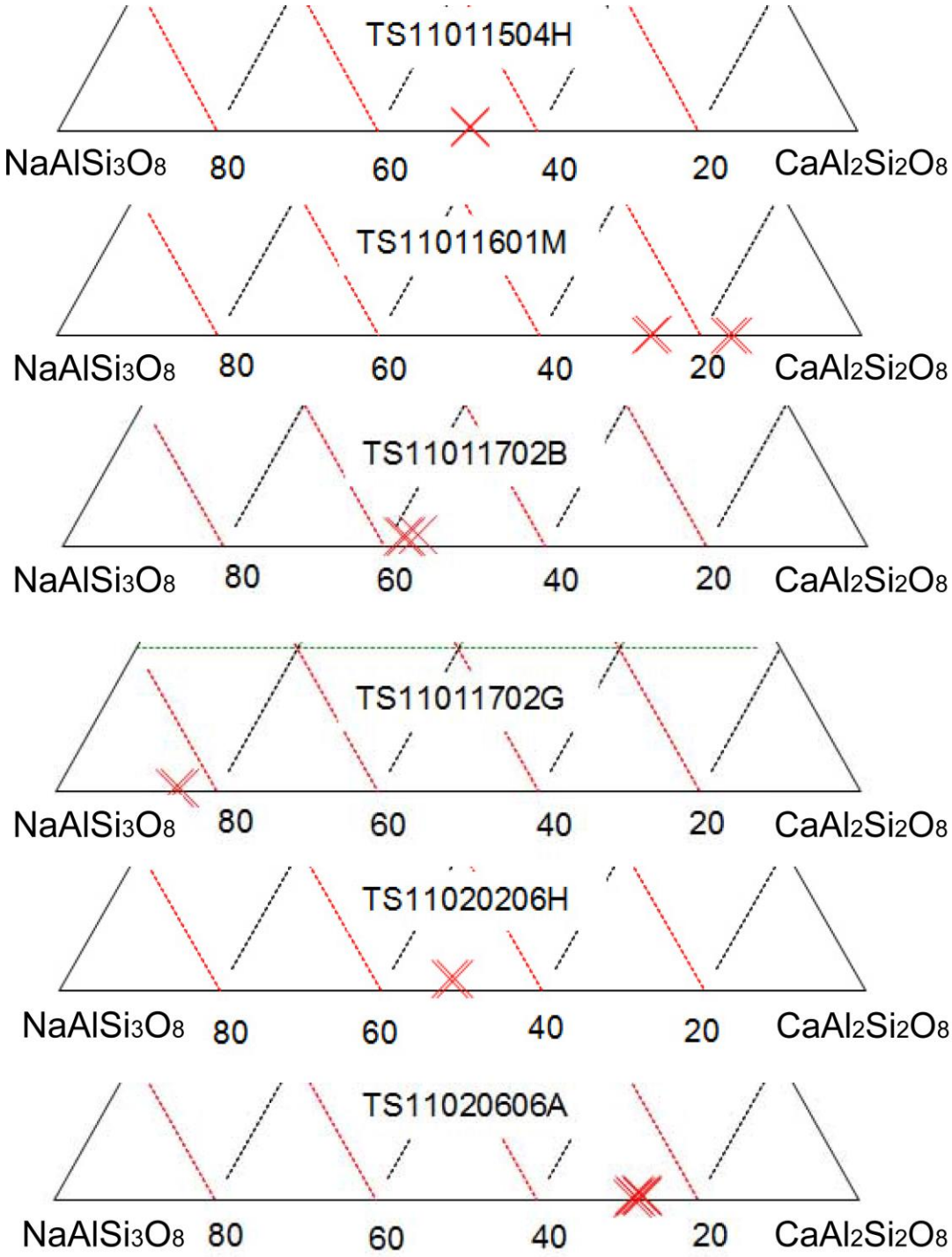

Fig. 13. Continued.

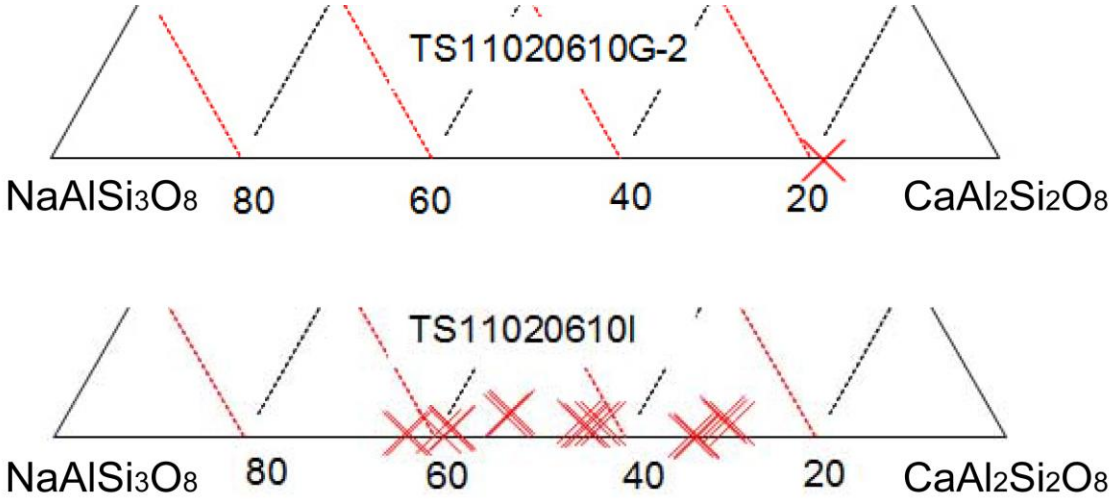

Fig. 13. Continued.

(Na+K)A≥ 0.50, Ti<0.5, CaB≥1.50.

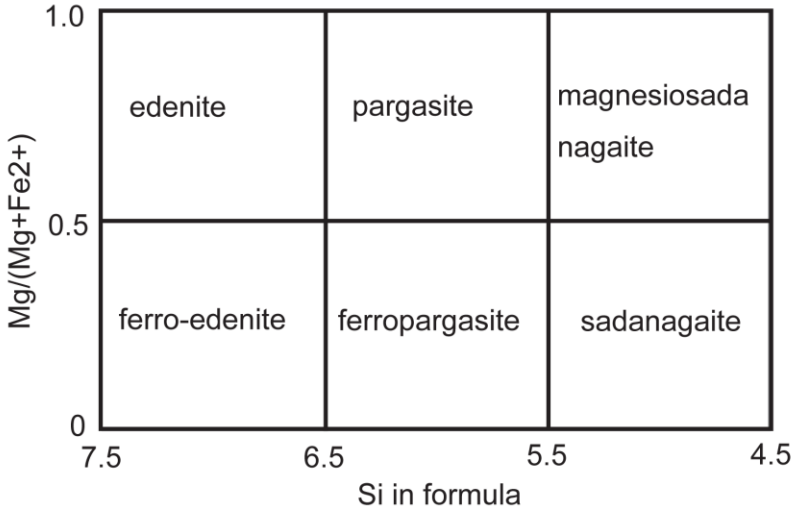

Fig.14-1. Classification of calcic amphiboles after Leake et al. (1978).

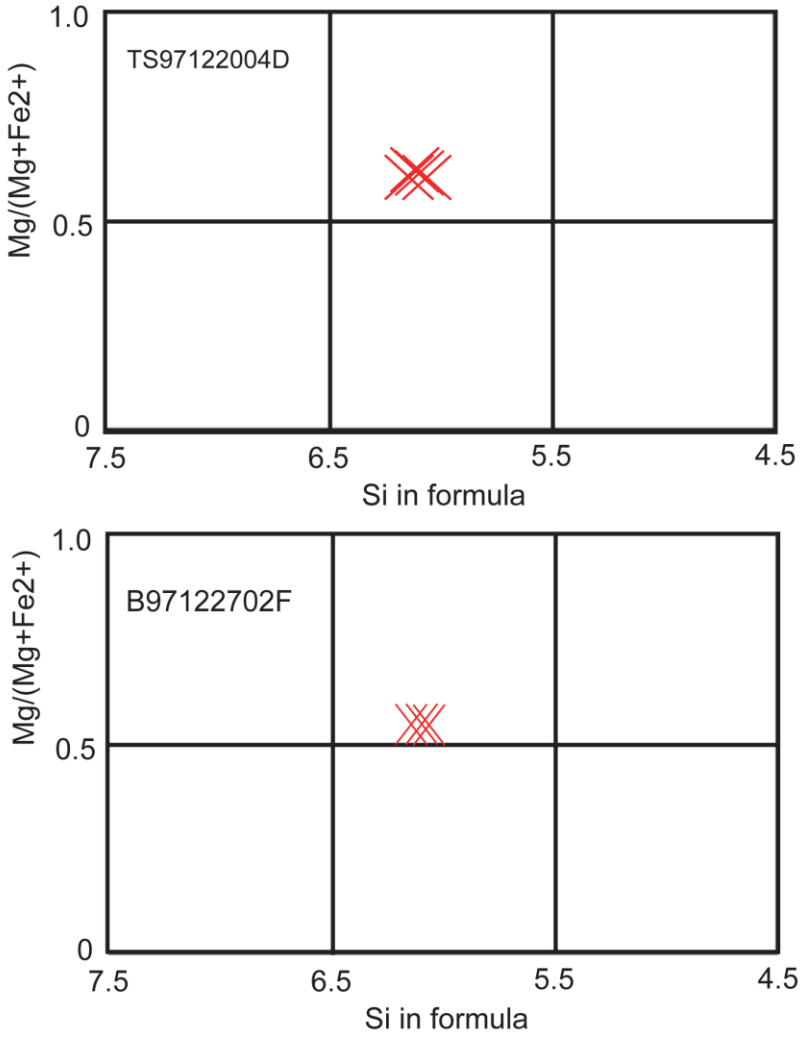

Fig. 14-2. Classification of calcic amphiboles in this study.

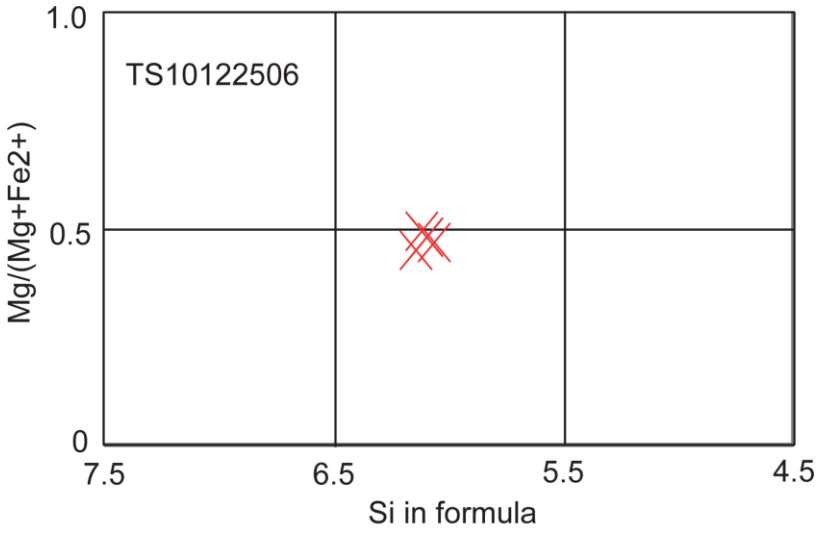

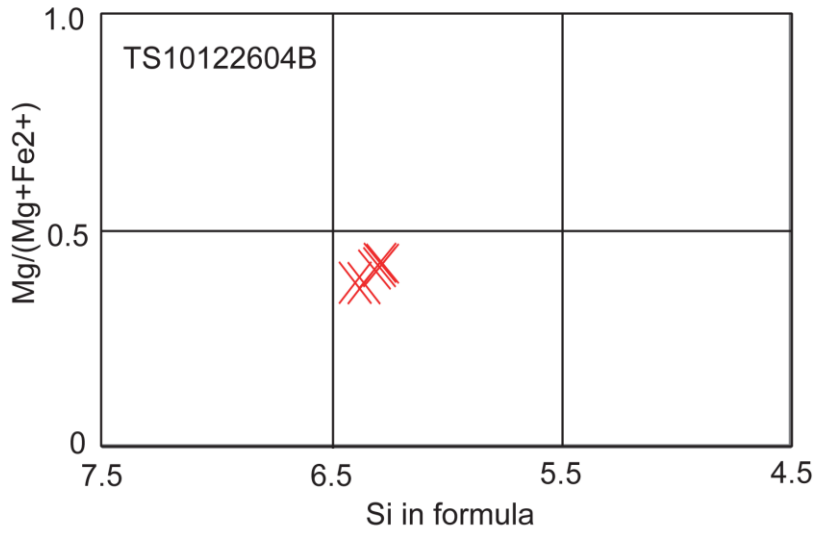

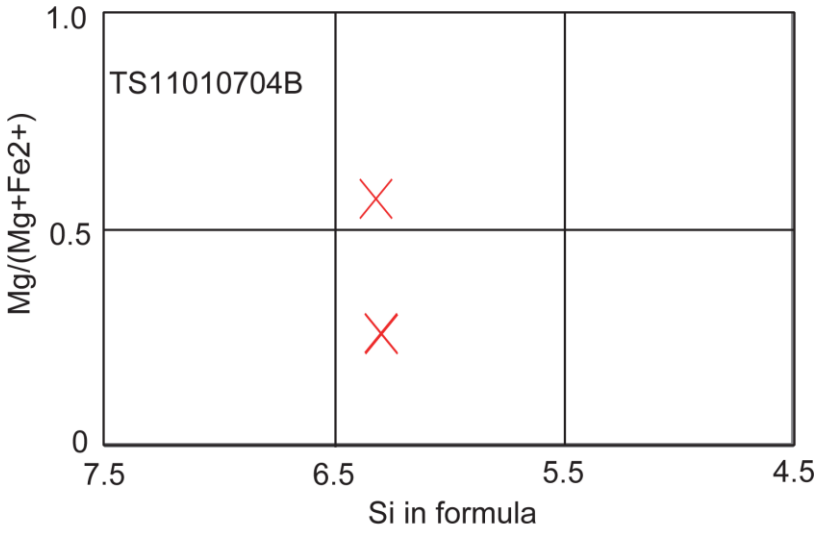

Fig. 14-2. Continued.

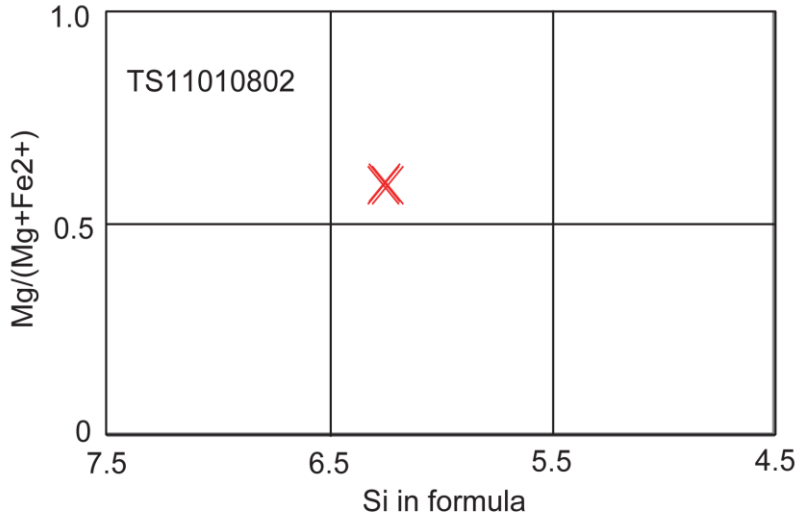

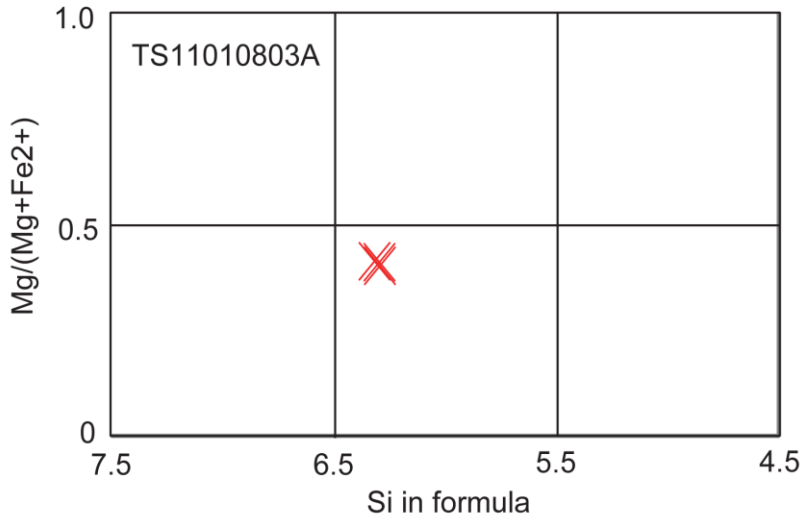

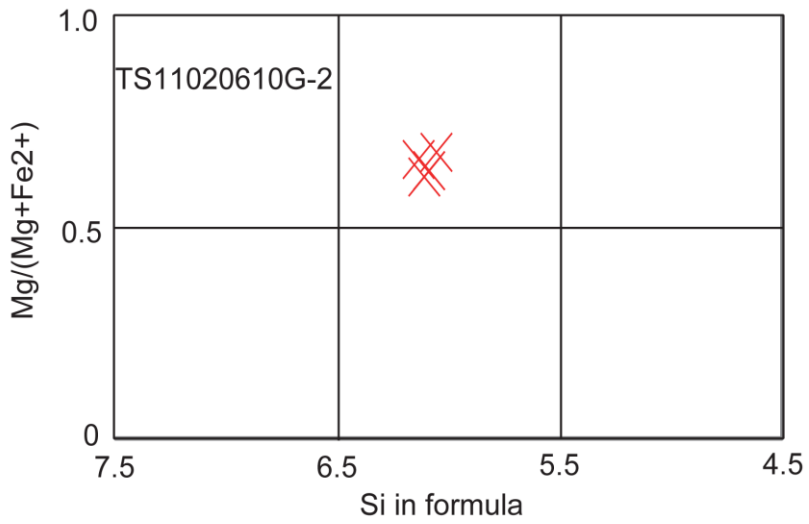

Fig. 14-2. Continued.

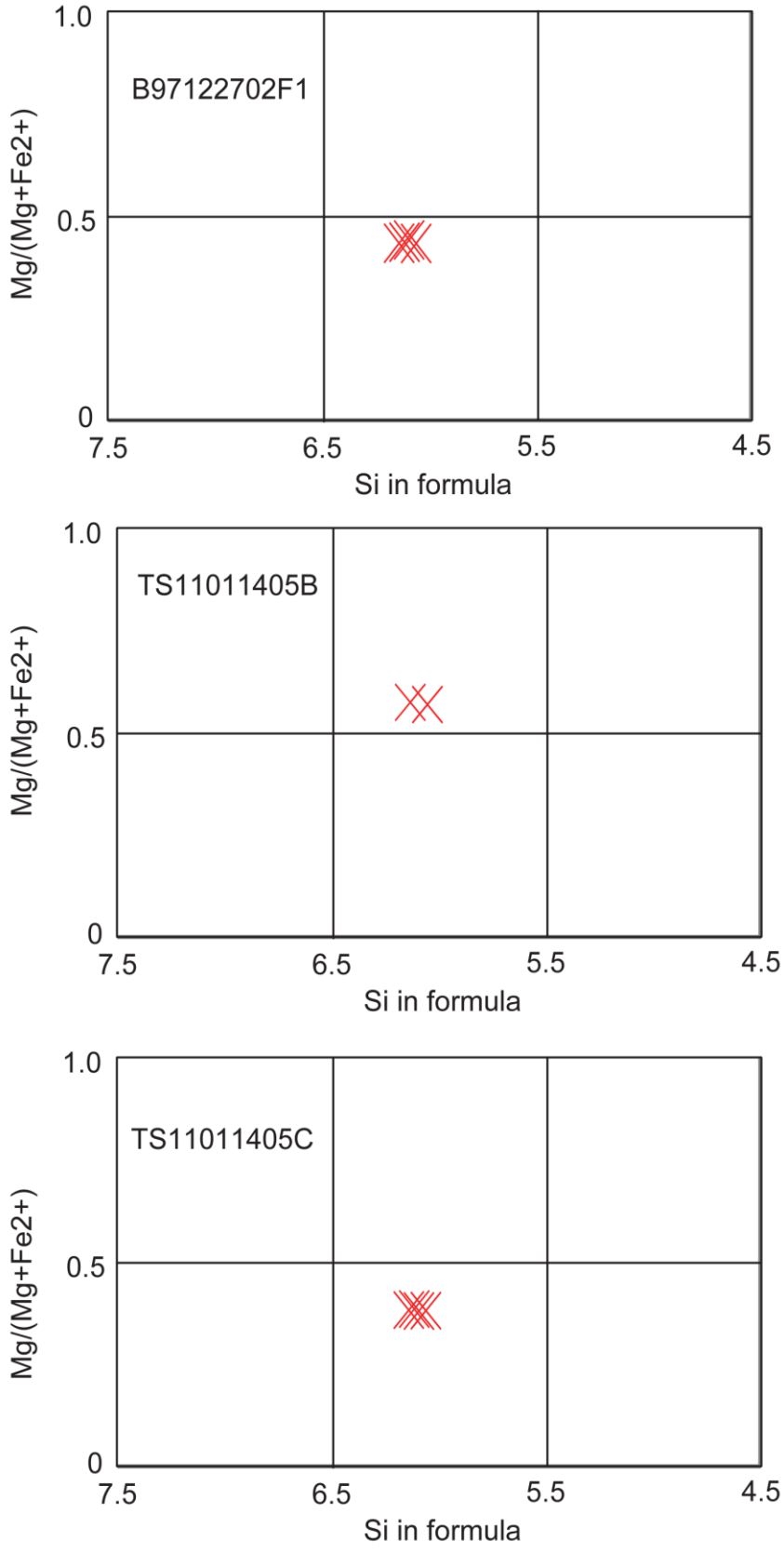

Fig. 14-2. Continued.

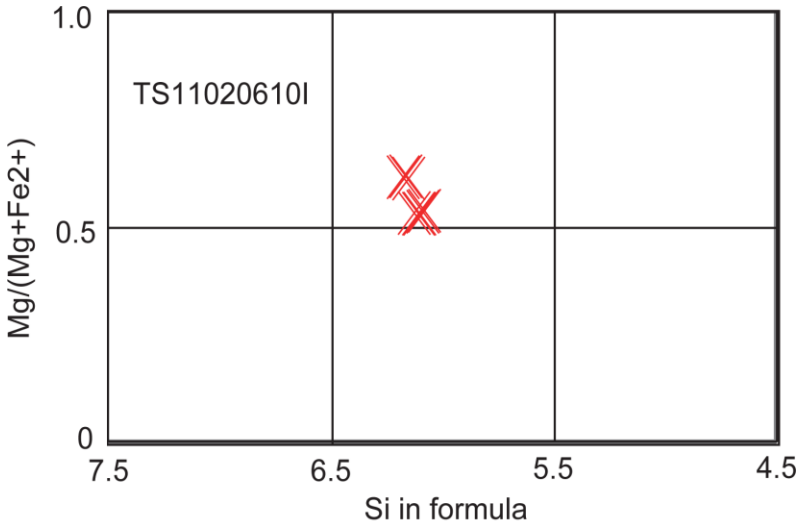

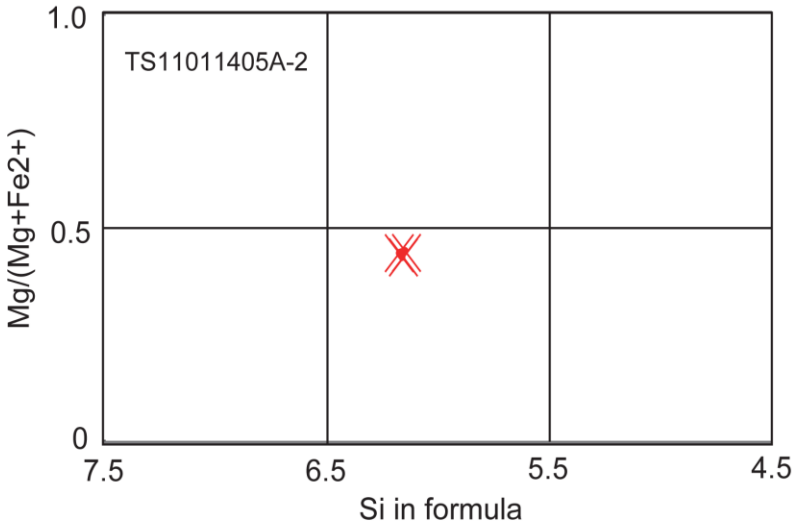

Fig. 14-2. Continued.

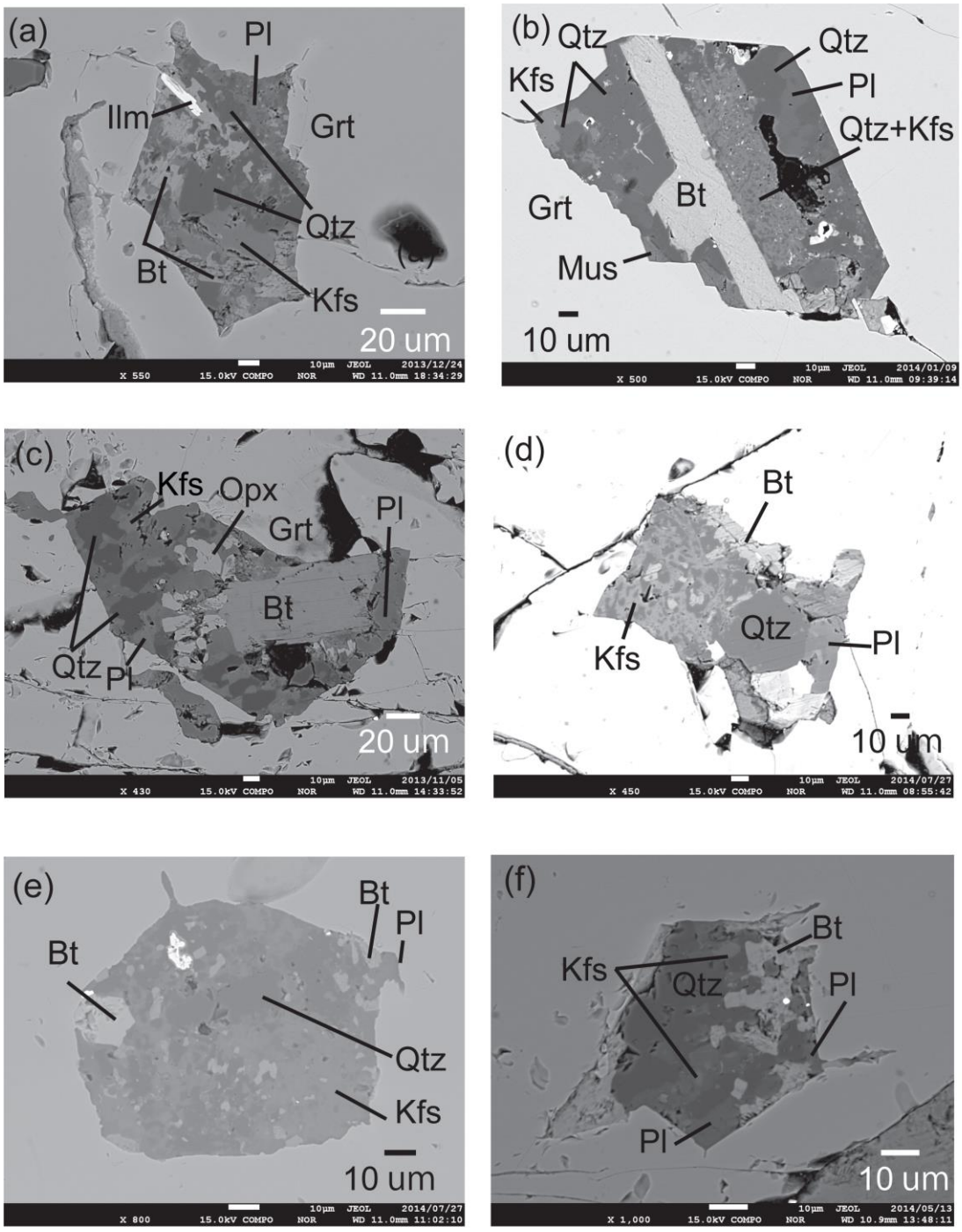

Fig. 15. Back Scattered Electron (BSE) images of CMI within mafic to ultramafic granulites. (a) CMI in the mafic granulite (sample TS10122506). (b) Muscovite-bearing CMI in ultramafic granulite (sample TS11010704B). (c) Orthopyroxene-bearing CMI in ultramafic granulite (sample TS11010802). (d) CMI in mafic granulite (sample B97122302F2) which contains rutile in garnet. (e) Irregular shaped CMI in garnet-two-pyroxene granulite (sample TS11011405A-2). (f) Negative crystal shape of CMI in garnet amphibolite (sample TS11020610I).

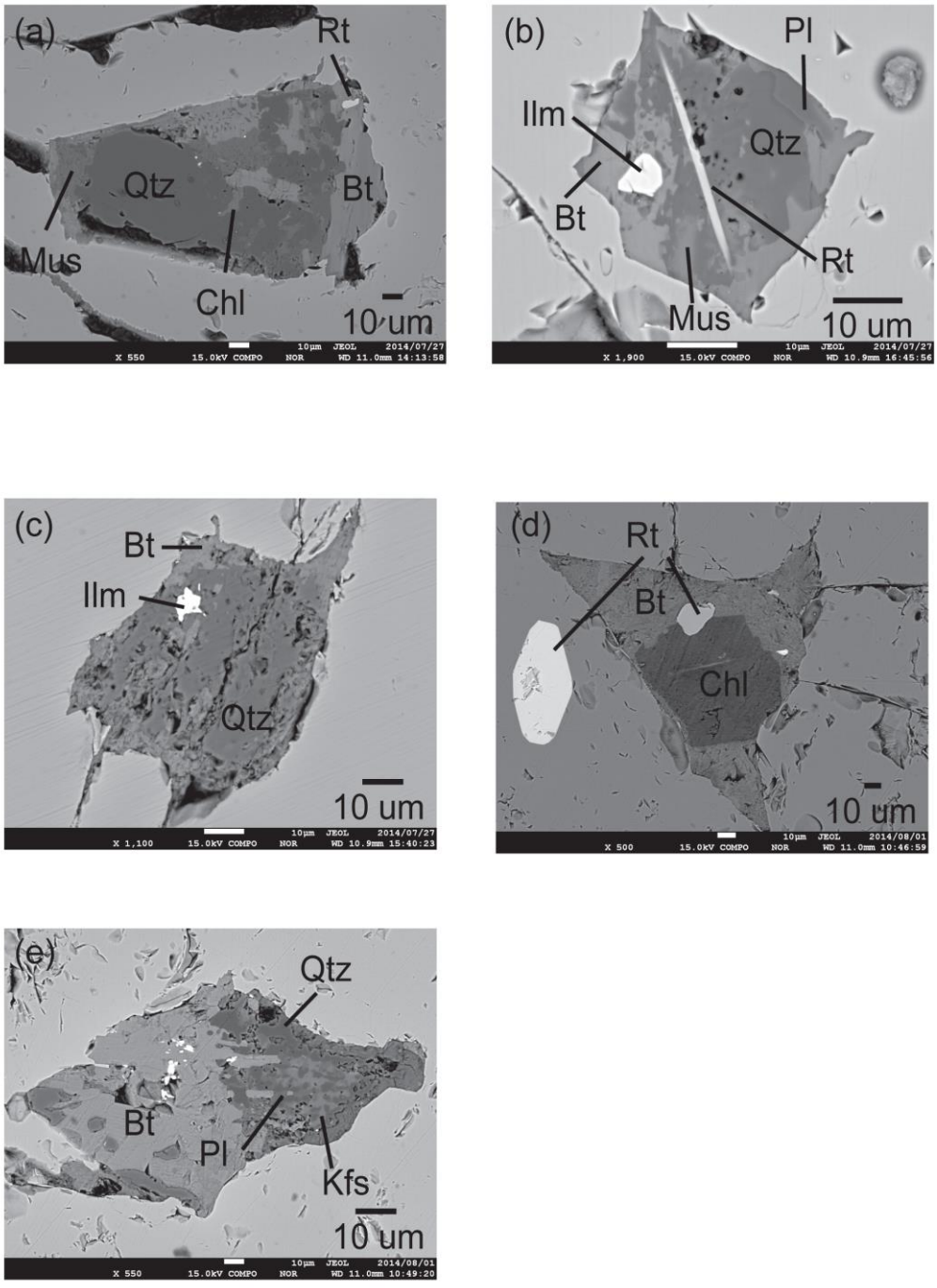

Fig. 16. Back Scattered Electron (BSE) images of CMI within pelitic to felsic granulites.
(a) CMIs in pelitic granulite (sample TS10122502B2). (b) Muscovite-bearing CMI in pelitic granulite. (sample TS10122502D). (c) Irregular shaped CMI in felsic granulite (sample B97122003-2). (d) CMI in garnet-biotite gneiss (sample TS11011504C). (e) Irregular shaped CMI in garnet-biotite gneiss(sample TS11011504C).

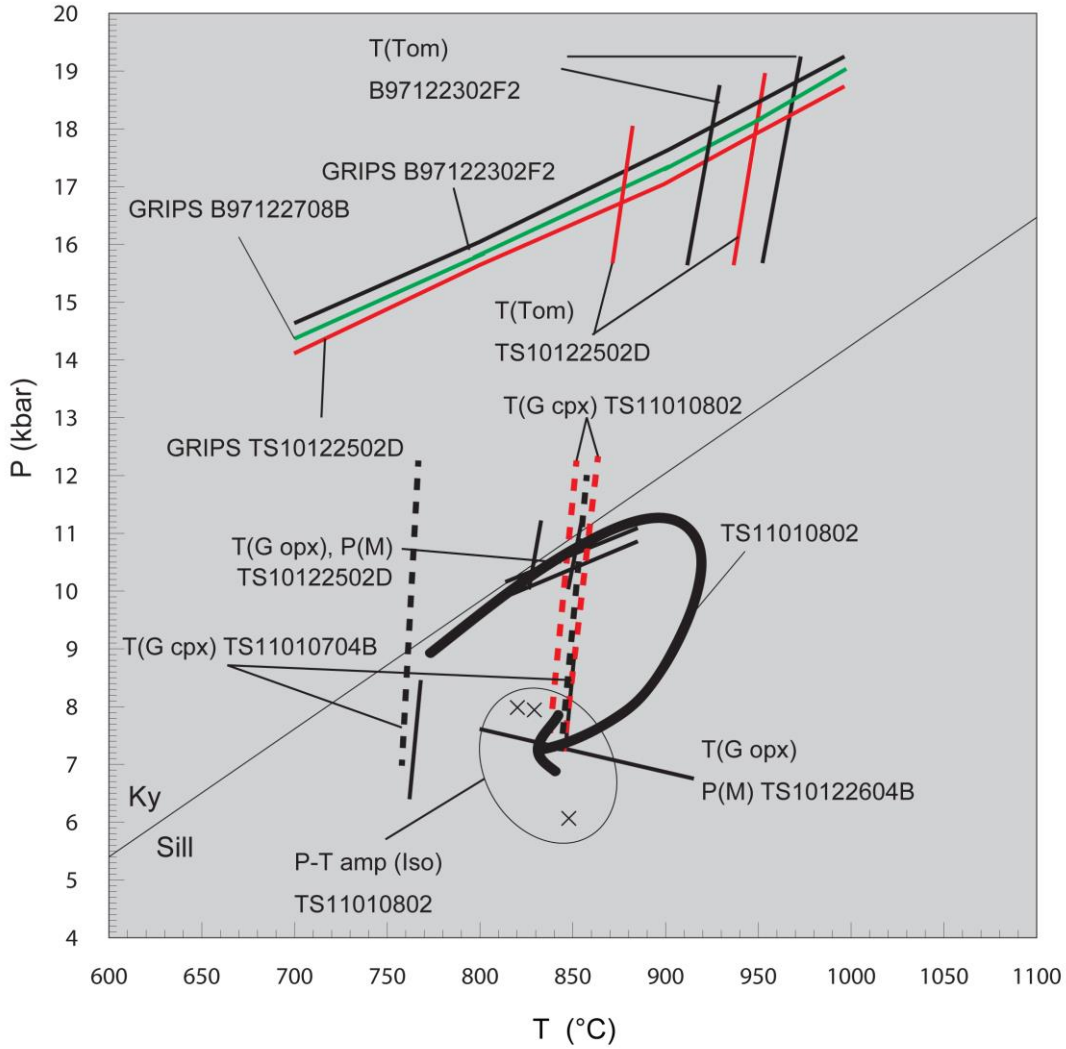

Fig. 17. Estimated *P-T* conditions obtained from Skallevikshalsen and Skallen.
P(M): Moecher et al. (1988), GRIPS: Bohlen and Liotta (1986), GASP: Spear (1993),
P-T amp (Iso): Ernst and Liu (1998), P(KS): Kohn and Spear (1990),
T(G cpx): Ganguly et al. (1996), T(G opx): Ganguly (1996), T(Tom): Tomkins et al. (2007),
T(GP): Graham and Powell (1987).

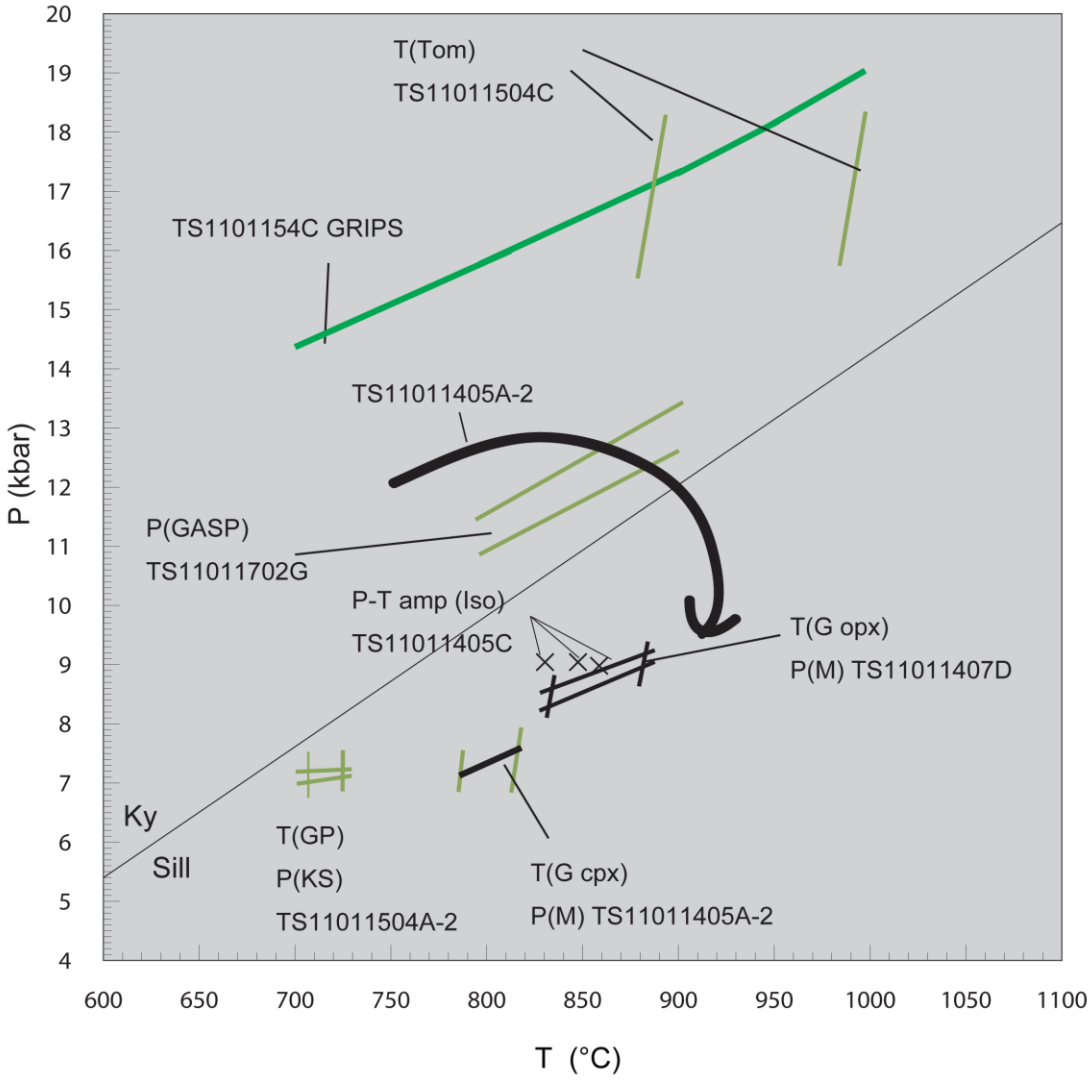

Fig. 18. Estimated *P-T* conditions obtained from Austhovde.
P(M): Moecher et al. (1988), GRIPS: Bohlen and Liotta (1986), GASP: Spear (1993),
P-T amp (Iso): Ernst and Liu (1998), P(KS): Kohn and Spear (1990),
T(G cpx): Ganguly et al. (1996), T(G opx): Ganguly (1996), T(Tom): Tomkins et al. (2007),
T(GP): Graham and Powell (1987).

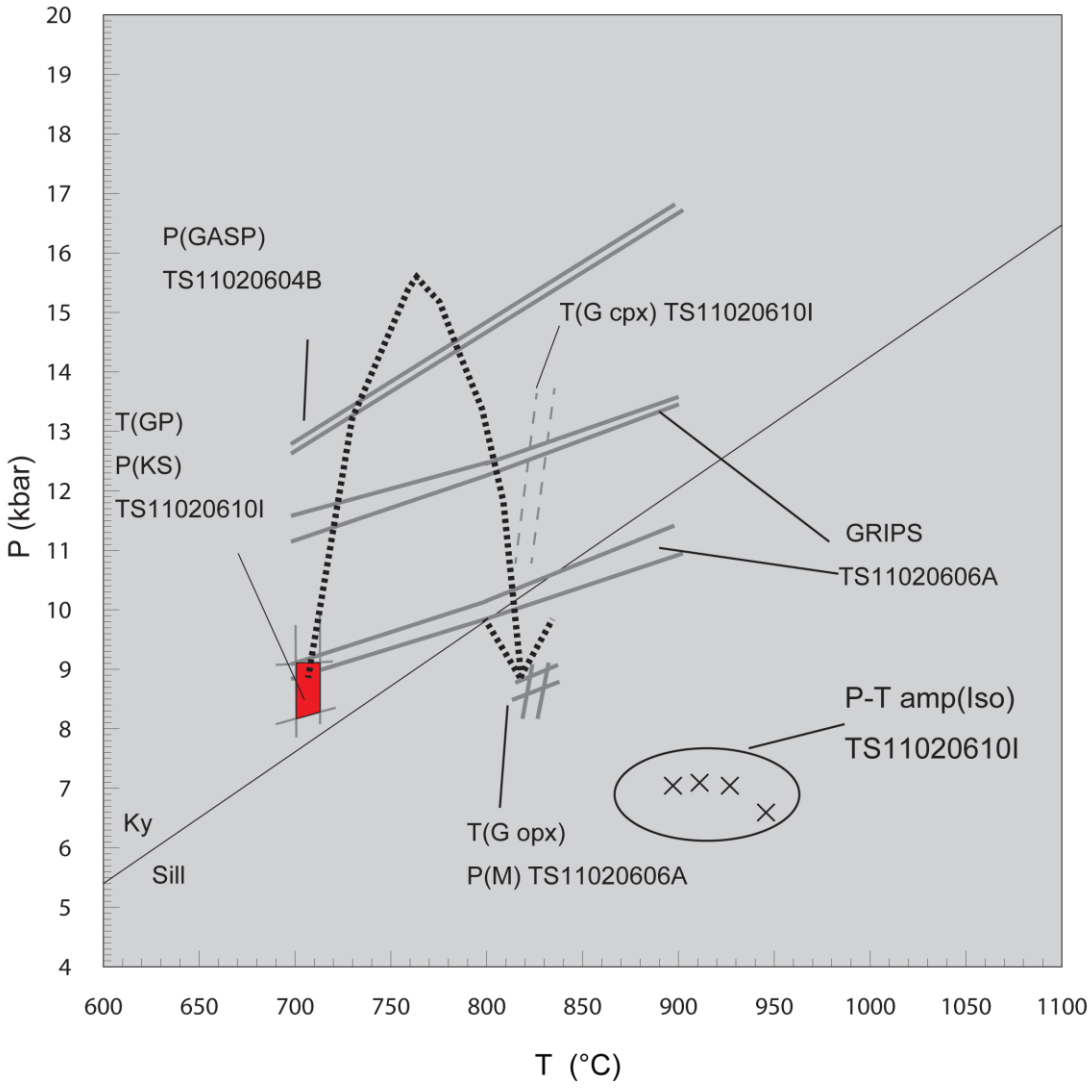

Fig. 19. Estimated *P-T* conditions obtained from Ongul.

P(M): Moecher et al. (1988), GRIPS: Bohlen and Liotta (1986), GASP: Spear (1993),

P-T amp (Iso): Ernst and Liu (1998), P(KS): Kohn and Spear (1990),

T(G cpx): Ganguly et al. (1996), T(G opx): Ganguly (1996), T(Tom): Tomkins et al. (2007),

T(GP): Graham and Powell (1987).

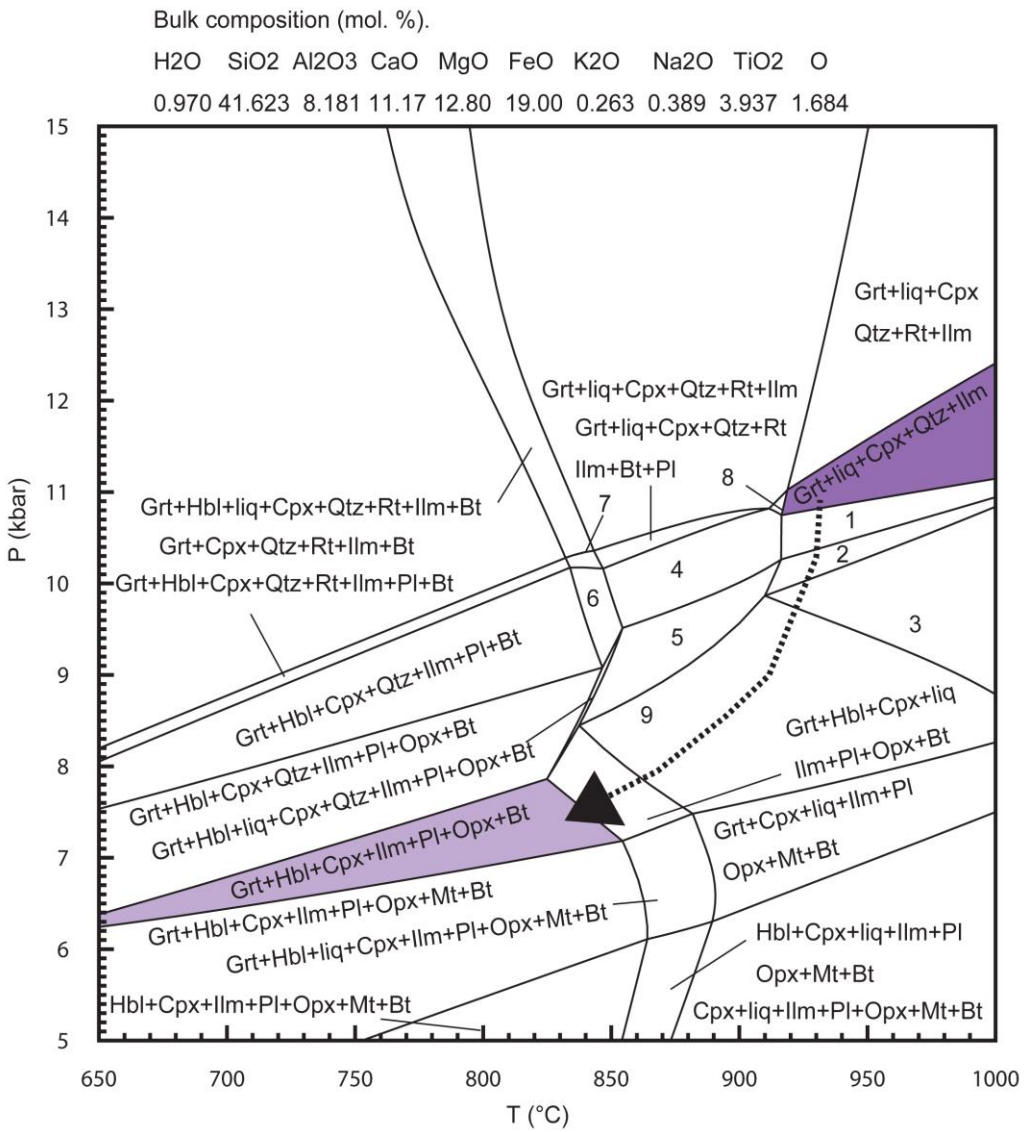

Fig. 20. *P-T* diagram showing calculated pseudosection of mineral assemblages in mafic granulite from Skallevikshalsen (sample TS11010802). Qtz: quartz, Pl: plagioclase, Cpx: clinopyroxene, Grt: garnet, Opx: orthopyroxene, Bt: biotite, Hbl: hornblende, Mt: magnetite, Ilm: ilmenite, Rt: rutile, liq: inferred melt.

1:Grt+liq+Cpx+Qtz+Ilm+Pl
2:Grt+liq+Cpx+Qtz+Ilm+Pl+Opx
3:Grt+liq+Cpx+Ilm+Pl+Opx
4:Grt+liq+Cpx+Qtz+Ilm+Pl+Bt
5:Grt+liq+Cpx+Qtz+Ilm+Pl+Bt+Opx
6:Grt+liq+Cpx+Qtz+Ilm+Pl+Bt+Hbl
7:Grt+liq+Cpx+Qtz+Ilm+Pl+Bt+Hbl+Rt
8:Grt+liq+Cpx+Qtz+Ilm+Bt
9: Grt+Cpx+liq+Ilm+Pl+Opx+Bt

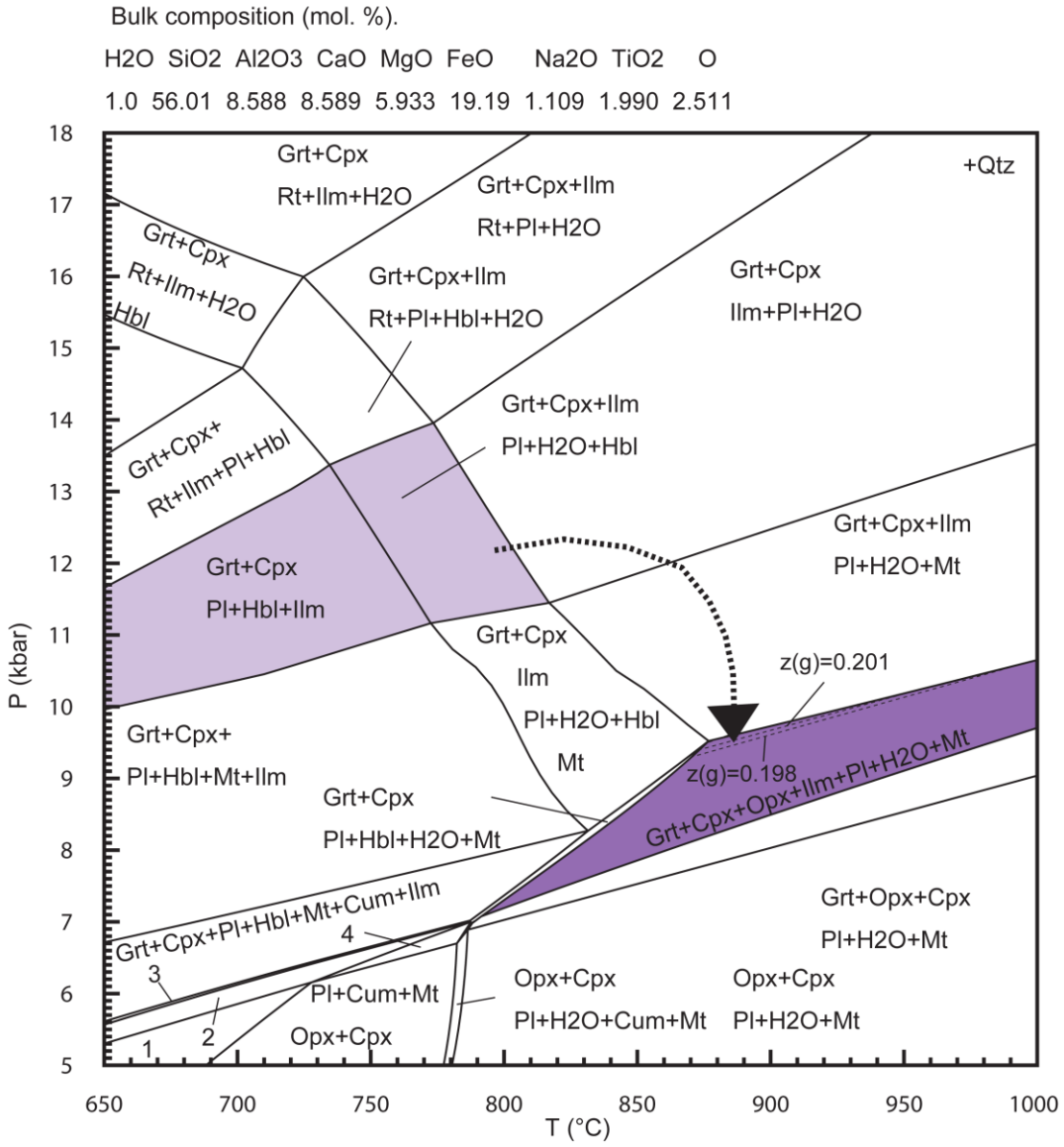

Fig. 21. *P-T* diagram showing calculated pseudosection of mineral assemblages in mafic granulite from Austhovde (sample TS11011405A-2). Qtz: quartz, Pl: plagioclase, Cpx: clinopyroxene, Grt: garnet, Opx: orthopyroxene, Bt: biotite, Hbl: hornblende, Mt: magnetite, Ilm: ilmenite, Rt: rutile, Cum: cummingtonite. z(g): grossular content of garnet.

1:Opx+Cpx+Pl+Mt+Ilm+Cum
2:Grt+Opx+Cpx+Pl+Mt+Ilm+Cum
3:Grt+Opx+Cpx+Pl+Mt+Ilm+Cum+Hbl
4:Grt+Pl+Cum+Mt+Opx+Cpx

Bulk composition (mol. %).

H2O	SiO2	Al2O3	CaO	MgO	FeO	K2O	Na2O	TiO2	O
0.994	48.205	11.669	10.496	11.967	12	0 .601	2.204	1.571	0.297

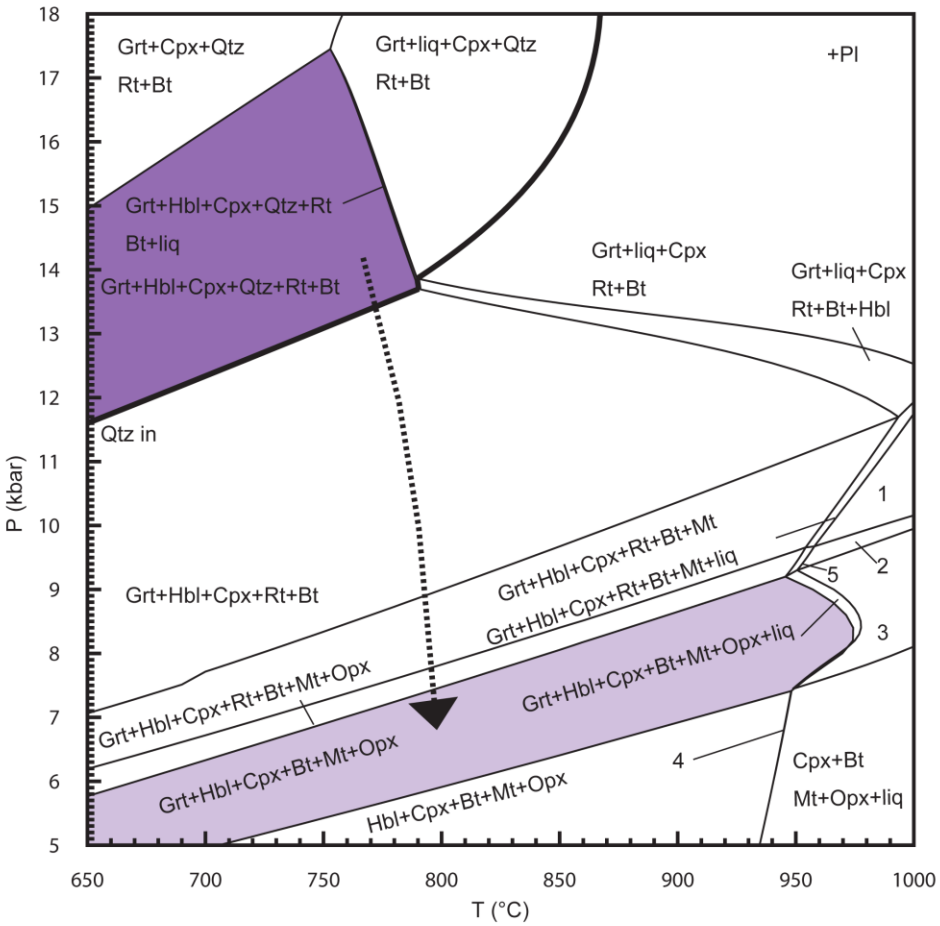

Fig. 22. *P-T* diagram showing calculated pseudosection of mineral assemblages in garnet amphibolite from Ongul (sample TS11020610I). Qtz: quartz, Pl: plagioclase, Cpx: clinopyroxene, Grt: garnet, Opx: orthopyroxene, Bt: biotite, Hbl: hornblende, Mt: magnetite, Ilm: ilmenite, Rt: rutile, liq: inferred melt.

1:Grt+liq+Cpx+Mt+Rt
2:Grt+liq+Cpx+Mt+Rt+Opx
3:Grt+liq+Cpx+Mt+Opx
4:Hbl+liq+Cpx+Bt+Opx
5:Grt+liq+Cpx+Mt+Rt+Opx+Hbl

Bulk composition (mol. %). @700 °C

H2O	SiO2	Al2O3	CaO	MgO	FeO	K2O	Na2O	TiO2	O	
0.97	41.62	8.18	11.17	12.79	19	0.26	0.39	3.94	1.68	(Bulk 100%)
6.37	42.45	7.79	9.03	12.11	16.34	0.65	0.5	3.39	1.38	(Bulk 85% Melt 15%)

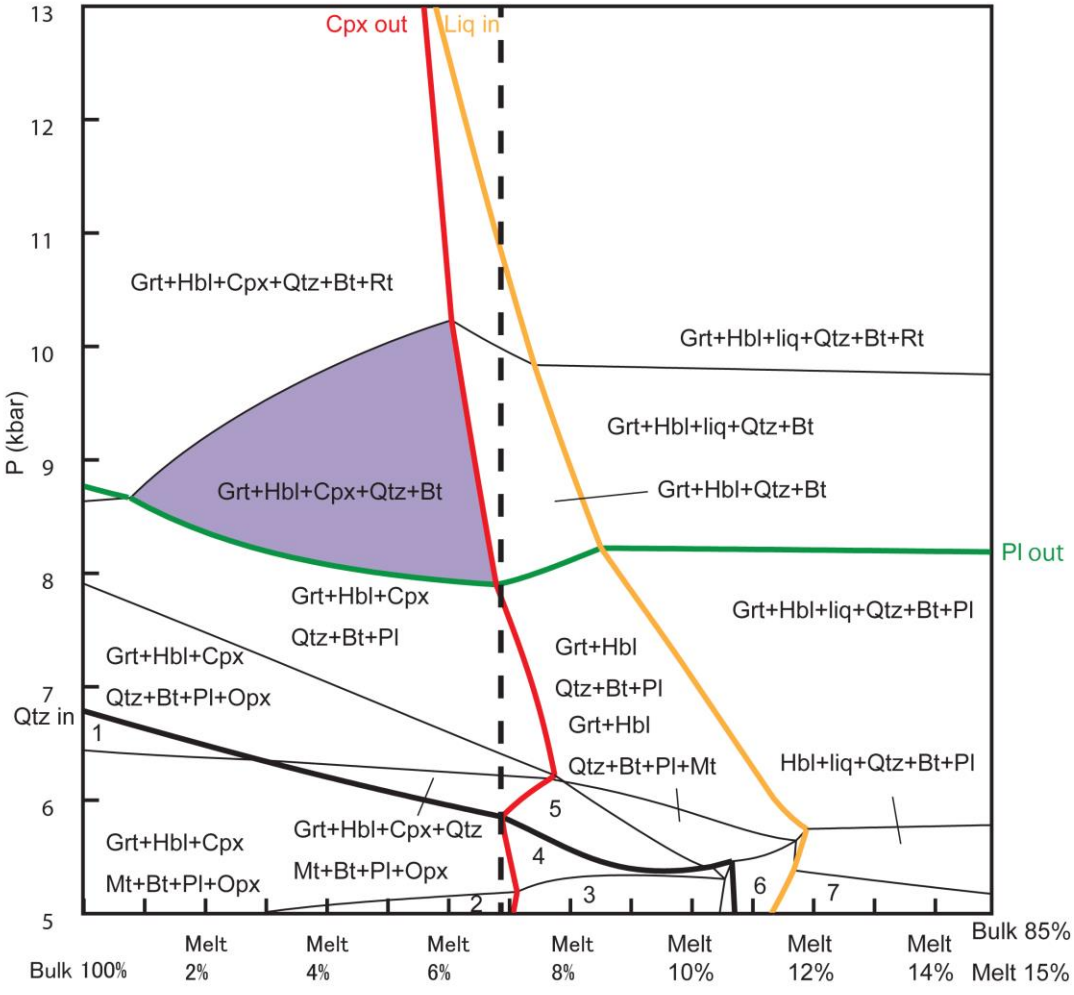

1:Grt+Hbl+Cpx+Bt+Pl+Opx
2:Hbl+Cpx+Mt+Bt+Pl+Opx
3:Hbl+Mt+Bt+Pl+Opx
4:Grt+Hbl+Mt+Bt+Pl+Opx
5:Grt+Hbl+Mt+Bt+Pl+Opx+Qtz
6:Hbl+Mt+Bt+Pl+Qtz
7:Hbl+Mt+Bt+Pl+liq+Qtz

Fig. 23. *P*-X diagram showing calculated pseudosection of mineral assemblages in mafic granulite from Skallevikshalsen (sample TS11010802). Qtz: quartz, Pl: plagioclase, Cpx: clinopyroxene, Grt: garnet, Opx: orthopyroxene, Bt: biotite, Hbl: hornblende, Mt: magnetite, Ilm: ilmenite, Rt: rutile.

Bulk composition (mol. %). @700 °C

H2O	SiO2	Al2O3	CaO	MgO	FeO	K2O	Na2O	TiO2	O
0.99	48.21	11.67	10.5	11.97	12	0.6	2.2	1.57	0.3 (Bulk 100%)
9.47	47.5	10.16	8.12	10.05	10.43	0.75	2	1.28	0.23 (Bulk 85% Melt 15%)

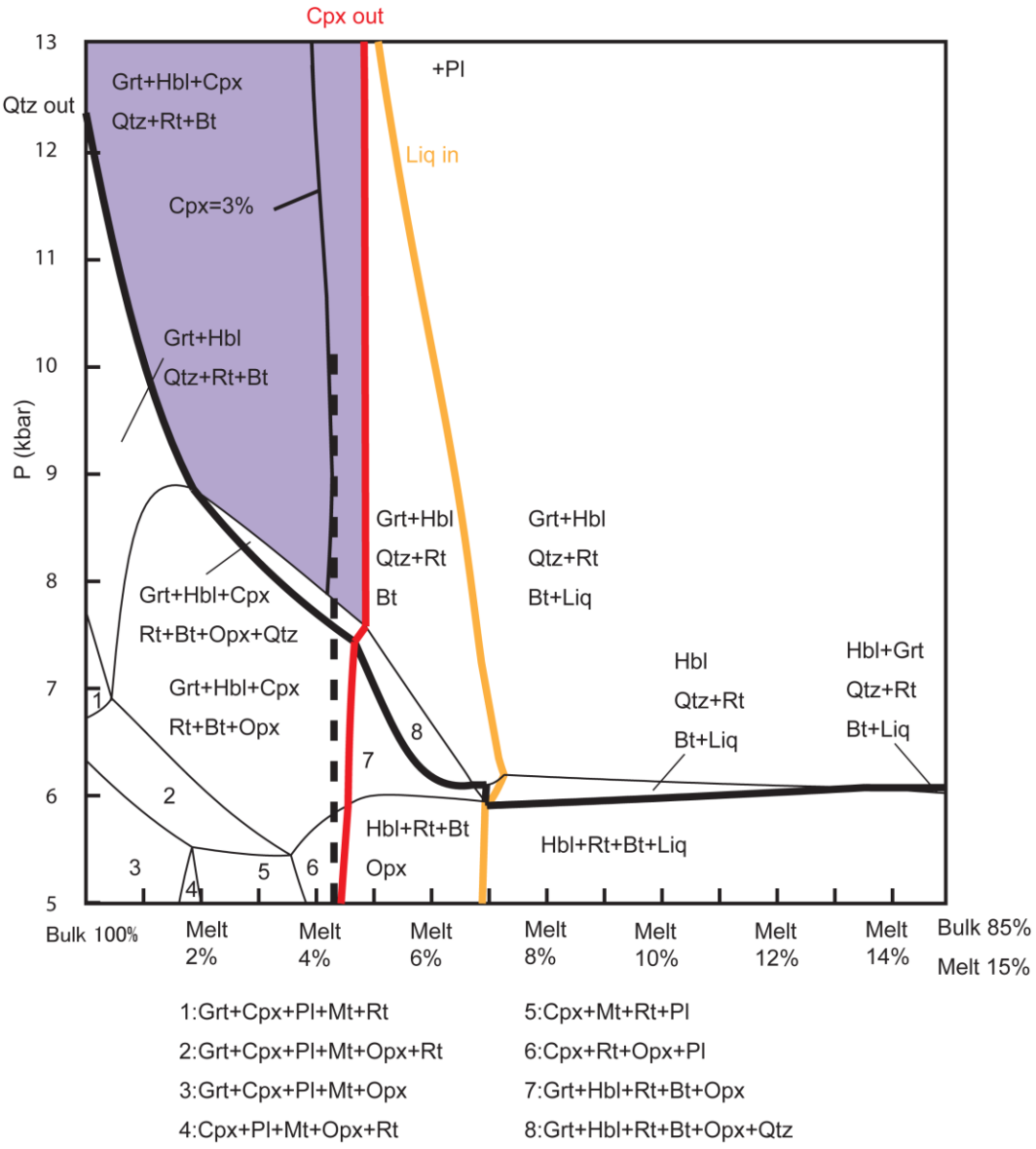

Fig. 24. *P*-X diagram showing calculated pseudosection of mineral assemblages in garnet amphibolite from Ongul (sample TS11020610I). Qtz: quartz, Pl: plagioclase, Cpx: clinopyroxene, Grt: garnet, Opx: orthopyroxene, Bt: biotite, Hbl: hornblende, Mt: magnetite, Ilm: ilmenite, Rt: rutile.

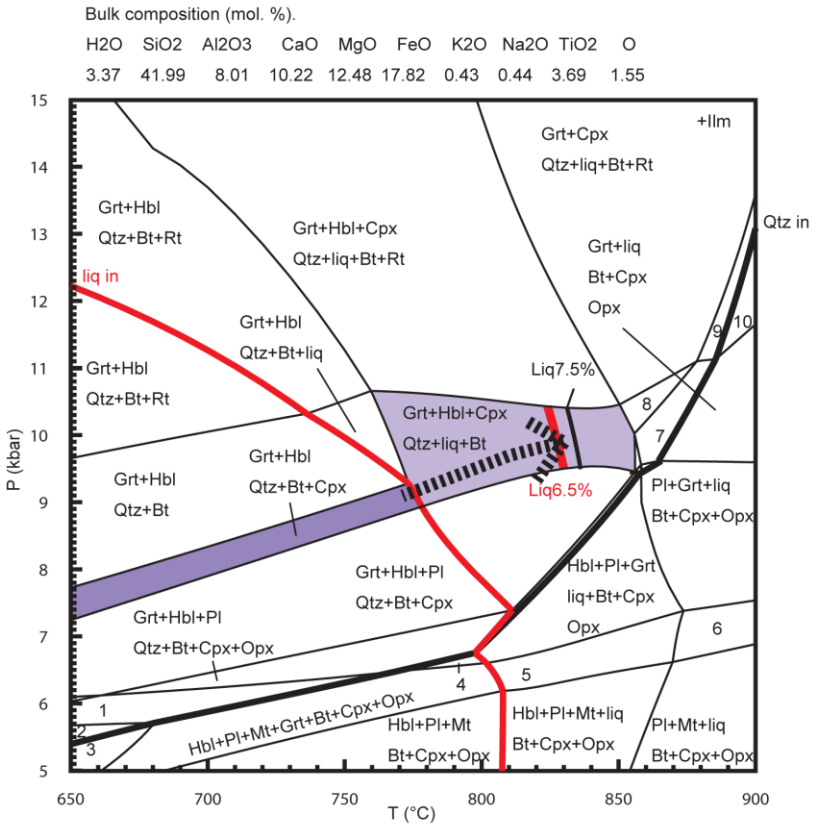

Fig. 25. *P-T* diagram showing calculated pseudosection of mineral assemblages in mafic granulite from Skallevikshalsen (sample TS11010802) with bulk rock chemistry of melt-integrated composition determined by Fig. 23. Qtz: quartz, Pl: plagioclase, Cpx: clinopyroxene, Grt: garnet, Opx: orthopyroxene, Bt: biotite, Hbl: hornblende, Mt: magnetite, Ilm: ilmenite, Rt: rutile.

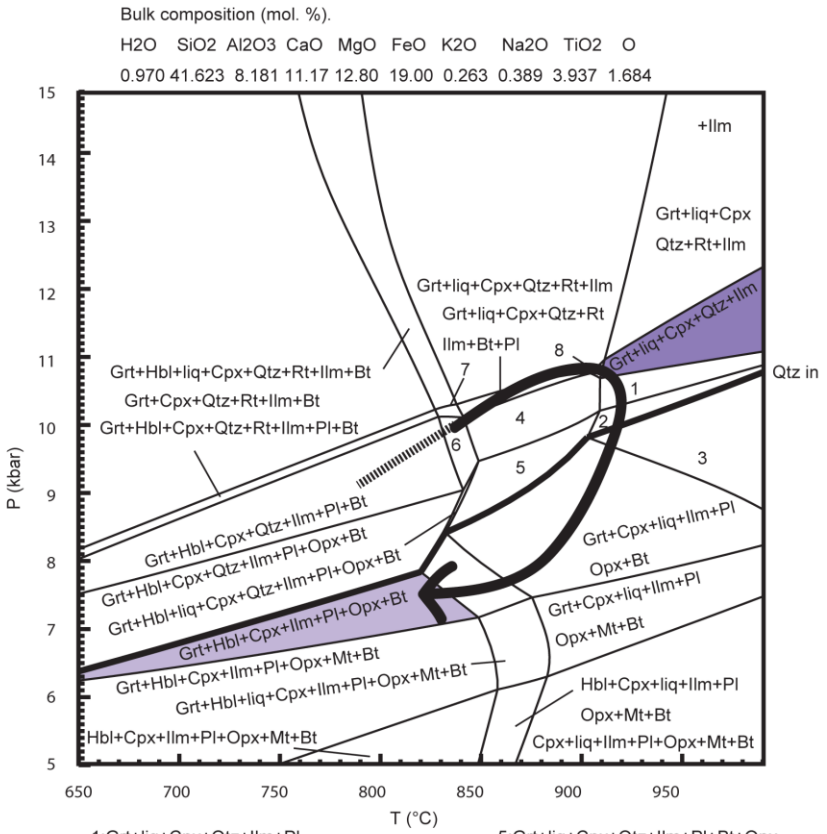

Fig. 26. *P-T* diagram showing calculated pseudosection of mineral assemblages in mafic granulite from Skallevikshalsen (sample TS11010802). Qtz: quartz, Pl: plagioclase, Cpx: clinopyroxene, Grt: garnet, Opx: orthopyroxene, Bt: biotite, Hbl: hornblende, Mt: magnetite, Ilm: ilmenite, Rt: rutile.

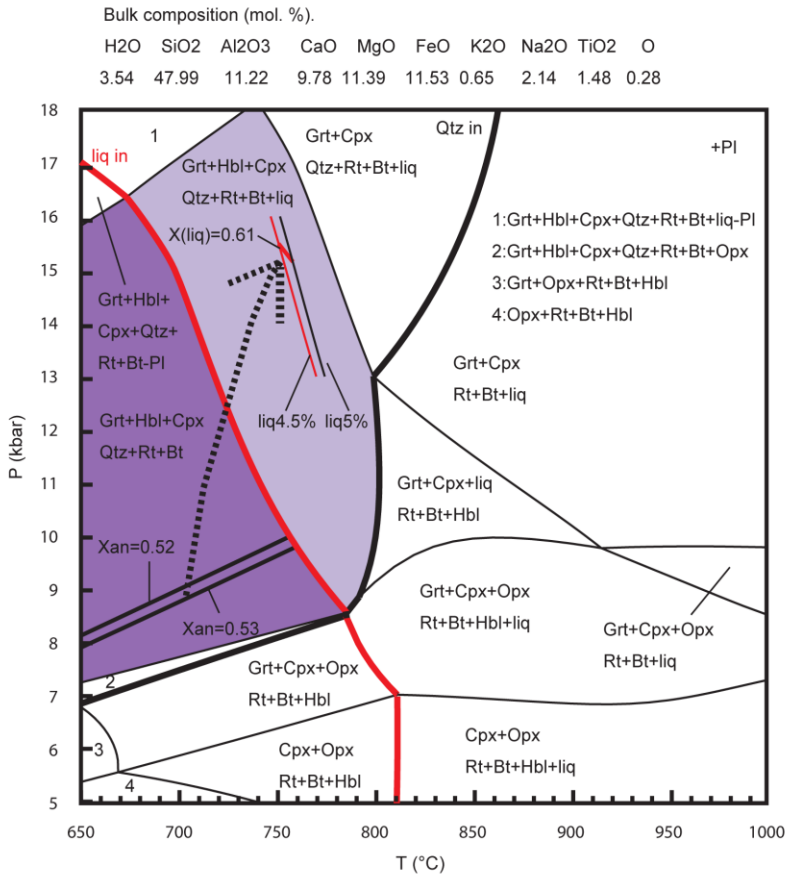

Fig. 27. *P-T* diagram showing calculated pseudosection of mineral assemblages in garnet amphibolite from Ongul (sample TS11020610I) with bulk rock chemistry of melt-integrated composition determined by Fig. 24. Qtz: quartz, Pl: plagioclase, Cpx: clinopyroxene, Grt: garnet, Opx: orthopyroxene, Bt: biotite, Hbl: hornblende, Mt: magnetite, Ilm: ilmenite, Rt: rutile. Xan: compositional isopleth of plagioclase. Xliq: compositional isopleth of liquid. liq4.5% and liq 5.5%: mode isopleth of liquid.

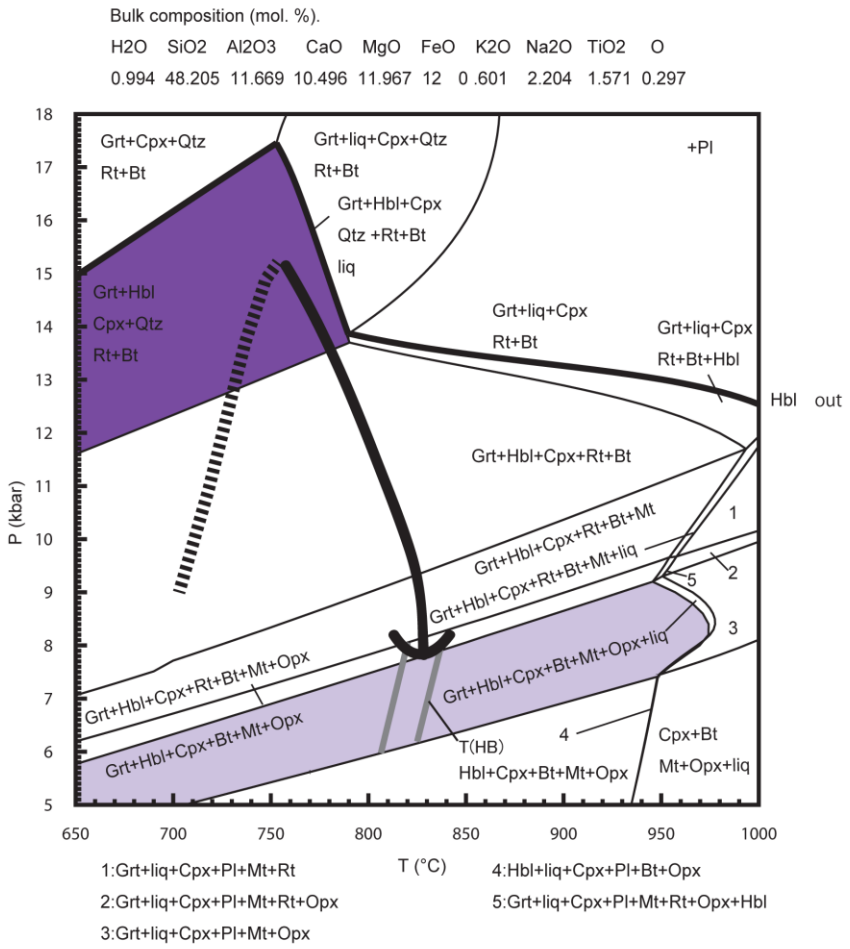

Fig. 28. *P-T* diagram showing calculated pseudosection of mineral assemblages in garnet amphibolite from Ongul (sample TS11020610I). Qtz: quartz, Pl: plagioclase, Cpx: clinopyroxene, Grt: garnet, Opx: orthopyroxene, Bt: biotite, Hbl: hornblende, Mt: magnetite, Ilm: ilmenite, Rt: rutile. T(HB)Holland and Blundy (1994).

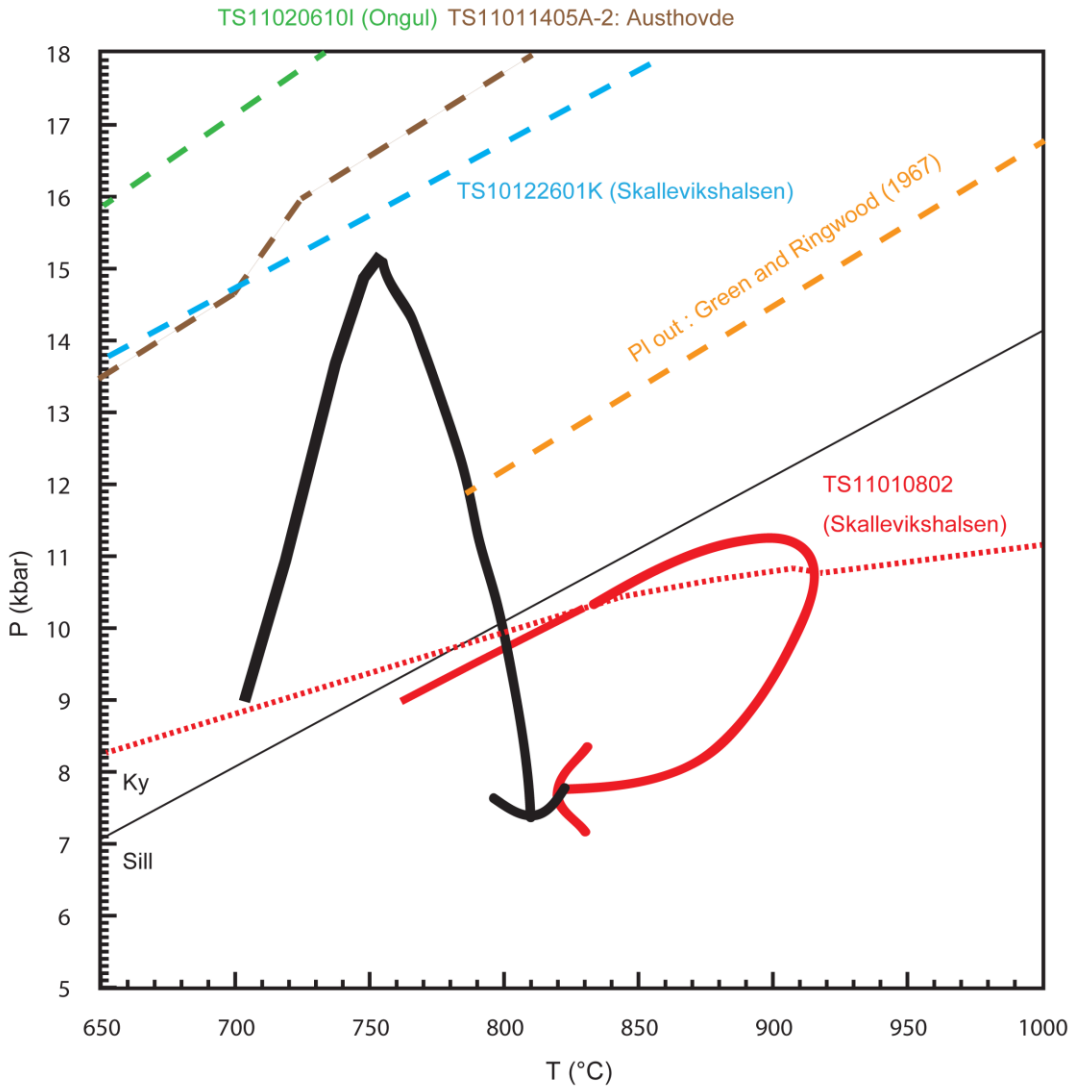

Fig. 29. Simplified *P-T* paths of the mafic granulite (sample TS11010802: red line from Skallevikshalsen) and garnet-amphibolite (sample TS11020610I: black line from Ongul). Dashed lines represent Pl-out line of each sample calculated by psuedosection.

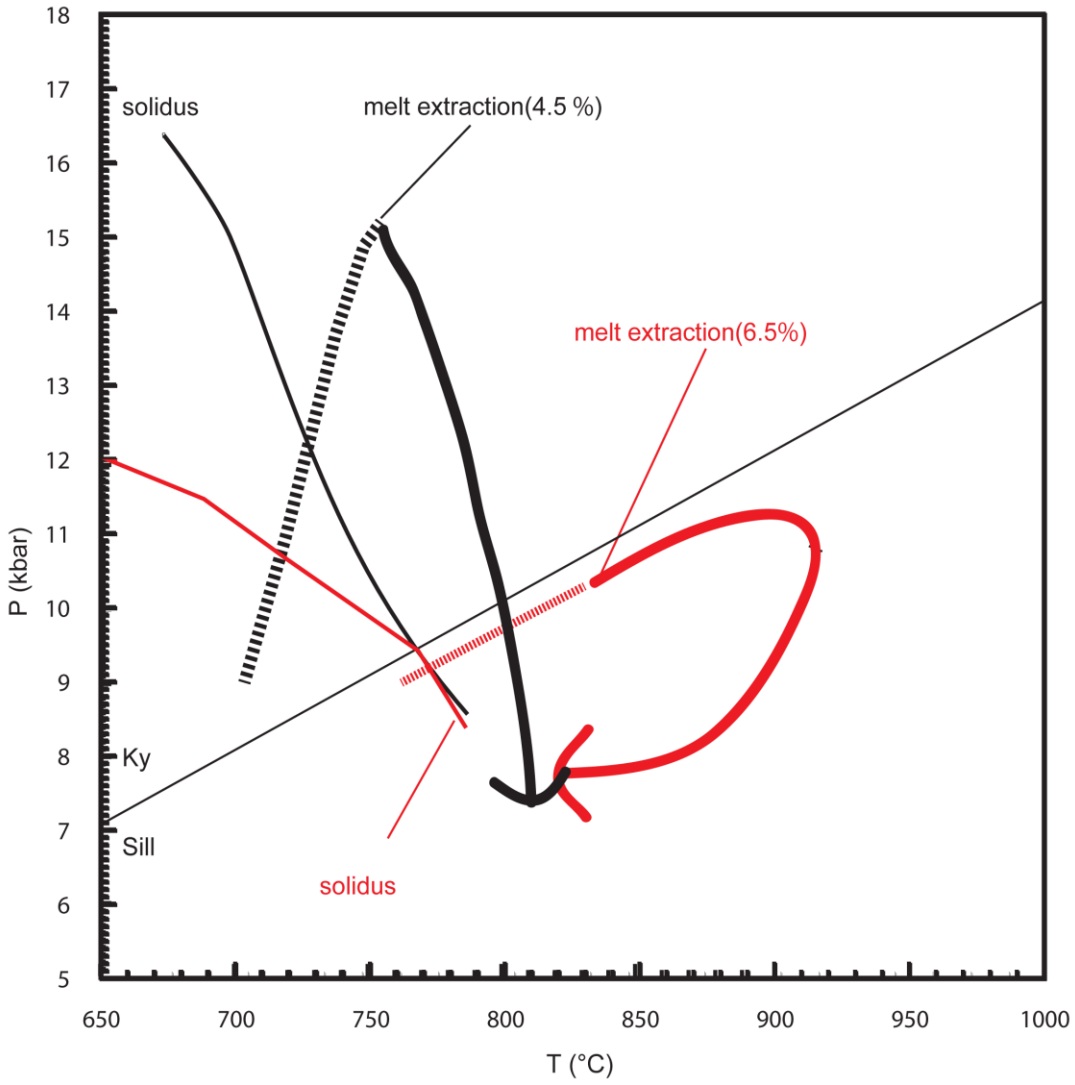

Fig. 30. Simplified *P-T* paths of the mafic granulite (sample TS11010802: red line) and garnet-amphibolite (sample TS11020610I: black line), and solidus of the examined samples. Dashed lines inferred the *P-T* paths before melt extraction.

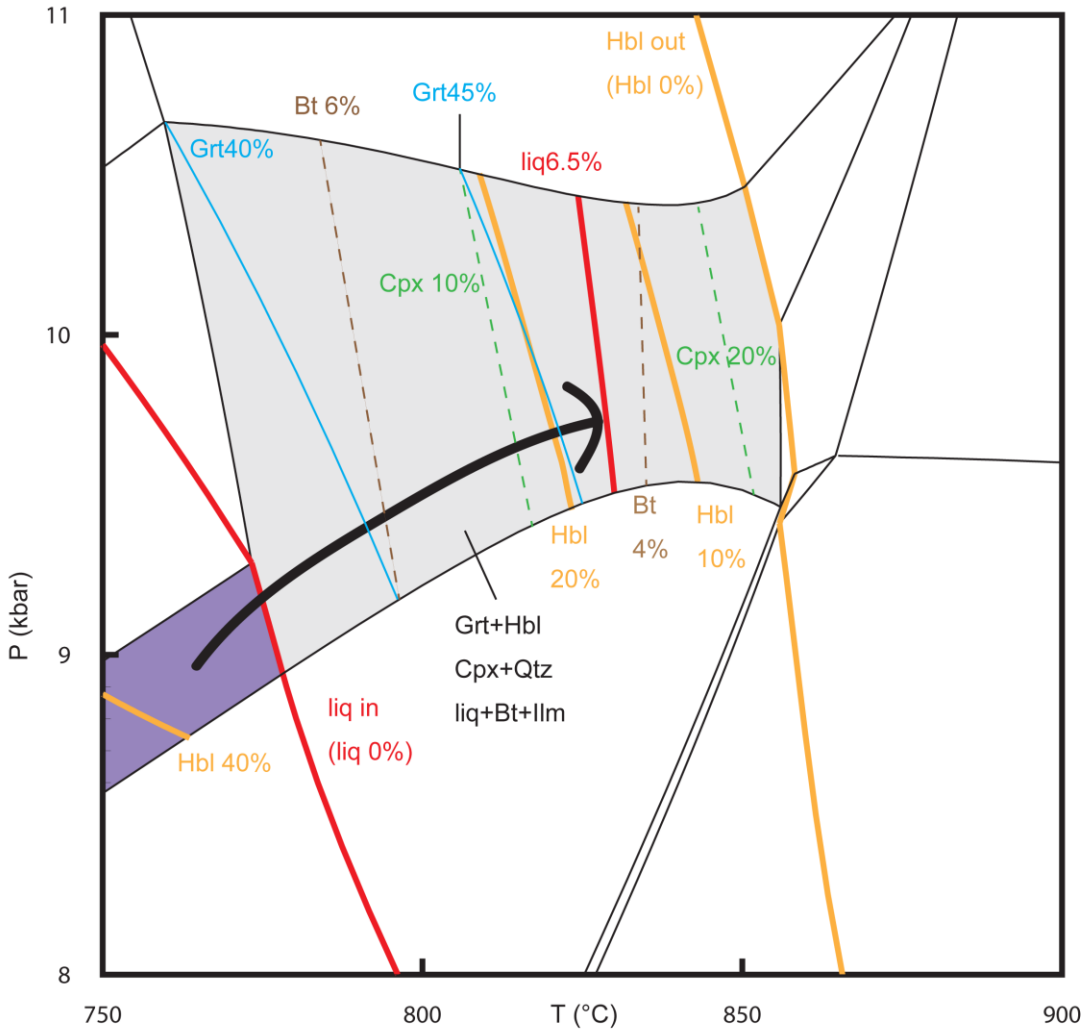

Fig. 31. *P-T* diagram showing calculated pseudosection of mineral assemblages in mafic granulite from Skallevikshalsen (sample TS11010802). Detailed *P-T* diagrams in Fig. 26. with mineral modal isopleth.

Qtz: quartz, Pl: plagioclase, Cpx: clinopyroxene, Grt: garnet, Opx: orthopyroxene, Bt: biotite, Hbl: hornblende, Mt: magnetite, Ilm: ilmenite, Rt: rutile.

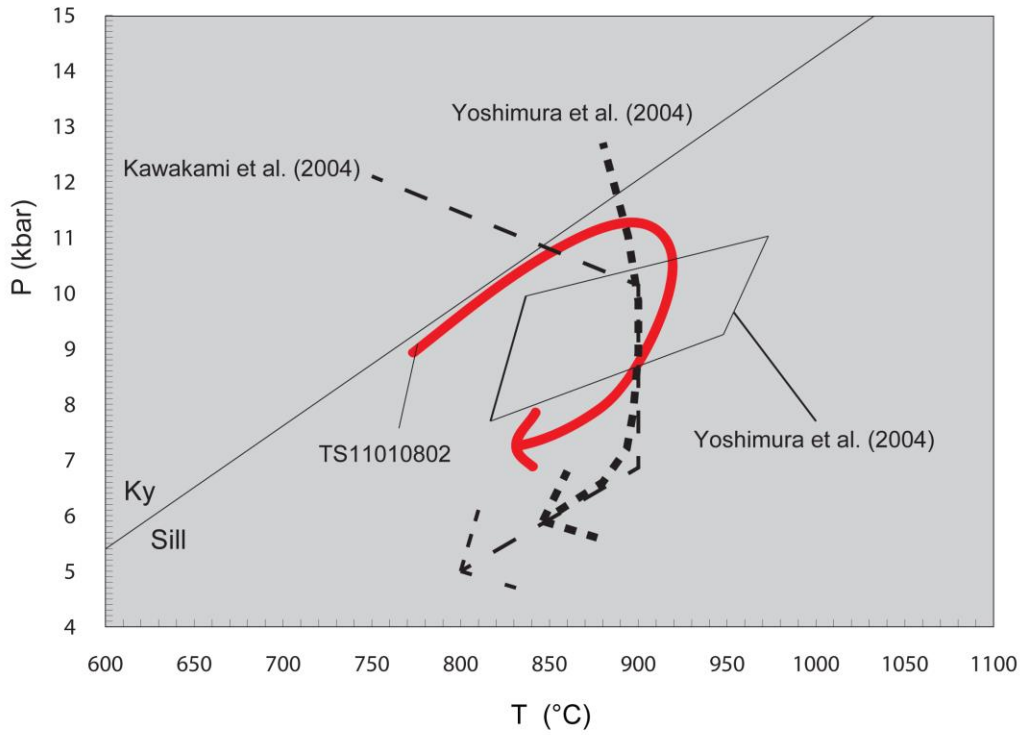

Fig. 32. Simplified *P-T* path of the mafic granulite (sample TS11010802: red line from Skallevikshalsen) and *P-T* paths and *P-T* conditions reported by Kawakami et al. (2004) and Yoshimura et al. (2004).

Table 1. Mineral name abbreviations

Mineral	abbreviations
Amp	amphibole
Ap	apatite
Bt	biotite
Cal	calcite
Grt	garnet
Ilm	Ilmenite
Kfs	alkali feldspar
Opq	opaque mineral
Opx	orthopyroxene
Pl	plagioclase
Qtz	quartz
Rt	rutile
Scp	scapolite
Sil	sillmanite
Sph	sphene
Spl	spinel
Zr	zircon

Table 2. Approximate abundance of minerals from the studied area

Sample	Grt	Sil	Kfs	Pl	Qtz	Bt	Spl	Rock type	Accessory	Locality
TS11011401A	10 15%	5-15%	5-15%	<5	25-35%	<1		5	Ilm, Rt	Austhovde
TS11011401K3	15-25%	10-15%	20-30%	5-15%	15-20%			2	Opq, Zr	〃
TS11011401N	15-20%		25-35%	10-20%	<2%	10-20%		6	Opq, Zr	〃
TS11011402A	10-15%	10-15%	10-15%	10-20%	20-30%	5-10%		5	Opq	〃
TS11011404B		3-5%	40-45%	3-5%		10-20%		8	Crn(3-5%)	〃
TS11011405D	3-5%		20-30%	10-15%		15-25%	10-20%	6	Opq	〃
TS11011502A	10-20%	10-20%	25-30%	5-15%	5-15%			5	Opq	〃
TS11011502D	10-20%		5-15%	15-25%	15-25%	5-15%	5-15%	2	Opq, Ap, Zr	〃
TS11011503C	20-30%	10-15%	30-40%		<5%			4	Opq, Bt	〃
TS11011504A	30-35%	5-10%	10-15%	5-10%		15-25%	5-15%	5	Qtz, Rt	〃
TS11011504C	40-45%	0-10%	<2%	5-15%		25-30%		2	Qtz,Rt,Spl,Ky	〃
TS11011601C	15-20%		30-35%	<2	10-15%	5-10%	<1	2	Opq, Ap	〃
TS11011601G	20-25%	5-10%	25-30%	5-10%	<1%	40-50%	10-15%	7	Opq	〃
TS11011601I	10-15%		25-35%	<5%	25-35%	5-10%		2	Opq	〃
TS11011601J	20-25%		25-35%	5-15%		10-15%	<5%	6	Opx, Pl, Bt	〃
TS11011601K	Cpx(10-15%)		Scp(60-70%)		Spn(<5)			8		〃

Rock type, 1:Grt-Cpx rock, 2:Grt-mafic granulite, 3:Mafic granulite, 4: Ultra-mafic granulite, 5: Grt-Sil gneiss 6. Grt-Bt gneiss, 7: Amphibolite, 8: Others

Table 2. Continued

Sample	Grt	Cpx	Opx	Pl	Qtz	Amp	Bt	Rock type	Accesory	Locality
TS11011401E		20-25%	15-20%	10-20%		<1%	5-15%	3	Opq, Zr	Austhovde
TS11011401F		20-30%	15-25%	10-15%		10-15%		3	Bt	〃
TS11011401G		15-25%	<5	25-35%		15-25%	>2%	3	Opq	〃
TS11011401I		<1%	5-15%	20-30%	10-15%	5-10%	10-15%	3	Ap, Ilm	〃
TS11011407B		5-15%	10-20%	5-15%	5-15%	10-15%	10-20%	6	Opq	〃
TS11011503B	10-15%	5-10%	10-15%	20-25%	20-25%	10-15%	<2%	2	Opq	〃
TS11011504D	<2%	10-15%	5-10%	5-15%	5-15%	5-15%	5-15%	2	Opq (5-15%), Ap, Zr	〃
TS11011505D		90-95%	<2%					8	Amp, Bt	〃
TS11011601D		10-15%	30-40%	25-35%	20-30%	>5		3	Bt	〃
TS110111701B		15-25%	<5	20-30%	<1%	20-25%		3	Opq	〃
TS11011601N	15-20%	10-15%	5-10%	15-20%	<1%	5-15%		2	Opq, Zr	Austhovde
TS11011701C		10-15%	15-25%	15-25%	<1%	10-20%	0-5%	3	Bt	〃
TS11011701E2		20-25%	20-25%	5-10%		15-25%	2-5%	3	Opq	〃
TS11011702C		10-15%	5-10%	10-15%	25-35%		0-5%	8	Ap, Ilm	〃

Rock type, 1:Grt-Cpx rock, 2:Grt-mafic granulite, 3:Mafic granulite, 4: Ultra-mafic granulite, 5: Grt-Sil gneiss 6. Grt-Bt gneiss, 7: Amphibolite, 8: Others

Table 2. Continued

Sample	Grt	Sil	Kfs	Pl	Qtz	Bt	Spl	Rock type	Accessory	Locality
TS11011601L	Cpx(75-80%)		Scp(5-10%)					8		Austhovde
TS11011602A	Cpx(5-10%)		Scp(70-80%)		Spn(<5)			8		〃
TS11011603			10-15%	20-25%	10-20%	5-10%		8	Opx,Hbl, Opq	〃
TS11011604A	15-20%	10-15%	25-35%	<1%	10-20%	5-10%		5	Opq	〃
TS11011604B	15-20%	10-15%	35-45%	<1%	<1%	5-10%		5		〃
TS11011604C	5-15%		20-30%	30-40%		5-10%	0-5%	6	Opq	〃
TS11011605A	5-10%		25-30%	10-15%	20-25%	5-10%	0-5%	6	Opq	〃
TS11011607A	5-15%		45-50%	<1%	5-10%	5-10%	0-5%	2	Opq, Ap, Zr	〃
TS11011607B	15-25%	10-15%	30-40%	5-10%	10-15%	5-15%		4	Spl	〃
TS11011701D	5-15%	5-10%	15-25%	25-35%	0-10%	2-5%	2-5%	5		〃
TS11011701F	40-45%		20-25%	15-20%	35-45%	0-5%		2		〃
TS11011702A	15-20%	10-15%	15-20%	5-15%	<1%	5-10%	10-15%	5	Opq, Ap	〃
TS11011702B	15-25%	10-15%	10-15%	5-10%	0-5%	10-15%	10-15%	7	Opq	〃
TS11011702B2	5-10%		15-20%	10-15%	25-30%	5-10%	5-10%	6	Opq	〃
TS11011702E	5-10%	10-15%	20-30%	20-30%	<1%	5-10%	10-15%	5	Opq	〃
TS11011702F	10-15%	0-5%	25-35%	<1%	25-35%			5		〃
TS11011702G	25%	2-3%			75-85%			8	Pl, Kfs, Ky	

Rock type, 1:Grt-Cpx rock, 2:Grt-mafic granulite, 3:Mafic granulite, 4: Ultra-mafic granulite, 5: Grt-Sil gneiss 6. Grt-Bt gneiss, 7: Amphibolite, 8: Others

Table 2. Continued

Sample	Grt	Cpx	Opx	Pl	Qtz	Amp	Bt	Rock type	Accesory	Locality
TS10122401C				20-25%		35-45%	15-20%	2	Opq, Zr	Skalleviks halsen
TS10122401D		85-90%	15-25%	5-7%				4	Opx	〃
TS10122401F		25-35%	25-35%	2-4%		5-10%	5-10%	3	Opq	〃
TS10122501K1	Scp(50-60%)					5-15%	5-15%	8		〃
TS10122501K2		5-10%		5-10%			3-5%	8	Scp(60-65%)	〃
TS10122601C		30-35%	20-25%			10-15%	10-15%	4	Opq	〃
TS10122601E		25-30%	20-25%	15-25%	2-5%			3	Opq (5-15%), Ap, Zr	〃

Sample	Grt	Sil	Kfs	Pl	Qtz	Bt	Spl	Rock type	Accessory	Locality
TS10122806B	5-7%	3-5%	20-25%	5-10%	10-15%	<1%	<1%	5		Skalleviks halsen
TS10122806B2	10-15%		45-55%	5-10%	5-10%	3-5%		8	Opx	〃
TS11010804	20-25%		10-15%	10-15%	5-7%	5-7%	5-7%	6		〃
TS11010903A	20-25%	5-7%	30-35%	2-3%	10-15%		2-3%	5	Rt	〃
TS11010903B	25-30%		10-15%	10-15%	15-20%	10-15%		6		〃

Rock type, 1:Grt-Cpx rock, 2:Grt-mafic granulite, 3:Mafic granulite, 4: Ultra-mafic granulite, 5: Grt-Sil gneiss 6. Grt-Bt gneiss, 7: Amphibolite, 8: Charnockite, 9: Others

Table 2. Continued

Sample	Grt	Sil	Kfs	Pl	Qtz	Bt	Spl	Rock type	Accessory	Locality
TS10122401A			50–55%	5–10%	10–15%	2–5%		8	Opx	Skalleviks halsen
TS10122502B2	15–20%		20–25%	<1%	10–15%	5–10%		6	Crd(10–15%)	〃
TS10122502C	20–25%		10–15%	10–15%	15–25%	10–15%		6		〃
TS10122502C-2	20–25%		20–30%	10–15%	15–20%	5–10%		6	Opq	〃
TS10122502D	15–25%		15–20%	15–20%	15–20%	2–3%		5	Opx(5–10%), Ky	〃
TS10122502G	25–35%	5–7%	30–45%	30–40%	5–7%	3–5%		6	Rt,Qtz	〃
TS10122503E	25–30%	5–7%	35–40%	5–10%	<1%	5–7%	Opx(2–3)	6	Opq	〃
TS10122504B	20–25%		10–15%	15–20%	10–15%	5–10%	0–5%	2	Opq, Ap, Zr,Rt	〃
TS10122505B	35–40%	5–10%	25–30%	<1%	10–15%	<1%		4	Rt, Spl	〃
TS10122505B-2	20–25%	5–10%	30–35%		10–15%	<1%	2–5%	5	Rt	〃
TS10122505C	10–15%		20–30%	5–7%	20–30%	5–7%		9	Rt	〃
TS10122601H	15–20%		25–35%	25–30%	<1%	3–5%	5–7%	9	Opq, Ap	〃
TS10122604F2	5–10%		10–15%	15–20%	10–15%	7–10%	2–5%	9	Opq	〃
TS10122604H	3–5%		40–45%	5–10%	20–30%	1–3%		6	Opq	〃
TS10122702C1	10–15%	10–15%	30–35%	20–25%	<1%	5–10%	10–15%	8	Opx(5–7%)	〃
TS10122702C2	5–10%	0–5%	20–25%	10–15%	25–30%	5–7%		8	Opx(3–5%)	〃

Rock type, 1:Grt–Cpx rock, 2:Grt–mafic granulite, 3:Mafic granulite, 4: Ultra–mafic granulite, 5: Grt–Sil gneiss 6. Grt–Bt gneiss, 7: Amphibolite, 8: Charnockite, 9: Others

Table 2. Continued

Sample	Grt	Sil	Kfs	Pl	Qtz	Bt	Spl	Rock type	Accessory	Locality
TS11020602A	5–7%		25–30%	15–20%	30–35%	3–5%		6		Ongul
TS11020602B	5–10%		35–45%	10–15%	30–35%	3–5%	<1%	6		〃
TS11020602C	15–20%		5–10%	15–20%	20–25%	10–15%	5–7%	6		〃
TS11020604B	10–15%	7–10%	10–15%	10–15%	20–25%	7–10%		6	Rt (2–3%)	〃
TS11020607B	35–40%	5–7%	10–15%	10–15%	15–20%	7–10%		6	Rt (3–5%)、Opq	〃
TS11020608B	30–35%	5–7%	35–40%	10–15%	15–20%	3–5%	Rt (2–4%)	8	Opx、Ilm (5–7%)	〃
TS10122502A1	15–25%	10–15%	35–40%		5–10%	5–10%		5	Opq, Ap, Pl, Bt	Skalleviks halsen
TS10122502E	20–25%	5–10%	15–20%	5–10%	15–20%	15–20%		4	Rt, Spl	〃
TS10122502H	25–30%		15–25%	10–15%	10–15%	10–15%		6	Opq	〃
TS10122502I	20–25%		5–10%	15–20%	25–30%		Opx (5–7%)	8	Bt, Rt	〃
TS10122503B	5–10%		30–35%	20–25%	10–15%	3–5%	Opx (2–3%)	9	Opq, Ap	〃
TS10122504B	15–20%		30–35%	10–15%	15–20%	5–7%		6	Opq	〃
TS10122601D	20–25%		25–35%	15–20%			10–15%	8	Opq, Bt	〃
TS10122601F2	15–20%		10–15%	5–10%	35–45%	1–3%		6	Opq	〃
TS10122601G	40–45%		15–20%	5–10%	20–25%	2–3%		6	Opq,	
TS10122601J	15–20%		35–40%	15–20%		2–3%	5–7%	8	Qtz	

Rock type, 1:Grt–Cpx rock, 2:Grt–mafic granulite, 3:Mafic granulite, 4: Ultra–mafic granulite, 5: Grt–Sil gneiss 6. Grt–Bt gneiss, 7: Amphibolite, 8: Others

Table 2. Continued

Sample	Grt	Cpx	Opx	Pl	Qtz	Amp	Bt	Rock type	Accesory	Locality
TS11020603C	30–35%		5–7%	20–25%		10–15%	5–7%	2	Opq, Zr, Qtz	Ongul
TS11020604A	30–35%		15–25%	5–10%	10–15%		7–10%	2	Opq (10–15%)	〃
TS11020605			15–20%	35–45%		10–15%	5–7%	3	Opq (5–7%), Cpx, Qtz	〃
TS11020606A	50–55%		5–10%	5–10%	5–10%	5–15%	5–15%	2	Ilm (7–10%)	〃
TS110206010C	7–10%	5–10%	5–10%	25–30%		15–20%	10–15%	2	Cpx, Opx	〃
TS11020610E		30–35%	45–55%			5–10%	10–15%	4	Opq	〃
TS11020611D	3–5%	25–30%	20–25%	10–15%	25–30%	3–5%		8	Kfs(15–20%)	〃
TS1122501K2		10–15%			Scp (60–70%)		5–10%	8	Sph (5–10%)	Skalleviks halsen
TS10122502F	20–25%	10–15%	15–20%	15–20%	10–15%			2	Cpx, Rt, Opq	〃
TS10122503C		5–10%	40–45%	30–35%	<1%			3	Opq, Qtz	〃
TS10122601A		10–15%			Scp (75–85%)			8	Sph	〃
TS10122601B		5–10%		5–10%		70–75%		7	Opx, Bt, Scp	〃
TS10122601I		5–10%		10–15%		20–25%	25–30%	7	Kfs (5–10%)	〃
TS10122601N	25–30%		10–15%	20–25%		20–25%	2–3%	2	Opq, Cpx	〃
TS10122602A	15–20%		15–20%	10–15%	20–25%	20–30%	5–10%	8	Opq, Rt	〃
TS10122602B	5–10%		20–25%	10–15%	15–20%		5–10%	8	Kfs(5–10%)	

Rock type, 1:Grt–Cpx rock, 2:Grt–mafic granulite, 3:Mafic granulite, 4: Ultra–mafic granulite, 5: Grt–Sil gneiss 6. Grt–Bt gneiss, 7: Amphibolite, 8: Others

Table 2. Continued

Sample	Grt	Cpx	Opx	Pl	Qtz	Amp	Bt	Rock type	Accesory	Locality
TS10122604G1		20–25%	15–20%	10–15%		15–20%	3–5%	3	Opq, Grt、Kfs(5–7%)	Skalleviks halsen
TS10122604I	15–20%		3–5%	10–15%	25–35%		5–10%	2	Opq (5–7%)	〃
TS11010602D	40–45%	10–15%	3–5%	10–15%		10–15%	5–7%	1	Opq	〃
TS11010901	40–45%		5–10%	10–15%	5–10%	10–15%	5–15%	8	Kfs (20–25%)	〃
TS11010902	15–25%	15–25%		5–10%		30–35%		2	Opq	〃
TS11011407E	40–45%			5–10%	30–35%			8	Opq	〃
TS11011501A		5–10%	10–15%	10–15%		40–45%	5–7%	3		Austhovde
TS11011503A	7–10%	10–15%	10–15%	20–25%		20–25%		2	Opq	〃
TS11011504C	2–3%	10–15%	15–20%	15–20%	10–15%	10–15%	7–10%	2	Opq	〃
TS11011504E		90–95%		2–3%				3	Opq	〃
TS11011601B	5–10%	10–15%		20–30%	15–25%	Scp (10–15%)		8	Sph	〃
TS11011601H		5–10%	3–5%	10–15%	5–10%		10–15%	8	Kfs (40–45%)	〃
TS11011602D		50–60%				Scp (25–35%)		7	Sph (2–3%)	〃
TS11011605B		20–25%		Scp (55–60%)			2–3%	2	Sph (3–5%)	〃
TS11011606A		25–35%	50–55%					8	Opq, Hbl, Bt	〃
TS11011702D	10–15%	10–15%	15–25%	20–25%	10–15%		5–10%	2	Opq (5–7%)	

Rock type, 1:Grt–Cpx rock, 2:Grt–mafic granulite, 3:Mafic granulite, 4: Ultra–mafic granulite, 5: Grt–Sil gneiss 6. Grt–Bt gneiss, 7: Amphibolite, 8: Others

Table 2. Continued

Sample	Grt	Sil	Kfs	Pl	Qtz	Bt	Spl	Rock type	Accessory	Locality
TS10122603A	45–50%		15–20%	5–10%		10–15%		6		Skalleviks halsen
TS10122603B	35–40%		10–15%	15–20%	10–15%	5–7%		6	Opq	〃
TS10122604A	Opx (10–15%)		10–15%	15–20%	20–25%	15–20%		8		〃
TS10122604K			45–55%	3–5%	15–20%		Opx (5–10%	6	Grt	〃
TS11010903C	30–35%	3–5%				5–7%		6	Spl, Opq	〃
TS11011502C	5–7%	5–7%	65–75%	10–15%	15–20%		3–5%	8	Pl	Austhovde

Sample	Grt	Cpx	Opx	Pl	Qtz	Amp	Kfs	Rock type	Accesory	Locality
TS11011201A	3–5%		3–5%	20–25%	10–15%	5–7%	60–65%		Opq, Zr、Pl	karamete
TS11011204A			3–5%	5–7%	15–25%		55–60%		Grt, Pl	〃
TS11011204B	2–4%	2–4%	4–5%		10–15%	2–3%	60–65%		Opq、Pl	〃
TS11011205B	2–4%	2–4%			10–15%	5–15%			Grt, Amp, Pl	〃
TS11011206A	2–4%		5–7%		10–15%	3–5%	45–55%			〃
TS11011206B	3–5%		2–4%		10–15%	5–10%	50–55%		Opq, Pl	〃
TS11011207			5–7%		10–15%	10–15%	55–60%		Pl, Zr	〃
TS11011208	3–5%	90–95%	<2%		20–15%	7–10%	40–45%		Opx, Cpx, Pl	〃

Rock type, 1:Grt–Cpx rock, 2:Grt–mafic granulite, 3:Mafic granulite, 4: Ultra–mafic granulite, 5: Grt–Sil gneiss 6. Grt–Bt gneiss, 7: Amphibolite, 8: Others

Table 2. Continued

Sample	Grt	Cpx	Opx	Pl	Qtz	Amp	Bt	Rock type	Accesory	Locality
TS10122405B	70–75%	10–15%				5–10 %		1	Scp	Skalleviksha lsen
TS10122503B	5–15%	10 20%	0–10%	35– 45%	15 20%	10–20%		2	Bt	〃
TS10122503D	10–20%	5–15%	10–20%	25–35%	10–20%	0 10 %		2		〃
TS10122506	10–20%	10–20%	10–20%	10–20%	10–20%	10–20%		2	Bt Opq	〃
TS10122601G	45–55%			0–10%	15–25%		0–10%	6	Hbl	〃
TS10122601K	20–30%		10–20%	5–15%		10–20%	5–15%	3	Qtz, Rt, Ilm, Mt, Cpx	〃
TS10122601L	20–30%		20–30%	5–15%		10–20%		2	Opq	〃
TS10122601N	10–20%		0–10%	15–25%		30–40%		2	Opq	〃
TS10122602A	10–20%		15–25%	10–20%	10–20%	10–20%	0–10%	2	Opq, Zr	〃
TS10122604B	30–40%		15–25%	5–15%	5–15%			2	Hbl, Bt, Ilm	〃
TS10122604G		10–20%	10–20%	10–20%		5–15%	10–15%	3	Grt, Opq	〃
TS10122604I	15–25%		0–10%	5–15%	20–30%	10–20%	0–10%	2	Opq	〃
TS10122702B			45–55%	10–20%	5–15%			3	Opq	〃
TS11010704A	30–40%	40–50%				0–10%		1	Pl, Opq	〃
TS11010704A3	50–60%	20–30%		0–10%				1	Hbl, Opq	〃
TS11010704B	20–25%	50–60%				5–10%		1	Opq	〃

Rock type, 1:Grt–Cpx rock, 2:Grt–mafic granulite, 3:Mafic granulite, 4: Ultra–mafic granulite, 5: Grt–Sil gneiss 6. Grt–Bt gneiss, 7: Others

Table 2. Continued

Sample	Grt	Cpx	Opx	Pl	Qtz	Amp	Bt	Rock type	Accesory	Locality
TS11010801	0–10%	0–10%		65–75%				6	Opq, Hbl	Skalleviks halsen
TS11010802	55–65%	15–25%	0–5%	0–5%		0–5%		1	Qtz,Opq, Bt	〃
TS11010803A	25–35%	40–50%						1	Ilm, Qtz, Pl, Ap, Amp	〃
TS11010803A-4	40–50%	30–40%	0–10%					1	Qtz, Ap, Ilm, Hbl	〃
TS11010803A-6	40–50%	30–40%						1	Qtz, Ap, Ilm, Hbl	〃
TS11010803C	50–60%	20–30%		5–15%				1	Opq, Hbl, Bt, Ap	〃
TS11010803D	0–10%	5–15%	5–15%	5–15%		15–25%	10–20%	2	Opq, Ap, Zr	〃
TS11010903D	30–40%	0–10%	15–25%	5–15%	0–10%	10–20%		2	Opq, Bt	〃
TS11011401L	55–65%			0–10%			0–10%	2	Opq (5–15%), Spl	Austhovde
TS11011405A	10–15%		0–10%	10–20%		30–40%	0–10%	2	Qtz, Opq	〃
TS11011405A-2	20–30%	15–20%	10–15%	10–15%	10–20%			2	Ilm, Ap	〃
TS11011405B	10–15%		20–30%	25–35%		10–15%		2	Ilm, Bt, Qtz	〃
TS11011405C	5–15%	5–10%		10–15%	10–15%	25–35%		2	Ilm	〃
TS11011407D	5–10%		10–15%	10–15%	35–45%	5–15%		7	Mag, Zr	〃
TS11011407E	55–65%			0–10%	15–25%			7	Opq, Bt	〃

Rock type, 1:Grt–Cpx rock, 2:Grt–mafic granulite, 3:Mafic granulite, 4: Ultra–mafic granulite, 5: Grt–Sil gneiss 6. Grt–Bt gneiss, 7: Others

Table 2. Continued

Sample	Grt	Cpx	Opx	Pl	Qtz	Amp	Bt	Rock type	Accesory	Locality
TS11011501A		0–10%	5–15%	10–20%		45–55 %	0–10%	7		Austhovde
TS11011504C	0–10%		5–15%	10–20%	5–15%	5–15%	5–15%	2	Opq, Zr	〃
TS11011504E		70–80%	0–10%			0–10%		4	Pl, Bt	〃
TS11011504H	40–50%		10–20%	0–10%			15–25%	4	Mag	〃
TS11011601M	10–15%	5–15%		15–25%		25–35%		2	Qtz, Ap, Ilm	〃
TS11020206D	35–45%			5–15%	10–20%		0–10%	6	Opq	Innhovde
TS11020206G	5–15%		15–25%	5–15%	0–10%		5–15%	2	Opq(0–10%)	〃
TS11020206H	15–25%		5–15%	5–15%	5–15%		5–15%	2	Opq (5–15%), Ap, Zr	〃
TS11020601		40–50%	30–40%			0–10%		4	Opq, Bt	Ongul
TS11020603A	5–15%		30–40%	5–15%		15–25%		2	Bt	〃
TS11020603B	35–45%	0–10%	5–15%	5–15%		0–10%		2	Opq(0–10%)	〃
TS11020609	50–60%		0–10%	0–10%		15–25%		2	Opq, Ap	〃
TS11020610F	35–45%					40–50%		7	Opx, Pl, Qtz	〃
TS11020610G	10–15%	5–10%	0–10%	15–25%	10–15%	20–25%		2	Opq	〃
TS11020610G-2	50–60%		5–10%	5–10%		20–30%		7	Bt	〃
TS11020610H			0–10%	45–55%		20–30%		7	Opq, Bt	〃

Rock type, 1:Grt–Cpx rock, 2:Grt–mafic granulite, 3:Mafic granulite, 4: Ultra–mafic granulite, 5: Grt–Sil gneiss 6. Grt–Bt gneiss, 7: Amphibolite, 8: Others

Table 2. Continued

Sample	Grt	Cpx	Opx	Pl	Qtz	Amp	Bt	Rock type	Accesory	Locality
TS11020610I	5–15%	0–10%	5–15%	30–40%		10–20%		2	Bt	Ongul
B97121902	15–25%			25–35%	5–10%		15–25%	6	Opx	Skallen
B97121903			15–25%	45–55%				8	Opq (0–10%)	〃
B97122001	0–5%		5–10%	15–25%	25–35%	5–15%	0–10%	2	Qpz,	〃
B97122002		20–30%	10–20%	10–20%	5–15%	0–10%		3	Opq	〃
B971220T01b	0–5%		15–25%	10–20%	35–45%		20–30%	6	Opq(0–10%)	〃
B97122101B			65–75%				10–15%	4		〃
B97122101D	0–10%	5–15%	0–10%	25–35%		0–10%	10–20%	2	Opq, Qtz	〃
B97122102	5–10%			15–25%	40–50%		5–15%	6	Opq	〃
B97122201A	35–45%	0–10%	5–15%	5–15%		0–10%		2	Opq(0–10%)	〃
B97122201B	10–15%			25–35%	10–15%		20–30%	6	Opq, Ap	〃
B97122201C				35–45%	5–10%		15–25%	8	Opq	〃
B97122201D		15–25%		30–40%	20–25%			8	Opq	〃
B97122201E	5–10%			15–25%	30–40%		10–15%	6	Opq, Amp	〃
B97122201F				45–55%		35–45%		7	Opq, Grt	〃

Rock type, 1:Grt-Cpx rock, 2:Grt-mafic granulite, 3:Mafic granulite, 4: Ultra-mafic granulite, 5: Grt-Sil gneiss 6. Grt-Bt gneiss, 7: Amphibolite, 8: Others

Table 2. Continued

Sample	Grt	Cpx	Opx	Pl	Qtz	Amp	Bt	Rock type	Accesory	Locality
B97122201G		10–15%		20–30%		20–30%	5–15%	7	Opx, Opq	Skallen
B97122201H	5–15%	25–35%	0–10%	20–30%	0–5%	0–10%		2	Opq, Zr	〃
B97122301A					80–90%		0–10%	8	Opq	〃
B97122301B				10–15%	55–65%		0–10%	8	Opq	〃
B97122301C		20–30%	15–25%	15–25%		5–15%		3	Opq	〃
B97122302B	10–15%			10–15%	0–10%		25–35%	6	Opq (0–10%), Opx	〃
B97122302D	5–10%				60–70%		10–15%	6	Opq, Ap	〃
B97122302E		5–15%	5–15%	20–30%		5–10%	15–25%	3	Opq, Ap	〃
B97122302F		20–30%	5–15%	15–25%	0–10%		20–30%	3	Opq, Qtz	〃
B97122302F2	5–15%		5–10%	15–25%		5–15%	15–20%	2	Opq, Cpx, Qtz	〃
B97122302G	0–10%		0–10%	5–15%	30–40%		15–25%	6	Opq	〃
B97122303A		40–50%	20–30%				0–10%	4	Opq, Ap	〃
B97122303B		20–30%	5–15%	10–15%	0–10%	10–20%	0–10%	3	Opq	〃
B97122303C		10–15%	20–30%	25–35%		10–15%	10–15%	3	Opq	〃
B97122303D		25–35%	15–25%	10–15%			10–15%	3	Opq, Ap	〃
B97122401B	15–25%			5–15%	10–20%		25–35%	6	Opx	〃

Rock type, 1:Grt-Cpx rock, 2:Grt-mafic granulite, 3:Mafic granulite, 4: Ultra-mafic granulite, 5: Grt-Sil gneiss 6. Grt-Bt gneiss, 7: Amphibolite, 8: Others

Table 2. Continued

Sample	Grt	Cpx	Opx	Pl	Qtz	Amp	Bt	Rock type	Accesory	Locality
B97122402				20–30%	35–45%		10–15%	8	Opq, Grt	Skallen
B97122404A	10–20%			15–25%	10–20%		25–35%	6	Opq, Zr	〃
B97122404B		10–15%	0–10%	20–30%		15–25%	10–15%	2	Opq	〃
B97122404B2		5–15%	0–10%	25–35%		5–15%	5–15%	2	Opq	〃
B97122503	0–10%			65–75%				8	Bt	〃
B97122601				45–55%		10–15%	10–15%	8	Opq	〃
B97122602A	0–10%			25–35%	35–45%		0–10%	6	Opq, Ap	〃
B97122602B	20–30%			25–35%			20–30%	6	Opq, Qtz	〃
B97122602C	15–25%			10–20%	10–20%		15–25%	6	Opq	〃
B97122602D	25–35%			15–25%	15–25%		5–15%	6	Zr, Opq	〃
B97122603A	0–5%	10–20%	0–10%	10–20%		25–35%	0–5%	7	Opq	〃
B97122603B	0–10%		5–15%	25–35%		20–30%		2	Opq, Qtz	〃
B97122701A			5–15%	25–35%	35–45%		0–10%	3	Opq, Grt	〃
B97122701B	0–10%			25–30%	35–45%		5–15%	6	Opq	〃
B97122701C		0–10%	0–10%	10–15%		45–55%	10–15%	7	Opq, Ap	〃
B97122702A	10–20%			55–65%		10–15%		7	Bt, Opq	〃

Rock type, 1:Grt–Cpx rock, 2:Grt–mafic granulite, 3:Mafic granulite, 4: Ultra–mafic granulite, 5: Grt–Sil gneiss 6. Grt–Bt gneiss, 7: Amphibolite, 8: Others

Table 2. Continued

Sample	Grt	Cpx	Opx	Pl	Qtz	Amp	Bt	Rock type	Accesory	Locality
B97122702B	0–10%			55–65%		15–25%		7	Opq, Cpx	Skallen
B97122702C			0–10%	20–30%		25–35%	10–20%	7	Opq	〃
B97122702D				40–50%		20–30%	10–15%	7	Opq	〃
B97122702F	5–15%	5–15%	10–20%	25–30%		20–25%		2	Opq ,Qtz	〃
B97122702G				80–90%				8		〃
B97122703A	5–15%			15–25%	30–40%		10–15%	6	Opq	〃
B97122703B		25–35%		15–20%		15–25%	5–10%	3	Opq, Ap	〃
B97122703C		20–30%		10–20%	10–20%		20–30%	3	kfs?	〃
B97122709	5–10%			15–25%	25–35%		20–30%	6	Opq	〃
B97122710	5–10%			25–35%	35–45%		5–15%	6	Zr, Opq	〃
B971227T01								8	Srp, Opx, Bt, Sph	〃
B97122801A					80–85%		0–10%	8		〃
B97122801B				0–10%	70–80%		10–15%	8	Opq, Grt	〃
B97122802A	0–10%		10–15%	10–20%	20–30%	5–10%	5–10%	2	Opq	〃
B97122802B	10–15%	5–15%	0–5%	10–15%	15–25%	5–15%		2	Opq, Bt	〃
B97122803B	5–15%			15–25%	35–45%			8	Opq, Rt	〃

Rock type, 1:Grt–Cpx rock, 2:Grt–mafic granulite, 3:Mafic granulite, 4: Ultra–mafic granulite, 5: Grt–Sil gneiss 6. Grt–Bt gneiss, 7: Amphibolite, 8: Others

Table 2. Continued

Sample	Grt	Cpx	Opx	Pl	Qtz	Amp	Bt	Rock type	Accesory	Locality
B97122803D	5–15%				80–90%			8	Bt	Skallen
B97122804B	10–20%	0–10%	10–15%	10–15%	15–25%			2	Opq	〃
B97122804C				5–15%	10–20%		50–60%	8	Opq, Zr, Ap	〃
B97122804E	25–35%			35–45%		20–25%		7	Opq ,Qtz	〃
B97122807				5–15%	70–80%			8	Grt	〃
B97122808		10–15%	5–15%	20–30%		20–35%	0–5%	3	Opq	〃
B971228T01	5–15%			35–40%	25–35%			8	Zr Cal (0–10%)	〃
B97123001A	0–10%		10–15%	20–30%		45–55%		7	Opq	〃
B97123001B		45–55%	0–10%	15–20%		5–15%		3	Opq	〃
TS97121901C	10–20%	0–10%	10–15%	30–40%	0–10%		10–15%	2	Zr, Opq, Hbl	〃
TS97121901D		5–15%	10–15%	10–20%	10–15%	15–25%	15–25%	3		〃
TS97121902A		65–75%						8	Sph, Scp (10–15%)	〃
TS97121903B						70–80%		8	Spl (10–15%)	〃
TS97121903D			Cal (85–95%)					8	Spl, Amp	〃
TS97122002A		25–35%	10–15%	15–25%	0–10%			3	Opq (0–10%)	〃
TS97122004A		15–25%	5–15%	10–15%	25–35%			8	Opq, Grt, Bt	〃

Rock type, 1:Grt–Cpx rock, 2:Grt–mafic granulite, 3:Mafic granulite, 4: Ultra–mafic granulite, 5: Grt–Sil gneiss 6. Grt–Bt gneiss, 7: Amphibolite, 8: Others

Table 2. Continued

Sample	Grt	Sil	Kfs	Pl	Qtz	Bt	Spl	Rock type	Accessory	Locality
TS10122505B	15–20%	10–15%	10–15%	5–10%	15–20%	0–10		5	Rt, Spl	Skalleviksha lsen
TS10122604H	0–10%		25–35%	5–15%	15–25%	0–10%		6	Opq, Zr	〃
TS10122806B	15–25%	5–15%	20–30%	10–20%	5–15%			5	Ilm,Zr, Spl	〃
TS10122806B2	5–15%		25–35	35–45				8	Qtz, Bt, Opx	〃
TS11010804	30–40%		15–25%	10–20%		0–10%	0–10%	6	Opq	〃
TS11010903A	20–30%	5–15%	10–20%	15–25%	0–5%		0–10%	5	Rt, Bt, Ilm	〃
TS11010903B	40–50%		0–10%	10–20%	5–15%	5–15%		6	Zr	〃
TS11011401K3	5–15%	15–25%	5–15%	10–20%	15–25%			5	Sph, Zr	Austhovde
TS11011502C	0–10%							8	unknown (70–80%), Bt	〃
TS11011702F	10–20%	5–15%		15–25%	20–30%			8	Ilm	〃
TS11020203A	0–10%	10–20%	20–30%		30–40%	0–10%		5	Opq	Innhovde
TS11020204A	10–20%		15–25%	10–20%	5–15%	10–20%		6	Ilm, Ap, Zr	〃
TS11020206A	30–40%			5–15%	10–20%	10–15%		6	Ilm, Ap (0–10%), Zr	〃
TS11020206F	10–15%		10–20%		35–45%	5–15%		6	Ilm, Ap, Zr	〃

Rock type, 1:Grt–Cpx rock, 2:Grt–mafic granulite, 3:Mafic granulite, 4: Ultra–mafic granulite, 5: Grt–Sil gneiss 6. Grt–Bt gneiss, 7: Amphibolite, 8: Others

Table 2. Continued

Sample	Grt	Sil	Kfs	Pl	Qtz	Bt	Spl	Rock type	Accessory	Locality
TS97122002B	25–35%	15–25%	20–30%					5	Opq. Qtz, Pl	Skallen
TS97122003	20–25%			45–50%	0–10%	0–10%		6	Opq, Rt, Sil	〃
TS97122004B			10–15%	15–25%	30–40%	10–20%		8		〃
TS97122004C			5–10%	45–55%	5–15%	5–10%		8	Grt	〃
TS97122005C	15–20%	0–10	35–45%		5–15%			5	Rt, Bt	〃
TS97122007	15–25%	35–45%				10–15%		6	Pl, Qtz	〃
TS97122302A-2	15–25%	5–15%		25–35%	10–15%	0–10%		5	Ilm, Rt	〃

Sample	Grt	Cpx	Opx	Pl	Qtz	Amp	Bt	Rock type	Accesory	Locality
TS97122004D	15–25%	10–15%	0–10	15–25%		25–35%		2	Qtz, Opq	Skallen
TS97122004E	0–10%	0–10%	0–10%	60–65%			0–10%	2	Opq	〃
TS97122005B	35–45%			0–10%	10–20%		10–15%	5	Sil (0–5%)	〃
TS97122005C	15–20%			35–45%	5–15%	20–25%		7	Opq ,Qtz	〃
TS97122005G			20–30%	20–30%	0–10%	10–20%	0–10%	3	Grt	〃
TS97122007	15–25%	10–15%	5–15%	20–30%		20–35%	0–5%	2	Opq	〃
TS97122402C		0–10%	70–80%					4	Spl (0–10%), Amp	〃

Rock type, 1:Grt–Cpx rock, 2:Grt–mafic granulite, 3:Mafic granulite, 4: Ultra–mafic granulite, 5: Grt–Sil gneiss 6. Grt–Bt gneiss, 7: Others

Table 3. Approximate grain size of minerals from the studied area. (mm)

Sample	Grt	Sil	Kfs	Pl	Qtz	Bt	Spl	Accessory
TS11011401A	0.1–10	0.01–2	0.05–1	0.05–0.2	0.01–1	0.01–0.1		Ilm
TS11011401K3	0.2–5	0.1–1.2	0.05–1.4	0.05–0.4	0.1–1.4			Rt, Bt
TS11011401N	0.2–2.5		0.1–1.2	0.1–1.2		0.05–1		Qtz
TS11011402A	0.2–7	0.1–0.6	0.1–0.9	0.2–0.5	0.05–5	0.1–0.7		Opq
TS11011404B		0.05–0.3	0.05–1.4	0.1–0.3		0.2–2	0.05–0.5	Opq
TS11011405D	1–1.9		0.1–0.4	0.1–0.9		0.1–2	0.05–0.5	Opq
TS11011502A	0.2–6	0.05–0.9	0.1–0.9	0.1–0.8	0.05–1.4		0.05–1	Opq, Zr
TS11011502D	0.2–3		0.1–0.8	0.02–0.7	0.05–2	0.05–0.5		Opq
TS11011503C	0.15–1.5	0.05–0.5	0.1–1		0.02–1.6			Pl, Opq
TS11011504A	0.3–10	0.02–0.5	0.1–0.7	0.02–0.5	0.1–4	0.02–0.85	0.05–1	Opq,Rt,Qtz
TS11011504C	1 to 7		0.02–0.4	0.05–0.4	0.2–2	0.04–1.2		Spl,Qtz,Rt,Ky
TS11011601C	0.2–2		0.1–0.7	0.15–0.7	0.05–2	0.07–0.8		Pl, Opq
TS11011601G	0.15–2	0.05–0.3	0.05–2	0.2–0.6		0.05–0.9	0.1–0.8	Hbl, Opq
TS11011601I	0.05–1.5	0.2–1.2	0.05–1.3		0.1–3	0.05–0.9		Pl, Opq
TS11011601J	0.2–1.4	0.2–2	0.03–1	0.05–1				Hbl, Opq
TS11011601K	Scp(0.15–1.4)		Cpx(0.1–1.2)		Spn(0.15–1.4)			Opq
TS11011702G	0.2–1.7	0.15–0.4			0.02–2			Kfs, Pl

Table 3. Continued (mm)

Sample	Grt	Cpx	Opx	Pl	Qtz	Amp	Bt	Rt	Accesory
TS11011401E		0.1–0.5	0.01–0.2	0.1–0.5	0.05–2				Amp.Opq
TS11011401F	0.2–5	0.2–2	0.1–0.5	0.1–0.5	>4	0.05–0.5			Opq
TS11011401G		0.1–0.8	0.05–0.2	0.1–0.5		0.2–1.2	0.6–1.2		
TS11011401I		0.1 – 1	0.1–0.8	0.2–1	0.05–1.8	0.2–2	0.1–1.5		Opq
TS11011407B		0.2–0.4	0.1–0.6	0.05–0.6	0.1–2	0.05–0.7	0.05–0.6		Opq
TS11011503B	0.1–1.4	0.2–0.8	0.05–0.2	0.02–1	0.05–4	0.05–0.8	0.05–2		Opq
TS11011504D	1–1.2	0.1–0.4	0.02–0.5	0.1–0.6	0.1–6	0.1–0.5	0.05–0.4		Opq
TS11011505D		0.4–2							Opx,Bt,Hbl
TS11011601D		0.05–0.8		0.15–1.2	0.1–2	0.05–1			Opq, Zr
TS11011701B		0.03–0.6	0.03–0.4	0.03–0.5		0.05–0.4			Hbl, Bt, Ilm
TS11011601N	0.1–1.4	0.1–0.6	0.1–0.4	0.05–0.5		0.05–1.1			Qtz.Opq, CMI
TS11011701C		0.2–0.4	0.03–0.5	0.1–0.9		0.1–0.8	0.05–0.6		Opq
TS110117011E2		0.05–0.5	0.05–0.5	0.1–0.5		0.05–0.6	0.1–0.7		
TS11011702C		0.1–0.3	0.05–0.5	0.02–0.3	0.02–2	0.2–2	0.05–0.2		Opq

Table 3. Continued (mm)

Sample	Grt	Sil	Kfs	Pl	Qtz	Bt	Spl	Accessory
TS11011601K	Scp(0.03-1.2)		Cpx(0.05-1.5)					Ilm
TS11011602A	Scp(0.05-1.5)		Cpx(0.1-1)		Spn(0.2-2)			
TS11011603			0.1-0.5	0.2-0.8	0.1-1.5	0.1-0.5		Opq, Opx,Hbl
TS11011604A	0.6-10	0.05-1	0.1-1.4	0.2-0.5	0.05-1.5	0.1-0.7		Opq
TS11011604B	0.3-1.4	0.1-0.6	0.05-1.5			0.05-2		Opq
TS11011604C	0.05-10		0.1-3	0.05-3		0.1-01.4	0.1-0.5	Opq
TS11011605A	0.4-1	0.05-0.9	0.1-2	0.2-0.6	0.1-3	0.05-0.6	0.05-1	Opq, Zr
TS11011607A	0.4-1		0.1-1.8		0.1-1.6	0.05-1.1	0.05-0.4	Opq,Pl
TS11011607B	0.2-1.2		0.05-1	0.1-0.6	0.05-1.6	0.05-0.6		Spl
TS11011701D	0.2-2		0.1-0.8	0.2-1.2	0.2-3	0.05-1	0.05-0.5	Opq
TS11011701F			0.1-0.8	0.2-0.8	0.05-2	0.05-0.8		Spl,Qtz,Rt,Ky
TS11011702A	0.2-1.7	0.05-2	0.1-1	0.2-0.8		0.1-0.9	0.02-0.5	Qtz Opq
TS11011702B	0.15-1.7	0.1-0.7	0.05-1	0.05-1.5	0.1-2	0.1-0.8	0.05-1	Opq
TS11011702B2	0.2-1.2	0.2-1.2	0.1-2	0.05-1.6	0.1-2	0.05-1.4	0.05-0.8	Opq
TS11011702E	0.15-1.9	0.05-0.7	0.05-1.7	0.2-1.7		0.02-0.9	0.03-1	QtzOpq
TS11011702F	0.2-1.4	0.05-0.5	0.03-0.8		0.1-1.4			Qtz
TS11011702G	0.2-1.7	0.15-0.4			0.02-2			Kfs, Pl

Table 3. Continued

Sample	Grt	Sil	Kfs	Pl	Qtz	Bt	Spl	Opx	Accessory
TS10122401A	0.1-10	0.01-2	0.1-0.6	0.2-0.6	0.1-1.5	0.1-0.7		0.1-0.9	Ilm
TS10122502B2	0.05-1.8		0.05-1.4	0.05-0.4	0.02-1.4	0.05-0.8	Crd(0.1-0.8)		Rt,
TS10122502C	0.2-2		0.05-0.7	0.05-0.8	0.1-2	0.05-0.9			
TS10122502C-2	0.4-1.7		0.05-1	0.05-1	0.02-1.9	0.05-0.9			Opq
TS10122502D	0.2-1.6		0.02-0.6	0.1-0.4	0.05-0.6	0.02-0.8	0.05-0.5	0.05-0.2	Ky, Rt, Ilm
TS10122502G	0.15-2	0.1-0.4	0.05-0.7	0.1-0.4		0.05-1.2			Opq
TS10122503E	>2		0.1-0.5	0.1-0.8	0.05-1.4	0.02-0.5	0.05-1	0.02-0.2	Opq, Zr
TS10122504B	0.05-2		0.05-1.6	0.02-0.6	0.02-1.2	0.05-0.9			Opq
TS10122505B	0.8-8	0.07-1.2	0.05-0.6		0.02-1.6				Pl, Opq
TS10122505B-2	0.7-2	0.05-2	0.02-0.7		0.1-1.2				Opq,Rt, Spl
TS10122505C	0.1-1.6		0.05-0.7	0.2-0.5	0.02-2	0.1-1.5			Rt
TS10122601H	0.05-2		0.05-1.1	0.1-1.3		0.03-0.2	0.03-0.7		Qtz
TS10122604F2	0.4-2	0.05-0.3	0.05-1.2	0.05-0.7	0.1-2	0.05-1	0.03-0.3		
TS10122604H	0.6-1.1	0.2-1.2	0.05-0.8	0.05-0.4	0.03-2	0.03-1.2			Opq
TS10122702C1	0.1-1.7	0.2-2	0.03-1.3	0.05-0.7		0.03-0.6		0.05-1.2	Opq
TS10122702C2	0.15-2		0.03-0.6	0.1-0.7	0.05-2	0.05-0.5		0.05-0.7	Opq

Table 3. Continued (mm)

Sample	Grt	Cpx	Opx	Pl	Qtz	Amp	Bt	Rt	Accesory
TS10122401C		0.1–0.5	0.01–0.2	0.1–0.8	0.05–2	0.1–0.9	0.05–0.6		Amp.Opq
TS10122401D		0.2–1.6		0.1–1.2					Opq
TS10122401F		0.3–0.6	0.4–1.4	0.05–1.3		0.1–1.2	0.05–0.2		
TS10122401K1		0.05–0.2	Scp(0.2–1.2)			0.1–1	0.1–1.4		Opq
TS10122401K2		0.1–0.4		0.3–1.2			0.05–1.6		Scp(0.2–1.2)
TS10122601C		0.2–1	0.2–1.7			0.1–1	0.05–1.4		Opq
TS10122601E	1–1.2	0.05–0.5	0.2–0.5	0.1–0.7	0.05–0.3				Opq, Spn, Rt

Sample	Grt	Sil	Kfs	Pl	Qtz	Bt	Spl	Opx	Accessory
TS10122806B	0.2–2	0.02–0.3	0.05–0.8	0.02–0.6	0.03–0.9	0.05–0.2			Ilm
TS10122806B2	0.6–1.4		0.03–1.2	0.05–0.5	0.03–1.1	0..1–1	Crd(0.1–0.8)		Rt,
TS11010804	0.07–2		0.03–1	0.07–1	0.03–2	0.03–0.6	0.02–0.6		
TS11010903A	0.2–2	0.07–0.9	0.05–0.6	0.1–0.3	0.05–0.8		0.03–0.2		Opq
TS11010903B	0.4–1.8		0.02–0.7	0.05–0.4	0.05–1.2	0.02–0.6			

Table 3. Continued (mm)

Sample	Grt	Sil	Kfs	Pl	Qtz	Bt	Spl	Opx	Accessory
TS11020602A	0.15–2		0.05–1.5	0.1–0.8	0.02–1.7	0.03–0.6			Ilm
TS11020602B	0.3–0.8		0.2–0.7	0.05–0.8	0.02–1	0..1–1	Crd(0.1–0.8)		Spl
TS11020602C	0.2–0.8		0.1–0.9	0.05–0.5	0.04–0.8	0.04–0.9	0.02–0.6		
TS11020604B	0.07–1	0.03–1	0.1–1.5	0.2–2	0.05–1.9	0.04–0.4			Rt
TS11020607B	0.2–1.2		0.03–1	0.03–1.5	0.05–2	0.03–1			Opq
TS11020608B	0.15–0.6			0.1–1.5	0.03–1.1	0.03–0.5			Opx, Opq
TS10122502A1	0.1–2	0.02–0.2	0.02–0.8		0.02–1				Opq, Pl, Bt
TS10122502E	0.4–1.2		0.2–0.8	0.1–0.4	0.05–1.8	0.05–1.2			Opq
TS10122502H	0.5–2		0.05–0.5	0.03–1	0.02–1.3	0.05–0.3			Opq
TS10122502I	0.3–2		0.05–0.3	0.02–0.4	0.03–1.2			0.02–0.1	Rt, Bt
TS10122503B	0.3–2		0.1–0.8	0.03–2	0.05–1.4	0.02–0.5		0.2–0.6	
TS10122504B	0.2–1.5		0.05–0.9	0.02–0.5	0.03–1.3	0.05–0.7	0.03–0.3		
TS10122601D	0.05–>2	0.2–1.2	0.03–1.5	0.1–0.8			0.02–0.4		Bt
TS10122601F2	0.2–>2		0.04–0.6	0.05–0.4	0.03–>2	0.03–0.2		0.05–1.2	Opq
TS10122601G	0.3–>10		0.03–1	0.1–1.3	0.03–>2	0.02–0.5			Opq
TS10122601J	0.05–>5	0.2–1.2	0.05–0.9	0.1–0.6		0.03–1	0.02–0.3		Opq, Qtz

Table 3. Continued (mm)

Sample	Grt	Cpx	Opx	Pl	Qtz	Amp	Bt	Rt	Accesory
TS11020603C	0.07-2		0.05-1.2	0.08-1.2	0.05-2	0.02-1.2	0.03-0.7		Cpx, Qtz
TS11020604A	0.15-0.8		0.07-0.35	0.1-1	0.02-1.7		0.03-0.7		Opq
TS11020605		0.03-0.6	0.4-1.4	0.15-01.4		0.07-0.6	0.05-0.4		Cpx, Grt, Opq
TS11020606A	0.05-0.7		0.03-0.1	0.03-0.5	0.03-0.7				Opq, Bt, Rt
TS110206010C	0.4-0.7		0.03-0.5	0.05-1.5		0.03-1	0.02-0.7		Cpx, Opq
TS11020610E		0.15-0.6	0.2-1			0.2-2			Opq
TS11020611D	0.05-1.2	0.05-0.5	0.2-0.5	0.1-0.9	0.05-2	0.04-2			Kfs (0.05-1.3),
TS1122501K2		0.05-1.2		Scp (0.03-2)			0.02-1		Sph (0.01-0.3)
TS10122502F	0.4-1.5		0.05-0.5	0.02-0.6	0.05-1		0.03-0.6		Opq, Zr, Cpx, Rt
TS10122503C		0.2-0.4	0.2-0.4	0.1-0.8					Opq, Qtz
TS10122601A		0.05-2		Scp (0.1-2)					Sph
TS10122601B	0.4-4	0.02-0.6		0.05-0.5	0.1-4	0.03-1.3			Opq, Bt, opx
TS10122601I		0.1-1.2		0.1-1.8	0.2-2	0.03-0.8	0.04-1.5		Kfs (0.1-1)Opq
TS10122601N	0.2-5		0.02-0.2	0.03-0.6		0.05-1	0.05-0.4		Cpx, Opq
TS10122602A	0.2-2		0.02-0.4	0.03-0.4	0.03-2		0.02-1		Rt, Opq
TS10122602B	0.1-1.2		0.03-0.3	0.04-1	0.03->2	0.2-1			Kfs (0.05-0.9), Opq

Table 3. Continued (mm)

Sample	Grt	Cpx	Opx	Pl	Qtz	Amp	Bt	Rt	Accesory
TS10122604G1	0.07-2	0.1-0.6	0.1-0.4	0.1-0.9	0.05-2	0.05-0.7	0.1-0.8	Kfs(0.05-0.7)	Opq
TS10122604I	0.4- >2		0.05-0.5	0.05-0.7	0.05 ->2		0.1-0.6		Opq
TS11010602D	0.2 ->2	0.1-1	0.05-0.4	0.03-0.6		0.03-0.9			
TS11010901	0.8 ->30		0.03-0.1	0.1-0.7	0.03-0.7	0.05-0.8		Kfs(0.1-0.9)	Opq
TS11010902	0.2 ->5	0.1-0.7		0.1-0.5		0.05-1.2			Opx, Opq
TS11011407E	0.1-1.4			0.1-0.3	0.1-1.3				Opq, Bt, Kfs
TS11011501A		0.2-0.4	0.2-0.9	0.03-0.9	0.05-2	0.05-1.2	0.05-1.2		
TS11011503A	0.15-1	0.05-1.5	0.02-0.3			0.1-0.5	0.02-1		
TS11011504C	0.8-1.4	0.04-0.3	0.05-0.4	0.1-0.6	0.05-1.6	0.03-0.6	0.02-0.4		Opq
TS11011504E		0.2-1.3		0.1-1.2					Opq, Hbl
TS11011601B	0.03->2	0.03-0.5		0.2-1	0.05-1.5		Scp (0.1-2)		Sph
TS11011601H	0.4-4		0.1-0.4	0.05-1.1	0.1-.2	0.03-1.3	Scp (0.1-1)		Kfs (0.03-1.2), Opq
TS11011602D		0.05-1.6		Sph (0.02-0.5)			Scp (0.1-1)		
TS11011605B	0.2-5	0.1-1.2	0.02-0.2	Sph (0.03-0.5)			0.05-0.9		Scp (0.05->2)
TS11011606A		0.05-0.4	0.1-0.7						Opq
TS11011702D	0.08-1.8	0.03-0.3	0.05-0.75	0.03-0.4	0.05->2	0.2-1			Opq (0.02-0.9)

Table 3. Continued (mm)

Sample	Grt	Sil	Kfs	Pl	Qtz	Bt	Spl	Opx	Accessory
TS10122603A	0.15–1.5		0.02–0.5	0.05–0.4		0.01–0.9			Ilm
TS10122603B	0.3–3		0.05–0.5	0.03–0.8	0.1–1.3	0.02–0.4			Opq
TS10122604A	0.2–0.8		0.1–01.2	0.2–1.4	0.1 –>2	0.05–1.2	0.02–0.6	0.05–1.3	Opq
TS10122604K	0.07–1	0.03–1	0.15–1.4	0.15–0.4	0.1–>2	0.04–0.4		0.1–1	Opq, Grt
TS11010903C	0.3 >2	0.03–0.2	0.1–1.2	0.1–0.6	0.03 –>2	0.05–0.6			Opq
TS11011502C	0.2–1.2	0.05–0.8	0.03– >2			0.03–0.5	0.02–0.7		Opq

Sample	Grt	Cpx	Opx	Pl	Qtz	Amp	Kfs		Accesory
TS11011201A	0.07–0.5	0.15–0.4	0.05–0.9		0.03–0.9	0.03–0.6	0.1–0.9		Opq, Pl
TS11011204A			0.03–0.7	0.3–0.7	0.1–1.2		0.05–1.2		Grt, Opq
TS11011204B	0.07–0.5	0.15–0.4	0.1–0.6		0.03–0.5	0.03–0.6	0.07–0.9		Pl, Opq
TS11011205B		0.05–0.5	0.2–0.4		0.05–1.2		0.03–1.4		Hbl,Pl, Grt
TS11011206A	0.1–0.5	0.05–0.2	0.05–0.5		0.05–1.2	0.05–0.6	0.03–1		Opq, Pl, Cpx
TS11011206B	0.2–0.6	0.1–0.4	0.05–0.6	0.3–1.2	0.03–1.2	0.05–0.5	0.02–1.2		Opq, Pl, Cpx
TS11011207	0.05–1.2				0.05–1	0.05–1.2	0.1–2		Opq
TS11011208	0.05–0.6		0.1–1.5		0.03–0.7	0.05–0.9	0.05–0.7		Cpx, Pl, Opq

Table 3. Continued (mm)

Sample	Grt	Cpx	Opx	Pl	Qtz	Amp	Bt	Rt	Accesory
TS10122405B	0.8–2	0.4–1				0.3–1			Scp
TS10122503B	0.2–5		0.2–0.6	0.2–1.8	>4				Bt
TS10122503D	0.2–3	0.3–0.8	0.4–0.6	0.2–1		0.1–0.6			
TS10122506	0.4–3	0.6–3	0.2–1	0.4–0.8	0.1–4	0.2–2	0.2–0.8		Bt Opq
TS10122601G	0.4–8			0.2–1.2	0.1–4				Hbl
TS10122601K	1.6–10		0.1–2	0.2–0.8		0.2–1.8	0.2–2		Opq
TS10122601L	0.4–12			0.3–0.8		0.2–2			Opq
TS10122601N	0.4–3		0.1–0.4	0.1–1		0.1–2			Opq
TS10122602A	0.6–2.5		0.05–0.6	0.1–0.8	0.1–3		0.05–1		Opq, Zr
TS10122604B	0.3–30		0.2–2	0.1–1.2	0.3–3				Hbl, Bt, Ilm
TS10122604G		0.2–0.8	0.1–0.8	0.2–1.4		0.1–1.2	0.2–1.2		Grt, Opq
TS10122604I	0.4–4		0.1–1	0.2–1.6	0.1–4		0.2–2		Opq
TS10122702B			0.1–0.8	0.2–1.4	0.2–2				Opq
TS11010704A	0.4–8	0.2–1.2				0.3–1.2			Pl, Opq
TS11010704A3	0.4–20	0.2–2		0.2–1					Hbl, Opq
TS11010704B	0.5–10	0.2–1.2				0.2–1			Opq

Table 3. Continued (mm)

Sample	Grt	Cpx	Opx	Pl	Qtz	Amp	Bt	Rt	Accesory
TS11010801	0.6–2	0.3–2.2		0.1–2					Opq, Hbl
TS11010802	0.8–6	0.4–3		0.2–3		0.3–0.8			Qtz,Opq, Bt, Opx, Pl
TS11010803A	0.8–2	0.3–1.2	0.2–0.4						Ilm, Qtz, Pl, Ap, Hbl
TS11010803A-4	0.8–3	0.4–1.6	0.5–1.2						Qtz, Ap, Ilm, Hbl
TS11010803A-6	0.6–3	0.4–0.8	0.3–0.6						Qtz, Ap, Ilm, Hbl
TS11010803C	0.2–2	0.4–0.8	0.4–0.8	0.2–0.6					Opq(0–10%), Hbl, Bt, Ap
TS11010803D	0.3–3	0.3–2	0.2–1.6	0.3–1.2		0.1–1.8	0.1–1.2		Opq, Ap, Zr
TS11010903D	0.3–3		0.1–1.6	0.2–0.8	0.1–3				Opq, Bt
TS11011401L	0.3–6			0.05–0.4			0.2–2		Opq (5–15%), Spl
TS11011405A	0.6–3		0.3–0.4	0.2–0.8	0.1–0.5	0.3–2	0.3–1		Qtz, Opq
TS11011405A-2	0.3–3	0.4–1	0.2–1	0.3–1	0.05–3				Ilm, Ap
TS11011405B	0.4–2		0.2–2	0.2–1		0.2–1.6			Ilm, Bt, Qtz
TS11011405C	0.4–3	0.3–1.5	0.2–1	0.3–1.2	0.3–1.6	0.2–2			Ilm
TS11011407D	0.2–1.3		0.2–1.4	0.2–1	0.2–3		0.1–1		Mag, Zr
TS11011407E	0.1–3			0.3–1.2	0.3–2.5				Opq, Bt

Table 3. Continued (mm)

Sample	Grt	Cpx	Opx	Pl	Qtz	Amp	Bt	Rt	Accesory
TS11011501A			0.2–1.4	0.2–1.4		0.4–2	0.3–1		
TS11011504C	0.3–1		0.1–0.6	0.1–0.8	0.2–2	0.2–1.4	0.2–0.8		Opq, Zr
TS11011504E		0.2–2.4	0.3–1			0.2–1			Pl, Bt
TS11011504H	0.1–3		0.2–2	0.1–1			0.1–1.4		Mag
TS11011601M	0.5–2	0.1–0.6	0.2–0.8	0.1–.6		0.2–2			Qtz, Ap, Ilm
TS11020206D	0.15–2			0.2–2	0.2–2.2		0.1–1.2		Opq
TS11020206G	0.1–1.6		0.1–2.4	0.05–1	0.1–2.4		0.05–1		Opq(0–10%)
TS11020206H	0.2–1.2		0.2–0.8	0.2–1.5	0.1–3		0.2–1.3		Opq (5–15%), Ap, Zr
TS11020601		0.3–4	0.2–10			0.4–2			Opq, Bt
TS11020603A	0.3–4		0.05–3.5	0.3–2		0.1–3			Bt
TS11020603B	0.3–4	0.6–2	0.2–3	0.2–2.5		0.1–1.2			Opq(0–10%)
TS11020609	0.4–3		0.05–1	0.2–0.8		0.3–2			Opq, Ap
TS11020610F	0.3–15					0.2–2.4			Opx, Pl, Qtz
TS11020610G	0.8–4		0.2–1	0.4–1.2		0.4–2	0.3–2		Opq
TS11020610G-2	0.1–40		0.1–1.2	0.1–1.2		0.6–4			Bt
TS11020610H		0.6–1	0.4–3			0.3–2.5			Opq, Bt

Table 3. Continued (mm)

Sample	Grt	Cpx	Opx	Pl	Qtz	Amp	Bt	Rt	Accesory
TS11020610I	0.2–4	>5	0.5–2.5	0.3–2.2		0.1–2.4			Bt
B97121902	1.2–7		>1.2	0.2–4	0.1–0.6		0.1–1.6		Opx
B97121903			0.1–0.4	0.05–1	>1.4				Opq (0–10%)
B97122001	0.5–0.6		0.1–0.6	0.3–1.2	0.2–10	0.1–0.8	0.1–0.8		Qpz,
B97122002		0.4–1.1	0.05–0.6	0.1–1.2	0.2–2	0.2–1.6			Opq
B971220T01b	0.4–1			0.4–1	0.5–3		0.2–1.6		Opq(0–10%)
B97122101B			0.3–1.2				0.2–2		
B97122101D	0.1–1.4	>1	0.3–1	0.3–0.7		0.4–1.2	0.5–2		Opq, Qtz
B97122102	1–1.6			0.6–1	1.4–1.5		0.3–0.6		Opq
B97122201A	0.3–1.8			0.05–1	0.2–2.5		0.1–1		
B97122201B	0.2–2			0.1–2	0.05–1.4		0.1–1.4		Opq, Ap
B97122201C				0.1–1.8	1.2–1.4		0.1–1.6		Opq
B97122201D		0.4–0.7		0.3–1.4		0.2–0.8			Opq
B97122201E	0.5–1.2			0.2–1.4	0.4–2		0.15–1		Opq, Amp
B97122201F				0.2–1		0.1–0.8			Opq, Grt

Table 3. Continued (mm)

Sample	Grt	Cpx	Opx	Pl	Qtz	Amp	Bt	Rt	Accesory
B97122201G		0.2–1		0.2–1.6		0.2–1.8	0.6–1		Opx, Opq
B97122201H	0.7–2	0.4–1.2	0.2–0.6	0.2–1.4	0.2–0.6	0.6–1.4			Opq, Zr
B97122301A					0.4–4		0.8–1.6		Opq
B97122301B				0.3–0.9	2–3 mm		0.2–0.6		Opq
B97122301C		0.3–1.2	0.05–1	0.2–2		0.2–3			Opq
B97122302B	0.4–2			0.1–1.5	0.05–1.8		0.1–1.3		Opq (0–10%), Opx
B97122302D	0.5–1.8				0.4–4		0.1–1.1		Opq, Ap
B97122302E		0.3–2.2	0.2–1.4	0.1–1.8		0.2–1.4	0.05–1.2		Opq, Ap
B97122302F		1.2–2	0.4–1.2	0.2–1.8	1.6–3		0.1–1		Opq, Qtz
B97122302F2	>5	0.6–3	0.2–1.2	0.1–1.1		0.5–1.3			Opq, Bt, Qtz
B97122302G	0.4–1.4		1–10 mm	0.8–1.8	0.1–3		0.2–1.4		Opq
B97122303A		1–4 mm	1–2 mm				0.2–2		Opq, Ap
B97122303B		1.9–3	0.1–2	0.1–1.2	2– 3mm	0.2–1.6	0.7–1		Opq
B97122303C		0.4–0.8	0.2–2	0.2–1.2		0.4–2	0.2–1		Opq
B97122303D		0.6–1	0.6–1.8	0.2–1.3			0.1–1.2		Opq, Ap
B97122401B	5–10 mm			0.1–2.5	0.1–4		0.1–1.3		Opx

Table 3. Continued (mm)

Sample	Grt	Cpx	Opx	Pl	Qtz	Amp	Bt	Rt	Accesory
B97122402				0.2–1.8	0.3–3		0.1–0.9		Opq, Grt
B97122404A	0.3–3			0.6–1.6	0.05–1.4		0.1–1.2		Opq, Zr
B97122404B		0.3–1	0.2–1.8	0.2–1.8		0.4–1.8	0.8–1.8		Opq
B97122404B2		0.2–1.4	0.1–4	0.1–3		0.1–1.4	0.2–1.4		Opq
B97122503	1.5–2			1.8–2					Bt
B97122601				0.5–2		0.6–2	0.6–1		Opq
B97122602A	0.4–1.4			0.1–1	0.05–2.5		0.05–1		Opq, Ap
B97122602B	0.8–3			0.1–2			0.1–0.9		Opq, Qtz
B97122602C	1.2–2			0.1–1.4	0.1–1.4		0.2–1.4		Opq
B97122602D	0.1–2.5			0.2–1.8	0.1–4		0.05–1.4		Zr, Opq
B97122603A	0.8–1.7	0.2–1.6	0.4–0.6	0.1–1.4		0.2–1.8	0.3–1.5		Opq
B97122603B	0.8–2		0.4–2.5	0.15–1.2		0.2–2			Opq, Qtz
B97122701A				0.3–0.8	0.3–2.5		0.1–0.6		Opq, Grt
B97122701B	0.2–1			0.2–0.8	0.2–1		0.1–0.8		Opq
B97122701C		0.2–1.8	0.4–2.5	0.1–2.2		0.1–1.8			Opq, Ap
B97122702A	0.2–3			0.1–2		0.2–1.8			Bt, Opq

Table 3. Continued (mm)

Sample	Grt	Cpx	Opx	Pl	Qtz	Amp	Bt	Spl	Accesory
B97122702B	1.2–2			0.4–2		0.2–2			Opq, Cpx
B97122702C			0.1–0.2	0.3–1.7		0.3–1.4	0.15–1.4		Opq
B97122702D				0.2–1.3		0.3–1.5	0.3–1.8		Opq
B97122702F	1.4–3	0.2–1.4	0.2–1.2	0.1–2		0.2–2.5			Opq ,Qtz
B97122702G				0.8–3					
B97122703A	0.7–1.4			0.2–2.5	0.2–4		0.6–1.8		Opq
B97122703B		0.3–2		0.1–1		0.2–2	0.1–1.3		Opq, Ap
B97122703C		2 mm		0.6–2	0.4–2		0.2–1.8		kfs?
B97122709	0.4–2.5			0.4–2	0.6–1.4		0.2–1.2		Opq
B97122710	0.8–2			0.4–1.6	0.4–3				Zr, Opq
B971227T01								4 mm	Srp (60–70%), Opx, Bt, Sph, Spl
B97122801A					1.4–5		0.3–1		
B97122801B				102–1.8	0.1–4		0.1–2		Opq, Grt
B97122802A	0.4–2.5		0.05–2	0.2–2	0.05–2.5	0.1–1	0.1–1.4		Opq
B97122802B	1.2–2.5	0.1–1.3	0.15–0.8	0.1–2	0.1–4	0.2–2			Opq, Bt
B97122803B	1.2–2			0.1–0.8	1.2–2.5				Opq, Rt

Table 3. Continued (mm)

Sample	Grt	Cpx	Opx	Pl	Qtz	Amp	Bt	Sil	Accesory
B97122803D	2 mm				3-4 mm				Bt
B97122804B	5 mm	0.2-1.6	0.1-0.2	0.4 mm	0.1-2.5				Opq
B97122804C				0.3-2	>2		0.05-1		Opq, Zr, Ap
B97122804E	1-4 mm			0.3-1.8			0.2-2.5	0.1-0.6	Opq ,Qtz
B97122807				0.1-1.2	0.2-5				Grt
B97122808		0.4-2	0.3-0.5	0.2-2		0.3-1.4	0.3 mm		Opq
B971228T01	1.2 mm			0.7-1.9	1.2-2				Zr Cal (0-10%)
B97123001A	5 mm		0.3-1	0.1-1.8		0.2-2			Opq
B97123001B		0.6-1.1	0.2-0.3	0.3-1.3		0.3-1.2			Opq
TS97121901C	3-4 mm	0.3-0.5	0.2-0.9	0.8-1.1	0.1-2		0.2-1		Zr, Opq, Hbl
TS97121901D		0.4-2	0.6-1.6	0.4-2	0.9-2.5	0.3-2	0.1-1.6		
TS97121902A		0.1-2.2							Sph, Scp (10-15%)
TS97121903B						0.3-4			Spl (10-15%)
TS97121903D									Cal (85-95%), Spl, Amp
TS97122002A		0.8-1.6	0.1-1.6	0.6-1.8	0.3-2				Opq (0-10%)
TS97122004A		0.9-1.8	0.1-1	0.4-0.8	1.2-4				Opq, Grt, Bt

Table 3. Continued mm

Sample	Grt	Sil	Kfs	Pl	Qtz	Bt	Spl		Accessory
TS10122505B	1-3 mm	0.1-3	0.4-0.8		0.4-2	0.1-0.4			Rt, Spl
TS10122604H	0.4-3		0.2-1.6	0.2-1.4	0.1-4	0.1-2			Opq, Zr
TS10122806B	0.8-3	0.05-0.8	0.1-1.8	0.2-1	0.1-2				Ilm,Zr, Spl
TS10122806B2	0.3-2.4		0.2-1		0.2-2.2	0.3-2.5			Qtz, Bt, Opx
TS11010804	0.4-4		0.2-1.4	0.1-1.2		0.1-1.2	0.05-1.6		Opq
TS11010903A	0.2-10	0.1-2	0.4-1.2	0.2-1.2	0.2-1.4		0.05-0.2		Rt, Bt, Ilm
TS11010903B	0.6-3		0.2-1	0.3-1.2	0.1-2	0.2-1.2			Zr
TS11011401K3	0.6-2.5	0.2-2	0.3-2.5		0.1-2				Sph, Zr
TS11011502C	0.4-2								unknown (70-80%), Bt
TS11011702F	0.4-2.4	0.1-0.6	0.2-1.4		0.05-3				Ilm
TS11020203A	0.2-1.4		0.2-2		0.2-3	0.1-1			Opq
TS11020204A	0.4-2		0.3-1.8	0.2-2	0.4-1.6	0.1-1.2			Ilm, Ap, Zr
TS11020206A	0.2-1.8			0.2-1	0.1-2.5	0.1-3			Ilm, Ap (0-10%), Zr
TS11020206F	0.3-1		0.5-4		0.1-4	0.2-1.2			Ilm, Ap, Zr

Table 3. Continued mm

Sample	Grt	Sil	Kfs	Pl	Qtz	Bt	Spl		Accessory
TS11020206J	2.5–3		0.8–1.6	0.2–2.5	0.1–2	0.2–1.4			Opq
TS11020602B	0.3–1.2		0.3–2	0.2–1.8	0.2–1				Opq, Zr
TS11020607B	0.2–2		0.2–2.5	0.1–3	0.2–5	0.1–1			Rt(0–10%)
B97121905	1 – 2 mm			0.2–0.8	0.4–4	1–1.4			Kfs
B97122401A	2–10 mm		0.4–2	0.1–5	0.1–0.2	0.1–1.4			Opq, Zr, Ap
B97122403			0.2–2	0.2–1.4		0.05–1			Rt, Bt, Ilm
B97122604	0.6–0.9		0.2–1.2	0.2–0.8	0.2–1.4	0.05–1.4			Opq
B97122708A			0.6–1.4	0.4–1.3	0.4–2				Zr
B97122708B	0.1–1.6		0.1–1.3	0.2–0.8	0.1–1.4	0.1–0.7			Zr, Ap
B97122803B	1.2–2	0.2–0.6	0.1–0.8		0.3–2.5				Opq, Rt
B97122803C		0.05–0.5	0.2–1.2	0.2–1	0.1–2.4				Grt, Opq
B97122804E	1–4 mm	0.1–0.6		0.3–1.8		0.2–2.5			Rt
TS97121901B		0.2–1.6	0.2–3	0.3–1.8					Grt, Qtz,
TS97122002B	0.4–2.4	0.2–0.6	0.1–1.7						Opq. Qtz, Pl
TS97122003	0.2–8			0.1–4	0.1–1.8	0.1–1.6			Opq, Rt, Sil
TS97122004B			0.3–2.5	0.3–2	0.1–3	0.05–2.4			

Table 3. Continued mm

Sample	Grt	Sil	Kfs	Pl	Qtz	Bt	Spl		Accessory
TS97122004C			0.6–1.6	0.4–2.2	0.2–1.8	0.2–0.8			Grt
TS97122005C	0.6–3	0.2–3	1.4 mm		0.2–1.8				Rt, Bt
TS97122007	1.5–10	0.3–2				0.2–1.2			Pl, Qtz
TS97122302A–2	1.4–4	0.1–0.4	0.2–0.9		0.1–2.5	0.7–1.4			Ilm, Rt, Chl
Sample	Grt	Cpx	Opx	Pl	Qtz	Amp	Bt	Sil	Accesory
TS97122004D	1.2–4	0.2–1.2	0.1–0.3	0.1–1.6		0.2–3			Qtz, Opq
TS97122004E	0.9–2.5	1.8 mm	0.4 mm	0.2–2			0.4–1.8		Opq
TS97122005B	2.5–3			0.2–1.8	0.2–2.5		0.2–1.5		Sil (0–5%)
TS97122005G			0.05–1.2	0.1–1.4	0.1–1.6	0.1–1.4			Grt
TS97122402C		0.2–2.2	0.2–2.2						Spl (0–10%), Amp

Table 4. Representative electron microprobe analyses of garnet.

Locality	Skallevikshalsen		Skallevikshalsen		Skallevikshalsen		Austhovde		Austhovde		Ongul		Ongul	
Rock types	TS11010802	TS11010802	TS10122604B	TS10122604B	TS11010704B	TS11010704B	TS11011405A-2	TS11011405A-2	TS11011601M	TS11011601M	TS11020610I	TS11020610I	TS11020610G	TS11020610G
Sample No.	Grt	Grt	Grt	Grt	Grt	Grt	Grt	Grt	Grt	Grt	Grt	Grt	Grt	Grt
Mineral Name	12	12	12	12	12	12	12	12	12	12	12	12	12	12
No. of oxygen	core	rim	core	rim	core	rim	core	rim	core	rim	core	rim	core	rim
Remarks	39.026	38.644	38.683	38.627	37.913	37.642	39.602	39.4	39.8	38.494	38.952	38.508	39.731	39.139
SiO2	21.757	21.549	21.878	21.486	20.936	21.015	22.014	21.574	23.084	22.22	21.289	21.396	22.281	22.082
Al2O3	0	0.093	0.095	0.017	0.099	0.038	0.049	0.041	0.051	0.017	0.101	0	0	0
TiO2	0.031	0.061	0	0.018	0	0.023	0.012	0	0.01	0.014	0.03	0	0	0
Cr2O3														
Fe2O3	25.998	26.764	30.15	30.136	29.9	30.118	29.242	29.536	25.47	27.074	24.646	25.905	21.854	24.054
FeO※	0.423	0.525	1.107	1.128	0.907	0.88	0.993	1.228	0.482	0.878	1.099	1.405	0.973	1.444
MnO	0	0	0	0.045	0.057	0	0.009	0	0	0.088	0.031	0		
NiO	6.787	5.942	3.565	3.109	2.204	2.307	3.848	3.209	7.266	5.645	7.319	6.772	9.444	7.626
MgO	6.597	6.751	6.899	7.088	8.253	8.168	7.098	7.209	6.457	6.229	5.703	5.495	5.87	5.621
CaO	0.013	0.039	0.015	0.029	0.024	0.01	0	0.001	0.004	0.044	0	0.038	0.021	0.024
Na2O	0.01	0.002	0	0.009	0	0	0	0	0.01	0	0.01	0.008	0	0
K2O	0.034	0.084	0	0	0.111	0.096	0	0	0	0.031	0	0		
ZnO	100.676	100.454	102.392	101.692	100.404	100.297	102.867	102.198	102.634	100.734	99.18	99.527	100.174	99.99
Total														
	3.005	3.000	2.994	3.015	3.013	2.997	3.030	3.046	2.986	2.982	3.029	3.007	3.012	3.010
Si	1.974	1.971	1.995	1.976	1.960	1.972	1.985	1.965	2.041	2.028	1.951	1.968	1.990	2.001
Al	0.000	0.005	0.006	0.001	0.006	0.002	0.003	0.002	0.003	0.001	0.006	0.000	0.000	0.000
Ti	0.002	0.004	0.000	0.001	0.000	0.001	0.001	0.000	0.001	0.001	0.002	0.000	0.000	0.000
Cr	0.000	0.000	0.000	0.000	0.000	0.000	0.000	0.000	0.000	0.000	0.000	0.000	0.000	0.000
Fe3+	1.673	1.737	1.951	1.967	1.986	2.005	1.871	1.909	1.598	1.754	1.602	1.691	1.385	1.546
Fe2+	0.028	0.035	0.073	0.075	0.061	0.059	0.064	0.080	0.031	0.058	0.072	0.093	0.062	0.094
Mn	0.000	0.000	0.000	0.003	0.004	0.000	0.001	0.000	0.000	0.005	0.002	0.000	0.000	0.000
Ni	0.778	0.687	0.411	0.362	0.261	0.274	0.439	0.370	0.812	0.651	0.848	0.788	1.066	0.874
Mg	0.544	0.561	0.572	0.593	0.702	0.697	0.582	0.597	0.519	0.517	0.475	0.459	0.477	0.463
Ca	0.002	0.006	0.002	0.004	0.004	0.002	0.000	0.000	0.001	0.007	0.000	0.006	0.003	0.004
Na	0.001	0.000	0.000	0.001	0.000	0.000	0.000	0.000	0.001	0.000	0.001	0.001	0.000	0.000
K	0.002	0.005	0.000	0.000	0.007	0.006	0.000	0.000	0.000	0.002	0.000	0.000	0.000	0.000
Zn	8.009	8.010	8.004	7.997	8.003	8.015	7.974	7.969	7.991	8.006	7.989	8.012	7.995	7.991
Total														
	0.32	0.28	0.17	0.16	0.12	0.12	0.19	0.16	0.34	0.27	0.35	0.32	0.44	0.36
Mg/(Fe+Mg)	55.4	57.5	64.9	65.7	66.0	66.1	63.3	64.6	54.0	58.9	53.5	55.8	46.3	51.9
Alm	25.7	22.8	13.7	12.1	8.7	9.0	14.8	12.5	27.4	21.9	28.3	26.0	35.7	29.3
Prp	18.0	18.6	19.0	19.8	23.3	23.0	19.7	20.2	17.5	17.3	15.8	15.2	15.9	15.6
Grs	0.91	1.14	2.41	2.49	2.03	1.96	2.18	2.72	1.03	1.93	2.41	3.06	2.09	3.16
Sps														
※Total Fe as FeO														

Table 4. Continued

Locality	Skallevikshalsen		Skallevikshalsen			Skallen		Austhovde	
Sample No.	TS10122502B	TS10122502B	TS10122502D	TS10122502D	TS10122502D	B97122003-2	B97122003-2	TS11011504C	TS11011504C
Mineral Name	Grt	Grt	Grt	Grt	Grt	Grt	Grt	Grt	Grt
No. of oxygen	12	12	12	12	12	12	12	12	12
Remarks	core	rim	core	rim	core	core	rim	core	rim
SiO2	39.42	38.374	38.659	38.645	39.217	38.569	38.672	38.781	38.164
Al2O3	21.795	21.388	21.592	21.788	21.542	21.209	20.992	21.381	21.052
TiO2	0	0.002	0.021	0	0.071	0.098	0.004	0.065	0.074
Cr2O3	0	0.067	0	0.048	0.026	0	0.046	0.029	0.117
Fe2O3									
FeO※	24.825	28.729	27.43	29.103	25.941	26.531	28.808	25.097	30.63
MnO	0.387	0.667	1.001	1.031	0.567	0.49	0.563	0.519	0.754
NiO			0.051	0	0			0	0.006
MgO	10.865	8.419	6.901	7.439	9.195	8.474	6.955	9.354	6.473
CaO	1.243	0.757	5.233	3.011	2.598	2.297	2.171	2.927	1.738
Na2O	0	0	0.039	0	0	0.001	0.054	0.023	0.018
K2O	0	0.014	0	0.01	0	0.013	0.016	0	0.029
ZnO			0	0	0.08			0.009	0.168
Total	98.535	98.417	100.927	101.075	99.237	97.682	98.281	98.185	99.223
Si	3.033	3.018	2.988	2.985	3.029	3.036	3.057	3.022	3.019
Al	1.976	1.982	1.967	1.983	1.961	1.967	1.955	1.963	1.962
Ti	0.000	0.000	0.001	0.000	0.004	0.006	0.000	0.004	0.004
Cr	0.000	0.004	0.000	0.003	0.002	0.000	0.003	0.002	0.007
Fe3+	0.000	0.000	0.000	0.000	0.000	0.000	0.000	0.000	0.000
Fe2+	1.597	1.889	1.772	1.879	1.675	1.746	1.904	1.635	2.026
Mn	0.025	0.044	0.066	0.067	0.037	0.033	0.038	0.034	0.051
Ni	0.000	0.000	0.003	0.000	0.000	0.000	0.000	0.000	0.000
Mg	1.245	0.986	0.795	0.856	1.058	0.994	0.819	1.086	0.763
Ca	0.102	0.064	0.433	0.249	0.215	0.194	0.184	0.244	0.147
Na	0.000	0.000	0.006	0.000	0.000	0.000	0.008	0.003	0.003
K	0.000	0.001	0.000	0.001	0.000	0.001	0.002	0.000	0.003
Zn	0.000	0.000	0.000	0.000	0.005	0.000	0.000	0.001	0.010
Total	7.979	7.989	8.030	8.023	7.985	7.976	7.969	7.994	7.995
Mg/(Fe+Mg)	0.44	0.34	0.31	0.31	0.39	0.36	0.30	0.40	0.27
Alm	53.8	63.3	57.8	61.6	56.1	58.9	64.7	54.5	67.8
Prp	41.9	33.1	25.9	28.0	35.4	33.5	27.8	36.2	25.5
Grs	3.4	2.1	14.1	8.2	7.2	6.5	6.2	8.1	4.9
Sps	0.85	1.49	2.14	2.21	1.24	1.10	1.28	1.14	1.69
※Total Fe as FeO									

Table 4. Continued

		Austhovde		Ongul		Ongul		Austhovde		
Locality		TS11011702B	TS11011702B	TS11020604B	TS11020604B	TS11020606A	TS11020606A	TS11011407D	TS11011407D	TS11011702G
Sample No.		Grt	Grt	Grt	Grt	Grt	Grt	Grt	Grt	Grt
Mineral Name		12	12	12	12	12	12	12	12	12
No. of oxygen		core	rim	core	rim	core	rim	core	rim	core
Remarks		38.313	38.548	39.308	39.401	39.484	39.281	39.014	39.533	38.338
SiO2		21.442	21.536	22.48	22.352	22.087	22.176	22.308	22.477	21.437
Al2O3		0.012	0	0.027	0	0	0.076	0	0	0
TiO2		0.087	0.041	0.031	0.035	0	0	0.047	0.012	0.006
Cr2O3								0	0	
Fe2O3		29.663	30.667	27.461	27.176	25.711	25.945	27.95	29.475	30.772
FeO※		1.219	1.208	0.38	0.369	0.463	0.387	0.792	0.817	0.55
MnO		0	0.044					0	0	
NiO		6.837	6.651	10.457	10.546	9.396	9.524	6.314	6.453	7.432
MgO		2.58	1.609	1.064	1.051	3.335	3.041	3.669	3.741	0.891
CaO		0	0.005	0	0	0	0.018	0	0.043	0
Na2O		0	0.014	0.004	0	0.002	0.011	0	0	0
K2O		0.129	0.066					0	0	
ZnO		100.282	100.389	101.212	100.93	100.478	100.459	100.094	102.551	99.426
Total										
		2.995	3.012	2.977	2.988	3.009	2.996	3.023	3.006	3.011
Si		1.975	1.983	2.006	1.998	1.983	1.993	2.037	2.014	1.984
Al		0.001	0.000	0.002	0.000	0.000	0.004	0.000	0.000	0.000
Ti		0.005	0.003	0.002	0.002	0.000	0.000	0.003	0.001	0.000
Cr		0.000	0.000	0.000	0.000	0.000	0.000	0.000	0.000	0.000
Fe3+		1.938	2.003	1.739	1.723	1.638	1.654	1.810	1.874	2.021
Fe2+		0.081	0.080	0.024	0.024	0.030	0.025	0.052	0.053	0.037
Mn		0.000	0.003	0.000	0.000	0.000	0.000	0.000	0.000	0.000
Ni		0.796	0.774	1.180	1.191	1.067	1.082	0.729	0.731	0.869
Mg		0.216	0.135	0.086	0.085	0.272	0.248	0.304	0.305	0.075
Ca		0.000	0.001	0.000	0.000	0.000	0.003	0.000	0.006	0.000
Na		0.000	0.001	0.000	0.000	0.000	0.001	0.000	0.000	0.000
K		0.007	0.004	0.000	0.000	0.000	0.000	0.000	0.000	0.000
Zn		8.014	7.997	8.017	8.012	7.999	8.006	7.958	7.990	7.997
Total										
		0.29	0.28	0.40	0.41	0.39	0.40	0.29	0.28	0.30
Mg/(Fe+Mg)		64.0	67.0	57.4	57.0	54.5	55.0	62.5	63.3	67.3
Alm		26.3	25.9	38.9	39.4	35.5	36.0	25.2	24.7	29.0
Prp		7.1	4.5	2.8	2.8	9.1	8.3	10.5	10.3	2.5
Grs		2.66	2.67	0.80	0.78	0.99	0.83	1.79	1.78	1.22
Sps										
※Total Fe as FeO										

Table 5. Representative electron microprobe analysis of pyroxene.

Locality	Skallevikshalsen					Austhovde	Ongul	
Sample No.	TS11010802	TS11010802	TS11010803A	TS11010803A	TS11010704B	TS1101405A-2	TS1101405A-2	TS11020610I
Mineral Name	Cpx	Cpx	Cpx	Cpx	Cpx	Cpx	Cpx	Cpx
No. oxygen	6	6	6	6	6	6	6	6
Remarks	core	rim	core	rim		core	rim	Matrix
SiO2	51.493	50.7	51.623	51.933	50.297	51.664	52.421	51.526
Al2O3	2.468	3.206	1.861	1.664	2.242	2.708	2.101	1.147
TiO2	0.331	0.268	0.267	0.143	0.296	0.301	0.201	0.364
Cr2O3	0	0.017	0.004	0.006	0	0	0	0.023
Fe2O3								
FeO※	11.912	11.132	14.802	14.925	19.614	15.625	15.316	9.721
MnO	0.117	0.108	0.13	0.122	0.278	0.114	0.196	0.191
NiO	0.031	0.007	0	0.04	0	0	0.032	
MgO	12.367	12.285	10.426	10.5	7.505	9.46	9.536	13.1
CaO	21.507	22.474	21.753	21.681	20.244	21.627	21.853	21.41
Na2O	0.402	0.3	0.301	0.321	0.534	0.359	0.397	0.376
K2O	0.002	0.001	0	0	0.008	0.004	0	0.005
ZnO	0	0	0	0	0.019		0	
Total	100.63	100.498	101.167	101.335	101.037	101.862	102.053	97.863
Si	1.934	1.907	1.954	1.962	1.947	1.946	1.968	1.972
Al	0.109	0.142	0.083	0.074	0.102	0.120	0.093	0.052
Ti	0.009	0.008	0.008	0.004	0.009	0.009	0.006	0.010
Cr	0.000	0.001	0.000	0.000	0.000	0.000	0.000	0.001
Fe3+	0.000	0.000	0.000	0.000	0.000	0.000	0.000	0.000
Fe2+	0.374	0.350	0.468	0.471	0.635	0.492	0.481	0.311
Mn	0.004	0.003	0.004	0.004	0.009	0.004	0.006	0.006
Ni	0.001	0.000	0.000	0.001	0.000	0.000	0.001	0.000
Mg	0.692	0.688	0.588	0.591	0.433	0.531	0.533	0.747
Ca	0.865	0.905	0.882	0.877	0.839	0.872	0.878	0.878
Na	0.029	0.022	0.022	0.023	0.040	0.026	0.029	0.028
K	0.000	0.000	0.000	0.000	0.000	0.000	0.000	0.000
Zn	0.000	0.000	0.000	0.000	0.001	0.000	0.000	0.000
Total	4.017	4.026	4.008	4.009	4.014	3.999	3.995	4.005
Mg/(Fe+Mg)	0.65	0.66	0.56	0.56	0.41	0.52	0.53	0.71
Acm	3.4	5.1	1.7	1.7	2.8	0.4	0.0	1.0
CaTs	6.6	9.3	4.6	3.8	5.3	5.3	3.2	2.8
Aug	73.2	71.8	78.9	80.1	73.2	74.7	80.8	82.2
※Total Fe as FeO								

Table 5. Continued.

Locality	Skallevikshalsen			Austhovde						Ongul
Sample No.	TS11010802	TS11010803A	TS10122604B	TS11011405B	TS11011405B	TS11020206H	TS11020206H	TS11011407D	TS10122502D	TS11020606A
Mineral Nam	Opx	Opx	Opx	Opx	Opx	Opx	Opx	Opx	Opx	Opx
No. oxygen	6	6	6	6	6	6	6	6	6	6
Remarks	symp	in Cpx	rim	core	rim	core	rim	rim	matrix	matrix
SiO2	51.753	50.202	50.147	52.343	52.954	51.759	51.301	50.585	51.352	51.975
Al2O3	1.687	1.127	0.837	2.232	1.888	2.806	2.547	2.334	2.346	2.722
TiO2	0.088	0.058	0.094	0.127	0.068	0	0.464	0	0.137	0.021
Cr2O3	0	0	0	0.021	0.039	0	0	0.039	0.115	0
Fe2O3								0		
FeO※	28.085	34.701	34.772	27.143	26.576	27.473	26.304	28.206	25.308	23.106
MnO	0.236	0.315	0.214	0.426	0.405	0.29	0.275	0.284	0.322	0.126
NiO	0	0.071	0	0	0	0	0.031	0.029	0.091	0
MgO	18.477	13.033	14.133	19.507	19.546	19.36	20.175	17.665	19.564	21.897
CaO	0.543	0.799	0.745	0.47	0.468	0.259	0.083	0.222	0.198	0.227
Na2O	0	0.044	0	0.016	0	0.028	0.027	0.04	0.032	0
K2O	0	0.006	0.045	0	0	0	0	0.013	0	0
ZnO	0.078	0.286	0.078			0.169	0.025	0	0.085	0.172
Total	100.947	100.642	101.065	102.285	101.944	102.212	101.232	99.417	99.55	100.246
Si	1.960	1.977	1.965	1.945	1.966	1.929	1.921	1.948	1.948	1.935
Al	0.075	0.052	0.039	0.098	0.083	0.123	0.112	0.106	0.105	0.119
Ti	0.003	0.002	0.003	0.004	0.002	0.000	0.013	0.000	0.004	0.001
Cr	0.000	0.000	0.000	0.001	0.001	0.000	0.000	0.001	0.003	0.000
Fe3+	0.000	0.000	0.000	0.000	0.000	0.000	0.000	0.000	0.000	0.000
Fe2+	0.889	1.143	1.139	0.843	0.825	0.856	0.823	0.908	0.803	0.719
Mn	0.008	0.011	0.007	0.013	0.013	0.009	0.009	0.009	0.010	0.004
Ni	0.000	0.002	0.000	0.000	0.000	0.000	0.001	0.001	0.003	0.000
Mg	1.042	0.765	0.825	1.080	1.081	1.075	1.125	1.013	1.106	1.214
Ca	0.022	0.034	0.031	0.019	0.019	0.010	0.003	0.009	0.008	0.009
Na	0.000	0.003	0.000	0.001	0.000	0.002	0.002	0.003	0.002	0.000
K	0.000	0.000	0.002	0.000	0.000	0.000	0.000	0.001	0.000	0.000
Zn	0.002	0.008	0.002	0.000	0.000	0.005	0.001	0.000	0.002	0.005
Total	4.000	3.997	4.014	4.003	3.990	4.010	4.011	4.000	3.995	4.005
Mg/(Fe+Mg)	0.54	0.40	0.42	0.56	0.57	0.56	0.58	0.53	0.58	0.63
XAl	0.04	0.03	0.02	0.05	0.04	0.06	0.06	0.05	0.05	0.06

Table 6. Representative electron microprobe analysis of plagioclase.

Locality	Skallevikshalsen				Austhovde			Skallen		Ongul	
Sample No.	TS11010802	TS11010802	TS11010803 A	TS10122604 B	TS11011405 A-2	TS11011405 C	TS11011405 C	B97122302F2	B97122302F2	TS11020610I	TS11020610I
Mineral Name	Pl	Pl	Pl	Pl	Pl	Pl	Pl	Pl	Pl	Pl	Pl
No. oxygen	8	8	8	8	8	8	8	8	8	8	8
Remarks	symp	mat			symp	mat	symp	in Grt	matrix	symp	matrix
SiO2	45.94	49.94	55.148	55.659	54.935	55.473	50.716	57.26	47.462	49.818	57.644
Al2O3	35.141	31.689	28.77	28.743	29.51	29.053	32.757	26.537	33.13	32.309	26.949
TiO2	0	0.04	0	0	0.014	0	0.018	0	0	0.011	0
Cr2O3	0.015	0.036	0	0.091	0.002	0	0	0.039	0	0	0.004
Fe2O3											
FeO※	0.169	0.179	0.074	0.119	0.368	0.06	0.316	0.154	0.137	0.048	0.048
MnO	0.021	0.006	0	0	0.007	0	0.017	0.034	0.011	0.026	0.009
NiO	0.022	0.06	0.029	0	0	0	0.031			0	0
MgO	0	0.022	0	0.017	0	0	0.013	0.019	0	0	0
CaO	18.57	14.625	10.949	11.245	12.309	10.872	14.627	8.864	16.413	15.635	9.079
Na2O	0.952	3.117	5.505	5.18	4.422	5.342	3.153	6.53	2.108	3.491	7.715
K2O	0.031	0.204	0.19	0.285	0.187	0.282	0.141	0.352	0.057	0.049	0.243
ZnO	0	0	0	0.022	0	0	0.133			0.101	0.025
Total	100.861	99.918	100.665	101.361	101.754	101.082	101.922	99.789	99.318	101.488	101.716
Si	2.100	2.282	2.473	2.479	2.442	2.474	2.272	2.578	2.191	2.251	2.557
Al	1.893	1.707	1.520	1.509	1.546	1.527	1.729	1.408	1.803	1.720	1.409
Ti	0.000	0.001	0.000	0.000	0.000	0.000	0.001	0.000	0.000	0.000	0.000
Cr	0.001	0.001	0.000	0.003	0.000	0.000	0.000	0.001	0.000	0.000	0.000
Fe3+	0.000	0.000	0.000	0.000	0.000	0.000	0.000	0.000	0.000	0.000	0.000
Fe2+	0.006	0.007	0.003	0.004	0.014	0.002	0.012	0.006	0.005	0.002	0.002
Mn	0.001	0.000	0.000	0.000	0.000	0.000	0.001	0.001	0.000	0.001	0.000
Ni	0.001	0.002	0.001	0.000	0.000	0.000	0.001	0.000	0.000	0.000	0.000
Mg	0.000	0.001	0.000	0.001	0.000	0.000	0.001	0.001	0.000	0.000	0.000
Ca	0.909	0.716	0.526	0.536	0.586	0.519	0.702	0.427	0.812	0.757	0.431
Na	0.084	0.276	0.478	0.447	0.381	0.462	0.274	0.570	0.189	0.272	0.588
K	0.002	0.012	0.011	0.016	0.011	0.016	0.008	0.020	0.003	0.003	0.014
Zn	0.000	0.000	0.000	0.001	0.000	0.000	0.004	0.000	0.000	0.003	0.001
Total	4.996	5.006	5.012	4.997	4.980	5.001	5.004	5.013	5.003	5.009	5.002
An	91.35	71.32	51.80	53.66	59.95	52.09	71.35	42.01	80.87	73.37	41.74
Ab	8.47	27.50	47.13	44.72	38.97	46.31	27.83	56.00	18.79	26.36	56.93
Or	2.05	3.97	2.17	3.38	2.64	3.25	2.78	3.31	1.72	1.02	2.23

Table 6. continued.

Locality	Skallen		Skallevikshalsen			Austhovde				Ongul	
Sample No.	B97122003-2	TS97122003-2	TS10122502D	TS10122502D	TS10122502B2	TS11011504C	TS11011504C	TS11011702B	TS11011702G	TS11020604B	TS11020606A
Mineral Name	Pl	Pl	Pl	Pl	Pl	Pl	Pl	Pl	Pl	Pl	Pl
No. oxygen	8	8	8	8	8	8	8	8	8	8	8
Remarks	in Grt	Matrix	matrix	matrix	in Grt	in Grt	matrix	mat	matrix	in Grt	
SiO2	54.488	58.987	54.662	57.979	60.481	57.825	57.196	57.731	65.156	61.33	50.318
Al2O3	27.212	27.097	28.768	26.573	24.402	26.144	26.638	26.741	22.175	24.959	31.994
TiO2	0	0	0	0	0.02	0	0.022	0	0	0.02	0
Cr2O3	0	0.015	0	0	0	0	0.014	0	0.016	0.022	0
Fe2O3											
FeO※	0.275	0.003	0.174	0.046	0.029	0.23	0.056	0.066	0.121	0.489	0.061
MnO	0.017	0.027	0	0	0	0	0.017	0	0	0.006	0
NiO		0	0.069	0.04		0.049	0	0			
MgO	0	0.029	0.01	0.009	0	0.001	0.026	0.02	0	0.008	0.041
CaO	10.045	8.686	11.294	8.611	6.794	7.772	8.753	8.831	3.041	6.294	14.767
Na2O	5.557	6.578	5.115	6.637	7.838	7.086	6.545	6.706	9.94	8.118	3.274
K2O	0.405	0.204	0.198	0.363	0.271	0.126	0.126	0.246	0.109	0.202	0.083
ZnO		0	0.049	0.003		0	0	0			
Total	97.999	101.626	100.339	100.261	99.835	99.233	99.393	100.341	100.558	101.448	100.538
Si	2.509	2.596	2.462	2.593	2.700	2.608	2.579	2.581	2.855	2.696	2.283
Al	1.477	1.405	1.527	1.400	1.284	1.390	1.415	1.409	1.145	1.293	1.710
Ti	0.000	0.000	0.000	0.000	0.001	0.000	0.001	0.000	0.000	0.001	0.000
Cr	0.000	0.001	0.000	0.000	0.000	0.000	0.000	0.000	0.001	0.001	0.000
Fe3+	0.000	0.000	0.000	0.000	0.000	0.000	0.000	0.000	0.000	0.000	0.000
Fe2+	0.011	0.000	0.007	0.002	0.001	0.009	0.002	0.002	0.004	0.018	0.002
Mn	0.001	0.001	0.000	0.000	0.000	0.000	0.001	0.000	0.000	0.000	0.000
Ni	0.000	0.000	0.002	0.001	0.000	0.002	0.000	0.000	0.000	0.000	0.000
Mg	0.000	0.002	0.001	0.001	0.000	0.000	0.002	0.001	0.000	0.001	0.003
Ca	0.495	0.409	0.545	0.412	0.325	0.375	0.423	0.423	0.143	0.296	0.717
Na	0.496	0.561	0.446	0.575	0.678	0.619	0.572	0.581	0.844	0.691	0.288
K	0.024	0.011	0.011	0.021	0.015	0.007	0.007	0.014	0.006	0.011	0.005
Zn	0.000	0.000	0.002	0.000	0.000	0.000	0.000	0.000	0.000	0.000	0.000
Total	5.012	4.987	5.003	5.005	5.004	5.010	5.002	5.012	4.997	5.008	5.008
An	48.8	41.7	54.3	40.9	31.9	37.5	42.2	41.5	14.4	29.7	71.0
Ab	48.9	57.1	44.5	57.0	66.6	61.8	57.1	57.1	85.0	69.2	28.5
Or	4.4	2.0	2.4	3.4	2.2	1.1	1.2	2.3	0.7	1.6	1.6

Table 7. Representative electron microprobe analysis of amphibole.

Locality	Skallevikshalsen			Austhovde	Ongul		Ongul	
Sample No.	TS11010802	TS11010803A	TS10122604B	TS11011405A-2	TS11020610I	TS11020610I	TS11020610G-2	TS11020610G-2
Mineral Name	Hbl	Hbl	Hbl	Hbl	Hbl	Hbl	Hbl	Hbl
No. oxygen	23	23	23	23	23	23	23	23
Remarks	symp		Matrix	in Grt	matrix	in Grt	in Grt	
SiO2	41.777	40.64	40.87	39.503	40.627	41.235	42.178	41.442
Al2O3	12.107	12.419	11.973	12.111	13.602	13.313	15.649	15.22
TiO2	1.769	2.024	2.244	2.618	2.989	3.137	0.325	0.374
Cr2O3	0.059	0.008	0.078	0.045	0.01	0.052	0	0.019
Fe2O3								
FeO※	14.919	20.538	19.409	18.329	15.398	12.602	10.181	12.268
MnO	0.039	0.048	0.06	0.032	0.219	0.081	0.085	0.044
NiO	0.04	0.018	0.007	0	0.002	0		
MgO	12.083	7.697	7.933	8.026	9.967	11.553	13.223	11.917
CaO	11.909	11.293	11.599	11.39	11.275	11.793	11.562	11.258
Na2O	1.723	2.302	1.226	1.27	2.237	2.31	1.973	1.971
K2O	2.096	1.12	1.975	2.733	1.56	1.425	1.877	1.832
ZnO	0.122	0	0	0	0.119	0		
Total	98.643	98.107	97.374	96.057	98.005	97.501	97.053	96.345
Si	6.237	6.231	6.295	6.186	6.106	6.144	6.208	6.208
Al	2.130	2.244	2.173	2.235	2.409	2.337	2.714	2.686
Ti	0.199	0.233	0.260	0.308	0.338	0.351	0.036	0.042
Cr	0.007	0.001	0.009	0.006	0.001	0.006	0.000	0.002
Fe3+	0.000	0.000	0.000	0.000	0.000	0.000	0.000	0.000
Fe2+	1.862	2.633	2.499	2.400	1.935	1.570	1.253	1.536
Mn	0.005	0.006	0.008	0.004	0.028	0.010	0.011	0.006
Ni	0.005	0.002	0.001	0.000	0.000	0.000	0.000	0.000
Mg	2.687	1.758	1.820	1.872	2.231	2.564	2.899	2.659
Ca	1.904	1.854	1.913	1.910	1.815	1.882	1.822	1.806
Na	0.498	0.684	0.366	0.385	0.651	0.667	0.563	0.572
K	0.399	0.219	0.388	0.546	0.299	0.271	0.352	0.350
Zn	0.013	0.000	0.000	0.000	0.013	0.000	0.000	0.000
Total	15.945	15.865	15.731	15.851	15.827	15.802	15.857	15.867
Mg/(Fe+Mg)	0.59	0.40	0.42	0.44	0.54	0.62	0.70	0.63
Si	6.24	6.23	6.29	6.19	6.11	6.12	6.21	6.21
NaA+K	0.90	0.83	0.75	0.93	0.950	0.940	0.97	0.92
		※Total Fe as FeO						

Table 8. Integrated composition of CMI (sample TS10122506).

		Qtz	Pl	Kfs	Ilm	Bt	Total
Mode ratio		0.333	0.189	0.164	0.016	0.298	
Mineral density		2.65	2.68	2.62	5.5	3.1	
Mineral weight		0.88	0.51	0.43	0.09	0.92	2.83
Volume density		0.31	0.18	0.15	0.03	0.33	1
		Qtz	Pl	Kfs	Ilm	Bt	
	SiO2	100	51.527	67.257	0.029	35.289	
	Al2O3		29.718	17.438	0.026	18.326	
	TiO2		0.109	0.035	51.609	0	
	Cr2O3		0	0.022	0.042	0	
	Fe2O3						
	FeO		0.858	0.526	45.932	18.311	
	MnO		0.024	0	0.168	0	
	NiO		0.041	0.015	0.053	0.002	
	MgO		0.137	0.012	0.718	12.133	
	CaO		12.331	0	0	0.035	
	Na2O		4.547	0.981	0	0.026	
	K2O		0.209	14.216	0.003	8.957	
	ZnO		0.055	0.095	0.077	0.03	
	Total		99.556	100.597	98.657	93.109	
Volume ratio* oxide component	SiO2	31.12	9.20	10.22	0.00	11.52	62.06
	Al2O3	0.00	5.31	2.65	0.00	5.98	13.94
	TiO2	0.00	0.02	0.01	1.64	0.00	1.66
	Cr2O3	0.00	0.00	0.00	0.00	0.00	0.00
	Fe2O3	0.00	0.00	0.00	0.00	0.00	0.00
	FeO	0.00	0.15	0.08	1.46	5.98	7.67
	MnO	0.00	0.00	0.00	0.01	0.00	0.01
	NiO	0.00	0.01	0.00	0.00	0.00	0.01
	MgO	0.00	0.02	0.00	0.02	3.96	4.01
	CaO	0.00	2.20	0.00	0.00	0.01	2.21
	Na2O	0.00	0.81	0.15	0.00	0.01	0.97
	K2O	0.00	0.04	2.16	0.00	2.93	5.12
	ZnO	0.00	0.01	0.01	0.00	0.01	0.04
	Total						97.72

Table 8. Continued (sample TS11010802).

				Qtz	Pl	Kfs	Opx	Bt	
		Mode ratio		0.231	0.254	0.113	0.090	0.313	
		Mineral density		2.65	2.7068	2.621	3.503	3.1	
		Mineral weight		0.61	0.69	0.30	0.32	0.97	2.88
		Volume density		0.212	0.238	0.102	0.110	0.337	1
				Qtz	Pl	Kfs	Opx	Bt	
			SiO2	100	53.703	64.257	50.904	38.256	
			Al2O3		27.882	17.645	1.813	13.207	
			TiO2		0.039	0.011	0.054	4.467	
			Cr2O3		0	0.033	0	0	
			Fe2O3						
			FeO		0.63	0.655	24.522	11.223	
			MnO		0.038	0.004	0.293	0.019	
			NiO		0.002	0.015	0.009	0.104	
			MgO		0.03	0.047	19.866	16.522	
			CaO		11.204	0.012	0.246	0	
			Na2O		4.984	1.432	0	0	
			K2O		0.079	13.985	0.021	9.906	
			ZnO		0.08	0.034	0.255	0.055	
			total	100	98.671	98.13	97.983	93.759	
Volume ratio* oxide component			SiO2	21.23	12.80	6.59	5.60	12.88	59.10
			Al2O3	0.00	6.65	1.81	0.20	4.45	13.10
			TiO2	0.00	0.01	0.00	0.01	1.50	1.52
			Cr2O3	0.00	0.00	0.00	0.00	0.00	0.00
			Fe2O3	0.00	0.00	0.00	0.00	0.00	0.00
			FeO	0.00	0.15	0.07	2.70	3.78	6.70
			MnO	0.00	0.01	0.00	0.03	0.01	0.05
			NiO	0.00	0.00	0.00	0.00	0.04	0.04
			MgO	0.00	0.01	0.00	2.19	5.56	7.76
			CaO	0.00	2.67	0.00	0.03	0.00	2.70
			Na2O	0.00	1.19	0.15	0.00	0.00	1.34
			K2O	0.00	0.02	1.43	0.00	3.34	4.79
			ZnO	0.00	0.02	0.00	0.03	0.02	0.07
			total	21.23	23.53	10.06	10.78	31.57	97.17

Table 8. Continued (sample TS11020610l).

					Bt	Kfs	Pl	Qtz	Total
			Mineral Mode		0.314	0.023	0.230	0.433	
			Mineral Density		3.100	2.621	2.67	2.65	
			Mineral Weight		0.97	0.06	0.61	1.15	2.79
			Volume ratio		0.35	0.02	0.22	0.41	1
			Mineral		Bt	Kfs	Pl	Qtz	
				SiO2	35.492	71.488	58.638	100	
				Al2O3	15.966	15.106	25.724		
				TiO2	1.055	0.016	0		
				Cr2O3	0	0.017	0		
				Fe2O3					
				FeO	22.943	0.908	0.948		
				MnO	0.095	0.03	0.053		
				NiO					
				MgO	8.336	0.044	0.059		
				CaO	0.249	0.227	6.829		
				Na2O	0.401	0.839	7.997		
				K2O	8.089	11.739	0.147		
				ZnO					
				Total	92.626	100.414	100.395		
Volume ratio * each oxide component				SiO2	12.371482	1.5382073	12.880775	41.0246	67.82
				Al2O3	5.5652846	0.3250358	5.6506882	0	11.54
				TiO2	0.3677424	0.0003443	0	0	0.37
				Cr2O3	0	0.0003658	0	0	0.00
				Fe2O3	0	0	0	0	0.00
				FeO	7.9972645	0.0195374	0.2082434	0	8.23
				MnO	0.0331142	0.0006455	0.0116423	0	0.05
				NiO	0	0	0	0	0.00
				MgO	2.9056879	0.0009467	0.0129603	0	2.92
				CaO	0.0867942	0.0048844	1.5000991	0	1.59
				Na2O	0.139777	0.0180528	1.756669	0	1.91
				K2O	2.8195908	0.2525881	0.0322909	0	3.10
				ZnO	0	0	0	0	0.00
				Total	32.286737	2.160608	22.053368	41.0246	97.53

Table 9. Results of *P-T* estimations.

Sample	Locality	Lithology	Grt-Cpx	Grt-Opx	Hbl-isopleth	Grt-Hbl	GRIPS	GASP	Zirconium in Rutile
TS10122502B2	Skallevikshalsen	Pelitic granulite							870-930 °C at 12 kbar
TS110122502D	Skallevikshalsen	Pelitic granulite		840-880 °C 10.5-11 kbar			15.2-15.4 kbar at 800 °C		850-910 °C at 12 kbar
TS110122604B	Skallevikshalsen	Ganrt-two-pyroxene granulite	740-780 °C 7.5-8 kbar	840-900 °C 8-9.5 kbar					
TS11010704B	Skallevikshalsen	Garnet-Cpx rock	820-920 °C at 12 kbar						
TS11010802	Skallevikshalsen	Garnet-Cpx rock	850-860°C at 12 kbar		820-860°C 6-8 kbar				
TS11010803A	Skallevikshalsen	Garnet-Cpx rock	790-800 °C at 12 kbar						
TS97122003-2	Skallen	Pelitic granulite							860-950 °C at 12 kbar
B97122302F2	Skallen	Mafic granulite					15.8-16 kbar at 800 °C		890-930 °C at 12 kbar
B97122708B	Skallen	Garnet-biotite gneiss					15.5-15.6 kbar at 800 °C		
TS11011405A-2	Austhovde	Ganrt-two-pyroxene granulite	790-840°C 7- 8 kbar	780-820 8-8.2 kbar		700-720 7-7.2 kbar			
TS11011405C	Austhovde	Ganrt-two-pyroxene granulite	720-750 °C 7-7.4 kbar		830-860°C 9 kbar				
TS11011407D	Austhovde	Felsic granulite		830-880 °C 8.5-9 kbar					
TS11011504C	Austhovde	Garnet-biotite gneiss					15.6-15.8 kbar at 800 °C		860-960 °C at 12 kbar
TS11011702G	Austhovde	Felsic granulite						11.5-11.6 kbar at 800 °C	
TS11020604B	Ongul	Pelitic granulite						14.7-15.3 kbar at 800 °C	
TS11020606A	Ongul	Intermediate granulite		810-840 °C 8.5-8.9kbar			8-8.5 kbar 12-12.7 kbar at 800 °C		
TS11020610G	Ongul	Garnet amphibolite				690-780 °C			
TS11020610I	Ongul	Garnet amphibolite	820-830 °C at 12 kbar		900-950°C 6-8 kbar	700-720 °C 8.1-9.1 kbar			

Table 10. Whole rock chemistry of the mafic granulites.

Sample number	SiO2	Al2O3	Fe2O3(T)	MnO	MgO	CaO	Na2O	K2O	TiO2	P205	LOI	Total
TS10122506	43.4	11.22	21.47	0.255	7.08	13.3	0.66	0.21	3.975	0.74	-1.45	100.9
TS11010704B	39.7	6.67	28.96	0.617	4.71	14.64	0.44	0.1	5.382	0.98	-1.57	100.7
TS11010802	39	13.33	24.33	0.376	7.94	10.74	0.41	0.38	4.856	0.63	-1.44	100.5
TS11010803A	36.5	13.41	29.89	0.766	5.16	10.34	0.17	0.07	3.854	1.01	-1.98	99.16
TS11011405A	42.5	12.88	22.52	0.361	6.47	9.73	1.22	0.26	4.252	0.53	0.1	100.9
TS11011601M	46.2	13.61	17.06	0.225	9.38	10.54	1.7	0.46	1.347	0.1	-0.11	100.6
TS11011601N	42.3	11.9	25.11	0.416	7.28	11.28	0.55	0.09	2.733	0.31	-1.1	100.8
TS11020206H	45	12.76	20.33	0.213	3.89	7.87	2.01	0.78	4.285	2.93	0.26	100.3
TS11020610G	44.1	14.88	12.45	0.144	12.01	10.99	1.9	1.71	0.552	0.02	1.88	100.6
TS11020610I	42.8	14.96	16.38	0.244	8.12	9.42	1.81	0.77	3.929	0.47	0.61	99.51